The dynamics of a tuningdisc vibratory gyroscope.

THE DYNAMICS OF A TUNING-DISC VIBRATORY GYROSCOPE

by

Getachew Temesgen Sedebo

Submitted in partial fulfillment of the requirements for the degree

DOCTOR TECHNOLOGIAE:

MATHEMATICAL TECHNOLOGY

in the

Department of Mathematics and Statistics

FACULTY OF SCIENCE

TSHWANE UNIVERSITY OF TECHNOLOGY

Supervisor: Prof SV Joubert

Co-Supervisor: Prof MY Shatalov

January 2019

"I hereby declare that this thesis submitted (in partial fulfillment) for the degree Doctor Technologiae: Mathematical Technology at the Tshwane University of Technology is my own original work and has not previously been submitted to any other institution of higher education. I further declare that all sources cited, or quoted are indicated and acknowledged by means of a comprehensive list of references."

Getachew Temesgen Sedebo

DEDICATION

I dedicate this work to:

- God Almighty, who is always faithful to me and has carried me thus far;
- My parents and friends, for their continuous and consistent support and love; and
- My wife Dr Ajebush Argaw, daughter Marina and son Yapheth for their support.

"Therefore I tell you, whatever you ask for in prayer, believe that you have received it, and it will be yours." Mark 11:24 NIV.

ACKNOWLEDGEMENTS

I would like to express my sincere gratitude and appreciation to the following individuals and institutions:

- Prof SV Joubert, my supervisor, for his unwavering help, inspiration, positive attitude and guidance;
- Prof MY Shatalov, my co-supervisor, for sharing his knowledge in the realm of science and innovation;
- Prof I Fedotov, for his inspiration and constructive suggestions;
- The late Dr C Coetzee, the then Head of the Department of Mathematics and Statistics, Tshwane University of Technology, for her support when I joined TUT;
- Dr EL Voges, for her constructive comments and suggestions;
- My wife, Dr Ajebush Argaw, thank you so much for your immense contributions. I am blessed to have you in my life;
- Mr Tedilaye, for helping me explore opportunities at Tshwane University of Technology;
- Ms Sesani and Mr Zukhile, the Research and Innovation Grant Administrators at TUT, for their kindness and outstanding professionalism;
- My undergraduate friend Fisseha Gashaw, at Addis Ababa University, for his immediate and timely responses to my requests;
- Mr Dominic Joubert and Mr Charl Joubert, for their professional assistance in quality sketches and language editing, respectively;
- The Department of Mathematics and Statistics of Tshwane University of Technology and TUT in general for the lecturing opportunities that I was offered;
- Tshwane University of Technology for the scholarship; and
- The National Research Foundation (NRF) of South Africa, for its Innovation Scholarship Grant.

ABSTRACT

Conventional configuration of the disc-vibratory gyroscope is based on in-plane axisymmetric vibrations of the disc with a prescribed circumferential wave number. Due to Bryan's effect, the vibrating pattern of the disc becomes sensitive to the axial component of inertial rotation of the disc. Rotation of the vibrating pattern relative to the disc is proportional to the inertial angular rate and is measured by sensors. Hence in the conventional configuration, the disc gyroscope is sensitive to the axial component of the external rotation. In this thesis, an attempt is made to design a single-body, disc-vibratory gyroscope which may replace the conventional three-body, disc-vibratory gyroscope. For this disc-vibratory gyroscope, both in-plane and out-of-plane vibrations (bending vibrations) are excited with different circumferential wave numbers. Inner and outer radii of the disc as well as the disc thickness are matched so that the natural frequencies of the in-plane and out-of-plane vibrations coincide, which is the "condition of tuning". In this case the tuning-disc gyroscope becomes sensitive to three components of inertial rotation, namely, the x-axis, the y-axis and the z-axis. Using the theory of linear elasticity and frequency tuning, a formula for the so-called "Bryan's factor" is derived to quantify a shift in angular velocity. In this thesis, analysis of the effects of elastic boundary conditions on the dynamics of thin-plate circular discs used as vibratory gyroscope resonators, is performed. The doctoral thesis is also devoted to the investigation of the dynamical aspects of disc vibration and realisation of the conditions of tuning. The thesis also includes the theory of imperfections of the vibratory gyroscope. The solutions to the equations of motion and analysis are presented using computer algebra systems (CASs) such as Mathematica and Maple.

TABLE OF CONTENTS

PAGE

DEDICATION iii

ACKNOWLEDGEMENTS iv

ABSTRACT v

LIST OF TABLES vii

LIST OF FIGURES viii

Chapter 1

INTRODUCTION 1

1.1 BACKGROUND 1

1.2 CLASSIFICATION OF GYROSCOPES 3

1.2.1 Mechanical gyroscopes 4

1.2.2 Optical gyroscopes 4

1.2.3 Vibratory gyroscopes 5

1.3 RESEARCH METHODOLOGY 8

1.4 PROBLEM STATEMENT 9

1.5 RESEARCH OBJECTIVES 9

1.6 SUMMARY OF CONTRIBUTIONS 10

1.7 OUTLINE OF THE THESIS 11

Chapter 2

LITERATURE REVIEW 13

Chapter 3

IN-PLANE DISC-VIBRATORY GYROSCOPE 17

3.1 INTRODUCTION 17

3.2 ELASTODYNAMICS 17

3.2.1 Strain-displacement relations 17

3.2.2 Hooke's law 18

3.2.3 Equilibrium equations 19

3.3 THE SINGLE-AXIS, DISC-VIBRATORY GYROSCOPE 19

3.3.1 Lagrangian and density 20

3.3.2 Generating equations 23

3.3.3 Explicit equations of motion 27

3.3.4 The explicit boundary conditions 30

3.4 NUMERICAL DETERMINATION OF THE EIGENVALUES AND EIGENFREQUENCIES OF THE IN-PLANE VIBRATIONS 31

3.4.1 Solid disc clamped at its edge 31

3.4.2 Annular disc clamped at both edges 34

3.4.3 Annular disc clamped at inner edge and free at outer edge 36

3.4.4 Annular disc free at the inner edge and clamped at the outer edge 40

3.5 CONCLUSION 43

Chapter 4

THE DYNAMICS OF THE OUT-OF-PLANE VIBRATIONS OF A DISC GYROSCOPE 44

4.1 INTRODUCTION 44

4.2 THIN PLATES 44

4.2.1 Classical or Kirchhof plate theory 44

4.3 EQUATIONS OF MOTION OF CIRCULAR PLATES 45

4.4 DERIVATION OF THE EQUATIONS OF MOTION USING THE VARIATIONAL PRINCIPLE 47

4.4.1 Kinetic energy of out-of-plane vibrations 47

4.4.2 Strain energy of the bending and torsional vibrations 48

4.4.3 Governing equation of motion 49

4.4.4 Boundary conditions in implicit form 52

4.4.5 Explicit form of the equations of motion of the vibrating plate 53

4.4.6 Explicit form of the boundary conditions 53

4.4.7 Boundary conditions in explicit form for the m^{th} vibrating mode 55

4.5 ANALYTICAL SOLUTION TO THE VIBRATING CIRCULAR PLATE 56

4.5.1 Solution for a circular plate with free vibration 57

4.5.2 Orthogonality of the eigenfunctions 59

4.5.3 Solution of a circular plate with a boundary excitation 60

4.5.4 Solution for a circular plate with a flexible foundation 61

4.5.5 Plates with varying thickness 62

4.6 NUMERICAL SOLUTIONS 62

4.6.1 Solid circular plate clamped at its edge 63

4.6.2 Annular plate with free edges 66

4.7 CONCLUSION 71

Chapter 5

THE DYNAMICS OF A TUNING DISC-VIBRATORY GYROSCOPE 72

5.1 INTRODUCTION 72

5.2 THE KINEMATICS OF THE 3D DISC-VIBRATORY GYROSCOPE 72

5.3 ENERGY 74

5.3.1 Kinetic energy 74

5.3.2 Potential energy 78
5.3.3 Lagrangian 80
5.4 THE EULER-LAGRANGE EQUATIONS OF MOTION 80
5.4.1 Homogeneous equations of motion 80
5.4.2 Non-homogeneous equations of motion 85
5.5 THE OPERATION PRINCIPLE OF THE DISC GYROSCOPE 86
5.6 INERTIAL ROTATION RATES AND BRYAN'S EFFECT 87
5.6.1 Inertial rotation rates 88
5.6.2 Bryan's factors 89
5.7 TUNING 90
5.8 EIGENFUNCTIONS FOR VARIOUS FREQUENCIES 92
5.9 CONCLUSION 94

Chapter 6

MASS IMPERFECTION IN A THREE-DIMENSIONAL, DISC-VIBRATORY GYROSCOPE 96
6.1 INTRODUCTION 96
6.2 ENERGY AND THE LAGRANGIAN 97
6.2.1 Kinetic energy 97
6.2.2 Potential energy 100
6.2.3 Lagrangian 100
6.3 THE EULER-LAGRANGE EQUATIONS OF MOTION FOR A DISC GYROSCOPE WITH MASS IMPERFECTIONS 101
6.4 FREQUENCY SPLIT 103
6.5 THEORETICAL ANALYTICAL DISCUSSION 105
6.5.1 Non-averaged solution 105
6.5.2 Averaging 107

6.6 CONCLUSION 108

Chapter 7

FINAL CONCLUSIONS AND RECOMMENDATIONS 110

7.1 SUMMARY OF CONCLUSIONS 110

7.2 RECOMMENDATIONS FOR FURTHER STUDY 112

REFERENCES 113

Appendix: A

MATHEMATICA AND MAPLE CODES 119

LIST OF TABLES

PAGE

Table 3.1 Material constants and geometric parameters of the solid disc 32

Table 3.2 The fundamental and the first five overtone vibration eigenvalues and the associated eigenfrequencies of a clamped solid disc vibrating at $m = 2$ 32

Table 3.3 The fundamental and the first five overtone vibration eigenvalues and the associated eigenfrequencies of an annular disc clamped at both edges and vibrating at $m = 2$ 35

Table 3.4 The fundamental and the first five overtone vibration eigenvalues and the associated eigenfrequencies of an annular disc clamped at the inner edge and free at the outer edge and vibrating at $m = 2$ 37

Table 3.5 The fundamental and the first five overtone vibration eigenvalues and the associated eigenfrequencies of an annular disc clamped at the outer edge and free at the inner edge and vibrating at $m = 2$ 42

Table 4.1 The fundamental and the first five overtone vibration eigenvalues and the associated eigenfrequencies of a clamped solid plate vibrating at $m = 3$ 64

Table 4.2 The fundamental and the first five overtone vibration eigenvalues and the associated eigenfrequencies of an annular plate free at the edges and vibrating at $m = 3$. 70

Table 5.1 Eigenfrequencies for an aluminium vibratory disc gyroscope for a fixed outer radius of b = 100 mm and inner radius of a=42.51 mm for various values of thickness 91

Table 5.2 Bryan's factor and auxiliary Bryan's factors for an aluminium vibratory-disc gyroscope for a fixed outer radius of b = 100 mm and inner radius of a = 42.51 mm, for various values of thickness h 91

Table 5.3 Eigenfrequencies for an aluminium vibratory-disc gyroscope for a fixed outer

radius of b = 100 mm and thickness of h = 4.824 mm for various values of inner radius a 91

Table 5.4 Bryan's factor and auxiliary Bryan's factors for an aluminium vibratory disc gyroscope with a fixed outer radius of b = 100 mm and thickness of h = 4.824 mm, for various values of inner radius a 92

LIST OF FIGURES

PAGE

Figure 1.1 The mechanical-wheel, spinning gyroscope 4

Figure 1.2 The ring-laser gyroscope 5

Figure 1.3 The Coriolis effect 6

Figure 1.4 Representation of the position vector relative to the inertial frame A and the rotating reference frame B 7

Figure 3.1 A slowly rotating annulus with inertial rotation rate $\mathbf{\Omega} = \varepsilon\Omega\hat{k}$, with inner radius a, outer radius b and thickness h with vibrating disc element of mass $dm = \rho h r dr d\varphi$ at its position of rest with polar coordinates $0r\varphi z$ 20

Figure 3.2 The function $f(\omega_d) = \ln|\det(\mathbf{M}_1)|$ produced by the CAS for a solid vibrating aluminium disc of radius $b = 1\,\mathrm{cm}$, circumferential wave number $m = 2$, density $\rho = 2.7 \times 10^3\,\mathrm{kg.\,m^{-3}}$, Young's modulus $E = 7 \times 10^{10}\,\mathrm{Pa}$ and Poisson's ratio $\upsilon = \frac{1}{3}$ 33

Figure 3.3 The eigenfunctions U (blue curve) and V (red curve) divided by their maximum-modulus corresponding to the eigenvalue $\omega_{2,0} = 1.362852\cdots\times 10^6\,\mathrm{rad.\,s^{-1}}$ for the aluminium solid disc clamped at the edge and mentioned in Figure 3.1 33

Figure 3.4 The function $f(\omega_d) = \ln|\det(\mathbf{D}_1)|$ produced by the CAS MATHEMATICA® for an annular vibrating aluminium disc of inner radius $a = 0.1\,\mathrm{cm}$, outer radius $b = 1\,\mathrm{cm}$ circumferential wave number $m = 2$, density $\rho = 2.7 \times 10^3\,\mathrm{kg.\,m^{-3}}$, Young's modulus $E = 7 \times 10^{10}\,\mathrm{Pa}$ and Poisson's ratio $\upsilon = \frac{1}{3}$ 36

Figure 3.5 The eigenfunctions $U(r)$ and $V(r)$ (divided by their maximum modulus) corresponding to the eigenvalue $\omega_{2,0} = 1.681977 \times 10^6\,\mathrm{rad.\,s^{-1}}$ for the aluminium disc clamped at both edges and mentioned in Figure 3.1 37

Figure 3.6 The function $f(\omega_d) = \ln|\det D_3|$ produced by the CAS MATHEMATICA® for a vibrating aluminium disc with inner radius $a = 0.1\,\mathrm{cm}$, outer radius $b = 1\,\mathrm{cm}$,

circumferential wave number $n = 2$, density $\rho = 2.7 \times 10^3\,\mathrm{kg.\,m^{-3}}$, Young's modulus $E = 7 \times 10^{10}\,\mathrm{Pa}$ and Poisson's ratio $\upsilon = \frac{1}{3}$ 38

Figure 3.7 The eigenfunctions $U(r)$ and $V(r)$ (divided by their maximum modulus) corresponding to the eigenvalue $\omega_{2,0} = 752771\,\mathrm{rad.\,s^{-1}}$ for the aluminium annular disc clamped at the inner boundary and free at the outer boundary 40

Figure 3.8 The function $f(\omega_d) = \ln|(\det M_4)|$ produced by the CAS MATHEMATICA® for a vibrating aluminium disc with inner radius $a = 0.1\,\mathrm{cm}$, outer radius $b = 1\,\mathrm{cm}$, circumferential wave number $m = 2$, density $\rho = 2.7 \times 10^3\,\mathrm{kg.\,m^{-3}}$, Young's modulus $E = 7 \times 10^{10}\,\mathrm{Pa}$ and Poisson's ratio $\upsilon = \frac{1}{3}$ 42

Figure 3.9 The eigenfunctions $U(r)$ and $V(r)$ (divided by their maximum modulus) corresponding to the eigenvalue $\omega_{2,0} = 1.511566 \times 10^5\,\mathrm{rad.\,s^{-1}}$ for the aluminium annular disc clamped at the outer boundary and free at the inner boundary 43

Figure 4.1 In this figure the shaded area represents the volume element of the vibrating point P. The position of rest of P is given by polar coordinates r and φ. The inner and outer arclengths are both assumed to be $rd\varphi$ as dr is verysmall, that is, $(r + dr)\,d\varphi \approx rd\varphi$ 46

Figure 4.2 The graph used to estimate the eigenvalues and eigenfrequencies of a clamped solid plate 65

Figure 4.3 The normalised eigenfunction $W(r)$ corresponding to the eigenvalue $\omega_{3,0} = 765736.6\,\mathrm{rad.\,s^{-1}}$ for a solid aluminium disc in its plate form clamped at the edge 65

Figure 4.4 The normalised eigenfunction $W(r)$ corresponding to the eigenvalue $\omega_{3,1} = 1.665943 \times 10^6\,\mathrm{rad.\,s^{-1}}$ for a solid aluminium disc in its plate form clamped at the edge 66

Figure 4.5 The graph used to estimate eigenvalues and eigenfrequencies of an annular plate free at both edges 70

Figure 4.6 The normalised eigenfunction $W(r)$ corresponding to the eigenvalue $\omega_{3,0} = 695335.3\,\mathrm{rad.\,s^{-1}}$ for the annular aluminium disc in its plate form, free at the edges 71

Figure 5.1 A thick disc, thin plate three dimensional vibratory gyroscope showing the three orthogonal axes with rotation rate components $\Omega_\zeta, \Omega_\eta$ and Ω_ξ 73

Figure 5.2 The graph used to estimate the tuned angular frequencies of in-plane and out-of-plane vibrations for $m = 2$ and $m = 3$, respectively, of an aluminium disc with inner radius $a = 42\ \mathrm{mm}$, outer radius $b = 100\ \mathrm{mm}$, density $\rho = 2.7 \times 10^3\ \mathrm{kg.\,m^{-3}}$, Young's modulus $E = 7 \times 10^{10}\ \mathrm{Pa}$ and Poisson's ratio $\upsilon = \frac{1}{3}$. The brown curve spike is used to approximate the out-of-plane eigenvalues and the red curve spikes are used to approximate the in-plane eigenvalues. Both eigenvalues are tuned approximately at $\omega \approx 688949.1598\ \mathrm{rad\,s^{-1}}$ 90

Figure 5.3 The normalised eigenfunctions U (blue curve), V (red curve) and W (brown curve) for an annular disc with clamped edges and scaled by their maximum modulus such that U and V are determined for mode number $m = 2$ while W is determined for mode number $m = 3$ and $\omega \approx 1.681977 \times 10^6\ \mathrm{rad\,s^{-1}}$ 92

Figure 5.4 The normalised eigenfunctions U (purple curve), V (red curve) and W (brown curve) for a clamped solid disc and scaled by their maximum modulus such that U and V are determined for mode number $m = 2$ while W is determined for mode number $m = 3$ and $\omega \approx 1.362852 \times 10^6\ \mathrm{rad\,s^{-1}}$ 93

Figure 5.5 The first five normalised radial eigenfunctions corresponding the first five eigenfrequencies for an annular-disc gyroscope clamped at both edges 93

Figure 5.6 The first five normalised tangential eigenfunctions corresponding the first five eigenfrequencies for an annular-disc gyroscope clamped at both edges 94

Figure 5.7 The first six normalised axial eigenfunctions corresponding to the first five eigenfrequencies for an annular-disc gyroscope clamped at both edges 95

Chapter 1

INTRODUCTION

1.1 BACKGROUND

The need for mathematical modelling in science and engineering is at its peak due to a wide range of applications of mathematical physics. Mathematical physics with a blend of vibrations and rotations has wide range applications in areas such as seismology, astronomy, inertial navigation, aerodynamics and many other fields. Mathematical modelling plays an essential role in engineering designs, scientific research, and technological innovations (Anandarajah, 2010, [1]). Mathematical modelling is essential in almost all areas of engineering, ranging from mechanical to civil, and aerospace to biological. Without appropriate mathematical modelling, the design and utilisation of automobiles, robots, aeroplanes, space shuttles, skyscrapers, bridges, roads and dams could not have been realised.

Vibrations and rotations are an integral part of most human activities such as hearing, breathing, speaking and walking. Thus, the study of vibrations and rotations has drawn the attention of most philosophers and mathematicians as far back as 4000 BC (Rao, 2011, [2]). One of the many instruments whose operation involves vibration and rotation is a “gyroscope”. The name “gyroscope” was derived from the Greek word $\gamma\eta\rho o\sigma$ (*gyros*) meaning "turn" and $\sigma\kappa o\pi o\varsigma$ (*skopos)* meaning ″view″ (Acar & Shkel, 2009, [3]). The French scientist Léon Foucault invented the gyroscope in 1852 in an attempt to measure the rotation of the earth (Lawrence, 1998, [4]). Although Foucault was given the credit for the discovery of the gyroscope, similar devices were made earlier by Johann Bohnenberger of Germany in 1817 and Walter Johnson of the United States of America in 1832 (Lawrence, 1998, [4]; Cooper, 1996, [5]; Sabageh, 2010, [6]).

A gyroscope is a sensor that measures the rate of rotation of an object (Acar & Shkel, 2009, [3]) or the angle of rotation of an object (Park, Horowitz & Tan, 2008, [7]) around a fixed axis with respect to an inertial space. Gyroscopes are used in aviation and space exploration, in the military industry, in digital camera stablisation, in rollover detection of vehicles and have many more consumer applications (Vineelal *et al*., 2014, [8]). Foucault’s pendulum as invented by Léon Fou-

cault was one of the first examples of a vibratory gyroscope (Loveday, 1999, [9], Cooper, 1996, [5]). Foucault used his pendulum to measure the rotation rate as an experiment to demonstrate the rotation of the earth. The swinging direction of the pendulum rotates with time at a rate proportional to the sine of the latitude due to the earth's rotation. The earliest gyroscopes, such as the Sperry gyroscope, utilised a rotating momentum wheel attached to a gimbal structure (Scarborough 1958, [10]). Rotating wheel gyroscopes have many disadvantages such as friction to and wear on bearings (Acar & Shkel, 2009, [3]).

The hemispherical-resonator gyroscope (HRG) and tuning-fork gyroscope eliminate rotation and avoid bearing problems. As technology develops and vibratory gyroscopes become smaller, cheaper and better-performing, many more applications will become possible (Loveday, 1999, [9]). High-performance technologies such as the fibre-optic gyroscope (FOG) and ring-laser gyroscope (RLG), based on the Sagnac effect, have been developed by eliminating nearly all mechanical limitations such as vibration, shock sensitivity and friction. Despite their high cost, optic gyroscopes have many high-end applications such as navigation aboard naval vessels (Zhang, 2015, [11]). Vibratory gyroscopes, due to their high performance, high reliability, and minute size are used in many diverse fields. These include navigation of air and marine vehicles, tracking control and rollover detection systems in cars (Azgin, 2007, [12]). Early efforts for the development of vibratory gyroscopes were motivated mostly by military applications such as missile guidance and stabilisation, gun, camera and antenna stabilisation, smart munitions including gun-fired munitions and GPS-augmented navigation (Loveday, 1999,[9]).

Bryan (1890, [13]) in his 1890 experiment explained the beating of sound produced by a ringing wine glass placed on a turntable. The foundation for the physics of present-day, hemispherical-resonator gyroscopes (HRGs) was laid by Bryan's experiment. In 1890, Bryan observed that when a vibrating structure is rotated with respect to inertial space, the vibrating pattern rotates at a rate proportional to the inertial rate of rotation (Shatalov *et al.* 2009, [14]). This effect, called "Bryan's effect" has numerous navigational applications in resonator gyroscopes (RGs) such as guidance systems in ships, aircraft and spacecraft (Coetzee, 2008, [15]). The mathematical principles of a resonator gyroscope have been discussed generally by Zhuravlev and Klimov (Joubert, Shatalov & Coetzee, 2014, [16]). Detailed analysis of the gyroscopic effects for a thin-shelled cylinder was done by Loveday and Rogers (1998, [17]). A commercial gyroscope based on Bryan's effect has a "three-body" array consisting of three hemispherical RGs with orthogonal axes of rotation. For

a fixed mode of vibration, Bryan (1890, [13]) made the following calculation for the constant of proportionality (known as Bryan's factor) or angular gain (Johari & Ayazi, 2007, [18]):

$$BF = \frac{\text{Rate of rotation of the vibrating pattern}}{\text{Inertial rate of rotation of the vibrating structure}}. \tag{1.1}$$

It is convenient to be able to calculate Bryan's factor quickly and accurately for RGs made from various substances, because it is used to calibrate each instrument. Its usefulness is confirmed by David Rozelle (2009, [19]). Rozelle states that the hemispherical-resonator gyroscope (HRG) "has been utilized in many applications over its developmental lifetime: aircraft navigation, strategic missile navigation, underground borehole navigation, communication satellite stabilization, precision pointing, and in deep space missions". He further states the following: "Small size, low noise, high performance and no wear-out has made the hemispherical resonator gyroscope (HRG) the choice for high-value space missions. After 14 years of production, the HRG boasts over 12-million operating gyrohours in space with 100% mission success". Regarding calibration, note that vibration patterns for various modes of vibration can be observed (see the holographic interferograms of a vibrating wineglass in Rossing (1994, [20])). Assume that the disc shown in Figure 3.1 is made of fused quartz and a free vibration mode is induced. Then, if a spot of paint is placed at a vibration node on the edge of the disc and the disc starts to rotate axially, the node moves away from the spot of paint and the rotation rate of the pattern can be calculated, because Bryan's factor BF in Equation (1.1) can be easily obtained. If this observation were made inside a space shuttle or submarine, then the rate of inertial rotation of the craft could be obtained.

It was in 1894 that Lord Rayleigh mentioned Bryan's effect (1894, [21]). Investigations of the latter effect appear to have lain dormant for 71 years, but reappeared in 1965 in the small Delco Wakefield Research and Development facility in Massachusetts in the USA (Rozell, 2009, [19]). Details of the working principles of the RG are scarce, mainly because of the secrecy involved in commercial manufacture.

1.2 CLASSIFICATION OF GYROSCOPES

Classification of gyroscopes can be made based on cost, operation principles, the type of material used for manufacture and the technology contained in the device. A number of classifications are in use but only a brief classification based on the technology and operation principles is presented here. Based on the existing technology, gyroscopes are broadly classified into the following main classes namely: Mechanical spinning-wheel gyroscopes; optical gyroscopes; fluidic gyroscopes;

vibratory gyroscopes; and non-vibratory gyroscopes (Sharma, 2013, [22]). In this section only mechanical, optical and vibratory gyroscopes are briefly discussed.

1.2.1 Mechanical gyroscopes

The mechanical gyroscope has a spinning disc mounted within the gimbal system. The disc moves freely with respect to the gimbal structure mounting points. This gyroscope is based on the principle of conservation of angular momentum and thus the axis of the rotor remains fixed in space and is used as an indicator of change in direction and attitude (Sabageh, 2010, [6]). Examples of mechanical gyroscopes include, for example: Dynamically-tuned gyroscopes (DTG); gas-bearing; and electrostatically-suspended spherical gyroscopes. The spinning-mass gyroscope is one of the highest-performance mechanical gyroscopes. However, its high cost, moving parts, longer start-up time and difficulty in miniaturisation remain challenges for batch fabrication (Dreyer, 2008, [23]). The mechanical-wheel spinning gyroscope (Sabageh, 2010, [6]) is shown in Figure 1.1.

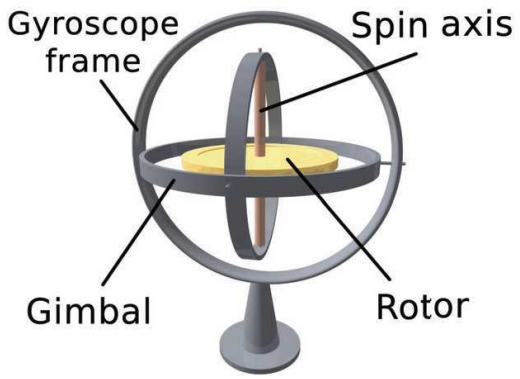

Figure 1.1: The mechanical-wheel, spinning gyroscope

1.2.2 Optical gyroscopes

This class of gyroscopes has two categories, namely, fibre-optic gyroscopes (FOGs) and ring-laser gyroscopes (RLGs). These gyroscopes are based on the Sagnac effect, which states that the phase shift between two beams measured by a ring interferometer is proportional to the angular velocity (Armensie *et al*., 2010, [24]). The Sagnac effect induces either a phase shift between two propagating signals or a frequency shift between two propagating resonant modes. A schematic diagram of a RLG is given in Hyvönen (2011, [25]).

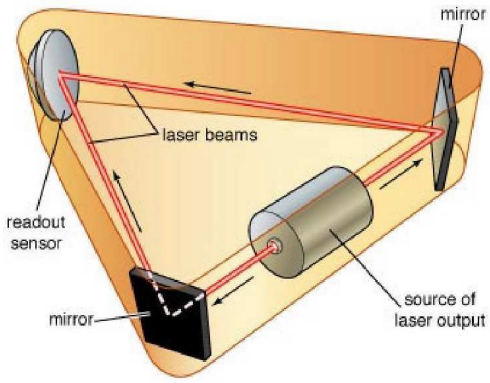

Figure 1.2: The ring-laser gyroscope

Optical gyroscopes were developed in the quest for improvement in heavy mechanical gyroscopes. They are much smaller than heavy mechanical gyroscopes and use more advanced technology and have higher performance and are thus steadily replacing their mechanical counterparts. Optical gyroscopes are widely used in inertial navigation units (INUs) in military and civilian aircraft. Unlike mechanical-wheel, spinning gyroscopes, optical gyroscopes have no bulky moving parts. However, due to their complex composition and components, and huge running costs due to intensive power use for rotation detection and cross-talk and locks, their reliability is sometimes questioned (Johari, 2008, [26]).

1.2.3 Vibratory gyroscopes

Both mechanical and optical gyroscopes are high precision gyroscopes, but due to bigger size and high cost, their use is limited to a few areas of application only. Vibratory gyroscopes are an alternative class of gyroscopes which use vibrating mechanical elements along with the Coriolis effect to measure rotation rate (Dreyer, 2008, [23]). The Coriolis force is an apparent inertial force that results from rotation and is proportional to the rotation rate. The Coriolis force appears when an object moves inside a rotating coordinate frame (Hyvönen, 2011, [25]). The Coriolis force was first observed by a French scientist Gaspar-Gustave Coriolis (1792–1843) in 1835 (Ansari, 2008, [27]). Vibratory gyroscopes do not have any moving and rotating parts and it is possible for them to be further miniaturised (Johari, 2008, [26]). Vibratory gyroscopes can be classified as angular, displacement-measuring, vibratory gyroscopes and angular-rate gyroscopes (Shkel, Acar

& Painter, 2005, [28]). The operation principle of all vibratory gyroscopes depends mainly on the exchange of energy between two vibration modes due to the Coriolis acceleration (Ansari, 2008, [27]). In order to demonstrate the Coriolis effect, assume a particle that travels in space with a velocity $\vec{V}$ and an observer seated on the x-axis of the xyz-coordinate system as shown in Figure 1.3, which has been adapted from (Ansari, 2008, [27]). Once the local coordinate system starts to rotate about the z-axis with an angular velocity $\vec{\Omega}$, then it appears for the observer on the x-axis that the particle is moving towards him/her along the $x-$axis with an acceleration of $\vec{a}_{cor} = 2\vec{\Omega} \times \vec{V}$. No force is applied to the particle but to the observer on the rotating frame (xyz) it appears that there is an apparent force which is proportional to the rotation rate $\vec{\Omega}$. The Coriolis effect is the basic operating principle of all vibratory gyroscopes.

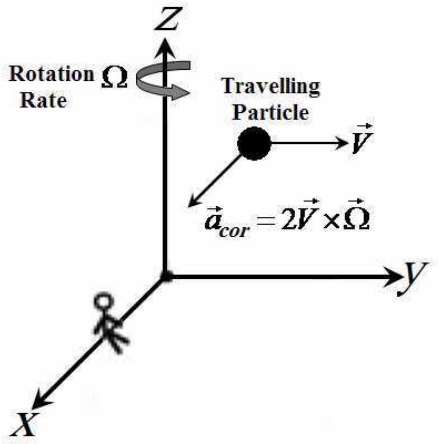

Figure 1.3: The Coriolis effect

Now consider the two reference frames A and B in Figure 1.4 as given in (Acar & Shkel, [3]), where A is an inertial or stationary frame and B is a rotating frame. Suppose also that $\mathbf{r}_A$ and $\mathbf{r}_B$ are the position vectors with respect to the stationary and rotating frames, respectively. Further assume that θ is the inclination of frame B with respect to frame A, Ω is the angular rate of the rotating frame and given as $\Omega = \dot{\theta}$, and $\mathbf{R}$ is the position vector of the rotating frame.

By means of the transport theorem (Spiegel, 1982, [29]) it is true that:

$$\dot{\mathbf{r}}_A = \dot{\mathbf{r}}_B + \boldsymbol{\Omega} \times \mathbf{r}_B. \tag{1.2}$$

From the vector representation in Figure 1.4, it can be seen that:

$$\mathbf{r}_A = \mathbf{R} + \mathbf{r}_B. \tag{1.3}$$

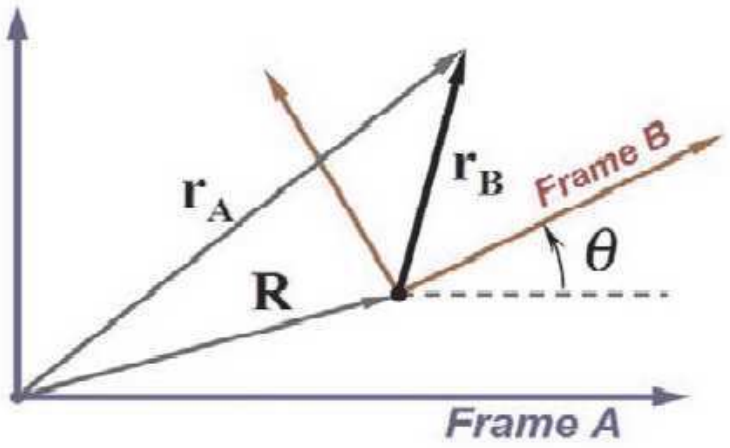

Figure 1.4: Representation of the position vector relative to the inertial frame A and the rotating reference frame B

Acceleration with respect to the inertial frame is given by (Acar & Shkel, 2009, [3]):

$$\mathbf{a}_A = \mathbf{A} + \mathbf{a}_B + \dot{\boldsymbol{\Omega}} \times \mathbf{r}_B + \boldsymbol{\Omega} \times (\boldsymbol{\Omega} \times \mathbf{r}_B) + 2\boldsymbol{\Omega} \times \mathbf{v}_B, \tag{1.4}$$

where $\mathbf{a}_B$ and $\mathbf{v}_B$ are the acceleration and velocity vectors with respect to the rotating frame B. Whereas $\mathbf{A}$ is the linear acceleration of the rotating frame, $\boldsymbol{\Omega}$ and $\dot{\boldsymbol{\Omega}}$, respectively, are the angular velocity and angular acceleration of the rotating frame. The term $\mathbf{A} + \mathbf{a}_B + \dot{\boldsymbol{\Omega}} \times \mathbf{r}_B$ is the acceleration of a vibrating object in the rotating frame whereas the term $\boldsymbol{\Omega} \times (\boldsymbol{\Omega} \times \mathbf{r}_B)$ is the centripetal acceleration and the last term $2\boldsymbol{\Omega} \times \mathbf{v}_B$ is the fictitious term called Coriolis acceleration.

In vibratory gyroscopes, the Coriolis effect is responsible for the coupling of energy between two modes of vibration. The drive mode, also called the primary mode, is responsible for setting the resonator (the vibrating element) in motion with constant amplitude. The sense mode, also called the secondary mode, is induced by the Coriolis effect and vibration of the primary mode. Measurement of the amplitude of the sense mode provides the required measure of the angular rate. Examples of vibratory gyroscopes may include: Disc-vibratory gyroscopes; hemispherical resonator gyroscopes; tuning-fork gyroscopes; ring gyroscope; and vibratory-wheel gyroscopes (Johari, 2008, [26]). The main focus of this thesis is the dynamics of the disc-vibratory gyroscope. The disc-vibratory gyroscope may consist of a fused-quartz resonator that is actuated by electrostatic force or electromagnetic force or piezoelectric means. The disc considered in this thesis is a thin disc made from isotropic material (Burdess & Wren, 1986, [30]).

1.3 RESEARCH METHODOLOGY

The research undertaken in this study considers both solid and annular discs that model the disc gyroscope vibrating in a plane as well as out-of-plane in the presence of non-constant, three-dimensional (3D), inertial rotation rate. Throughout this study, Hamilton's variational principle which deals with determination of the extrema of a functional is used to derive equations of motion. Using the same method, the natural and prescribed boundary conditions are formulated. Various models of the disc gyroscope are considered. Firstly, a disc gyroscope that vibrates and rotates in its plane is considered, where all dynamics and boundary conditions of the in-plane vibration of the disc for both rotating and non-rotating disc gyroscopes is detailed in depth. The analytical solutions in terms of Bessel's functions for a non-rotating disc vibrating in its plane is determined. Later the eigenfunctions associated with the non-rotating disc is used to determine the eigenvalues when the disc is slowly rotating. Secondly, the out-of-plane vibration of the disc gyroscope is modelled using a circular plate that is subjected to bending out of its plane. Similar to the in-plane vibration, analytical solutions to the vibration problem are determined in terms of Bessel's and modified Bessel's functions. Using various boundary conditions, the frequency equations are formulated and the corresponding eigenvalues and eigenfrequencies are numerically computed using MATHEMATICA and MAPLE.

Thirdly, a disc gyroscope vibrating both in its plane and out-of-plane and subjected to a slow 3D-inertial rotation rate is considered. The strain energies of in-plane and out-of-plane vibrations are considered independent of one another and thus the total strain energy of the disc is obtained as a sum of the two. The Lagrangian of the system vibrating with mode numbers $m = 2$ in-plane and $m = 3$ out-of-plane is determined in terms of the generalised coordinates C, S, A and B. A system of gyroscopic equations for the disc with 2-ω_I and 3-ω_o vibrating patterns in terms of the generalised coordinates is obtained.

The operation principles of the 3D-disc gyroscope, Bryan's effect and Bryan's factors are investigated. The eigenvalues, eigenfrequencies and Bryan's factors for various boundary conditions are determined and analysed using tables and graphs generated by means of CASs. To eliminate the frequency split between the in-plane modes and the out-of-plane modes, appropriate thickness and/or radii of the disc are selected. To account for structural non-idealities, the case of mass imperfections is included.

1.4 PROBLEM STATEMENT

Gyroscopes operating in single axis and dual-axis forms are widely developed and batch-fabricated (Tsai & Sue, 2008, [31]). A number of applications which require 3D motion has necessitated the need for a detailed study of 3D-vibratory gyroscopes. Sung (2013, [32]) used three devices comprising of a yaw, a pitch and a roll integrated into a single chip to sense tri-axial rotation. Johari, Shah and Ayazi (2008, [33]) designed and used a thick (100) silicon, high-frequency, single-disc gyroscope capable of sensing the rotation rate around the x and z-axes. The main problems that this thesis tries to investigate and answer are the following:

- Is it possible to derive a mathematical model for a single disc gyroscope that is capable of sensing inertial rotation rates in multiple axes?
- If so, how can the equations of motion that describe the dynamics of the system be derived?
- What is the system of equations for this dynamic system?
- What are the analytical solutions for the vibratory system if the rotation rate is neglected?
- What are the operation principles of such a single 3D-disc gyroscope?
- What are the formulas for the components of inertial rotation rate?
- What are the models for Bryan's effect and Bryan's factors for a slowly rotating 3D-disc gyroscope?
- What are the techniques used to tune eigenfrequencies of in-plane modes and out-of-plane modes to maximise the sensitivity of this disc gyroscope?

1.5 RESEARCH OBJECTIVES

The principal objectives of this thesis are:

- To model mathematically a single 3D-solid and annular disc gyroscope that is capable of sensing rotation rates around three mutually-perpendicular axes;
- To derive the equations of motion and expressions for various associated boundary conditions for the disc gyroscope that is capable of measuring rotation rates in three axes;
- To establish the various boundary conditions and solve the associated frequency equations to determine the approximate eigenvalues of the vibrating system;
- To determine the eigenfunctions associated with both in-plane and out-of-plane modes graphically;

- To show how the tuning of natural frequencies of both modes can be achieved to maximise the performance of the disc gyroscope; and
- To determine the approximate values of Bryan's factor and the auxiliary Bryan's factors for the disc-vibratory gyroscope.

1.6 SUMMARY OF CONTRIBUTIONS

The main contributions of this work are the derivation of equations of motion, formulation of boundary conditions, and the numerical determination of the eigenvalues and eigenfrequencies. The components of the rotation rate for a 3D disc gyroscope are formulated analytically. Bryan's factor and auxiliary Bryan's factors are derived. In general, a mathematical model for a disc-vibratory gyroscope that is subjected to a 3D rotation rate is developed. The contributions are summarised in the peer-reviewed publications and conference presentations as listed below.

[1] SEDEBO, G.T., JOUBERT, S.V. & SHATALOV, M.Y. 2018. An analytical theory for a three-dimensional thick-disc thin-plate vibratory gyroscope. *Journal of Physics: Conference Series*, **991(1)** 012072: 1-8. [Online]: doi:10.1088/17426596/991/1/012072.

[2] JOUBERT, S.V., SHATALOV, M.Y., FAY, T.H. & SEDEBO, G.T. 2017. *On Bryan's law and anisotropic non-linear damping*. International Congress on Sound and Vibration (ICSV24), 23-27 July 2017, London, United Kingdom: 1-8. [Online]:

http://iiav.org/icsv24/content/papers/papers/full_paper_689_20170416152259242.pdf.

[3] SEDEBO, G.T., JOUBERT, S.V. & SHATALOV, M.Y. 2016. *The dynamics of a 3-dimensional vibrating and rotating disc gyroscope*. 18th International Conference on Applied Physics and Mathematics (ICAPM 2016), 8-9 September 2016, Singapore. Won best oral presentation award. [Online]: https://waset.org/abstracts//52286.

[4] SEDEBO, G.T., JOUBERT, S.V. & SHATALOV, M.Y. 2017. *On the dynamics of a 3D vibratory-disc gyroscope.* Science Faculty research day, TUT, 8 September 2017.

[5] SEDEBO, G.T., JOUBERT, S.V. & SHATALOV, M.Y. 2015. *The dynamics of a thin disc-vibratory gyroscope.* Postgraduate Seminar in Mathematics, 29 November - 3 December 2015, Nelson Mandela Metropolitan University, Port Elizabeth, South Africa.

1.7 OUTLINE OF THE THESIS

This thesis is organised in seven chapters. Chapter 2 provides a comprehensive literature review for the disc-vibratory gyroscope and Bryan's effect. The dynamics of the in-plane, disc-vibratory gyroscope is discussed in Chapter 3. This study is not limited to the vibration of thin-shelled disc gyroscopes (as is the case for almost all of the results in the literature). The derivation of equations of motion for the disc-vibratory gyroscope is undertaken using the variational principle. Various boundary conditions and frequency equations are established and the associated eigenvalues and eigenfrequencies are calculated numerically. In Chapter 4 the out-of-plane vibration of the disc-vibratory gyroscope is modelled by the bending vibration of a thin circular plate. Similar to Chapter 3, the equations of motion for the out-of-plane vibration are derived using the variational principle. The eigenvalues and the eigenfrequencies as well as the eigenfunctions relating to the bending vibration of the disc-vibratory gyroscope are determined numerically.

Chapter 5 discusses the derivation of equations of motion of a tuning, disc-vibratory gyroscope subjected to slow 3D-rotation. The kinetic energy and strain energy of the slowly-rotating and vibrating disc are described in terms of four generalised coordinates namely, C, S, A and B. The analytical theory of the tuning, disc-vibratory gyroscope with tuned resonant frequencies of the in-plane and out-of-plane modes is presented. Numerical examples of tuning of frequencies of both modes are investigated for various dimensions of the disc gyroscope. Investigations of Bryan's effect in terms of the integrals of the eigenfunctions are presented in this chapter including quantitative examples of Bryan's factor and auxiliary Bryan's factors. The operation principle for this 3D-disc gyroscope is discussed and analytical determination of the components of the inertial rotation is provided. The results of this contribution is published in Sedebo, Joubert and Shatalov (2018, [34]).

Chapter 6 introduces the notion of mass imperfection to the vibratory-disc gyroscope. Imperfections such as mass imperfection are the major sources of limitations in the performance of vibratory-disc gyroscope, if left uncorrected. A coupled system of gyroscopic equations with mass imperfections are derived. Frequency splitting as a result of mass imperfections in the in-plane modes and out-of-plane modes of the disc-vibratory gyroscope are discussed. Both non-averaged and averaged equations are obtained and qualitative inferences are included.

Chapter 7 summarises and concludes the thesis. Potential future research areas are identified and recommendations are made. A list of contributions to this study in local and international conferences and refereed scientific journals is summarised.

Chapter 2

LITERATURE REVIEW

A disc and its vibration properties subjected to classical boundaries have been widely studied and are well-documented. Substantial amounts of information on the nature of both in-plane and out-of-plane vibrations can be found in literature. Circular discs are used and applied in widely different areas, amongst others, in nozzle covers, pressure vessels, pump diaphragms, turbine disks, submarines, airplanes, railway wheels, brakes, hard drive discs and as sensors (Bashmal, Bhat & Rakheja, 2011, [36]). Love (1893, [35]) derived the equations of motion for a thin circular disc with a free edge and obtained an analytical solution. The bending of circular plates with various boundary conditions are thoroughly discussed by Timoshenko and Woinowsky-Krieger (1959, [37]). Bashmal, Bhat and Rakheja (2011, [36]) investigated and analysed the in-plane free vibration of an annular disc with an elastic support at a point. The Rayleigh-Ritz method was used to determine the various frequency parameters and the associated mode shapes. Leissa (1969, [38]) and Leissa and Qatu (2011, [39]) presented analytical solutions for both solid and annular plates in terms of the Bessel functions subjected to various boundary conditions. Theoretical as well as experimental results for frequencies and ratios of radii for nodal circles were calculated.

Analytical solutions for a rotor consisting of multiple flexible discs were obtained by Jia, Chun and Lee (1997, [40]). The authors also investigated the effect of a flexible disc on the coupled longitudinal vibrations that link the disc and shaft. A car brake disc, regarded as an annular plate, was investigated by Ouyang *et al*. (2000, [41]) and its equation of motion was derived using the theory of a thin plate. The equations of motion were purely those of a thin circular plate because the authors intentionally dropped the dynamics of the in-plane vibrations that involve gyroscopic effects. The first disc gyroscope based on Piezoelectric material was investigated by Burdess and Wren (1986, [30]). The authors proposed a thin piezoelectric disc gyroscope that utilises its in-plane vibration properties to detect the rotation rate. The authors neglected the stresses in the transverse direction of the disc to derive both constitutive and field equations. Singh and Gorain (2004, [42]) reported another piezoelectric disc gyroscope which uses the piezoelectric material PZT-5H for both excitation of vibration and detection of rotation. The disc structure has certain advantages as compared to other structures, due to its symmetry, and it is less sensitive to

bogus vibrations. The vibrating disc is not sensitive to temperature and hence the sensitivity is not affected by temperature variations (Singh & Gorain, 2004, [42]).

The authors Hao, Pourkamali and Ayazi (2004, [43]) reported a single, silicon-capacitive, disc resonator based on an elliptic bulk-mode which is modelled as a solid circular thin plate with a free edge and a support beam. The authors also calculated the mode shape and presented both theoretical and numerical results. The disc resonator presented by Hao, Pourkamali and Ayazi (2004, [43]), similar to the one reported by Burdess and Wren (1986, [30]) and Singh and Gorain (2004, [42]) uses the in-plane vibration mode properties with mode number $m = 2$, to measure the rotation rate. Tsai *et al.* (2010, [44]) reported the design of a reciprocally, micro-disc gyroscope driven electromagnetically. In their innovative design, the micro-disc gyroscope had a two-dimensional angular rate, the first dimension "spinning" as a result of the electromagnetic drive force and the second "tilting" as a result of the Coriolis effect. A high-quality, high-frequency, single-crystal, silicon (SCS) disc resonator driven by capacitive means and operating at its elliptic mode with a mode number $m = 2$ was reported by Pourkamali, Hao and Ayazi (2004, [45]) as a continuation of their work in part I (2004, [43]). They provided the details of implementation and characterisation of the SCS. Another elliptical mode (SCS) disc resonator was also presented by Wei and Seshia (2014, [46]), where the frequency split between the in-plane modes is analytically formulated. Johari and Ayazi (2007, [18]) presented a capacitive, bulk-acoustic disc gyroscope which also operates in elliptic mode with $m = 2$, in its plane. They compared the performance parameters of the disc gyroscope for both silicon (100) and (111) substrates.

Despite their high precision, mechanical, optic or ring-laser gyroscopes are all too bulky and too expensive and these factors limit their use in recent emerging applications. Miniaturisation of mechanical gyroscopes is very difficult and this has created an opportunity for vibratory gyroscopes that can effectively be miniaturised using micro-machining technology. The size of vibratory gyroscopes can be shrunken by an order of magnitude reducing their fabrication costs considerably. Micro-fabrication also allows designers to integrate the electronics on the same chip, further reducing the overall size of the gyroscope. Micro-electromechanical systems (MEM) are a technology that combines electrical and mechanical systems at a micro level (Acar & Shkel, 2009, [3]). As a result of miniaturisation, extremely complex electromechanical parts can be assembled together to create complete and sophisticated systems on a chip. This provides an opportunity for mass-production of low-cost gyroscopes.

Conventional gyroscopes such as mechanical, optic or ring-laser gyroscopes can only measure rotation rates around one axis at a time. If there is a need to measure the rotation rate around three mutually-perpendicular axes, one of these gyroscopes has to be used at a time for each axis. Gyroscopes operating in single-axis and dual-axis are widely developed and batch-fabricated (Tsai & Sue, 2010, [47]). A number of applications which require 3D motion has necessitated the need for a detailed study of multi–axis vibratory gyroscopes. Cooper (1996, [5]) proposed a gyroscope that is able to measure rotation rates around all three, mutually-perpendicular axes. His investigation was mainly of qualitative nature with finite element (FE) analysis. Sung (2013, [32]) used three devices such as a yaw, a pitch and a roll integrated into a single chip to sense tri-axial rotation. Johari, Shah and Ayazi (2008, [33]) designed and implemented a thick (100) silicon, high-frequency, single-disc gyroscope capable of sensing the rotation rate around the x and z-axes. Despite using the same disc, the sensitivity for each in-plane axis was measured at different times. Another multi-axis gyroscope using the ring element as a resonator was investigated and the operation principle was detailed by Gallacher *et al*. (2006, [48]). The authors presented the principle of a 3-axis, ring gyroscope and outlined the process of prototype fabrication using MEMS techniques.

Johari (2008, [26]) introduced a single disc gyroscope capable of sensing rotation rates along the x and z-axes, operating at high frequency. The operation principle is based on the Coriolis coupling of in-plane and out-of-plane vibrations. The implementation of this gyroscope involved revised the high aspect-ratio, poly and single-crystalline silicon (HARPSS) fabrication process and used 40 μm-thick SOI substrates. A successful, mode-matched hollow-disc, dual-axis gyroscope was reported by Sung, Dalal and Ayazi (2011, [49]). The gyroscope uses three in-plane and out-of-plane resonant modes to achieve maximum sensitivity. Furthermore, the gyroscope uses its in-plane elliptical mode as a drive mode and the two other orthogonal out-of-plane modes as sense modes. Although the device reported on was capable of sensing rates of rotation around more than one axis, it needed to be integrated to the yaw-disc to exploit it for measuring rotation rates around three mutually-perpendicular axes.

G.H. Bryan (1890, [13]) in his 1890 experiment explained that the angular rate of a vibrating pattern of a rotating ring is proportional to the inertial angular rate of the ring structure. This effect is called Bryan's effect and the proportionality constant is called "Bryan's factor". Bryan's effect laid the foundation for the physics of present-day, vibratory-disc resonator gyroscopes (VDRGs) and hemispherical resonator gyroscopes (HRGs). Bryan's effect has many applications such as

in the fields of navigation, seismology and cosmology (Coetzee, 2008, [15]). Coetzee (2008, [15]) investigated the dependence of Bryan's factor on various physical and geometric parameters of a spherical body. Bryan's effect for a cylinder with a vibrating lateral side was discussed by Voges (2006, [50]). Joubert, Shatalov and Fay (2009, [51]) obtained approximate but extremely accurate values for Bryan's factor in terms of integrals for isotropic rotating structures. Pretorius (2007, [52]) studied Bryan's effect for a thin disc subjected to an inertial rotation. Analysis of the effects of isotropic, non-linear damping on Bryan's effect was performed by Joubert, Shatalov and Manzhirov (2013, [53]).

To date, there is no example with sufficient detail, of a 3D, single-disc vibratory gyroscope, available in the literature. For this reason, this thesis is devoted to the investigation of a single-disc vibratory gyroscope that is capable of measuring 3D rotation rates. To accomplish this investigation, the equations of motion that describe the dynamics of the 3D-disc vibratory gyroscope are derived, the operation principle is devised, the rotation rates are determined analytically and Bryan's factors are investigated in subsequent chapters.

Chapter 3

IN-PLANE DISC-VIBRATORY GYROSCOPE

3.1 INTRODUCTION

In this chapter, the in-plane vibrations of the disc-vibratory gyroscope are investigated. The equations of motion and boundary conditions describing the in-plane vibration of the disc are derived and discussed. Only the vibration of the disc in its plane mode resulting from extension and shear are emphasised in this chapter.

3.2 ELASTODYNAMICS

Elasticity of materials is defined as the subject that deals with the stress, strain and displacement of an elastic solid (Sadd, 2009, [54]). The main idea behind the theory of elasticity is that the deformation of the body due to an external load is small with respect to unity, which allows for the establishment of various mathematical models in numerous areas of application in engineering and science. A perfectly elastic body returns to its natural undeformed state when all loads or external forces are removed (Achenbach, 1973, [55]). Throughout this thesis, wherever applicable, only aspects of linear elasticity are used. Fan (2011, [56]) reduces the basic assumptions of elasticity to the following core ideas:

- Continuity of the medium: The medium in which the field variables are considered is uniform. From this, it follows that the field variables are continuously differentiable functions of the spatial coordinates.
- Homogeneity of the medium: The physical constants of the medium do not depend on spatial coordinates.
- Small deformations: The strain components as a result of deformation are less than unity.
- Rigid body motions are not part of the deformation of the body.

3.2.1 Strain-displacement relations

If an elastic body undergoes deformation due to external loads, its shape or volume varies. Below,

the strain-displacement relations are shown for the cylindrical coordinates $(r,\ \varphi,\ z)$ of an elastic body that undergoes deformation:

$$\epsilon_r = \frac{\partial u}{\partial r},\ \epsilon_\varphi = \frac{1}{r}\left(u + \frac{\partial v}{\partial \varphi}\right),\ \epsilon_z = \frac{\partial w}{\partial z}, \tag{3.1}$$

where u is radial displacement, v is tangential displacement, w is axial displacement, ϵ_r is a tensile strain in the radial direction, ϵ_φ is a tensile strain in the tangential direction and ϵ_z is a tensile strain in the axial direction. The shear strains are given as follows:

$$\epsilon_{r\varphi} = \frac{1\partial u}{r\partial \varphi} + \frac{\partial v}{\partial r} - \frac{v}{r},\ \epsilon_{rz} = \frac{\partial u}{\partial z} + \frac{\partial w}{\partial r} \text{ and } \epsilon_{\varphi z} = \frac{1\partial w}{r\partial \varphi} + \frac{\partial v}{\partial z}. \tag{3.2}$$

For the deformation of a perfectly elastic body, the infinitesimal or differential displacement is a continuous function of the coordinate axis. Tensile strains given by Equation (3.1) are obtained from the diagonal elements of the displacement-gradient matrix, while shear strains given by Equations (3.2) may be obtained from the symmetry of the displacement-gradient matrix (Yenwong-Fai, 2008, [57]).

3.2.2 Hooke's law

Hooke's law for isotropic material in cylindrical coordinates may be written in its general form as:

$$\begin{aligned} \sigma_r &= \lambda\left(\epsilon_r + \epsilon_\varphi + \epsilon_z\right) + 2\mu\epsilon_r; \\ \sigma_\varphi &= \lambda\left(\epsilon_r + \epsilon_\varphi + \epsilon_z\right) + 2\mu\epsilon_\varphi; \text{ and} \\ \sigma_z &= \lambda\left(\epsilon_r + \epsilon_\varphi + \epsilon_z\right) + 2\mu\epsilon_z; \end{aligned} \tag{3.3}$$

where σ_r, σ_φ and σ_z are the tensile stresses, in radial, tangential and axial directions respectively, λ and μ are the Lamè coefficients. The shear stresses are:

$$\begin{aligned} \sigma_{r\varphi} &= \mu\epsilon_{r\varphi}; \\ \sigma_{rz} &= \mu\epsilon_{rz}; \text{ and} \\ \sigma_{\varphi z} &= \mu\epsilon_{\varphi z}. \end{aligned} \tag{3.4}$$

For an isotropic material the strain-stress relationship in cylindrical coordinates is summarised by and represented in the matrix shown below (Reddy, 2004, [58]):

$$\begin{pmatrix} \epsilon_r \\ \epsilon_\varphi \\ \epsilon_z \\ \frac{1}{2}\epsilon_{r\varphi} \\ \frac{1}{2}\epsilon_{\varphi z} \\ \frac{1}{2}\epsilon_{rz} \end{pmatrix} = \frac{1}{E}\begin{pmatrix} 1 & -\eta & -\eta & 0 & 0 & 0 \\ -\eta & 1 & -\eta & 0 & 0 & 0 \\ -\eta & -\eta & 1 & 0 & 0 & 0 \\ 0 & 0 & 0 & 1+\eta & 0 & 0 \\ 0 & 0 & 0 & 0 & 1+\eta & 0 \\ 0 & 0 & 0 & 0 & 0 & 1+\eta \end{pmatrix}\begin{pmatrix} \sigma_r \\ \sigma_\varphi \\ \sigma_z \\ \sigma_{r\varphi} \\ \sigma_{\varphi z} \\ \sigma_{rz} \end{pmatrix}, \tag{3.5}$$

where E-is modulus of elasticity, η-is Poisson's ratio. The Lamè constants are:

$$\lambda = \frac{\eta E}{(1+\eta)(1-2\eta)}; \text{ and } \mu = G = \frac{E}{2(1+\eta)}. \tag{3.6}$$

The following relationships can be obtained from Equation (3.6) (Redwood, 1960, [59]):

$$E = \frac{\mu(3\lambda+2\mu)}{\lambda+\mu},\ \eta = \frac{\lambda}{2(\lambda+\mu)} \text{ and } k = \lambda + \frac{2}{3}\mu. \tag{3.7}$$

Here $\mu = G$-is shear modulus and k-is bulk modulus..

3.2.3 Equilibrium equations

The equilibrium equations or Navier's equations for an isotropic solid with a material density ρ in cylindrical coordinates (Redwood, 1960, [59]) are:

$$\mu\left(\nabla^2 u - \frac{u}{r^2} - \frac{2}{r^2}\frac{\partial v}{\partial \varphi}\right) + (\lambda+\mu)\frac{\partial}{\partial r}\left(\frac{1}{r}\frac{\partial}{\partial r}(ru) + \frac{1}{r}\frac{\partial v}{\partial \varphi} + \frac{\partial w}{\partial z}\right) = \rho\frac{\partial^2 u}{\partial t^2}; \tag{3.8}$$

$$\mu\left(\nabla^2 v - \frac{v}{r^2} + \frac{2}{r^2}\frac{\partial u}{\partial \varphi}\right) + (\lambda+\mu)\frac{\partial}{\partial \varphi}\left(\frac{1}{r}\frac{\partial}{\partial r}(ru) + \frac{1}{r}\frac{\partial v}{\partial \varphi} + \frac{\partial w}{\partial z}\right) = \rho\frac{\partial^2 v}{\partial t^2}; \text{ and} \tag{3.9}$$

$$\mu\nabla^2 w + (\lambda+\mu)\frac{\partial}{\partial z}\left(\frac{1}{r}\frac{\partial}{\partial r}(ru) + \frac{1}{r}\frac{\partial v}{\partial \varphi} + \frac{\partial w}{\partial z}\right) = \rho\frac{\partial^2 w}{\partial t^2}. \tag{3.10}$$

3.3 THE SINGLE-AXIS, DISC-VIBRATORY GYROSCOPE

Consider an annular disc of thickness h with inner radius a and outer radius b that is rotating slowly at rate $\mathbf{\Omega} = \varepsilon\Omega\hat{k}$. Assume that $dm = \rho h r dr d\varphi$ is an infinitesimal element of the disc located at a distance r from the origin as shown in Figure 3.1 on the disc, with radial displacement given as u and tangential displacement as v from the position of rest. The element dm has a polar angle φ, measured from the x-axis with terms: mass density ρ of the disc and Poisson's ratio η. It is also assumed that the thickness h is much smaller than the typical in-plane dimensions of the disc, that is, $h << \min(a,b)$ and hence the disc is "thin".

Assume that the disc rotates around its axis (z) with an inertial angular rate of $\mathbf{\Omega} = \varepsilon\Omega\hat{k}$ where ε is a small parameter and $\hat{k}$ is the unit vector in the direction of increasing z. From this, the absolute velocity of the element dm is:

$$\vec{V} = \begin{pmatrix} \dot{u} & \dot{v} & \dot{w} \end{pmatrix}^T + \mathbf{\Omega} \times \vec{R}; \tag{3.11}$$

with:

$$\mathbf{\Omega} = \begin{pmatrix} 0 & 0 & \varepsilon\Omega \end{pmatrix}^T; \text{ and} \tag{3.12}$$

$$\vec{R} = \begin{pmatrix} r+u & v & 0 \end{pmatrix}^T; \tag{3.13}$$

and T is the transpose of a matrix, while $\dot{u}$, $\dot{v}$ and $\dot{w} = 0$ are the derivatives of u, v and w respectively with respect to time. The absolute linear velocity can now be written as (Joubert, Shatalov & Fay, 2009, [51]):

$$\vec{V} = (\dot{u} - \varepsilon\Omega v)\,\hat{r} + (\dot{v} + \varepsilon\Omega(r+u))\,\hat{\varphi} + 0\hat{k}; \tag{3.14}$$

were $\hat{r}$, $\hat{\varphi}$ and $\hat{k}$ are the unit vectors in the increasing directions of r, φ and z, respectively.

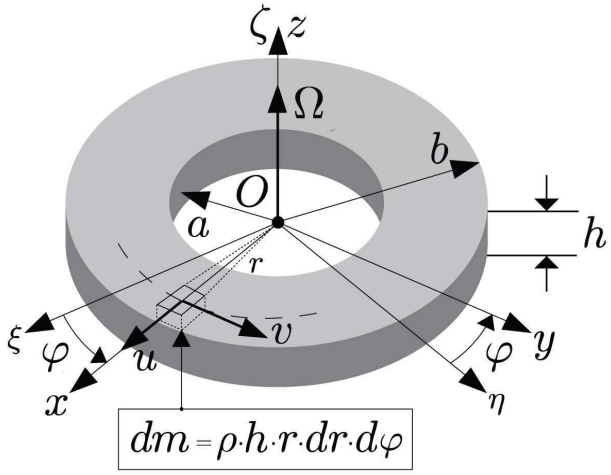

Figure 3.1: A slowly rotating annulus with inertial rotation rate $\boldsymbol{\Omega} = \varepsilon\Omega\hat{k}$, with inner radius a, outer radius b and thickness h with vibrating disc element of mass $dm = \rho h r dr d\varphi$ at its position of rest with polar coordinates $0r\varphi z$

3.3.1 Lagrangian and density

The kinetic energy of the vibrating and slowly-rotating disc (Joubert, Shatalov & Fay, 2009, [51]) is given by:

$$\begin{aligned} K &= \frac{1}{2}\int_0^h \int_0^{2\pi} \int_a^b \rho(\vec{V}\cdot\vec{V}) r d\varphi dr dz \\ &= \int_0^{2\pi} \int_a^b \frac{\rho h r}{2} \left((\dot{u} - \varepsilon\Omega v)^2 + (\dot{v} + \varepsilon\Omega(r+u))^2\right) dr d\varphi. \end{aligned} \tag{3.15}$$

Assuming that the inertial rotation $\varepsilon\Omega$ is much smaller than the lowest eigenvalue of the system, terms of order $O(\varepsilon^2)$ are neglected. The centrifugal forces that are proportional to $(\varepsilon\Omega)^2$ are also neglected. The term $2\varepsilon r\Omega\dot{v}$ in the expression of the kinetic energy is neglected because it disappears in the Euler-Lagrange equations. Thus one obtains the following approximate expression for

the kinetic energy:

$$K \approx \int_0^{2\pi} \int_a^b \frac{\rho h r}{2} \left(\dot{u}^2 + \dot{v}^2 - 2\varepsilon\Omega \left(\dot{u}v - u\dot{v} \right) \right) dr d\varphi. \tag{3.16}$$

Please take note of the dot and prime notations used for derivatives elsewhere in this chapter:

$$\dot{u} = \frac{\partial u}{\partial t},\ \dot{v} = \frac{\partial v}{\partial t},\ u'_r = \frac{\partial u}{\partial r},\ u'_\varphi = \frac{\partial u}{\partial \varphi},\ v'_r = \frac{\partial v}{\partial r},\ v'_\varphi = \frac{\partial v}{\partial \varphi}; \tag{3.17}$$

$$\ddot{u} = \frac{\partial^2 u}{\partial t^2},\ u''_{rr} = \frac{\partial^2 u}{\partial r^2},\ u''_{\varphi\varphi} = \frac{\partial^2 u}{\partial \varphi^2},\ u''_{r\varphi} = \frac{\partial^2 u}{\partial r \varphi}; \tag{3.18}$$

$$\ddot{v} = \frac{\partial^2 v}{\partial t^2},\ v''_{rr} = \frac{\partial^2 v}{\partial r^2},\ v''_{\varphi\varphi} = \frac{\partial^2 v}{\partial \varphi^2};\ \text{and}\ v''_{r\varphi} = \frac{\partial^2 v}{\partial r \varphi}. \tag{3.19}$$

In order to calculate the strain energy (the potential energy) it is assumed that the in-plane displacements u and v and their derivatives do not influence the mid-plane curvatures (χ_1 and χ_2) and torsion ($\tilde{\tau}$). This assumption corresponds to the simplification of the Novozhilov's theory of thin shells to the Novozhilov-Goldenveizer theory of shallow shells (Leissa, 1993, [60], Novozhilov, 1970, [61]). In the Novozhilov-Goldenveizer theory, it is accepted that the curvatures and torsion become (Soedel, 2004, [62]):

$$\chi_1 \approx -\frac{1}{A_1}\frac{\partial}{\partial \alpha_1}\left(\frac{1}{A_1}\frac{\partial w}{\partial \alpha_1} \right) - \frac{1}{A_1 A_2^2}\frac{\partial A_1}{\partial \alpha_2}\frac{\partial w}{\partial \alpha_2} = 0; \tag{3.20}$$

$$\chi_2 \approx -\frac{1}{A_2}\frac{\partial}{\partial \alpha_2}\left(\frac{1}{A_2}\frac{\partial w}{\partial \alpha_2} \right) - \frac{1}{A_1^2 A_2}\frac{\partial A_2}{\partial \alpha_1}\frac{\partial w}{\partial \alpha_1} = 0;\ \text{and} \tag{3.21}$$

$$\tilde{\tau} \approx -\frac{1}{A_1 A_2}\left(\frac{\partial^2 w}{\partial \alpha_1 \partial \alpha_2} - \frac{1}{A_1}\frac{\partial A_1}{\partial \alpha_2}\frac{\partial w}{\partial \alpha_1} - \frac{1}{A_2}\frac{\partial A_2}{\partial \alpha_1}\frac{\partial w}{\partial \alpha_2} \right) = 0; \tag{3.22}$$

where A_1 and A_2 are the Lamé parameters and the axial displacement is $w = 0$. The parametrisation of the mid-plane of the disc is as follows:

$$x = \alpha_1 \cos\alpha_2; \quad y = \alpha_1 \sin\alpha_2; \quad z = 0; \tag{3.23}$$

where:

$$\alpha_1 = r; \quad \alpha_2 = \varphi. \tag{3.24}$$

The corresponding curvatures are:

$$\lim_{R_1 -> \infty} \frac{1}{R_1} = 0; \quad \frac{1}{R_2} = \frac{1}{r}; \tag{3.25}$$

The strains in the mid-plane of the disc are then calculated as: (Soedel, 2004, [62])

$$\varepsilon_1 = \frac{1}{A_1}\frac{\partial u_1}{\partial \alpha_1} + \frac{1}{A_1 A_2}\frac{\partial A_1}{\partial \alpha_1}u_2 + \frac{u_3}{R_1} = \frac{\partial u}{\partial r} = u'_r; \tag{3.26}$$

$$\varepsilon_1 = \frac{1}{A_2}\frac{\partial u_2}{\partial \alpha_2} + \frac{1}{A_1 A_2}\frac{\partial A_2}{\partial \alpha_1}u_1 + \frac{u_3}{R_2} = \frac{1}{r}\left(u + \frac{\partial v}{\partial \varphi} \right) = \frac{1}{r}\left(u + v'_\varphi \right);\ \text{and} \tag{3.27}$$

$$\Upsilon = \frac{A_1}{A_2}\frac{\partial}{\partial \alpha_2}\frac{u_1}{A_1} + \frac{A_2}{A_1}\frac{\partial}{\partial \alpha_1}\frac{u_2}{A_2} = \frac{1}{r}\left(\frac{\partial u}{\partial \varphi} - v \right) + \frac{\partial v}{\partial r} = \frac{1}{r}\left(u'_\varphi + v'_r \right) - v. \tag{3.28}$$

In accordance with the theory of a thin shell (Soedel, 2004, [62]), it can be seen that:

$$u_1 = u; \quad u_2 = v; \quad u_3 = w = 0; \tag{3.29}$$

and the metric coefficients are:

$$\begin{aligned} A_1 &= \sqrt{\left(\frac{\partial x}{\partial \alpha_1}\right)^2 + \left(\frac{\partial y}{\partial \alpha_1}\right)^2 + \left(\frac{\partial z}{\partial \alpha_1}\right)^2} = 1; \text{ and} \\ A_2 &= \sqrt{\left(\frac{\partial x}{\partial \alpha_2}\right)^2 + \left(\frac{\partial y}{\partial \alpha_2}\right)^2 + \left(\frac{\partial z}{\partial \alpha_2}\right)^2} = r. \end{aligned} \tag{3.30}$$

The strain energy of deformation in thin shells (Novozhilov, 1970, [61]) is:

$$\begin{aligned} P_t &= \int_0^{2\pi}\int_a^b \frac{Eh}{2(1-\eta^2)}\left[\varepsilon_1^2 + \varepsilon_2^2 + 2\eta\varepsilon_1\varepsilon_2 + \frac{1-\eta}{2}\Upsilon^2\right] r dr d\varphi dz \\ &\quad + \int_0^{2\pi}\int_a^b \frac{Eh^3}{24\left(1-\eta^2\right)}\left[\chi_1^2 + \chi_2^2 + 2\eta\chi_1\chi_2 + 2\left(1-\eta\right)\tilde{\tau}^2\right] r dr d\varphi dz. \end{aligned} \tag{3.31}$$

The first part of Equation (3.31) is the strain energy of extension and shear, whereas the second part is the strain energy of bending and torsion. The terms ε_1, ε_2 and Υ are given by Equations (3.26), (3.27) and (3.28), respectively, whereas the terms χ_1, χ_2 and $\tilde{\tau}$ are given by Equations (3.20), (3.20) and (3.22), respectively. In an attempt to model a 3D (multi-axis) disc-vibratory gyroscope, it is assumed that the in-plane and out-of plane vibrations are independent (Rourke, McWilliam & Fox, 2005, [63]). Hence, the strain energy of in-plane vibrations after substitution of Equations (3.20), (3.20), (3.22), (3.26), (3.27) and (3.28) into Equation (3.31) yields:

$$\begin{aligned} P &= \int_0^h\int_0^{2\pi}\int_a^b \frac{E}{2(1-\eta^2)}\left[\varepsilon_1^2 + \varepsilon_2^2 + 2\eta\varepsilon_1\varepsilon_2 + \frac{1-\eta}{2}\Upsilon^2\right] r dr d\varphi dz \\ &= h\int_0^{2\pi}\int_a^b \frac{E}{2(1-\eta^2)}\left[u_r'^2 + \frac{1}{r^2}\left(u + v_\varphi'\right)^2 + \frac{2\eta}{r}u_r'\left(u + v_\varphi'\right) + \right. \\ &\qquad \left. \frac{1-\eta}{2}\left[\frac{1}{r}\left(u_\varphi' + v_r'\right) - v\right]^2\right] r dr d\varphi. \end{aligned} \tag{3.32}$$

The Lagrangian of the system with regard to in-plane vibration is:

$$\begin{aligned} \mathbb{L} &= K - P \\ &= h\int_0^{2\pi}\int_a^b \frac{r}{2}\left\{\rho\left(\dot{u}^2 + \dot{v}^2 - 2\varepsilon\Omega\left(\dot{u}v - u\dot{v}\right)\right) - \right. \\ &\qquad \frac{E}{(1-\eta^2)}\left[u_r'^2 + \frac{1}{r^2}\left(u + v_\varphi'\right)^2 + \frac{2\eta}{r}u_r'\left(u + v_\varphi'\right) + \right. \\ &\qquad \left.\left. \frac{1-\eta}{2}\left[\frac{1}{r}\left(u_\varphi' + v_r'\right) - v\right]^2\right]\right\} dr d\varphi. \end{aligned} \tag{3.33}$$

The *Lagrangian density function* is the integrand of the Lagrangian given in Equation (3.33):

$$\begin{aligned}\Pi &= \frac{r}{2}\left\{\rho\left(\dot{u}^2+\dot{v}^2-2\varepsilon\Omega\left(\dot{u}v-u\dot{v}\right)\right)-\right.\\ &\qquad \frac{E}{(1-\eta^2)}\left[u_r'^2+\frac{1}{r^2}\left(u+v_\varphi'\right)^2+\frac{2\eta}{r}u_r'\left(u+v_\varphi'\right)+\right.\\ &\qquad \left.\left.\frac{1-\eta}{2}\left[\frac{1}{r}\left(u_\varphi'-v\right)+v_r'\right]^2\right]\right\};\end{aligned} \tag{3.34}$$

then:

$$\Pi=\Pi\left(\dot{u},\dot{v},u_r',v_r',u_\varphi',v_\varphi',u,v\right); \tag{3.35}$$

and the Lagrangian is:

$$\mathbb{L}=h\int_0^{2\pi}\int_a^b \Pi\left(\dot{u},\dot{v},u_r',v_r',u_\varphi',v_\varphi',u,v\right)drd\varphi. \tag{3.36}$$

Note here that the Lagrangian density function Π for in-plane vibration does not depend on the thickness of the disc, which helps the tuning of in-plane natural frequency of the disc with its out-of-plane natural frequency.

3.3.2 Generating equations

Hamilton's variational principle (Goldstein, Poole & Safco, 2000, [64]) states that of all possible paths by which a point in the system could travel from, its position at time t_1 to its position at time t_2, the system takes the path for which the action integral A_d is stationary. The action integral (Goldstein, Poole & Safco, 2000, [64]) is given by:

$$A_d=\int_{t_1}^{t_2}\mathbb{L}d\tau. \tag{3.37}$$

By means of Hamilton's variational principle, the variation of action is mathematically written as:

$$\delta A_d=\delta\int_{t_1}^{t_2}\mathbb{L}d\tau=\int_{t_1}^{t_2}\delta\mathbb{L}d\tau=0, \tag{3.38}$$

provided that

$$\delta u\left(t=t_1\right)=\delta u\left(t=t_2\right)=0 \tag{3.39}$$

and

$$\delta v\left(t=t_1\right)=\delta v\left(t=t_2\right)=0. \tag{3.40}$$

In what follows, Hamilton's variational principle is used to derive the equations of motion as well as a set of possible boundary conditions, assuming that $\varepsilon\Omega=0$ in Equation (3.34).

The variation of A_d for a vibrating disc using Equation (3.36) is:

$$\begin{aligned}\delta A_d &= \int_0^t \int_0^h \int_0^{2\pi} \int_a^b \delta\Pi dr d\varphi dz d\tau \\ &= h \int_0^t \int_0^{2\pi} \int_a^b \delta\Pi dr d\varphi d\tau; \end{aligned} \tag{3.41}$$

where it is assumed that:

$$t_1 = 0, \quad t_2 = t \tag{3.42}$$

and

$$\delta A_d = 0 \quad \text{with} \quad \delta u|_{\tau=0,t} = \delta v|_{\tau=0,t} = 0. \tag{3.43}$$

From Equation (3.35), $\delta\Pi$ can be calculated as follows:

$$\begin{aligned}\delta\Pi &= \frac{\partial\Pi}{\partial\dot{u}}\delta\dot{u} + \frac{\partial\Pi}{\partial\dot{v}}\delta\dot{v} + \frac{\partial\Pi}{\partial u'_r}\delta u'_r + \frac{\partial\Pi}{\partial v'_r}\delta v'_r + \\ &\qquad \frac{\partial\Pi}{\partial u'_\varphi}\delta u'_\varphi + \frac{\partial\Pi}{\partial v'_\varphi}\delta v'_\varphi + \frac{\partial\Pi}{\partial u}\delta u + \frac{\partial\Pi}{\partial v}\delta v. \end{aligned} \tag{3.44}$$

Keeping the product rule of differentiation in mind, an example would be:

$$\frac{\partial}{\partial r}\left(\frac{\partial\Pi}{\partial u'_r}\delta u\right) = \frac{\partial}{\partial r}\frac{\partial\Pi}{\partial u'_r}\delta u + \frac{\partial\Pi}{\partial u'_r}\delta u'_r; \tag{3.45}$$

and so the third term of Equation (3.44) is:

$$\frac{\partial\Pi}{\partial u'_r}\delta u'_r = \frac{\partial}{\partial r}\left(\frac{\partial\Pi}{\partial u'_r}\delta u\right) - \frac{\partial}{\partial r}\frac{\partial\Pi}{\partial u'_r}\delta u. \tag{3.46}$$

Continuing in this fashion with all the terms in Equation (3.44) the following is obtained:

$$\begin{aligned}\delta\Pi &= \frac{\partial}{\partial\tau}\left(\frac{\partial\Pi}{\partial\dot{u}}\delta u + \frac{\partial\Pi}{\partial\dot{v}}\delta v\right) + \\ &\qquad \frac{\partial}{\partial r}\left(\frac{\partial\Pi}{\partial u'_r}\delta u + \frac{\partial\Pi}{\partial v'_r}\delta v\right) + \\ &\qquad\qquad \frac{\partial}{\partial\varphi}\left(\frac{\partial\Pi}{\partial u'_\varphi}\delta u + \frac{\partial\Pi}{\partial v'_\varphi}\delta v\right) - \\ &\qquad \left(\frac{\partial}{\partial\tau}\frac{\partial\Pi}{\partial\dot{u}} + \frac{\partial}{\partial r}\frac{\partial\Pi}{\partial u'_r} + \frac{\partial}{\partial\varphi}\frac{\partial\Pi}{\partial u'_\varphi} - \frac{\partial\Pi}{\partial u}\right)\delta u - \\ &\qquad\qquad \left(\frac{\partial}{\partial\tau}\frac{\partial\Pi}{\partial\dot{v}} + \frac{\partial}{\partial r}\frac{\partial\Pi}{\partial v'_r} + \frac{\partial}{\partial\varphi}\frac{\partial\Pi}{\partial v'_\varphi} - \frac{\partial\Pi}{\partial v}\right)\delta v. \end{aligned} \tag{3.47}$$

Hence, substituting Equation (3.47) into Equation (3.41) the variation of action becomes:

$$\begin{aligned}
\delta A_d &= h\int_0^{2\pi}\int_a^b\int_0^t \frac{\partial}{\partial\tau}\left(\frac{\partial\Pi}{\partial\dot{u}}\delta u+\frac{\partial\Pi}{\partial\dot{v}}\delta v\right)d\tau dr d\varphi + \\
&\quad h\int_0^t\int_0^{2\pi}\int_a^b \frac{\partial}{\partial r}\left(\frac{\partial\Pi}{\partial u'_r}\delta u+\frac{\partial\Pi}{\partial v'_r}\delta v\right)dr d\varphi d\tau + \\
&\quad h\int_0^t\int_a^b\int_0^{2\pi} \frac{\partial}{\partial\varphi}\left(\frac{\partial\Pi}{\partial u'_\varphi}\delta u+\frac{\partial\Pi}{\partial v'_\varphi}\delta v\right)d\varphi dr d\tau - \\
&\quad h\int_0^t\int_0^{2\pi}\int_a^b \left(\frac{\partial}{\partial\tau}\frac{\partial\Pi}{\partial\dot{u}}+\frac{\partial}{\partial r}\frac{\partial\Pi}{\partial u'_r}+\frac{\partial}{\partial\varphi}\frac{\partial\Pi}{\partial u'_\varphi}-\frac{\partial\Pi}{\partial u}\right)\delta u dr d\varphi d\tau - \\
&\quad h\int_0^t\int_0^{2\pi}\int_a^b \left(\frac{\partial}{\partial\tau}\frac{\partial\Pi}{\partial\dot{v}}+\frac{\partial}{\partial r}\frac{\partial\Pi}{\partial v'_r}+\frac{\partial}{\partial\varphi}\frac{\partial\Pi}{\partial v'_\varphi}-\frac{\partial\Pi}{\partial v}\right)\delta v dr d\varphi d\tau. \qquad (3.48)
\end{aligned}$$

Performing integration on the first, second and third terms of Equation (3.48) yields the following:

$$\begin{aligned}
\delta A_d &= h\int_0^{2\pi}\int_a^b \left(\frac{\partial\Pi}{\partial\dot{u}}\delta u\Big|_{\tau=0}^{\tau=t}+\frac{\partial\Pi}{\partial\dot{v}}\delta v\Big|_{\tau=0}^{\tau=t}\right)dr d\varphi + \\
&\quad h\int_0^t\int_0^{2\pi} \left(\frac{\partial\Pi}{\partial u'_r}\delta u\Big|_{r=a}^{r=b}+\frac{\partial\Pi}{\partial v'_r}\delta v\Big|_{r=a}^{r=b}\right)d\varphi d\tau + \\
&\quad h\int_0^t\int_a^b \left(\frac{\partial\Pi}{\partial u'_\varphi}\delta u\Big|_{\varphi=0}^{\varphi=2\pi}+\frac{\partial\Pi}{\partial v'_\varphi}\delta v\Big|_{\varphi=0}^{\varphi=2\pi}\right)dr d\tau - \\
&\quad h\int_0^t\int_0^{2\pi}\int_a^b \Big[\left(\frac{\partial}{\partial\tau}\frac{\partial\Pi}{\partial\dot{u}}+\frac{\partial}{\partial r}\frac{\partial\Pi}{\partial u'_r}+\frac{\partial}{\partial\varphi}\frac{\partial\Pi}{\partial u'_\varphi}-\frac{\partial\Pi}{\partial u}\right)\delta u - \\
&\qquad \left(\frac{\partial}{\partial\tau}\frac{\partial\Pi}{\partial\dot{v}}+\frac{\partial}{\partial r}\frac{\partial\Pi}{\partial v'_r}+\frac{\partial}{\partial\varphi}\frac{\partial\Pi}{\partial v'_\varphi}-\frac{\partial\Pi}{\partial v}\right)\delta v\Big]dr d\varphi d\tau. \qquad (3.49)
\end{aligned}$$

The method of variation requires that $\delta u|_{\tau=t} = \delta u|_{\tau=0} = \delta v|_{\tau=t} = \delta v|_{\tau=0} = 0$. Furthermore, due to the continuity of the disc in the circumferential direction, $\delta u|_{\varphi=0} = \delta u|_{\varphi=2\pi}$, $\delta v|_{\varphi=0} = \delta v|_{\varphi=2\pi}$, $\left.\frac{\partial\Pi}{\partial u'_\varphi}\right|_{\varphi=0} = \left.\frac{\partial\Pi}{\partial u'_\varphi}\right|_{\varphi=2\pi}$ and $\left.\frac{\partial\Pi}{\partial v'_\varphi}\right|_{\varphi=0} = \left.\frac{\partial\Pi}{\partial v'_\varphi}\right|_{\varphi=2\pi}$. Hence $\frac{\partial\Pi}{\partial u'_\varphi}\delta u\Big|_{\varphi=0}^{\varphi=2\pi} = \frac{\partial\Pi}{\partial v'_\varphi}\delta v\Big|_{\varphi=0}^{\varphi=2\pi} = 0$. This means that Equation (3.49) simplifies to:

$$\begin{aligned}
\delta A_d &= h\int_0^t\int_0^{2\pi} \left(\frac{\partial\Pi}{\partial u'_r}\delta u\Big|_{r=a}^{r=b}+\frac{\partial\Pi}{\partial v'_r}\delta v\Big|_{r=a}^{r=b}\right)d\varphi d\tau + \\
&\quad h\int_0^t\int_0^{2\pi}\int_a^b \Big[\left(\frac{\partial}{\partial\tau}\frac{\partial\Pi}{\partial\dot{u}}+\frac{\partial}{\partial r}\frac{\partial\Pi}{\partial u'_r}+\frac{\partial}{\partial\varphi}\frac{\partial\Pi}{\partial u'_\varphi}-\frac{\partial\Pi}{\partial u}\right)\delta u - \\
&\qquad \left(\frac{\partial}{\partial\tau}\frac{\partial\Pi}{\partial\dot{v}}+\frac{\partial}{\partial r}\frac{\partial\Pi}{\partial v'_r}+\frac{\partial}{\partial\varphi}\frac{\partial\Pi}{\partial v'_\varphi}-\frac{\partial\Pi}{\partial v}\right)\delta v\Big]dr d\varphi d\tau. \qquad (3.50)
\end{aligned}$$

By means of inspection, *if* displacements u and v could be determined such that:

$$\frac{\partial}{\partial\tau}\frac{\partial\Pi}{\partial\dot{u}}+\frac{\partial}{\partial r}\frac{\partial\Pi}{\partial u'_r}+\frac{\partial}{\partial\varphi}\frac{\partial\Pi}{\partial u'_\varphi}-\frac{\partial\Pi}{\partial u} = 0; \qquad (3.51a)$$

$$\frac{\partial}{\partial\tau}\frac{\partial\Pi}{\partial\dot{v}}+\frac{\partial}{\partial r}\frac{\partial\Pi}{\partial v'_r}+\frac{\partial}{\partial\varphi}\frac{\partial\Pi}{\partial v'_\varphi}-\frac{\partial\Pi}{\partial v} = 0; \qquad (3.51b)$$

$$\left.\frac{\partial \Pi}{\partial u_r'}\delta u\right|_{r=a}^{r=b} = 0; \text{ and} \tag{3.52}$$

and

$$\left.\frac{\partial \Pi}{\partial v_r'}\delta v\right|_{r=a}^{r=b} = 0; \tag{3.53}$$

then this would "solve" the equation $\delta A_d = 0$.

From Equation (3.52):

$$\left.\frac{\partial \Pi}{\partial u_r'}\delta u\right|_{r=a}^{r=b} = \left.\frac{\partial \Pi}{\partial u_r'}\delta u\right|_{r=b} - \left.\frac{\partial \Pi}{\partial u_r'}\delta u\right|_{r=a} = 0. \tag{3.54}$$

The above would occur if:

$$\left.\frac{\partial \Pi}{\partial u_r'}\delta u\right|_{r=b} = 0; \tag{3.55}$$

and

$$\left.\frac{\partial \Pi}{\partial u_r'}\delta u\right|_{r=a} = 0. \tag{3.56}$$

But Equation (3.55) implies that:

$$\left.\frac{\partial \Pi}{\partial u_r'}\right|_{r=a} = 0 \quad \text{or} \quad \delta u|_{r=a} = 0;$$

which would occur if:

$$\left.\frac{\partial \Pi}{\partial u_r'}\right|_{r=a} = 0 \quad \text{or} \quad u|_{r=a} = 0. \tag{3.57}$$

Similarly, Equation (3.56) occurs if:

$$\left.\frac{\partial \Pi}{\partial u_r'}\right|_{r=b} = 0 \quad \text{or} \quad u|_{r=b} = 0. \tag{3.58}$$

Similar arguments result in the following combinations of boundary conditions (BCs) that, together with the partial differential equations (PDEs) (3.51a) and (3.51b) satisfy $\delta A_d = 0$:

$$\begin{aligned} r = a: & \left.\frac{\partial \Pi}{\partial u_r'}\right|_{r=a} = 0 \text{ or } u|_{r=a} = 0 \text{ and } \left.\frac{\partial \Pi}{\partial v_r'}\right|_{r=a} = 0 \text{ or } v|_{r=a} = 0; \text{ and} \\ r = b: & \left.\frac{\partial \Pi}{\partial u_r'}\right|_{r=b} = 0 \text{ or } u|_{r=b} = 0 \text{ and } \left.\frac{\partial \Pi}{\partial v_r'}\right|_{r=b} = 0 \text{ or } v|_{r=b} = 0. \end{aligned} \tag{3.59}$$

For example, boundary conditions $u|_{r=a} = 0$ and $v|_{r=a} = 0$ correspond to *fixed edges* of the disc while $\left.\frac{\partial \Pi}{\partial v_r'}\right|_{r=a} = 0$ and $\left.\frac{\partial \Pi}{\partial u_r'}\right|_{r=a} = 0$ correspond to *free edges at* $r = a$.

The variational method provides boundary conditions for free edges of the disc that are unambiguous. Indeed, $\left.\frac{\partial \Pi}{\partial u_r'}\right|_{r=b} = 0$ is equivalent to setting $\sigma_r|_{r=b} = 0$ (that is, there are no radial forces at $r = b$) while $\left.\frac{\partial \Pi}{\partial v_r'}\right|_{r=b} = 0$ is equivalent to setting $\sigma_{r\varphi}|_{r=b} = 0$ (that is, there are no shear forces at $r = b$). Hence, assuming that there are no tangential forces at $r = b$ (that is choosing $\sigma_\varphi|_{r=b} = 0$) does not yield the correct boundary condition. Setting $\sigma_\varphi = 0$ as a boundary condition for a free

edge is an infamous historical error that was corrected using the variational method.

3.3.3 Explicit equations of motion

It is important to keep in mind that the *primary goal* is to determine the displacements $u(r, \varphi, t)$ and $v(r, \varphi, t)$, assuming that inertial rotation $\varepsilon\Omega = 0$. By substituting the Lagrangian density given by Equation (3.34) into the two PDEs (3.51), the following is obtained:

$$\frac{\rho(1-\eta)}{E} r\ddot{u} - ru''_{rr} - u'_r - \frac{1-\eta}{2r}u''_{\varphi\varphi} + \frac{1}{r}u - \frac{1+\eta}{2}v''_{r\varphi} + \frac{3-\eta}{2r}v'_\varphi = 0; \quad (3.60a)$$

$$\frac{\rho(1-\eta)}{E} r\ddot{v} - \frac{1+\eta}{2}u''_{r\varphi} - \frac{3-\eta}{2r}u'_\varphi - \frac{1-\eta}{2}rv''_{rr} - \frac{1-\eta}{2}v'_r - \frac{1}{r}v''_{\varphi\varphi} + \frac{1-\eta}{2r}v = 0. \quad (3.60b)$$

Following standard methods in the linear theory of elasticity (Landau & Lifshitz, 1975, [65]) and using the "grad-curl" representation of the displacements (*vector functions*) u and v yields the following:

$$\begin{bmatrix} u \\ v \end{bmatrix} = \begin{bmatrix} \Phi'_r + \frac{1}{r}\Psi'_\varphi \\ \frac{1}{r}\Phi'_\varphi - \Psi'_r \end{bmatrix}, \quad (3.61)$$

where $\Phi = \Phi(r, \varphi, t)$ and $\Psi = \Psi(r, \varphi, t)$ are *scalar functions*, called *potential* functions. The usual prime notations ($'$ and $''$) are used for first and second partial differentiations, respectively with respect to the subscript variable. These potential functions are considered to be new variables. The derivatives of u and v are given as follows:

$$u'_r = \Phi''_{rr} - \frac{1}{r^2}\Psi'_\varphi + \frac{1}{r}\Psi''_{\varphi r}; \quad (3.62)$$

$$\begin{aligned} u''_{rr} &= \Phi'''_{rrr} + \frac{2}{r^3}\Psi'_\varphi - \frac{1}{r^2}\Psi''_{\varphi r} - \frac{1}{r^2}\Psi''_{\varphi r} + \frac{1}{r}\Psi'''_{\varphi rr} \\ &= \Phi'''_{rrr} + \frac{2}{r^3}\Psi'_\varphi - \frac{2}{r^2}\Psi''_{\varphi r} + \frac{1}{r}\Psi'''_{\varphi rr}; \end{aligned} \quad (3.63)$$

$$u''_{r\varphi} = \Phi'''_{rr\varphi} - \frac{1}{r^2}\Psi''_{\varphi\varphi} + \frac{1}{r}\Psi'''_{\varphi r\varphi}; \quad (3.64)$$

$$u'_\varphi = \Phi''_{r\varphi} + \frac{1}{r}\Psi''_{\varphi\varphi}; \text{ and} \quad (3.65)$$

$$u''_{\varphi\varphi} = \Phi'''_{r\varphi\varphi} + \frac{1}{r}\Psi'''_{\varphi\varphi\varphi}; \quad (3.66)$$

and the second-order derivative of u with respect t becomes:

$$\ddot{u} = \ddot{\Phi}'_r + \frac{1}{r}\ddot{\Psi}'_\varphi. \quad (3.67)$$

Similarly, the derivatives of v are obtained as follows:

$$v'_r = -\frac{1}{r^2}\Phi'_\varphi + \frac{1}{r}\Phi_{\varphi r} - \Psi_{rr}; \tag{3.68}$$

$$v''_{rr} = \frac{2}{r^3}\Phi'_\varphi - \frac{2}{r^2}\Phi''_{\varphi r} + \frac{1}{r}\Phi'''_{\varphi rr} - \Psi'''_{rrr}; \tag{3.69}$$

$$v'_\varphi = \frac{1}{r}\Phi''_{\varphi\varphi} - \Psi''_{r\varphi}; \tag{3.70}$$

$$v''_{\varphi\varphi} = \frac{1}{r}\Phi'''_{\varphi\varphi\varphi} - \Psi''_{r\varphi\varphi}; \text{ and} \tag{3.71}$$

$$v''_{r\varphi} = -\frac{1}{r^2}\Phi''_{\varphi\varphi} + \frac{1}{r}\Phi'''_{\varphi r\varphi} - \Psi'''_{rr\varphi}; \tag{3.72}$$

and the second-order derivative of v with respect t becomes:

$$\ddot{v} = \frac{1}{r}\ddot{\Phi}'_\varphi - \ddot{\Psi}'_r. \tag{3.73}$$

Substitution of Equations (3.62), (3.63), (3.64), (3.65) (3.66) and (3.67) into Equations (3.60a) and Equations (3.68), (3.69), (3.70), (3.71) (3.72) and (3.73) into Equation (3.60b) after extensive simplification (see Pretorius (2007, [52])) yields:

$$r\frac{\partial}{\partial r}\left\{\frac{\rho(1-\eta^2)}{E}\ddot{\Phi} - \nabla^2\Phi\right\} + \frac{\partial}{\partial\varphi}\left\{\frac{\rho(1-\eta^2)}{E}\ddot{\Psi} - \frac{1-\eta}{2}\nabla^2\Psi\right\} = 0; \text{ and} \tag{3.74}$$

$$\frac{\partial}{\partial\varphi}\left\{\frac{\rho(1-\eta^2)}{E}\ddot{\Phi} - \nabla^2\Phi\right\} - r\frac{\partial}{\partial r}\left\{\frac{\rho(1-\eta^2)}{E}\ddot{\Psi} - \frac{1-\eta}{2}\nabla^2\Psi\right\} = 0; \tag{3.75}$$

where:

$$\nabla^2 = \frac{\partial^2}{\partial r^2} + \frac{1}{r}\frac{\partial}{\partial r} + \frac{1}{r^2}\frac{\partial^2}{\partial\varphi^2}; \tag{3.76}$$

is the *Laplace operator in polar coordinates*. If one can determine scalar functions Φ and Ψ that solve the partial differential equations (PDEs) given by Equations (3.74) and (3.75), then these solutions yield solutions for u and v given by Equation (3.61). By inspection, if one makes the choice that the scalar potential functions Φ and Ψ must satisfy the partial differential equations:

$$\frac{\rho(1-\eta^2)}{E}\ddot{\Phi} = \nabla^2\Phi; \tag{3.77}$$

$$\frac{2\rho(1+\eta)}{E}\ddot{\Psi} = \nabla^2\Psi; \tag{3.78}$$

then these functions satisfy Equations (3.74) and (3.75). From the standard theory of linear partial differential equations (PDEs) (Asmar, 2005, [66]), harmonic solutions of the form:

$$\Phi(r,t,\varphi) = \phi(r)\cos(\omega_d t + \theta)\cos m\varphi; \text{ and} \tag{3.79}$$

$$\Psi(r,t,\varphi) = \psi(r)\cos(\omega_d t + \theta)\sin m\varphi; \tag{3.80}$$

are suitable candidate functions that solve PDEs in Equations (3.77) and (3.78), respectively. Here

ω_d is the circular frequency (eigenvalue) or *angular frequency*[1], with θ as some phase angle and the positive integer m is the *circumferential wave number* that is obtained from the fact that both Φ and Ψ are periodic in the variable φ with period 2π. Substituting Equations (3.79) and (3.80) into Equations (3.77) and (3.78), respectively, yields two ordinary differential equations (ODEs):

$$\frac{d^2\phi}{dr^2} + \frac{1}{r}\frac{d\phi}{dr} + \left[\left(D_E\omega_d\right)^2 - \frac{m^2}{r^2}\right]\phi = 0; \tag{3.81}$$

$$\frac{d^2\psi}{dr^2} + \frac{1}{r}\frac{d\psi}{dr} + \left[\left(D_G\omega_d\right)^2 - \frac{m^2}{r^2}\right]\psi = 0; \tag{3.82}$$

where:

$$D_E = \sqrt{\frac{\rho(1-\eta^2)}{E}}; \tag{3.83}$$

and

$$D_G = \sqrt{\frac{2\rho(1+\eta)}{E}}. \tag{3.84}$$

Both of the ODEs in Equations (3.81) and (3.82) are Bessel's ODEs of order m and have respective solutions (O'Neil, 2007, [67]) of the form:

$$\phi(r) = C_1 J_m(k_1 r) + C_2 Y_m(k_1 r); \text{ and} \tag{3.85}$$

$$\psi(r) = C_3 J_m(k_2 r) + C_4 Y_m(k_2 r); \tag{3.86}$$

where J_m is Bessel's function of the first kind of order m and Y_m is Bessel's function of the second kind of order m with $C_{i=1,2,3,4}$ being arbitrary constants. Furthermore, $k_1 = \omega_d D_E = \omega_d\sqrt{\frac{\rho(1-\eta^2)}{E}}$ and $k_2 = D_G\omega_d = \omega_d\sqrt{\frac{2\rho(1+\eta)}{E}}$.

Now Equations (3.85) and (3.86) are substituted into Equation (3.61). Using a CAS such as MATHEMATICA® or MAPLE™ or by using the well-known identity:

$$\frac{d}{dr}J_m(\alpha r) = \frac{m}{r}J_m(\alpha r) - \alpha J_{m+1}(\alpha r); \tag{3.87}$$

solutions for the displacements are found to be:

$$u(r,\varphi,t) = U(r)\cos\left(\omega_d t + \theta\right)\cos m\varphi; \tag{3.88}$$

and

$$v(r,\varphi,t) = V(r)\cos\left(\omega_d t + \theta\right)\sin m\varphi; \tag{3.89}$$

where the functions $U(r)$ and $V(r)$ are the eigenfunctions (form-factors) which have to be deter-

[1] The angular frequency $\omega_d = 2\pi f$ where f is the frequency of vibration of the disc.

mined, namely:

$$\begin{aligned} U(r) &= \frac{1}{2}C_1 D_E\omega_d(J_{m-1}(D_E\omega_d r) - J_{m+1}(D_E\omega_d r)) + \\ &\quad \frac{1}{2}C_2 D_E\omega_d(Y_{m-1}(D_E\omega_d r) - Y_{m+1}(D_E\omega_d r)) + \\ &\quad \frac{m(C_3 J_m(D_G\omega_d r) + C_4 Y_m(D_G\omega_d r))}{r}; \text{ and} \qquad (3.90) \\ V(r) &= -\frac{m(C_1 J_m(D_E\omega_d r) + C_2 Y_m(D_E\omega_d r))}{r} - \\ &\quad \frac{1}{2}C_3 D_G\omega_d(J_{m-1}(D_G\omega_d r) - J_{m+1}(D_G\omega_d r)) - \\ &\quad \frac{1}{2}C_4 D_G\omega_d(Y_{m-1}(D_G\omega_d r) - Y_{m+1}(D_G\omega_d r)). \qquad (3.91) \end{aligned}$$

For a solid disc with $a = 0$, the Neumann's function $Y_m(\alpha r)$ is singular at $r = a = 0$, thus $C_2 = C_4 = 0$, because the amplitude of vibrations is finite. Consequently, the eigenfunctions have the form:

$$U(r) = \frac{1}{2}C_1 D_E\omega_d(J_{m-1}(D_E\omega_d r) - J_{m+1}(D_E\omega_d r)) + \frac{mC_3 J_m(D_G\omega_d r)}{r}; \qquad (3.92)$$

and

$$V(r) = -\frac{mC_1 J_m(D_E\omega_d r)}{r} - \frac{1}{2}C_3 D_G\omega_d(J_{m-1}(D_G\omega_d r) - J_{m+1}(D_G\omega_d r)). \qquad (3.93)$$

3.3.4 The explicit boundary conditions

Substitution of the Lagrangian density from Equation (3.34) into the boundary conditions in Equation (3.59), gives:

$$\begin{aligned} r = a, b \qquad u|_{r=a,b} &= 0 \text{ or } \left[u'_r + \frac{\eta}{r}\left(v'_\varphi + u\right)\right]_{r=a,b} = 0; \\ \text{and} \quad v|_{r=a,b} &= 0 \text{ or } \left[v'_r + \frac{1}{r}\left(u'_\varphi - v\right)\right]_{r=a,b} = 0; \qquad (3.94) \end{aligned}$$

respectively.

Substitution of Equations (3.88) and (3.89) into Equation (3.94) for the non-trivial case yields:

$$\begin{aligned} r = a, b \qquad U(r)|_{r=a,b} &= 0 \text{ or } \left[U'(r) + \frac{\eta}{r}\left(mV(r) + U(r)\right)\right]_{r=a,b} = 0; \\ \text{and} \quad V(r)|_{r=a,b} &= 0 \text{ or } \left[V'(r) - \frac{1}{r}\left(mU(r) + V(r)\right)\right]_{r=a,b} = 0. \qquad (3.95) \end{aligned}$$

Consequently, when $a \neq 0$ there are four arbitrary constants in Equations (3.90) and (3.91) and four boundary conditions in Equations (3.95) and hence eigenfunctions $U(r)$ and $V(r)$ can be determined explicitly. On the other hand, if the disc is not annular with $a = 0$, there are two arbitrary constants in Equations (3.90) and (3.91) with two boundary conditions at the outer edge of the disc, that is:

$$\begin{aligned} r = b \qquad U(r)|_{r=b} &= 0 \text{ or } \left[U'(r) + \frac{\eta}{r}\left(mV(r) + U(r)\right)\right]_{r=b} = 0; \\ \text{and} \qquad V(r)|_{r=b} &= 0 \text{ or } \left[V'(r) - \frac{1}{r}\left(mU(r) + V(r)\right)\right]_{r=b} = 0; \end{aligned} \tag{3.96}$$

and consequently eigenfunctions $U(r)$ and $V(r)$ can be determined explicitly. In the next section, solutions of a flat disc vibrating in its plane with various boundary conditions are investigated.

3.4 NUMERICAL DETERMINATION OF THE EIGENVALUES AND EIGENFREQUENCIES OF THE IN-PLANE VIBRATIONS

In this section both solid and annular-disc boundary conditions are considered. The eigenvalues and eigenfrequencies are determined numerically and the normalised displacements are obtained graphically taking the mode number $m = 2$ as an example.

3.4.1 Solid disc clamped at its edge

For a solid disc clamped at its edge, the boundary conditions in explicit form using Equation (3.96) can be written as:

$$r = b \qquad U(r)|_{r=b} = 0 \text{ and } V(r)|_{r=b} = 0. \tag{3.97}$$

Now substitution of Equations (3.90) and (3.91) into Equation (3.97) gives a matrix equation which may be written as:

$$\underbrace{\begin{pmatrix} a_{11} & a_{12} \\ a_{21} & a_{22} \end{pmatrix}}_{\mathbf{M}_1} \begin{pmatrix} C_1 \\ C_3 \end{pmatrix} = 0; \text{ where:} \tag{3.98}$$

$$\begin{aligned} a_{11} &= \frac{1}{2} D_E \omega_d \left[J_{m-1}(D_E \omega_d b) - J_{m+1}(D_E \omega_d b)\right]; \\ a_{12} &= \frac{m J_m(D_G \omega_d b)}{b}; \\ a_{21} &= -\frac{m J_m(D_E \omega_d b)}{b}; \text{ and} \\ a_{22} &= -\frac{1}{2} D_G \omega_d \left[J_{m-1}(D_G \omega_d b) - J_{m+1}(D_G \omega_d b)\right]. \end{aligned}$$

The functions Y_{m-1}, Y_m and Y_{m+1} in Equations (3.90) and (3.91) are singular at $a = 0$, thus

$C_2 = C_4 = 0$. If $C1 = 1$, then:

$$C_3 = -\frac{a_{11}(\omega_d)}{a_{12}(\omega_d)} = -\frac{\frac{1}{2}D_E\omega_d\left[J_{m-1}(D_E\omega_d b) - J_{m+1}(D_E\omega_d b)\right]}{\frac{mJ_m(D_G\omega_d b)}{b}}. \tag{3.99}$$

The only unknown quantity in Equation (3.99) is the angular frequency ω_d. For a non-trivial solution of Equation (3.98) the determinant of the coefficient matrix vanishes. That is:

$$\Delta(\omega_d) = \det(\mathbf{M}_1) = 0. \tag{3.100}$$

Table 3.1: Material constants and geometric parameters of the solid disc

Parameter name	Parameter symbol	Unit	Value
Thickness	h	m	1.7106×10^{-3}
Radius	b	m	10^{-2}
Poisson's ratio	η		3.3×10^{-1}
Material density	ρ	$\mathrm{kg\,m^{-3}}$	2.7×10^{3}
Young's modulus	E	Pa	70×10^{9}

Equation (3.100) is known as the characteristic equation of the boundary value problem (BVP). Using a CAS to solve this transcendental characteristic equation yields, for each circumferential wave number m, a sequence of eigenvalues $\omega_{dm,k}$ $(k = 0, 1, 2, 3, \cdots)$ with:

$$\omega_{dm,0} < \omega_{dm,1} < \omega_{dm,2} < \cdots. \tag{3.101}$$

The eigenvalue $\omega_{dm,0}$ is called the fundamental vibration eigenvalue while $\omega_{dm,1}$ is called the first overtone vibration *eigenvalue,* and so forth. Results for the fundamental and the first five overtone vibration eigenvalues and the associated *eigenfrequencies* are given in Table 3.2 for the disc clamped at its edge for $m = 2$.

Table 3.2: The fundamental and the first five overtone vibration eigenvalues and the associated eigenfrequencies of a clamped solid disc vibrating at $m = 2$

k	$\omega_{d2,k}\,(\mathrm{rad\,s^{-1}})$	$f_{2,k} = \frac{\omega_{d2,k}}{2\pi}\,(\mathrm{Hz})$
0	1.362852×10^{6}	216904.6854
1	1.784281×10^{6}	283977.2867
2	1.904047×10^{6}	303038.5248
3	3.126511×10^{6}	497599.7893
4	3.621574×10^{6}	576391.5361
5	4.093600×10^{6}	651516.8309

A plot of the function $f(\omega_d) = \ln|\Delta(\omega_d)|$ appears in Figure 3.2. The radial and tangential displacements (eigenfunctions) of a clamped solid disc vibrating at circumferential wave number $m = 2$ are shown in Figure 3.3. It can be clearly seen from the figure that both tangential and ra-

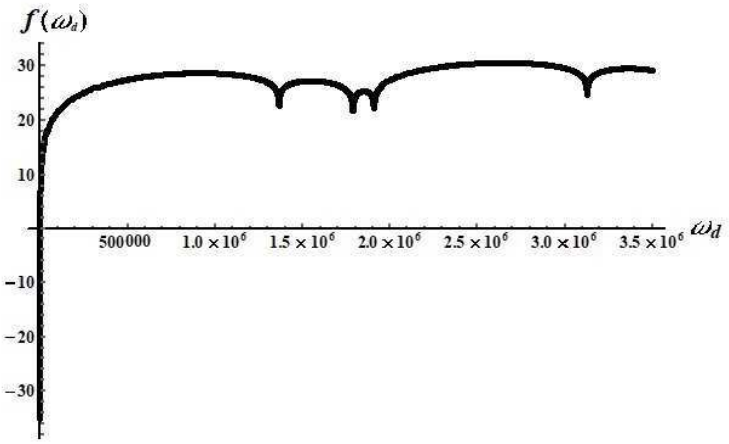

Figure 3.2: The function $f(\omega_d) = \ln|\det(\mathbf{M}_1)|$ produced by the CAS for a solid vibrating aluminium disc of radius $b = 1\,\mathrm{cm}$, circumferential wave number $m = 2$, density $\rho = 2.7\times10^3\,\mathrm{kg.m^{-3}}$, Young's modulus $E = 7\times10^{10}\,\mathrm{Pa}$ and Poisson's ratio $\upsilon = \frac{1}{3}$

dial displacements are zero at the clamped edge of the disc. Local maxima for both displacements seem to be at about half-way between the centre and the clamped edge of the disc. It is also evident from the solution that the displacements are not equal to zero at the centre of the disc. Note that this approximate calculation is made for the fundamental eigenvalue $\omega_{d2,0} = 1.362852\times10^6\,\mathrm{rad\,s^{-1}}$ of the disc gyroscope vibrating in its plane with mode number $m = 2$.

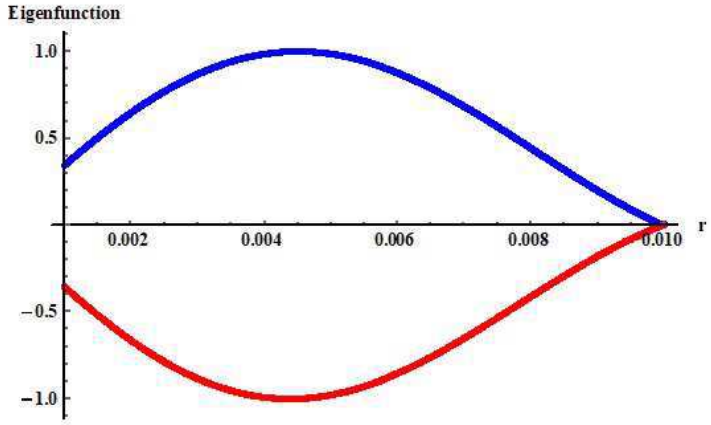

Figure 3.3: The eigenfunctions U (blue curve) and V (red curve) divided by their maximum-modulus corresponding to the eigenvalue $\omega_{2,0} = 1.362852\cdots\times10^6\,\mathrm{rad.\,s^{-1}}$ for the aluminium solid disc clamped at the edge and mentioned in Figure 3.1

3.4.2 Annular disc clamped at both edges

As before the disc is assumed to be isotropic and obeys Hooke's law. The boundary conditions for the annular disc clamped at both edges can be written as:

$$U(r)|_{r=a,b} = 0 \text{ and } V(r)|_{r=a,b} = 0. \tag{3.102}$$

Once again substituting Equations (3.90) and (3.91) into Equation (3.102) results in the frequency (characteristic) equation in its matrix form as:

$$\underbrace{\begin{pmatrix} a_{11} & a_{12} & a_{13} & a_{14} \\ a_{21} & a_{22} & a_{23} & a_{24} \\ a_{31} & a_{32} & a_{33} & a_{34} \\ a_{41} & a_{42} & a_{43} & a_{44} \end{pmatrix}}_{\mathbf{D}_1} \begin{pmatrix} C_1 \\ C_2 \\ C_3 \\ C_4 \end{pmatrix} = 0; \tag{3.103}$$

with:

$$\begin{aligned}
a_{11} &= \frac{mJ_m\left(k_1\left(\omega_d\right)a\right)}{a} - J_{m+1}\left(k_1\left(\omega_d\right)a\right)k_1\left(\omega_d\right); \\
a_{12} &= \frac{m}{a}Y_m\left(k_1\left(\omega_d a\right)\right) - Y_{m+1}\left(k_1\left(\omega_d\right)a\right)k_1\left(\omega_d\right); \\
a_{13} &= \frac{m}{a}J_m\left(k_2\left(\omega_d\right)a\right); \\
a_{14} &= \frac{m}{a}Y_m\left(k_2\left(\omega_d\right)a\right); \\
a_{21} &= -\frac{m}{a}J_m\left(k_1\left(\omega_d\right)a\right); \\
a_{22} &= -\frac{m}{a}Y_m\left(k_1\left(\omega_d\right)a\right); \\
a_{23} &= -\frac{mJ_m\left(k_2\left(\omega_d\right)a\right)}{a} + J_{m+1}\left(k_2\left(\omega_d\right)a\right)k_2\left(\omega_d\right); \text{ and} \\
a_{24} &= -\frac{mY_m\left(k_2\left(\omega_d\right)a\right)}{a} + Y_{m+1}\left(k_2\left(\omega_d\right)a\right)k_2\left(\omega_d\right);
\end{aligned}$$

at $r = a$ and:

$$\begin{aligned}
a_{31} &= \frac{mJ_m\left(k_1\left(\omega_d\right)b\right)}{b} - J_{m+1}\left(k_1\left(\omega_d\right)b\right)k_1\left(\omega_d\right); \\
a_{32} &= \frac{m}{b}Y_m\left(k_1\left(\omega_d b\right)\right) - Y_{m+1}\left(k_1\left(\omega_d\right)b\right)k_1\left(\omega_d\right); \\
a_{33} &= \frac{m}{b}J_m\left(k_2\left(\omega_d\right)b\right); \\
a_{34} &= \frac{m}{b}Y_m\left(k_2\left(\omega_d\right)b\right); \\
a_{41} &= -\frac{m}{b}J_m\left(k_1\left(\omega_d\right)b\right); \\
a_{42} &= -\frac{m}{b}Y_m\left(k_1\left(\omega_d\right)b\right); \\
a_{43} &= -\frac{mJ_m\left(k_2\left(\omega_d\right)b\right)}{b} + J_{m+1}\left(k_2\left(\omega_d\right)b\right)k_2\left(\omega_d\right); \text{ and} \\
a_{44} &= -\frac{mY_m\left(k_2\left(\omega_d\right)b\right)}{b} + Y_{m+1}\left(k_2\left(\omega_d\right)b\right)k_2\left(\omega_d\right);
\end{aligned}$$

at $r = b$.

The eigenfunctions $U(r)$ and $V(r)$ can thus be written as:

$$\begin{aligned} U(r) &= C_1\left(\frac{mJ_m(k_1(\omega_d)r)}{r} - J_{m+1}(k_1(\omega_d)r)k_1(\omega_d)\right) + \\ & C_2\left(\frac{m}{r}Y_m(k_1(\omega_d r)) - Y_{m+1}(k_1(\omega_d)r)k_1(\omega_d)\right) \\ & +\frac{m}{r}C_3(J_m(k_2(\omega_d)r)) + \frac{m}{r}C_4(rY_m(k_2(\omega_d)r)); \end{aligned} \tag{3.104}$$

and:

$$\begin{aligned} V(r) &= -\frac{m}{r}C_1J_m(k_1(\omega_d)r) - \frac{m}{r}C_2Y_m(k_1(\omega_d)r) \\ & C_3\left(-\frac{mJ_m(k_2(\omega_d)r)}{r} + J_{m+1}(k_2(\omega_d)r)k_2(\omega_d)\right) \\ & C_4\left(-\frac{mY_m(k_2(\omega_d)r)}{r} + Y_{m+1}(k_2(\omega_d)r)k_2(\omega_d)\right). \end{aligned} \tag{3.105}$$

As in the previous section the characteristic equation of the matrix $\mathbf{D}_1$ of Equation (3.103) needs to be zero for non-trivial solutions of $\begin{pmatrix} C_1, & C_2, & C_3, & C_4 \end{pmatrix}^{\mathrm{T}}$. The roots of the resulting characteristic equation give the eigenvalues for the vibrating disc. The *fundamental eigenvalue* and the first five *overtone eigenvalues* with the *fundamental eigenfrequency* and the first five *overtone eigenfrequencies* for a disc clamped at both edges are given in Table 3.3. In this case, once again $m = 2$.

Table 3.3: The fundamental and the first five overtone vibration eigenvalues and the associated eigenfrequencies of an annular disc clamped at both edges and vibrating at $m = 2$

k	$\omega_{d2,k}\left(\mathrm{rad\,s^{-1}}\right)$	$f_{2,k} = \frac{\omega_{d2,k}}{2\pi}\,(\mathrm{Hz})$
0	1.681977×10^6	267695
1	1.202229×10^6	350495
2	1.249287×10^6	517140
3	3.628088×10^6	577482
4	3.355487×10^6	693197
5	4.204516×10^6	828324

For annular disc clamped at both edges, both radial and shear forces are non-zero at either edges. Thus, as can be seen from Figure 3.5, with an increase in the inner radius, both radial and tangential displacements decrease, but both displacements completely vanish at the edges. The shear and radial forces are stronger at the clamped edges than elsewhere on the disc.

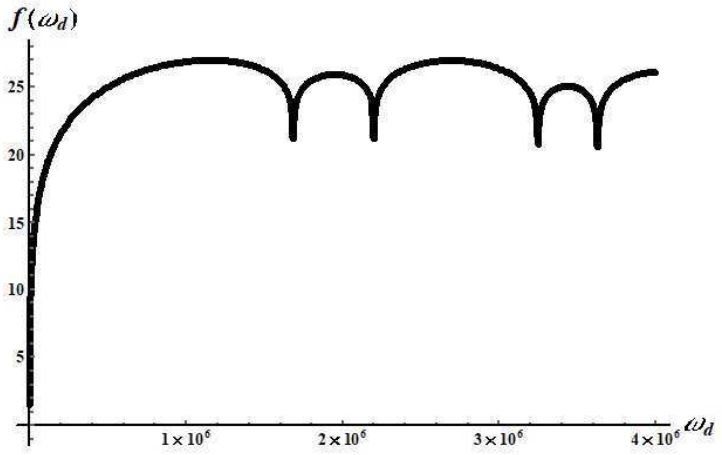

Figure 3.4: The function $f(\omega_d) = \ln|\det(\mathbf{D}_1)|$ produced by the CAS MATHEMATICA® for an annular vibrating aluminium disc of inner radius $a = 0.1\,\mathrm{cm}$, outer radius $b = 1\,\mathrm{cm}$ circumferential wave number $m = 2$, density $\rho = 2.7 \times 10^3\,\mathrm{kg.\,m^{-3}}$, Young's modulus $E = 7 \times 10^{10}\,\mathrm{Pa}$ and Poisson's ratio $\upsilon = \frac{1}{3}$

3.4.3 Annular disc clamped at inner edge and free at outer edge

This section demonstrates how to obtain an explicit approximate solution and hence the eigenvalue ω_d and corresponding eigenfunctions $U(r)$ and $V(r)$ for a disc with fixed inner boundary and free outer boundary, that is:

$$U(a) = 0, \quad V(a) = 0; \tag{3.106}$$

and

$$bU'(b) + \eta\left(mV(b) + U(b)\right) = 0, \quad bV'(b) - \left(mU(b) + V(b)\right) = 0. \tag{3.107}$$

By substituting Equations (3.90) and (3.91) into Equations (3.106) and (3.107), a system of 4×4 equations is obtained and can be written in matrix form as:

$$\underbrace{\begin{pmatrix} a_{11} & a_{12} & a_{13} & a_{14} \\ a_{21} & a_{22} & a_{23} & a_{24} \\ a_{31} & a_{32} & a_{33} & a_{34} \\ a_{41} & a_{42} & a_{43} & a_{44} \end{pmatrix}}_{\mathbf{D}_3} \begin{pmatrix} C_1 \\ C_2 \\ C_3 \\ C_4 \end{pmatrix} = 0. \tag{3.108}$$

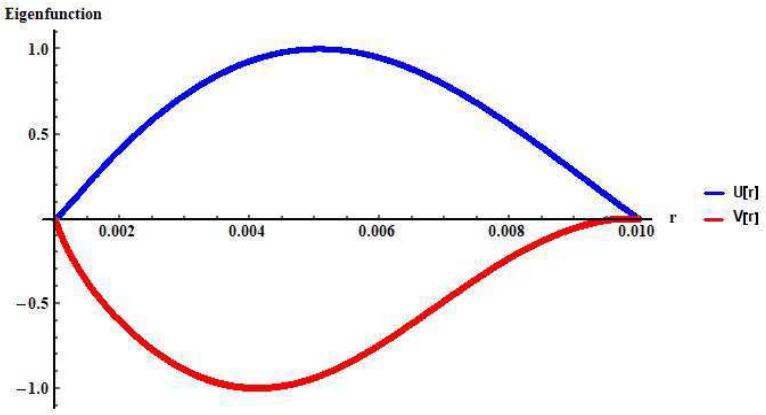

Figure 3.5: The eigenfunctions $U(r)$ and $V(r)$ (divided by their maximum modulus) corresponding to the eigenvalue $\omega_{2,0} = 1.681977 \times 10^6 \,\mathrm{rad.\,s^{-1}}$ for the aluminium disc clamped at both edges and mentioned in Figure 3.1

Table 3.4: The fundamental and the first five overtone vibration eigenvalues and the associated eigenfrequencies of an annular disc clamped at the inner edge and free at the outer edge and vibrating at $m = 2$

k	$\omega_{d2,k}\,(\mathrm{rad s^{-1}})$	$f_{2,k} = \frac{\omega_{d2,k}}{2\pi}\,(\mathrm{Hz})$
0	752771×10^5	119807
1	1.350581×10^6	214952
2	2.530764×10^6	402784
3	2.788630×10^6	443824
4	3.757043×10^6	597952
5	4.444012×10^6	707287

The first line of the matrix equation from Equation (3.108) is given by:

$$U(a) = C_1 \left(\frac{m}{a} J_m\left(k_1\left(\omega_d\right) a\right) - J_{m+1}(k_1\left(\omega_d\right) a) k_1\left(\omega_d\right) \right) + C_2 \left(\frac{m}{a} Y_m\left(k_1\left(\omega_d\right) a\right) - Y_{m+1}(k_1\left(\omega_d\right) a) k_1\left(\omega_d\right) \right) + \frac{m(C_3 J_m(k_2\left(\omega_d\right) a) + C_4 Y_m(k_2\left(\omega_d\right) a)}{a} = 0. \tag{109}$$

Similarly, $V(a)$ and the terms in Equation (3.107) can be determined, with all components being:

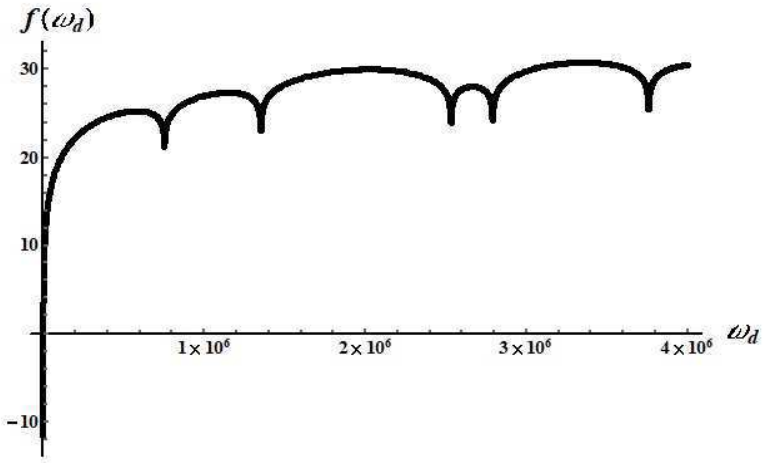

Figure 3.6: The function $f(\omega_d) = \ln|\det D_3|$ produced by the CAS MATHEMATICA® for a vibrating aluminium disc with inner radius $a = 0.1\,\mathrm{cm}$, outer radius $b = 1\,\mathrm{cm}$, circumferential wave number $n = 2$, density $\rho = 2.7 \times 10^3\,\mathrm{kg.\,m^{-3}}$, Young's modulus $E = 7 \times 10^{10}\,\mathrm{Pa}$ and Poisson's ratio $\upsilon = \frac{1}{3}$

$$
\begin{aligned}
a_{11} &= \frac{m}{a} J_m\left(k_1\left(\omega_d\right) a\right) - J_{m+1}(k_1\left(\omega_d\right) a) k_1\left(\omega_d\right); \\
a_{12} &= \frac{m}{a} Y_m\left(k_1\left(\omega_d\right) a\right) - Y_{m+1}(k_1\left(\omega_d\right) a) k_1\left(\omega_d\right); \\
a_{13} &= \frac{m J_m(k_2\left(\omega_d\right) a)}{a}; \\
a_{14} &= \frac{m Y_m(k_2\left(\omega_d\right) a)}{a}; \\
a_{21} &= -\frac{m J_m(k_1\left(\omega_d\right) a)}{a}; \\
a_{22} &= -\frac{m Y_m(k_1\left(\omega_d\right) a)}{a}; \\
a_{23} &= -\frac{m}{a} J_m\left(k_2\left(\omega_d\right) a\right) - J_{m+1}(k_2\left(\omega_d\right) a) k_2\left(\omega_d\right); \\
a_{24} &= -\frac{m}{a} Y_m\left(k_2\left(\omega_d\right) a\right) - Y_{m+1}(k_2\left(\omega_d\right) a) k_2\left(\omega_d\right); \\
a_{31} &= \left(-k_1\left(\omega_d\right)^2 - \frac{m\left(m-1\right)\left(\eta-1\right)}{b^2}\right) J_m\left(k_1\left(\omega_d\right) b\right) - \\
&\quad k_1\left(\omega_d\right)\left(\eta-1\right) J_{m+1}\left(k_1\left(\omega_d\right) b\right); \\
a_{32} &= \left(-k_1\left(\omega_d\right)^2 - \frac{m\left(m-1\right)\left(\eta-1\right)}{b^2}\right) Y_m\left(k_1\left(\omega_d\right) b\right) - \\
&\quad k_1\left(\omega_d\right)\left(\eta-1\right) Y_{m+1}\left(k_1\left(\omega_d\right) b\right); \\
a_{33} &= -\frac{m\left(m-1\right)\left(\eta-1\right)}{b^2} J_m\left(k_2\left(\omega_d\right) b\right) + \frac{k_2\left(\omega_d\right) m\left(\eta-1\right) J_{m+1}\left(k_2\left(\omega_d\right) b\right)}{b};
\end{aligned}
$$

$$
\begin{aligned}
a_{34} &= -\frac{m\,(m-1)\,(\eta-1)}{b^2}Y_m\left(k_2\left(\omega_d\right)b\right)+\frac{k_2\left(\omega_d\right)m\,(\eta-1)\,J_{m+1}\left(k_2\left(\omega_d\right)b\right)}{b};\\
a_{41} &= -\frac{2m\,(m-1)\,J_m\left(k_1\left(\omega_d\right)b\right)}{b^2}+\frac{2J_{m+1}\left(k_1\left(\omega_d\right)b\right)k_1\left(\omega_d\right)b}{b};\\
a_{42} &= -\frac{2m\,(m-1)\,Y_m\left(k_1\left(\omega_d\right)b\right)}{b^2}+\frac{2Y_{m+1}\left(k_1\left(\omega_d\right)b\right)k_1\left(\omega_d\right)b}{b};\\
a_{43} &= \left(k_2\left(\omega_d\right)^2-\frac{2m\,(m-1)}{b^2}\right)J_m\left(k_2\left(\omega_d\right)b\right)-\frac{2k_2\left(\omega_d\right)J_{m+1}\left(k_2\left(a\right)b\right)}{b};\ \text{and}\\
a_{44} &= \left(k_2\left(\omega_d\right)^2-\frac{2m\,(m-1)}{b^2}\right)Y_m\left(k_2\left(\omega_d\right)b\right)-\frac{2k_2\left(\omega_d\right)Y_{m+1}\left(k_2\left(a\right)b\right)}{b}.
\end{aligned}
$$

As before it is evident that the only "unknown" quantity in the values a_{ij} is the angular frequency ω_d, that is:

$$a_{ij} = a_{ij}(\omega_d), \quad i,j = 1,2,3,4. \tag{3.110}$$

The Equation (3.108) has a non-trivial solution if the determinant of $\mathbf{D}_3 = \mathbf{D}_3(\omega_d)$ is zero, that is:

$$\Delta(\omega_d) = \det \mathbf{D}_3(\omega_d) = 0. \tag{3.111}$$

Equation (3.111) is known as the characteristic equation of the boundary value problem (BVP). Using a CAS to solve this transcendental characteristic equation yields, for each circumferential wave number m, *a sequence of eigenvalues* $\omega_{dm,k}$ $(k = 0,1,2,3,\cdots)$ with:

$$\omega_{dm,0} < \omega_{dm,1} < \omega_{dm,2} < \cdots. \tag{3.112}$$

The eigenvalue $\omega_{dm,0}$ is called the *fundamental vibration eigenvalue* while $\omega_{dm,1}$ is called the *first overtone vibration eigenvalue,* and so forth. A plot of the function $f(\omega_d) = \ln\left(|\det \mathbf{D}_3(\omega_d)|\right)$ appears in Figure 3.6 for an aluminium disc where the "spikes" point towards the roots of the function $\det \mathbf{D}_3(\omega_d)$, showing the sequence of eigenvalues depicted in inequality in Equation (3.112). Note that the eigenvalues are not linearly spaced along the ω_d-axis.

Now, an integer k with $k \geq 0$ is fixed and the eigenvalue $\omega_{dm,k}$ is substituted back into Equation (3.108). By performing Gaussian elimination on the augmented matrix of Equation (3.108) it is now possible to choose any one of C_1, C_2, C_3, and C_4 as being free. Hence, choosing any non-zero value for C_4 (say $C_4 = 1$), the value of C_1 can be obtained using Cramer's rule:

$$C_1 = \frac{\det\begin{pmatrix} -a_{14}C_4 & a_{12} & a_{13} \\ -a_{24}C_4 & a_{22} & a_{23} \\ -a_{34}C_4 & a_{32} & a_{33} \end{pmatrix}}{\det\begin{pmatrix} a_{11} & a_{12} & a_{13} \\ a_{21} & a_{22} & a_{23} \\ a_{31} & a_{32} & a_{33} \end{pmatrix}}; \tag{3.113}$$

similarly for C_2 and C_3. Consequently, with these values of $C_{i=1,2,3,4}$ the eigenfunctions $U(r)$ and

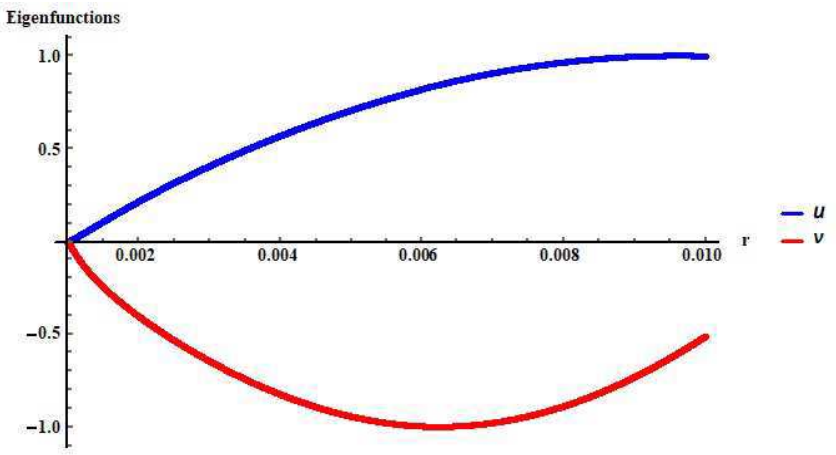

Figure 3.7: The eigenfunctions $U(r)$ and $V(r)$ (divided by their maximum modulus) corresponding to the eigenvalue $\omega_{2,0} = 752771\,\mathrm{rad.\,s^{-1}}$ for the aluminium annular disc clamped at the inner boundary and free at the outer boundary

$V(r)$ corresponding to $\omega_d = \omega_{dm,k}$ can be calculated (see Figure 3.7). These eigenfunctions are also referred to as the *form factors* of the m-ω_d-vibrating pattern or mode.

3.4.4 Annular disc free at the inner edge and clamped at the outer edge

In this sub-section the eigenvalue ω_d and corresponding eigenfunctions $U(r)$ and $V(r)$ for a disc with a fixed outer boundary and a free inner boundary are shown. The boundary conditions for the annular disc vibrating in its plane where its inner edge is free and its outer edge is clamped are written as:

$$aU'(a) + \eta\left(mV(a) + U(a)\right) = 0, \quad aV'(a) - \left(mU(a) + V(a)\right) = 0. \tag{3.114}$$

$$U(b) = 0, \quad V(b) = 0. \tag{3.115}$$

By substituting Equations (3.90) and (3.91) into Equations (3.114) and (3.115), the characteristic equation in matrix form can be written as:

$$\underbrace{\begin{pmatrix} a_{11} & a_{12} & a_{13} & a_{14} \\ a_{21} & a_{22} & a_{23} & a_{24} \\ a_{31} & a_{32} & a_{33} & a_{34} \\ a_{41} & a_{42} & a_{43} & a_{44} \end{pmatrix}}_{\mathbf{D}_4} \begin{pmatrix} C_1 \\ C_2 \\ C_3 \\ C_4 \end{pmatrix} = 0;$$

with:

$$
\begin{aligned}
a_{11} &= \left(-k_1(\omega_d)^2 - \frac{m(m-1)(\eta-1)}{a^2}\right) J_m(k_1(\omega_d)a) - \\
&\quad k_1(\omega_d)(\eta-1) J_{m+1}(k_1(\omega_d)a); \\
a_{12} &= \left(-k_1(\omega_d)^2 - \frac{m(m-1)(\eta-1)}{a^2}\right) Y_m(k_1(\omega_d)a) - \\
&\quad k_1(\omega_d)(\eta-1) Y_{m+1}(k_1(\omega_d)a); \\
a_{13} &= -\frac{m(m-1)(\eta-1)}{a^2} J_m(k_2(\omega_d)a) + \frac{k_2(\omega_d) m(\eta-1) J_{m+1}(k_2(\omega_d)a)}{a}; \\
a_{14} &= -\frac{m(m-1)(\eta-1)}{a^2} Y_m(k_2(\omega_d)a) + \frac{k_2(\omega_d) m(\eta-1) J_{m+1}(k_2(\omega_d)a);}{a} \\
a_{21} &= -\frac{2m(m-1) J_m(k_1(\omega_d)a)}{a^2} + \frac{2J_{m+1}(k_1(\omega_d)a) k_1(\omega_d) a}{a}; \\
a_{22} &= -\frac{2m(m-1) Y_m(k_1(\omega_d)a)}{a^2} + \frac{2Y_{m+1}(k_1(\omega_d)a) k_1(\omega_d) a}{a}; \\
a_{23} &= \left(k_2(\omega_d)^2 - \frac{2m(m-1)}{a^2}\right) J_m(k_2(\omega_d)a) - \frac{2k_2(\omega_d) J_{m+1}(k_2(a)a)}{a}; \\
a_{24} &= \left(k_2(\omega_d)^2 - \frac{2m(m-1)}{a^2}\right) Y_m(k_2(\omega_d)a) - \frac{2k_2(\omega_d) Y_{m+1}(k_2(a)a)}{a}; \\
a_{31} &= \frac{m}{b} J_m(k_1(\omega_d)b) - J_{m+1}(k_1(\omega_d)b) k_1(\omega_d); \\
a_{32} &= \frac{m}{b} Y_m(k_1(\omega_d)b) - Y_{m+1}(k_1(\omega_d)b) k_1(\omega_d); \\
a_{33} &= \frac{m J_m(k_2(\omega_d)b)}{b}; \\
a_{34} &= \frac{m Y_m(k_2(\omega_d)b)}{b}; \\
a_{41} &= -\frac{m J_m(k_1(\omega_d)b)}{b};
\end{aligned}
$$

$$
\begin{aligned}
a_{42} &= -\frac{m Y_m(k_1(\omega_d)b)}{b}; \\
a_{43} &= -\frac{m}{b} J_m(k_2(\omega_d)b) - J_{m+1}(k_2(\omega_d)b) k_2(\omega_d); \text{ and} \\
a_{44} &= -\frac{m}{b} Y_m(k_2(\omega_d)b) - Y_{m+1}(k_2(\omega_d)b) k_2(\omega_d).
\end{aligned}
$$

It is only ω_d that is an "unknown" quantity in a_{ij}, that is:

$$a_{ij} = a_{ij}(\omega_d), \quad i,j = 1,2,3,4. \tag{3.116}$$

It is well-known from linear algebra, that the Equation (3.108) has a non-trivial solution if the determinant of $\mathbf{M}_4 = \mathbf{M}_4(\omega_d)$ is zero, that is:

$$\Delta(\omega_d) = \det \mathbf{M}_4(\omega_d) = 0. \tag{3.117}$$

Equation (3.117) is known as the characteristic equation of the BVP. Using a CAS to solve this transcendental characteristic equation yields, for each circumferential wave number m, *a sequence*

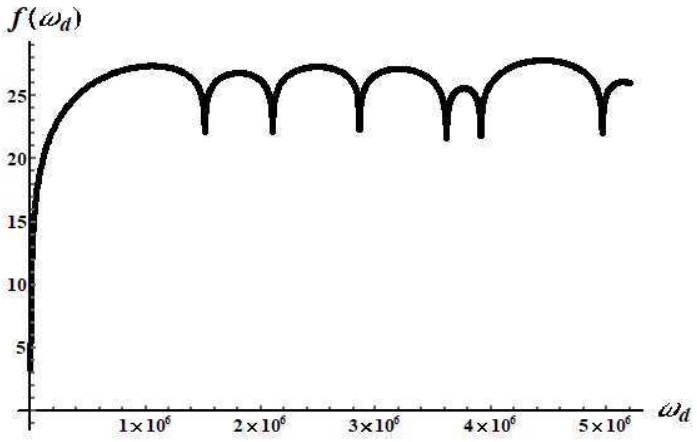

Figure 3.8: The function $f(\omega_d) = \ln|(\det M_4)|$ produced by the CAS MATHEMATICA® for a vibrating aluminium disc with inner radius $a = 0.1\,\mathrm{cm}$, outer radius $b = 1\,\mathrm{cm}$, circumferential wave number $m = 2$, density $\rho = 2.7 \times 10^3\,\mathrm{kg.\,m^{-3}}$, Young's modulus $E = 7 \times 10^{10}\,\mathrm{Pa}$ and Poisson's ratio $\upsilon = \frac{1}{3}$

of eigenvalues $\omega_{dm,k}$ $(k = 0, 1, 2, 3, \cdots)$ with:

$$\omega_{dm,0} < \omega_{dm,1} < \omega_{dm,2} < \cdots. \tag{3.118}$$

Similarly, the plot of the function $f(\omega_d) = \ln|(\det \mathbf{M}_4(\omega_d))|$ appears in Figure 3.8 for an aluminium disc where the "spikes" point towards the roots of the function $f(\omega_d)$, showing the sequence of eigenvalues depicted in inequality given by Equation (3.118). As for the previous cases, the eigenvalues are not linearly-spaced along the ω_d-axis.

Table 3.5: The fundamental and the first five overtone vibration eigenvalues and the associated eigenfrequencies of an annular disc clamped at the outer edge and free at the inner edge and vibrating at $m = 2$

k	$\omega_{d2,k}\,(\mathrm{rad\,s^{-1}})$	$f_{2,k} = \frac{\omega_{d2,k}}{2\pi}\,(\mathrm{Hz})$
0	1.511566×10^5	240573
1	2.098169×10^6	333934
2	2.861315×10^6	455392
3	3.613884×10^6	575167
4	3.912401×10^6	622678
5	4.964034×10^6	790051

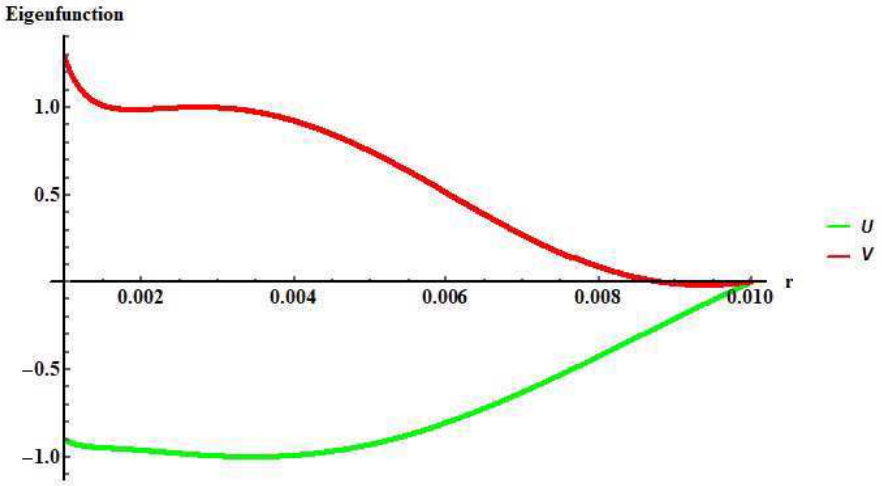

Figure 3.9: The eigenfunctions $U(r)$ and $V(r)$ (divided by their maximum modulus) corresponding to the eigenvalue $\omega_{2,0} = 1.511566 \times 10^5\,\mathrm{rad.\,s^{-1}}$ for the aluminium annular disc clamped at the outer boundary and free at the inner boundary

3.5 CONCLUSION

In this chapter, the variational principle is used to derive the governing equations of motion of the single-axis disc gyroscope. For in-plane vibration of the disc gyroscope, only potential energy resulting from extension and shear is considered. The eigenvalues and the eigenfrequencies corresponding to the in-plane vibration of the disc gyroscope are calculated numerically. The in-plane eigenfunctions are presented graphically.

For a clamped solid disc vibrating at circumferential wave number $m = 2$, it is evident from Figure 3.3 that both tangential and radial displacements vanish at the edge for the fundamental eigenvalue $\omega_{d2,0} = 1.362852 \times 10^6\,\mathrm{rad\,s^{-1}}$. Note that both displacements are non-zero at the centre of the disc. If the annular disc is clamped at both edges, with an increase in the inner radius, both the radial and tangential displacements decrease (as seen in Figure 3.5), but similar to the solid clamped disc, both displacements completely vanish at the edges, because of the shear forces at either edge. The dynamics of the out-of-plane vibration of the disc gyroscope are discussed in Chapter 4.

Chapter 4

THE DYNAMICS OF THE OUT-OF-PLANE VIBRATIONS OF A DISC GYROSCOPE

4.1 INTRODUCTION

Chapter 3 of this thesis dealt with in-plane vibrations of the disc-vibratory gyroscope. In this chapter, the equations of motion and boundary conditions describing the out-of-plane vibration of the disc are derived and discussed. Vibration of the disc in its out-of plane mode is modelled as circular-plate vibration and hence the vibration resulting from bending only, is emphasised in this chapter.

4.2 THIN PLATES

Venstel and Krauthammer (2001, [68]) describe plates as flat structures bounded by two parallel faces and an edge. The separation between the plane faces of the plate are called thickness. The thickness characterises the plate and it is significantly smaller than the other typical dimensions (length, breadth) of the faces of the plate. Plates are widely used in almost all fields of engineering, in architectural structures, bridges, hydraulic structures, pavements, containers, airplanes, missiles, ships, instruments and machine parts, just to name a few applications. The latter-mentioned authors categorise plates as follows below, into three main groupings based on the ratio of the typical plane dimension (a) to the thickness (h) of the plate:

- *Thick plates*: If the ratio $\frac{a}{h} \leq 8...10$. In this case the analysis of the plate uses the theory of three-dimensional elasticity.
- *Membranes*: If the ratio $\frac{a}{h} \geq 80...100$. This type of plate does not have flexural rigidity.
- *Thin plates*: These are the intermediate types of plates with $8...10 \leq \frac{a}{h} \leq 80...100$. They are the most widely-used type of plates which can also be sub-categorised into *stiff* or *flexibe* based on the ratio of maximum deflection of the plate to its thickness.

4.2.1 Classical or Kirchhof plate theory

Wherever applicable in this thesis, Kirchhof's theory of plates is assumed. The following is a list

of the widely-accepted assumptions of this theory:

- The material of the plate is elastic, homogeneous and isotropic.
- Initially, the plate is assumed to be flat.
- The displacement of deformation perpendicular to the plane of the plate is substantially small compared to the thickness of the plate. Hence the square of the gradient of the deflected surface is much smaller than unity.
- The straight lines, initially normal to the middle plane before bending, remain straight and normal to the middle surface during deformation.
- The stress, normal to the middle plane σ_z is small compared to the other stress components and can be neglected in the stress-strain relationships.
- The middle surface remains unstrained after bending, because the displacements of the plate are assumed to be small.

4.3 EQUATIONS OF MOTION OF CIRCULAR PLATES

Circular plates are elements of the structures which are important in application domains such as aeroplanes, submarines, discs, pressure vessels and many more. The dynamics of a circular plate are used to describe vibration properties of out-of-plane vibrations of the vibratory disc gyroscope. Therefore, in this thesis, the terms plate vibration and bending vibration are used interchangeably to model the out-of-plane vibrations of the disc gyroscope.

The classical plate equation in rectangular coordinates for free vibration is (Leissa & Qatu, 2011, [39]):

$$D\left(\frac{\partial^4 w}{\partial x^4}+2\frac{\partial^4 w}{\partial x^2\partial y^2}+\frac{\partial^4 w}{\partial y^4}\right)+\rho h\frac{\partial^2 w}{\partial t^2}=0; \tag{4.1}$$

where:

$$D=\frac{Eh^3}{12\left(1-\eta^2\right)}; \tag{4.2}$$

is flexural rigidity, E is Young's modulus, w is the transverse displacement and η is the Poisson's ratio. It is more convenient to write the equation in polar coordinates. The coordinate transformation as discussed and shown below is used to re-write the equation (See Figure 4.1 adapted from Spoelstra (2015, [69]).

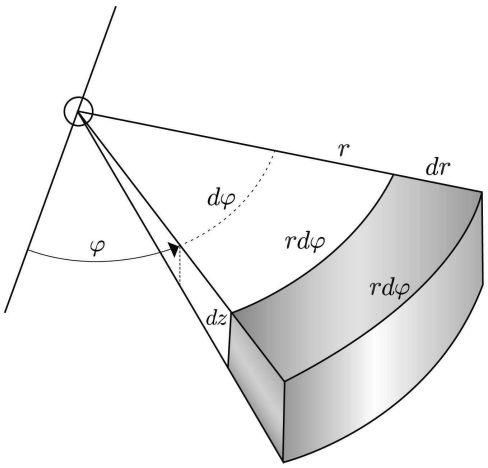

Figure 4.1: In this figure the shaded area represents the volume element of the vibrating point P. The position of rest of P is given by polar coordinates r and φ. The inner and outer arclengths are both assumed to be $rd\varphi$ as dr is verysmall, that is, $(r + dr)\, d\varphi \approx rd\varphi$

If $(r,\ \varphi)$ are the polar coordinates, then the rectangular coordinates are given by:

$$x = r\cos\varphi, \text{ and } y = r\sin\varphi. \tag{4.3}$$

Thus:

$$r^2 = x^2 + y^2,\ \varphi = \tan^{-1}\frac{y}{x}. \tag{4.4}$$

By differentiation, the following is obtained:

$$\frac{\partial r}{\partial x} = \frac{x}{r} = \frac{r\cos\varphi}{r} = \cos\varphi \text{ and } \frac{\partial r}{\partial y} = \frac{y}{r} = \sin\varphi. \tag{4.5}$$

In addition to the above, the following expressions are also valid:

$$\frac{\partial \varphi}{\partial x} = -\frac{y}{r^2} = -\frac{\sin\varphi}{r}; \text{ and } \frac{\partial \varphi}{\partial y} = \frac{x}{r^2} = \frac{\cos\varphi}{r}. \tag{4.6}$$

Since the deflection w is a function of both r and φ, the relations from the application of the chain rule, as shown below, are obtained:

$$\begin{aligned}\frac{\partial w}{\partial x} &= \frac{\partial w}{\partial r}\frac{\partial r}{\partial x} + \frac{\partial w}{\partial \varphi}\frac{\partial \varphi}{\partial x} \\ &= \frac{\partial w}{\partial r}\cos\varphi - \frac{1}{r}\frac{\partial w}{\partial \varphi}\sin\varphi.\end{aligned} \tag{4.7}$$

Differentiating Equation (4.7) with respect to x, once again, yields:

$$\begin{aligned}\frac{\partial^2 w}{\partial x^2} &= \cos\varphi\frac{\partial}{\partial r}\left(\frac{\partial w}{\partial x}\right) - \frac{1}{r}\sin\varphi\frac{\partial}{\partial \varphi}\left(\frac{\partial w}{\partial x}\right) \\ &= \frac{\partial^2 w}{\partial r^2}\cos^2\varphi - \frac{\partial^2 w}{\partial \varphi \partial r}\frac{\sin 2\varphi}{r} + \frac{\partial w}{\partial r}\frac{\sin^2\varphi}{r} + \frac{\partial w}{\partial \varphi}\frac{\sin 2\varphi}{r^2} + \frac{\partial^2 w}{\partial \varphi^2}\frac{\sin^2\varphi}{r^2}.\end{aligned} \tag{4.8}$$

Similarly:

$$\frac{\partial^2 w}{\partial y^2} = \frac{\partial^2 w}{\partial r^2}\sin^2\varphi + \frac{\partial^2 w}{\partial r \partial \varphi}\frac{\sin 2\varphi}{r} + \frac{\partial w}{\partial r}\frac{\cos^2\varphi}{r} - \frac{\partial w}{\partial \varphi}\frac{\sin 2\varphi}{r^2} + \frac{\partial^2 w}{\partial \varphi^2}\frac{\cos^2\varphi}{r^2}; \tag{4.9}$$

and

$$\frac{\partial^2 w}{\partial x \partial y} = \frac{\partial^2 w}{\partial r^2}\frac{\sin 2\varphi}{2} + \frac{\partial^2 w}{\partial r \partial \varphi}\frac{\cos 2\varphi}{r} - \frac{\partial w}{\partial \varphi}\frac{\cos 2\varphi}{r^2} - \frac{\partial w}{\partial r}\frac{\sin 2\varphi}{2r} - \frac{\partial^2 w}{\partial \varphi^2}\frac{\sin 2\varphi}{2r^2}. \tag{4.10}$$

Substitution of Equations (4.8), (4.9) and (4.10) by repeating differentiation twice on each part into Equation (4.1), yields:

$$D\left(\nabla^2\left(\nabla^2 w\right)\right) + \rho h \frac{\partial^2 w}{\partial t^2} = 0; \tag{4.11}$$

where:

$$\nabla^2\left(\nabla^2 w\right) = \left(\frac{\partial^2}{\partial r^2} + \frac{1}{r}\frac{\partial}{\partial r} + \frac{1}{r^2}\frac{\partial^2}{\partial \varphi^2}\right)\left(\frac{\partial^2 w}{\partial r^2} + \frac{1}{r}\frac{\partial w}{\partial r} + \frac{1}{r^2}\frac{\partial^2 w}{\partial \varphi^2}\right). \tag{4.12}$$

The expression in Equation (4.12) after expansions and simplifications yields:

$$\frac{\partial^4 w}{\partial r^4} + \frac{2}{r}\frac{\partial^3 w}{\partial r^3} - \frac{1}{r^2}\frac{\partial^2 w}{\partial r^2} + \frac{1}{r^3}\frac{\partial w}{\partial r} + \frac{2}{r^2}\frac{\partial^4 w}{\partial r^2 \partial \varphi^2} - \frac{2}{r^3}\frac{\partial^3 w}{\partial \varphi^2 \partial r} + \frac{4}{r^4}\frac{\partial^2}{\partial \varphi^2} + \frac{1}{r^4}\frac{\partial^4 w}{\partial \varphi^4}; \tag{4.13}$$

where t is time and ∇^4 is a biharmonic differential operator. Equation (4.11) is the well known classical differential equation of motion of plate in polar coordinates with respect to the transverse displacement w of the plate.

4.4 DERIVATION OF THE EQUATIONS OF MOTION USING THE VARIATIONAL PRINCIPLE

To build the theory of a three-dimensional disc gyroscope, assume that in-plane vibrations of the disc (u, v) and its out-of-plane vibrations (w) are independent (Rourke, McWilliam & Fox, 2005, [63]). Hence, it is possible to consider strain energy of the disc as the sum of two strain energies, namely, the strain energy of the in-plane vibrations of the disc discussed in Chapter 3 (see Equation 3.32) and the strain energy of its out-of-plane vibrations. The out-of-plane vibrations are considered as the bending vibrations of the disc in its out-of-plane direction (in other words, considered as the vibration of the circular plate).

4.4.1 Kinetic energy of out-of-plane vibrations

Neglecting in-plane vibrations (Novozhilov, 1970, [61]) as well as in-plane displacements of the plate (u, v), the kinetic energy of the plate in terms of of the axial deformation (w) is given by (Hagedorn & DasGupta, 2007, [70]):

$$K_p = \int_0^{2\pi}\int_a^b \frac{\rho h}{2}\dot{w}^2 r dr d\varphi. \tag{4.14}$$

The expression in Equation (4.14) is obtained by assuming pure bending of the plate where the angular rate of rotation along all inertial axes are assumed to be zero, that is, $\Omega_\eta = \Omega_\xi = \Omega_\zeta = 0$.

4.4.2 Strain energy of the bending and torsional vibrations

The strain energy of bending and torsion for out-of-plane vibrations can be written as (Landau & Lifshitz, 1975, [65]), (Venstel & Krauthammer, 2001, [68]):

$$P_p = \int_0^{2\pi} \int_a^b \frac{Eh^3}{24\left(1-\eta^2\right)} \left(\chi_1^2 + \chi_2^2 + 2\eta\chi_1\chi_2 + 2\left(1-\eta\right)\tilde{\tau}^2\right) r dr d\varphi; \tag{4.15}$$

with:

$$\chi_1 = -\frac{1}{A_1}\frac{\partial}{\partial\alpha_1}\left(\frac{1}{A_1}\frac{\partial w}{\partial\alpha_1}\right) - \frac{1}{A_1 A_2^2}\frac{\partial A_1}{\partial\alpha_2}\frac{\partial w}{\partial\alpha_2}; \tag{4.16}$$

$$\chi_2 = -\frac{1}{A_2}\frac{\partial}{\partial\alpha_2}\left(\frac{1}{A_2}\frac{\partial w}{\partial\alpha_2}\right) - \frac{1}{A_1^2 A_2}\frac{\partial A_2}{\partial\alpha_1}\frac{\partial w}{\partial\alpha_1}; \text{ and} \tag{4.17}$$

$$\tilde{\tau} = -\frac{1}{A_1 A_2}\left(\frac{\partial^2 w}{\partial\alpha_1\partial\alpha_2} - \frac{1}{A_1}\frac{\partial A_1}{\partial\alpha_2}\frac{\partial w}{\partial\alpha_1} - \frac{1}{A_2}\frac{\partial A_2}{\partial\alpha_1}\frac{\partial w}{\partial\alpha_2}\right); \tag{4.18}$$

and where χ_1 and χ_2 represent bending strains and $\tilde{\tau}$ represents torsional strain. For the sake of disc geometry, from Equations (3.24) and (3.30) the parameters in Equations (4.16), (4.17) and (4.18) can be replaced by:

$$\alpha_1 = r;\ \alpha_2 = \varphi;\ A_1 = 1; \text{ and } A_2 = r. \tag{4.19}$$

According to the Novozhilov-Goldenveizer theory of thin shells (Leissa, 1993, [60]), the tangential displacements (u, v) are neglected. Thus, terms χ_1, χ_2 and $\tilde{\tau}$ can be evaluated using only axial displacement w. Substitution of Equation (4.19) into Equations (4.16), (4.17) and (4.18) results in:

$$\chi_1 = -\frac{\partial^2 w}{\partial r^2}; \tag{4.20}$$

$$\chi_2 = -\frac{1}{r}\frac{\partial w}{\partial r} - \frac{1}{r^2}\frac{\partial^2 w}{\partial\varphi^2}; \text{ and} \tag{4.21}$$

$$\tilde{\tau} = -\frac{1}{r}\frac{\partial^2 w}{\partial r\partial\varphi} + \frac{1}{r^2}\frac{\partial w}{\partial\varphi}. \tag{4.22}$$

Substitution of Equations (4.20), (4.21) and (4.22) into Equation (4.15) yields:

$$\begin{aligned} P_p &= \int_0^{2\pi}\int_a^b \frac{Eh^3}{24\left(1-\eta^2\right)}\left(\chi_1^2 + \chi_2^2 + 2\eta\chi_1\chi_2 + 2\left(1-\eta\right)\tilde{\tau}^2\right) r dr d\varphi \\ &= \int_0^{2\pi}\int_a^b \frac{Eh^3}{24\left(1-\eta^2\right)} \left\{ \begin{array}{c} \left(-\frac{\partial^2 w}{\partial r^2}\right)^2 + \left(-\frac{1}{r}\frac{\partial w}{\partial r} - \frac{1}{r^2}\frac{\partial^2 w}{\partial\varphi^2}\right)^2 + \\ 2\eta\left(-\frac{\partial^2 w}{\partial r^2}\right)\left(-\frac{1}{r}\frac{\partial w}{\partial r} - \frac{1}{r^2}\frac{\partial^2 w}{\partial\varphi^2}\right) + \\ 2\left(1-\eta\right)\left(-\frac{1}{r}\frac{\partial^2 w}{\partial r\partial\varphi} + \frac{1}{r^2}\frac{\partial w}{\partial\varphi}\right)^2 \end{array} \right\} r dr d\varphi. \end{aligned} \tag{4.23}$$

The Lagrangian of the plate can thus be written as:

$$\begin{aligned} L_p &= K_p - P_p \\ &= \int_0^{2\pi}\int_a^b \Lambda dr d\varphi; \end{aligned} \tag{4.24}$$

where:

$$\Lambda = \rho\frac{h}{2}\dot{w}^2 r - \frac{Eh^3 r}{24\left(1-\eta^2\right)}\left\{\left(w''_{rr}\right)^2 + \frac{1}{r^2}\left(w'_r + \frac{1}{r}w''_{\varphi\varphi}\right)^2 + \frac{2\eta}{r}\left(w'_r + \frac{1}{r}w''_{\varphi\varphi}\right)w''_{rr} + \frac{2\left(1-\eta\right)}{r^2}\left(w''_{r\varphi} - \frac{1}{r}w'_{\varphi}\right)^2\right\}; \quad (4.25)$$

is the Lagrangian density, with:

$$\dot{w} = \frac{\partial w}{\partial t} = \frac{\partial w}{\partial \tau};\ w'_r = \frac{\partial w}{\partial r};\ w'_{\varphi} = \frac{\partial w}{\partial \varphi};\ w''_{rr} = \frac{\partial^2 w}{\partial r^2};\ w''_{\varphi\varphi} = \frac{\partial^2 w}{\partial \varphi^2};\ \text{and } w''_{r\varphi} = \frac{\partial^2 w}{\partial r \partial \varphi}. \quad (4.26)$$

The Lagrangian density in implicit form can be written as:

$$\Lambda = \Lambda\left(\dot{w}, w''_{rr},\ w''_{r\varphi},\ w''_{\varphi\varphi},\ w'_r,\ w'_{\varphi}\right). \quad (4.27)$$

4.4.3 Governing equation of motion

The functional of an action is given by (Goldstein, Poole & Safco, 2000, [64]):

$$A_p = \int_0^t L_p d\tau = \int_0^t \int_0^{2\pi} \int_a^b \Lambda dr d\varphi d\tau. \quad (4.28)$$

According to Hamilton's variational principle (Goldstein, Poole & Safco, 2000, [64]), the variation of action (δA_p) satisfies:

$$\delta A_p = 0;$$

provided that

$$\delta w|_{\tau=0} = \delta w|_{\tau=t} = 0;$$

thus:

$$\delta A_p = \int_0^t \delta L_p d\tau = \int_0^t \int_0^{2\pi} \int_a^b \delta\Lambda dr d\varphi d\tau = 0. \quad (4.29)$$

The variation of the Lagrangian density ($\delta\Lambda$) can be calculated as follows:

$$\begin{aligned}\delta\Lambda &= \frac{\partial\Lambda}{\partial\dot{w}}\delta\dot{w}+\frac{\partial\Lambda}{\partial w'_r}\delta w'_r+\frac{\partial\Lambda}{\partial w'_\varphi}\delta w'_\varphi+\frac{\partial\Lambda}{\partial w''_{rr}}\delta w''_{rr}+\\ &\qquad \frac{\partial\Lambda}{\partial w''_{r\varphi}}\delta w''_{r\varphi}+\frac{\partial\Lambda}{\partial w''_{\varphi\varphi}}\delta w''_{\varphi\varphi}\\ &= \frac{\partial}{\partial\tau}\left(\frac{\partial\Lambda}{\partial\dot{w}}\delta w\right)+\frac{\partial}{\partial\varphi}\left(\frac{\partial\Lambda}{\partial w'_\varphi}\delta w+\frac{\partial\Lambda}{\partial w''_{r\varphi}}\delta w'_r+\frac{\partial\Lambda}{\partial w''_{\varphi\varphi}}\delta w'_\varphi\right)+\\ &\quad \frac{\partial}{\partial r}\left(\frac{\partial\Lambda}{\partial w'_r}\delta w_r+\frac{\partial\Lambda}{\partial w''_{rr}}\delta w'_r\right)-\left(\frac{\partial}{\partial\tau}\frac{\partial\Lambda}{\partial\dot{w}}+\frac{\partial}{\partial r}\frac{\partial\Lambda}{\partial w'_r}+\frac{\partial}{\partial\varphi}\frac{\partial\Lambda}{\partial w'\varphi}\right)\delta w\\ &\quad -\frac{\partial}{\partial\varphi}\frac{\partial\Lambda}{\partial w''_{\varphi\varphi}}\delta w'_\varphi-\left(\frac{\partial}{\partial r}\frac{\partial\Lambda}{\partial w'_{rr}}+\frac{\partial}{\partial\varphi}\frac{\partial\Lambda}{\partial w''_{r\varphi}}\right)\delta w'_r. \end{aligned} \tag{4.30}$$

Rearranging the right-hand side of Equation (4.30) gives:

$$\begin{aligned}\delta\Lambda &= \frac{\partial}{\partial\tau}\left(\frac{\partial\Lambda}{\partial\dot{w}}\delta w\right)+\frac{\partial}{\partial\varphi}\left\{\left(\frac{\partial\Lambda}{\partial w'_\varphi}-\frac{\partial}{\partial\varphi}\frac{\partial\Lambda}{\partial w''_{\varphi\varphi}}\right)\delta w+\right.\\ &\quad \left.\frac{\partial\Lambda}{\partial w''_{r\varphi}}\delta w'_r+\frac{\partial\Lambda}{\partial w''_{\varphi\varphi}}\delta w'_\varphi\right\}+\frac{\partial}{\partial r}\left\{\left(\frac{\partial\Lambda}{\partial w'_r}-\frac{\partial}{\partial r}\frac{\partial\Lambda}{\partial w''_{rr}}-\frac{\partial}{\partial\varphi}\frac{\partial\Lambda}{\partial w''_{r\varphi}})\right)\delta w\right.\\ &\quad \left.+\frac{\partial\Lambda}{\partial w''_{rr}}\delta w'_r\right\}-\\ &\quad \left\{\frac{\partial}{\partial\tau}\left(\frac{\partial\Lambda}{\partial\dot{w}}\right)+\frac{\partial}{\partial r}\left(\frac{\partial\Lambda}{\partial w'_r}\right)+\frac{\partial}{\partial\varphi}\left(\frac{\partial\Lambda}{\partial w'_\varphi}\right)-\frac{\partial^2}{\partial r^2}\left(\frac{\partial\Lambda}{\partial w''_{rr}}\right)-\right.\\ &\quad \left.-\frac{\partial^2}{\partial r\partial\varphi}\left(\frac{\partial\Lambda}{\partial w''_{r\varphi}}\right)-\frac{\partial^2}{\partial\varphi^2}\left(\frac{\partial\Lambda}{\partial w'_{\varphi\varphi}}\right)\right\}\delta w. \end{aligned} \tag{4.31}$$

Substitution of the first term of the right-hand side of Equation (4.31) into Equation (4.29) and changing the order of integration yields:

$$\begin{aligned}\int_0^{2\pi}\int_a^b\left\{\int_0^t\frac{\partial}{\partial\tau}\left(\frac{\partial\Lambda}{\partial\dot{w}}\delta w\right)d\tau\right\}drd\varphi &= \\ \int_0^{2\pi}\int_a^b\left\{\left(\frac{\partial\Lambda}{\partial\dot{w}}\right)_{\tau=t}(\delta w)_{\tau=t}-\left(\frac{\partial\Lambda}{\partial\dot{w}}\right)_{\tau=0}(\delta w)_{\tau=0}\right\}drd\varphi &= 0; \end{aligned} \tag{4.32}$$

since $\delta w|_{\tau=0}=\delta w|_{\tau=t}=0$. Again by substitution of the second group of terms of Equation (4.31) into Equation (4.29) and then by changing the order of integration and by 2π-periodicity

and continuity of the disc over the polar angle φ yields:

$$\int_0^t \int_a^b \left\{ \int_0^{2\pi} \frac{\partial}{\partial \varphi} \left(\left(\frac{\partial \Lambda}{\partial w'_\varphi} - \frac{\partial}{\partial \varphi} \frac{\partial \Lambda}{\partial w'_{\varphi\varphi}} \right) \delta w + \frac{\partial \Lambda}{\partial w''_{r\varphi}} \delta w'_r + \frac{\partial \Lambda}{\partial w''_{\varphi\varphi}} \delta w'_\varphi \right) d\varphi \right\} dr d\tau$$

$$= \int_0^t \int_a^b \left\{ \left(\frac{\partial \Lambda}{\partial w'_\varphi} - \frac{\partial}{\partial \varphi} \frac{\partial \Lambda}{\partial w'_{\varphi\varphi}} \right)_{\varphi=2\pi} (\delta w)_{\varphi=2\pi} - \left(\frac{\partial \Lambda}{\partial w'_\varphi} - \frac{\partial}{\partial \varphi} \frac{\partial \Lambda}{\partial w'_{\varphi\varphi}} \right)_{\varphi=0} (\delta w)_{\varphi=0} + \right.$$

$$+ \left(\frac{\partial \Lambda}{\partial w''_{r\varphi}} \delta w'_r \right)_{\varphi=2\pi} (\delta w'_r)_{\varphi=2\pi} - \left(\frac{\partial \Lambda}{\partial w''_{r\varphi}} \delta w'_r \right)_{\varphi=0} (\delta w'_r)_{\varphi=0} +$$

$$\left. + \left(\frac{\partial \Lambda}{\partial w''_{\varphi\varphi}} \right)_{\varphi=2\pi} \left(\delta w'_\varphi\right)_{\varphi=2\pi} - \left(\frac{\partial \Lambda}{\partial w''_{\varphi\varphi}} \right)_{\varphi=0} \left(\delta w'_\varphi\right)_{\varphi=0} \right\} dr d\tau = 0. \tag{4.33}$$

Note that:

$$\begin{aligned} (\delta w)_{\varphi=0} &= (\delta w)_{\varphi=2\pi} \text{ and} \\ \left(\frac{\partial \Lambda}{\partial w'_\varphi} - \frac{\partial}{\partial \varphi} \frac{\partial \Lambda}{\partial w'_{\varphi\varphi}} \right)_{\varphi=0} &= \left(\frac{\partial \Lambda}{\partial w'_\varphi} - \frac{\partial}{\partial \varphi} \frac{\partial \Lambda}{\partial w'_{\varphi\varphi}} \right)_{\varphi=2\pi}. \end{aligned} \tag{4.34}$$

Now consider the third group of terms of Equation (4.31) which after performing integration result in:

$$\int_0^t \int_0^{2\pi} \left\{ \int_a^b \frac{\partial}{\partial r} \left[\left(\frac{\partial \Lambda}{\partial w'_r} - \frac{\partial}{\partial r} \frac{\partial \Lambda}{\partial w''_{rr}} - \frac{\partial}{\partial \varphi} \frac{\partial \Lambda}{\partial w''_{r\varphi}} \right) \delta w + \frac{\partial \Lambda}{\partial w''_{rr}} \delta w'_r \right] dr \right\} d\varphi d\tau$$

$$= \int_0^t \int_0^{2\pi} \left\{ \left[\frac{\partial \Lambda}{\partial w'_r} - \frac{\partial}{\partial r} \frac{\partial \Lambda}{\partial w''_{rr}} - \frac{\partial}{\partial \varphi} \frac{\partial \Lambda}{\partial w''_{r\varphi}} \right]_{r=b} [\delta w]_{r=b} + \left[\frac{\partial \Lambda}{\partial w''_{rr}} \right]_{r=b} [\delta w'_r]_{r=b} \right.$$

$$\left. - \left[\frac{\partial \Lambda}{\partial w'_r} - \frac{\partial}{\partial r} \frac{\partial \Lambda}{\partial w''_{rr}} - \frac{\partial}{\partial \varphi} \frac{\partial \Lambda}{\partial w''_{r\varphi}} \right]_{r=a} [\delta w]_{r=a} - \left[\frac{\partial \Lambda}{\partial w''_{rr}} \right]_{r=a} [\delta w'_r]_{r=a} \right\} d\varphi d\tau. \tag{4.35}$$

Combining the fourth group of terms of the right-hand side of Equation (4.31) together with Equations (4.32), (4.33) and (4.35) into Equation (4.31), for variation of action, gives the following:

$$\begin{aligned} \delta A_p = & \int_0^t \int_0^{2\pi} \left\{ \left[\frac{\partial \Lambda}{\partial w'_r} - \frac{\partial}{\partial r} \frac{\partial \Lambda}{\partial w''_{rr}} - \frac{\partial}{\partial \varphi} \frac{\partial \Lambda}{\partial w''_{r\varphi}} \right]_{r=b} [\delta w]_{r=b} + \left[\frac{\partial \Lambda}{\partial w''_{rr}} \right]_{r=b} [\delta w'_r]_{r=b} \right. \\ & \left. - \left[\frac{\partial \Lambda}{\partial w'_r} - \frac{\partial}{\partial r} \frac{\partial \Lambda}{\partial w''_{rr}} - \frac{\partial}{\partial \varphi} \frac{\partial \Lambda}{\partial w''_{r\varphi}} \right]_{r=a} [\delta w]_{r=a} - \left[\frac{\partial \Lambda}{\partial w''_{rr}} \right]_{r=a} [\delta w'_r]_{r=a} \right\} d\varphi d\tau \\ & - \int_0^t \int_0^{2\pi} \int_a^b \left[\frac{\partial}{\partial \tau} \left(\frac{\partial \Lambda}{\partial \dot{w}} \right) + \frac{\partial}{\partial r} \left(\frac{\partial \Lambda}{\partial w'_r} \right) + \frac{\partial}{\partial \varphi} \left(\frac{\partial \Lambda}{\partial w'_\varphi} \right) - \frac{\partial^2}{\partial r^2} \left(\frac{\partial \Lambda}{\partial w''_{rr}} \right) - \right. \\ & \left. \frac{\partial^2}{\partial r \partial \varphi} \left(\frac{\partial \Lambda}{\partial w''_{r\varphi}} \right) - \frac{\partial^2}{\partial \varphi^2} \left(\frac{\partial \Lambda}{\partial w'_{\varphi\varphi}} \delta w \right) \right] dr d\varphi d\tau. \end{aligned} \tag{4.36}$$

But from Equation (4.29), $\delta A_p = 0$. Thus, for the right-hand side of Equation (4.36) to be zero, one has to impose certain conditions. However, from the fact that the variations such as $[\delta w]_{r=a,\,b}$ and $[\delta w'_r]_{r=a,\,b}$ are arbitrary and by the First Fundamental Lemma of the Calculus of Variations (Soedel, 2004, [62]), the following implicit form of equation with the corresponding boundary

conditions is obtained as:

$$\begin{aligned} & \frac{\partial}{\partial \tau}\left(\frac{\partial \Lambda}{\partial \dot{w}}\right)+\frac{\partial}{\partial r}\left(\frac{\partial \Lambda}{\partial w_r'}\right)+\frac{\partial}{\partial \varphi}\left(\frac{\partial \Lambda}{\partial w_\varphi'}\right)-\frac{\partial^2}{\partial r^2}\left(\frac{\partial \Lambda}{\partial w_{rr}''}\right)- \\ & -\frac{\partial^2}{\partial r \partial \varphi}\left(\frac{\partial \Lambda}{\partial w_{r\varphi}''}\right)-\frac{\partial^2}{\partial \varphi^2}\left(\frac{\partial \Lambda}{\partial w_{\varphi\varphi}''}\right) \\ = \; & 0. \end{aligned} \tag{4.37}$$

Note that Equation (4.37) is the implicit form of the governing equation of motion of the circular bending plate in polar coordinates.

4.4.4 Boundary conditions in implicit form

Keeping Equation (4.36) in mind and from the Fundamental Lemma of the Calculus of Variations (Soedel, 2004, [62]), the implicit form of the boundary condition for a circular plate vibrating in the transverse direction can be written as:

$$\begin{aligned} w|_{r=a,\,b} &= 0 \text{ or } \left[\frac{\partial \Lambda}{\partial w_r'}-\frac{\partial}{\partial r}\left(\frac{\partial \Lambda}{\partial w_{rr}''}\right)-\frac{\partial}{\partial \varphi}\left(\frac{\partial \Lambda}{\partial w_{r\varphi}''}\right)\right]_{r=a,\,b}=0; \\ \text{and } \left.\frac{\partial w}{\partial r}\right|_{r=a,\,b} &= 0 \text{ or } \left.\frac{\partial \Lambda}{\partial w_{rr}''}\right|_{r=a,\,b}=0. \end{aligned} \tag{4.38}$$

4.4.5 Explicit form of the equations of motion of the vibrating plate

Substitution of Equation (4.25) into Equation (4.37) gives the following equations for each part:

$$\frac{\partial}{\partial \tau}\left(\frac{\partial \Lambda}{\partial \dot{w}}\right) = \rho h \ddot{w} r; \tag{4.39}$$

$$\frac{\partial}{\partial r}\left(\frac{\partial \Lambda}{\partial w'_r}\right) = -\frac{Eh^3}{24\left(1-\eta^2\right)}\left\{2\eta w'''_{rrr} + \frac{2}{r}w''_{rr} - \frac{2}{r^2}w'_r - \right. \tag{4.40}$$

$$\left. \frac{4}{r^3}w''_{\varphi\varphi} + \frac{2}{r^3}w'''_{r\varphi\varphi}\right\}; \tag{4.41}$$

$$\frac{\partial}{\partial \varphi}\left(\frac{\partial \Lambda}{\partial w'_\varphi}\right) = \frac{Eh^3}{24\left(1-\eta^2\right)}\left\{\frac{4\left(1-\eta\right)}{r^2}w'''_{r\varphi\varphi} - \frac{4\left(1-\eta\right)}{r^3}w''_{\varphi\varphi}\right\}; \tag{4.42}$$

$$\frac{\partial^2}{\partial r^2}\left(\frac{\partial \Lambda}{\partial w''_{rr}}\right) = -\frac{Eh^3}{24\left(1-\eta^2\right)}\left\{2r w''''_{rrrr} + 4w'''_{rrr} + 2\eta w'''_{rrr} + \frac{4\eta}{r^3}w''_{\varphi\varphi} - \right. \tag{4.43}$$

$$\left. \frac{4}{r^2}w'''_{r\varphi\varphi} + \frac{2\eta}{r}w''''_{rr\varphi\varphi}\right\}; \tag{4.44}$$

$$\frac{\partial^2}{\partial r \partial \varphi}\left(\frac{\partial \Lambda}{\partial w''_{r\varphi}}\right) = -\frac{Eh^3}{24\left(1-\eta^2\right)}\left\{-\frac{8\left(1-\eta\right)}{r^2}w'''_{r\varphi\varphi} + \frac{4\left(1-\eta\right)}{r}w''''_{rr\varphi\varphi} + \right. \tag{4.45}$$

$$\left. \frac{8}{r^3}\left(1-\eta\right)w''_{\varphi\varphi}\right\}; \text{ and} \tag{4.46}$$

$$\frac{\partial^2}{\partial \varphi^2}\left(\frac{\partial \Lambda}{\partial w''_{\varphi\varphi}}\right) = -\frac{Eh^3}{24\left(1-\eta^2\right)}\left[\frac{2}{r^3}w''''_{\varphi\varphi\varphi\varphi} + \frac{2\eta}{r}w''''_{rr\varphi\varphi} + \frac{2}{r^2}w'''_{r\varphi\varphi}\right]. \tag{4.47}$$

Substitution of Equations (4.39)-(4.47) into Equation (4.37) yields:

$$\frac{12\left(1-\eta^2\right)}{Eh^2}\ddot{w} + \left\{\begin{array}{c} w''''_{rrrr} + \frac{2}{r}w'''_{rrr} - \frac{w''_{rr}}{r^2} + \frac{w'_r}{r^3} + \frac{2}{r^2}w''''_{rr\varphi\varphi} - \frac{2}{r^3}w'''_{r\varphi\varphi} \\ + \frac{4w''_{\varphi\varphi}}{r^4} + \frac{1}{r^4}w''''_{\varphi\varphi\varphi\varphi} \end{array}\right\} = 0; \tag{4.48}$$

which can be rewritten as:

$$\frac{12\rho\left(1-\eta^2\right)}{Eh^2}\ddot{w} + \nabla^4 w = 0; \tag{4.49}$$

where ∇^4 (del fourth) is the biharmonic differential operator defined as $\nabla^4 = \nabla^2\left(\nabla^2\right)$, and:

$$\nabla^2 = \frac{\partial^2}{\partial r^2} + \frac{1}{r}\frac{\partial}{\partial r} + \frac{1}{r^2}\frac{\partial^2}{\partial \varphi^2}; \tag{4.50}$$

is the *Laplace operator* in polar coordinates. Equation (4.49) is the equation of the circular plate in polar coordinates.

4.4.6 Explicit form of the boundary conditions

To derive formulas for boundary conditions in explicit form, Equations (4.38) and (4.25) are used.

Indicated differentiations are carried out on equations:

$$\left[\frac{\partial\Lambda}{\partial w'_r}-\frac{\partial}{\partial r}\left(\frac{\partial\Lambda}{\partial w''_{rr}}\right)-\frac{\partial}{\partial\varphi}\left(\frac{\partial\Lambda}{\partial w''_{r\varphi}}\right)\right]_{r=a,\,b}=0; \tag{4.51}$$

and:

$$\left.\frac{\partial\Lambda}{\partial w''_{r\varphi}}\right|_{r=a,\,b}=0. \tag{4.52}$$

Now substitution of the Lagrangian density Λ into Equation (4.51) for each term gives:

$$\frac{\partial\Lambda}{\partial w'_r} = \frac{-Eh^3r}{24\left(1-\eta^2\right)}\left\{\frac{2}{r^2}\left(w'_r+\frac{1}{r}w''_{\varphi\varphi}\right)+\frac{2\eta}{r}w''_{rr}\right\}; \tag{4.53}$$

$$\frac{\partial\Lambda}{\partial w''_{rr}} = \frac{-Eh^3r}{24\left(1-\eta^2\right)}\left\{2w''_{rr}+\frac{2\eta}{r}\left(w'_r+\frac{1}{r}w''_{\varphi\varphi}\right)\right\}r;\ \text{then}$$

$$\begin{aligned}\frac{\partial}{\partial r}\left(\frac{\partial\Lambda}{\partial w''_{rr}}\right) = {} & \frac{-Eh^3r}{24\left(1-\eta^2\right)}\left\{2w'''_{rrr}-\frac{2\eta}{r^2}\left(w'_r+\frac{1}{r}w''_{\varphi\varphi}\right)+\right.\\ & \left.\frac{2\eta}{r}\left(w''_{rr}-\frac{1}{r^2}w''_{\varphi\varphi}+\frac{1}{r}w'''_{\varphi\varphi r}\right)\right\}-\\ & \frac{-Eh^3}{24\left(1-\eta^2\right)}\left\{2w''_{rr}+\frac{2\eta}{r}\left(w'_r+\frac{1}{r}w''_{\varphi\varphi}\right)\right\};\end{aligned} \tag{4.54}$$

$$\frac{\partial\Lambda}{\partial w''_{r\varphi}} = \frac{-Eh^3r}{24\left(1-\eta^2\right)}\left\{\frac{4\left(1-\eta\right)}{r^2}\left(w''_{r\varphi}-\frac{1}{r}w'_{\varphi}\right)\right\};\ \text{then}$$

$$\frac{\partial}{\partial\varphi}\left(\frac{\partial\Lambda}{\partial w''_{r\varphi}}\right) = \frac{-Eh^3r}{24\left(1-\eta^2\right)}\left\{\frac{4\left(1-\eta\right)}{r^2}w'''_{r\varphi\varphi}-\frac{4\left(1-\eta\right)}{r^3}w''_{\varphi\varphi}\right\}. \tag{4.55}$$

Combining Equations (4.53), (4.54) and (4.55) into Equation (4.120) gives:

$$\begin{aligned}&\frac{-Eh^3}{24\left(1-\eta^2\right)}\left\{\frac{2}{r}\left(w'_r+\frac{1}{r}w''_{\varphi\varphi}\right)+2\eta w''_{rr}\right\}+\\ &\frac{Eh^3}{24\left(1-\eta^2\right)}\left\{2rw'''_{rrr}-\frac{2\eta}{r}\left(w'_r+\frac{1}{r}w''_{\varphi\varphi}\right)+\right.\\ &\left.2\eta\left(w''_{rr}-\frac{1}{r^2}w''_{\varphi\varphi}+\frac{1}{r^2}w'''_{\varphi\varphi r}\right)\right\}+\\ &\frac{Eh^3}{24\left(1-\eta^2\right)}\left\{2w''_{rr}+\frac{2\eta}{r}\left(w'_r+\frac{1}{r}w''_{\varphi\varphi}\right)\right\}+\\ &\frac{Eh^3}{24\left(1-\eta^2\right)}\left\{\frac{4\left(1-\eta\right)}{r^2}w'''_{r\varphi\varphi}-\frac{4\left(1-\eta\right)}{r^2}w''_{\varphi\varphi}\right\}=0.\end{aligned} \tag{4.56}$$

Division of Equation (4.56) throughout by $\dfrac{Eh^3}{12\left(1-\eta^2\right)r}$ after simplification yields:

$$\begin{aligned}&w'''_{rrr}+\frac{w''_{rr}}{r}-\frac{1}{r^2}w'_r+\left(\frac{-3+\eta}{r^3}\right)w''_{\varphi\varphi}+\left(\frac{2-\eta}{r^2}\right)w'''_{r\varphi\varphi}\\ = {} & \left[w'''_{rrr}+\frac{w''_{rr}}{r}-\frac{1}{r^2}w'_r+\frac{2-\eta}{r^2}w'''_{r\varphi\varphi}-\frac{3-\eta}{r^3}w''_{\varphi\varphi}\right]\Bigg|_{r=a,\,b}=0.\end{aligned} \tag{4.57}$$

The other boundary condition for the free edge of the plate is:

$$\frac{\partial \Lambda}{\partial w''_{rr}} = \frac{-Eh^3 r}{24\left(1-\eta^2\right)}\left\{2w''_{rr} + \frac{2\eta}{r}\left(w'_r + \frac{1}{r}w''_{\varphi\varphi}\right)\right\} = 0. \tag{4.58}$$

Taking the non-trivial case which satisfies Equation (4.58) yields:

$$\begin{aligned} 2w''_{rr} + \frac{2\eta}{r}\left(w'_r + \frac{1}{r}w''_{\varphi\varphi}\right) &= 0; \text{ and} \\ w''_{rr} + \frac{\eta}{r}\left(w'_r + \frac{1}{r}w''_{\varphi\varphi}\right) &= 0. \end{aligned} \tag{4.59}$$

The boundary conditions in explicit form of the circular plate vibration are summarised as follows:

$$r = a,\, b:\; w|_{r=a,\,b} = 0; \tag{4.60}$$

or

$$\left[w'''_{rrr} + \frac{1}{r}w''_{rr} - \frac{1}{r^2}w'_r + \frac{2-\eta}{r^2}w'''_{r\varphi\varphi} - \frac{3-\eta}{r^3}w''_{\varphi\varphi}\right]_{r=a,\,b} = 0; \tag{4.61}$$

and

$$r = a,\, b:\; w'|_{r=a,\,b} = 0 \text{ or } \left[w''_{rr} + \frac{\eta}{r}\left(w'_r + \frac{1}{r}w''_{\varphi\varphi}\right)\right]_{r=a,b} = 0. \tag{4.62}$$

In the above boundary conditions: $[w]_{r=a,\,b} = 0$ and $[w']_{r=a,\,b} = 0$ correspond to the fixed rims of the plate, while the other boundary conditions:

$$\left[w'''_{rrr} + \frac{1}{r}w''_{rr} - \frac{1}{r^2}w'_r + \frac{2-\eta}{r^2}w'''_{r\varphi\varphi} - \frac{3-\eta}{r^3}w''_{\varphi\varphi} = 0\right]_{r=a,\,b};$$

and

$$\left[w''_{rr} + \frac{\eta}{r}\left(w'_r + \frac{1}{r}w''_{\varphi\varphi}\right) = 0\right];$$

correspond to the free boundaries or the free rims of the plate.

4.4.7 Boundary conditions in explicit form for the m^{th} vibrating mode

The explicit boundary conditions for a modal vibration of the form:

$$w\left(r,\varphi,t\right) = W\left(r\right)\cos\left(m\varphi\right)e^{i\omega t}; \tag{4.63}$$

can be obtained by substituting Equation (4.63) into Equations (4.60), (4.61) and (4.62), respectively. After performing the indicated differentiation the following is obtained:

$$\begin{aligned} r = a, b \text{ (respectively)} \qquad W|_{r=a,b} &= 0; \\ \text{or } \left[W'''_{rrr} + \frac{1}{r}W''_{rr} - \frac{\left(2-\eta\right)m^2+1}{r^2}W'_r + \left(\frac{3-\eta}{r^3}\right)m^2 W\right]_{r=a,b} &= 0; \end{aligned} \tag{4.64}$$

and

$$\begin{aligned} r = a, b \text{ (respectively)} \qquad W'_r|_{r=a,b} &= 0; \\ \text{or } \left[W''_{rr} + \frac{\eta}{r}W'_r + -\frac{\eta m^2}{r^2}W\right]_{r=a,b} &= 0. \end{aligned} \tag{4.65}$$

4.5 ANALYTICAL SOLUTION TO THE VIBRATING CIRCULAR PLATE

Assume that the transverse vibration of the plate vibrating at its m^{th}-mode is given by the time-harmonic solution of the form shown in Equation (4.63). Then substitution of Equation (4.63) into Equation (4.49) results in a fourth-order ODE. The procedure is demonstrated using Equation (4.63) as follows:

$$\frac{\partial^2 w}{\partial t^2} = \ddot{w} = -\omega^2 W \cos(m\varphi)\, e^{i\omega t}; \tag{4.66}$$

$$\begin{aligned}\nabla^2 w &= \frac{\partial^2 w}{\partial r^2} + \frac{1}{r}\frac{\partial w}{\partial r} + \frac{1}{r^2}\frac{\partial^2 w}{\partial \varphi^2} \\ &= \frac{\partial^2 W}{\partial r^2}\cos(m\varphi)\, e^{i\omega t} + \frac{1}{r}\frac{\partial W}{\partial r}\cos(m\varphi)\, e^{i\omega t} \\ &\quad -\frac{m^2}{r^2} W \cos(m\varphi)\, e^{i\omega t}.\end{aligned} \tag{4.67}$$

For the purpose of calculation, the procedure is as follows:

$$\nabla^2\nabla^2 w = \nabla^2\left(\frac{\partial^2 w}{\partial r^2}\right) + \nabla^2\left(\frac{1}{r}\frac{\partial w}{\partial r}\right) + \nabla^2\left(\frac{1}{r^2}\frac{\partial^2 w}{\partial \varphi^2}\right); \tag{4.68}$$

and differentiation is applied separately for each term. Using *Mathematica*'s symbolic computation makes the process effortless. Now differentiating Equation (4.67) twice with respect to r term by term gives:

$$\frac{\partial^2}{\partial r^2}\left[\frac{\partial^2 W}{\partial r^2}\cos(m\varphi)\, e^{i\omega t}\right] = \frac{\partial^4 W}{\partial r^4}\cos(m\varphi)\, e^{i\omega t}; \tag{4.69}$$

$$\frac{\partial^2}{\partial r^2}\left[\frac{1}{r}\frac{\partial W}{\partial r}\cos(m\varphi)\, e^{i\omega t}\right] = \left(\frac{2}{r^3}\frac{\partial W}{\partial r} - \frac{2}{r^2}\frac{\partial^2 W}{\partial r^2} + \frac{1}{r}\frac{\partial^3 W}{\partial r^3}\right)\cos(m\varphi)\, e^{i\omega t}; \text{ and} \tag{4.70}$$

$$\frac{\partial^2}{\partial r^2}\left[-\frac{m^2}{r^2} W \cos(m\varphi)\, e^{i\omega t}\right] = \left(-\frac{6m^2}{r^4} W + \frac{4m^2}{r^3}\frac{\partial W}{\partial r} - \frac{m^2}{r^2}\frac{\partial^2 W}{\partial r^2}\right)\cos(m\varphi)\, e^{i\omega t} \tag{4.71}$$

For the part $\dfrac{1}{r}\dfrac{\partial}{\partial r}$, it follows that:

$$\frac{1}{r}\frac{\partial}{\partial r}\left[\frac{\partial^2 W}{\partial r^2}\cos(m\varphi)\, e^{i\omega t}\right] = \frac{1}{r}\frac{\partial^3 W}{\partial r^3}\cos(m\varphi)\, e^{i\omega t}; \tag{4.72}$$

$$\frac{1}{r}\frac{\partial}{\partial r}\left[\frac{1}{r}\frac{\partial W}{\partial r}\cos(m\varphi)\, e^{i\omega t}\right] = \left(-\frac{1}{r^3}\frac{\partial W}{\partial r} + \frac{1}{r^2}\frac{\partial^2 W}{\partial r^2}\right)\cos(m\varphi)\, e^{i\omega t}; \text{ and} \tag{4.73}$$

$$\frac{1}{r}\frac{\partial}{\partial r}\left[-\frac{m^2}{r^2} W \cos(m\varphi)\, e^{i\omega t}\right] = \left(\frac{2m^2}{r^4} W - \frac{m^2}{r^3}\frac{\partial W}{\partial r}\right)\cos(m\varphi)\, e^{i\omega t}. \tag{4.74}$$

Similarly, for the part $\frac{1}{r^2}\frac{\partial^2}{\partial\varphi^2}$, differentiation yields:

$$\frac{1}{r^2}\frac{\partial^2}{\partial\varphi^2}\left[\frac{\partial^2 W}{\partial r^2}\cos(m\varphi)\,e^{i\omega t}\right] = -\frac{m^2}{r^2}\frac{\partial^2 W}{\partial r^2}\cos(m\varphi)\,e^{i\omega t}; \tag{4.75}$$

$$\frac{1}{r^2}\frac{\partial^2}{\partial\varphi^2}\left[\frac{1}{r}\frac{\partial W}{\partial r}\cos(m\varphi)\,e^{i\omega t}\right] = -\frac{m^2}{r^3}\frac{\partial W}{\partial r}\cos(m\varphi)\,e^{i\omega t};\ \text{and} \tag{4.76}$$

$$\frac{1}{r^2}\frac{\partial^2}{\partial\varphi^2}\left[-\frac{m^2}{r^2}W\cos(m\varphi)\,e^{i\omega t}\right] = \frac{m^4}{r^4}W\cos(m\varphi)\,e^{i\omega t}. \tag{4.77}$$

Substitution of Equations (4.66) to (4.77) into (4.49) gives:

$$\begin{aligned}\frac{12\rho(1-\eta^2)}{Eh^2}\ddot{w}+\nabla^4 w = &\left\{\frac{-12\rho(1-\eta^2)}{Eh^2}\omega^2 W+\left[\frac{\partial^4 W}{\partial r^4}+\left(\frac{1}{r}+\frac{1}{r}\right)\frac{\partial^3 W}{\partial r^3}+\right.\right.\\ &\left(\frac{2}{r^2}-\frac{m^2}{r^2}+\frac{1}{r^2}-\frac{m^2}{r^2}\right)\frac{\partial^2 W}{\partial r^2}+\\ &+\left(\frac{2}{r^3}+\frac{2m^2}{r^2}+\frac{2m^2}{r^2}-\frac{1}{r^3}-\frac{m^2}{r^3}-\frac{m^2}{r^3}\right)\frac{\partial W}{\partial r}+\\ &\left.\left.+\left(\frac{-6m^2}{r^4}+\frac{2m^2}{r^4}+\frac{m^4}{r^4}\right)W\right]\right\}\cos(m\varphi)\,e^{i\omega t}=0.\end{aligned} \tag{4.78}$$

The eigenfunction W is a function of only r and thus the differential equation becomes an ODE. Equation (4.78) after simplification becomes:

$$\begin{aligned}\frac{12\rho(1-\eta^2)}{Eh^2}\ddot{w}+\nabla^4 w = &\left\{\frac{-12\rho(1-\eta^2)}{Eh^2}\omega^2 W+\left[\frac{d^4 W}{dr^4}+\frac{2}{r}\frac{d^3 W}{dr^3}-\right.\right.\\ &-\left(\frac{2m^2+1}{r^2}\right)\frac{d^2 W}{dr^2}+\left(\frac{2m^2+1}{r^3}\right)\frac{dW}{dr}+\\ &\left.\left.+\frac{m^4-4m^2}{r^4}W\right]\right\}\cos(m\varphi)\,e^{i\omega t}=0.\end{aligned} \tag{4.79}$$

Due to the periodic nature of φ for a non-trivial case Equation (4.79) reduces to:

$$\begin{aligned}&\frac{d^4 W}{dr^4}+\frac{2}{r}\frac{d^3 W}{dr^3}-\left(\frac{2m^2+1}{r^2}\right)\frac{d^2 W}{dr^2}+\\ &\left(\frac{2m^2+1}{r^3}\right)\frac{dW}{dr}+\left[\frac{m^4-4m^2}{r^4}-\frac{12\rho(1-\eta^2)}{Eh^2}\omega^2\right]W=0.\end{aligned} \tag{4.80}$$

Note that the function $W(r)$ is the eigenfunction of the vibrating circular plate with a mode number m.

4.5.1 Solution for a circular plate with free vibration

Assume that the vibration of the circular plate under consideration is free and given by Equation (4.63) thus, Equation (4.80) can be rewritten as:

$$\nabla^4 W-\beta^4 W=0; \tag{4.81}$$

where:

$$\beta^4 = \frac{12\rho\left(1-\eta^2\right)\omega^2}{Eh^2} = \frac{12\left(1-\eta^2\right)\rho\omega^2 h}{Eh^3} = \frac{\rho\omega^2 h}{D}; \tag{4.82}$$

with $D = \dfrac{Eh^3}{12\left(1-\eta^2\right)}$ is the flexural rigidity of the plate. Thus Equation (4.81) can now be rewritten as:

$$\left(\nabla^4 - \beta^4\right) W = 0; \text{ or} \tag{4.83}$$

$$\left(\nabla^2 + \beta^2\right)\left(\nabla^2 - \beta^2\right) W = 0. \tag{4.84}$$

Now define two functions $W_1$and W_2 such that:

$$w_1\left(r,\varphi,t\right) = W_1\left(r\right)\cos\left(m\varphi\right)e^{i\omega t}; \tag{4.85}$$

and

$$w_2\left(r,\varphi,t\right) = W_2\left(r\right)\cos\left(m\varphi\right)e^{i\omega t}; \tag{4.86}$$

with

$$\left(\nabla^2 + \beta^2\right) W_1 = 0; \tag{4.87}$$

and

$$\left(\nabla^2 - \beta^2\right) W_2 = 0. \tag{4.88}$$

The operators $\left(\nabla^2 + \beta^2\right)$ and $\left(\nabla^2 - \beta^2\right)$ commute, thus by the theory of linear differential equations (Zill & Cullen, 2009, [71]), the solution to Equation (4.84) is given by the superpositions of the solutions to W_1 and W_2. Substitution of Equations (4.85) and (4.86), respectively, into Equations (4.87) and (4.88) yields:

$$\frac{d^2W_1}{dr^2} + \frac{1}{r}\frac{dW_1}{dr} + \left(\beta^2 - \frac{m^2}{r^2}\right) W_1 = 0; \text{ and} \tag{4.89}$$

$$\frac{d^2W_2}{dr^2} + \frac{1}{r}\frac{dW_2}{dr} - \left(\beta^2 + \frac{m^2}{r^2}\right) W_2 = 0. \tag{4.90}$$

Solving the Bessel equations shown above yields solutions of the form:

$$W_1\left(r\right) = A_1 J_m\left(\beta r\right) + A_2 Y_m\left(\beta r\right); \tag{4.91}$$

and

$$W_2\left(r\right) = A_3 I_m\left(\beta r\right) + A_4 K_m\left(\beta r\right); \tag{4.92}$$

meaning that the general solution to Equation (4.84) is given by the superposition of Equations (4.91) and (4.92) as:

$$W\left(r\right) = A_1 J_m\left(\beta r\right) + A_2 Y_m\left(\beta r\right) + A_3 I_m\left(\beta r\right) + A_4 K_m\left(\beta r\right); \tag{4.93}$$

where the coefficients A_1, A_2, A_3 and A_4 determine the mode shapes. A more general solution to

the vibrating plate in polar coordinates can be written as (Leissa, 1969, [38]):

$$w(r,\varphi,t) = \sum_{m=0}^{\infty}\left[A_1 J_m(\beta r) + A_2 Y_m(\beta r) + A_3 I_m(\beta r) + A_4 K_m(\beta r)\right]\cos(m\varphi)\, e^{i\omega t} + \sum_{m=1}^{\infty}\left[A_1 J_m(\beta r) + A_2 Y_m(\beta r) + A_3 I_m(\beta r) + A_4 K_m(\beta r)\right]\sin(m\varphi)\, e^{i\omega t}. \quad (4.94)$$

Here $J_m(\beta r)$ and $Y_m(\beta r)$ are Bessel functions of the first and second kind, respectively, of order m. The functions $I_m(\beta r)$ and $K_m(\beta r)$ are modified Bessel functions of the first and second kind, respectively, of order m. The arbitrary constants of integration A_1, A_2, A_3 and A_4 are determined from the boundary conditions and they determine the mode shape. Note that unless stated otherwise, throughout this thesis the vibration mode number investigated for the out-of-plane vibration of the disc is $m = 3$ and hence a solution of the form given by Equation (4.93) is used in all investigations with regard to the out-of-plane vibrations of the disc.

4.5.2 Orthogonality of the eigenfunctions

Consider the differential equation as given by Equation (4.83) and suppose two eigenfunctions W_r and W_s related to the equation with the corresponding eigenvalues ω_r and ω_s of Equation (4.80), such that:

$$D\nabla^4 W_r - \omega_r^2 \rho h W_r = 0; \text{ and} \quad (4.95)$$

$$D\nabla^4 W_s - \omega_s^2 \rho h W_s = 0. \quad (4.96)$$

Multiplication of Equation (4.95) by W_s and Equation (4.96) by W_r and integrating the difference of the two over the domain (area A) of the plate gives:

$$\int_A \left[DW_s\nabla^4 W_r - DW_r\nabla^4 W_s - \left(\omega_r^2 - \omega_s^2\right)\rho h W_r W_s\right] dA = 0. \quad (4.97)$$

The bi-harmonic operator ∇^4 can be written as $\nabla^4 = \nabla\cdot[\nabla(\nabla\cdot\nabla W)]$ and rewriting Equation (4.97) by using the Gauss divergence theorem (Reddy, 2004, [58]), (Stroud & Booth, 2003, [72]) yields:

$$D\oint_S \left[\begin{array}{c} W_r\hat{n}\cdot\nabla\left(\nabla^2 W_s\right) - W_s\hat{n}\cdot\nabla\left(\nabla^2 W_r\right) + \nabla^2 W_r\hat{n}\cdot\nabla W_s - \\ \nabla^2 W_s\hat{n}\cdot\nabla W_r \end{array}\right] dS - \left(\omega_r^2 - \omega_s^2\right)\int_A \rho h W_r W_s dA = 0. \quad (4.98)$$

Here S is the boundary of the plate area A and $\hat{n}$ is the unit outward normal vector to the boundary S. If $\omega_r \neq \omega_s$ and:

$$\oint_S \left[\begin{array}{c} W_r\hat{n}\cdot\nabla\left(\nabla^2 W_s\right) - W_s\hat{n}\cdot\nabla\left(\nabla^2 W_r\right) + \nabla^2 W_r\hat{n}\cdot\nabla W_s - \\ \nabla^2 W_s\hat{n}\cdot\nabla W_r \end{array}\right] dS = 0; \quad (4.99)$$

then it can be concluded from Equation (4.98) that:

$$\int_A \rho h W_r W_s dA = 0; \tag{4.100}$$

which is the orthogonality relationship for arbitrary eigenfunctions of the plate for clamped, free or with any form of boundary conditions. It can be seen from Equation (4.99) that the eigenfunctions are self-adjoint.

4.5.3 Solution of a circular plate with a boundary excitation

In this sub-section an annular circular plate of inner radius a and outer radius b mounted on a massless rigid load is considered. Assume that the excitation is only at the inner edge of the plate and that the outer edge is free. Now consider an axisymmetrical excitation force along the z-axis of the plate as:

$$f = \hat{f} \sin \nu t; \tag{4.101}$$

where $\hat{f}$ is the amplitude of the excitation force, ν is the angular frequency of the excitation force and t is time. In this case only the boundary of the disc is excited and hence the governing equation of the out-of-plane vibration remains unchanged. Thus the governing equation of motion of the out-of-plane vibration of the disc is:

$$\frac{12\rho\left(1-\eta^2\right)}{Eh^2}\ddot{w} + \nabla^4 w = 0;$$

with explicit boundary conditions:

$$W_r'|_{r=a} = 0; \tag{4.102}$$

or

$$\left[W_{rrr}''' + \frac{1}{r}W_{rr}'' - \frac{(2-\eta)\,m^2+1}{r^2}W_r' + \left(\frac{3-\eta}{r^3}\right)m^2 W\right]\Bigg|_{r=a} = \frac{-\hat{f}\sin\nu t}{2\pi a}; \tag{4.103}$$

and

$$\left[W_{rrr}''' + \frac{1}{r}W_{rr}'' - \frac{(2-\eta)\,m^2}{r^2}W_r' + \left(\frac{3-\eta}{r^3}\right)m^2 W\right]\Bigg|_{r=b} = 0; \tag{4.104}$$

or

$$\left[W_{rr}'' + \frac{\eta}{r}W_r' + \frac{\eta m^2}{r^2}W\right]\Bigg|_{r=b} = 0. \tag{4.105}$$

The modified solution of the equation with respect to the given boundary conditions can be given as:

$$w\left(r,\varphi,t\right) = W\left(r\right)\cos\left(m\varphi+\gamma_m\right)\sin\left(\nu t\right); \tag{4.106}$$

where:

$$W\left(r\right) = A_1 J_m\left(\beta r\right) + A_2 Y_m\left(\beta r\right) + C_3 I_m\left(\beta r\right) + C_4 K_m\left(\beta r\right); \tag{4.107}$$

is the eigenfunction of the out-of-plane vibration, and γ_m is the phase angle. Since the boundary forcing introduced here is along the z-axis, the solution is independent of m and thus has the form:

$$w(r,\varphi,t) = [A_1 J_0(\beta r) + A_2 Y_0(\beta r) + A_3 I_0(\beta r) + A_4 K_0(\beta r)] \sin(\nu t); \tag{4.108}$$

in which the order of each Bessel function is $m = 0$. The unknowns A_1, A_2, A_3 and A_4 can be obtained by substituting the solution given by Equation (4.108) into the boundary conditions given in Equations (4.102) to (4.105) and solving the resulting matrix equation.

4.5.4 Solution for a circular plate with a flexible foundation

Suppose that a circular disc in the form of a plate is supported by or embedded in an elastic massless foundation with a stiffness constant K. The derivation of the equations of motion follows from Section 4.4 and can be written as:

$$\frac{12\rho(1-\eta^2)}{Eh^2}\ddot{w} + \nabla^4 w + Kw = 0; \tag{4.109}$$

where K is the stiffness of the elastic foundation. As before, suppose a harmonic solution of the form:

$$w(r,\varphi,t) = W(r)\cos(m\varphi)\, e^{i\omega t}. \tag{4.110}$$

Substitution of Equation (4.110) into Equation (4.109) can be simplified to yield:

$$\begin{aligned}
\frac{12\rho(1-\eta^2)}{Eh^2}\ddot{w} + \nabla^4 w + Kw &= 0; \\
-\rho h\omega^2 W + D\nabla^4 W + KW &= 0; \\
\nabla^4 W - \left(\frac{\rho h\omega^2 - K}{D}\right) W &= 0; \text{ and} \\
\nabla^4 W - \tilde{\beta}^4 W &= 0;
\end{aligned} \tag{4.111}$$

with

$$\tilde{\beta}^4 = \left(\frac{\rho h\omega^2 - K}{D}\right). \tag{4.112}$$

The analytical solution to Equation (4.111) is given in simplified form as:

$$W(r) = A_1 J_m\left(\tilde{\beta} r\right) + A_2 Y_m\left(\tilde{\beta} r\right) + A_3 I_m\left(\tilde{\beta} r\right) + A_4 K_m\left(\tilde{\beta} r\right), \tag{4.113}$$

where $\tilde{\beta}^4$ is given by Equation (4.112). The general solution to the plate with a flexible elastic foundation then becomes:

$$w(r,\varphi,t) = \left[A_1 J_m\left(\tilde{\beta} r\right) + A_2 Y_m\left(\tilde{\beta} r\right) + A_3 I_m\left(\tilde{\beta} r\right) + A_4 K_m\left(\tilde{\beta} r\right)\right] \cos(m\varphi)\, e^{i\omega t}. \tag{4.114}$$

4.5.5 Plates with varying thickness

The discussions covered so far with respect to the out-of-plane vibration of the disc gyroscope were based on a constant thickness h, to simplify the model. However, circular plates of non-uniform thickness are not uncommon (Timoshenko & Woinowsky-Krieger, 1959, [37]). Examples of circular plates with variable thickness are encountered in machine parts, steam turbines and the pistons of reciprocating engines.

Hagedorn and DasGupta (2007, [70]) have demonstrated the equation of free vibration of a rectangular plate with varying thickness in rectangular coordinates as:

$$\rho h\ddot{w} + \nabla^2\left(D\nabla^2 w\right) - (1-\eta)\left(D''_{xx}w''_{yy} - 2D''_{xy}w''_{xx} + D''_{yy}w''_{xx}\right) = 0. \tag{4.115}$$

The equations of motion for a circular plate with varying thickness after manipulation of Equation (4.115) in polar coordinates yields:

$$\rho h\ddot{w} + \nabla^2\left(D\nabla^2 w\right) - (1-\eta)\left(D_{rr}\left(\frac{1}{r}w'_r + \frac{1}{r^2}w''_{\varphi\varphi}\right) + \frac{1}{r}D'_r w''_{rr}\right) = 0; \tag{4.116}$$

with $h = h\,(r)$, and

$$D = D\,(r) = \frac{Eh\,(r)}{12\,(1-\eta^2)}.$$

If the deflection of the disc in its out-of-plane direction is given by:

$$w\,(r,\varphi,t) = W\,(r)\,e^{im\varphi}e^{i\omega t}; \tag{4.117}$$

then substitution of Equation (4.117) into Equation (4.116) for the non-trivial case gives:

$$W''''_{rrrr} + g_3 W'''_{rrr} + g_2 W''_{rr} + g_1 W'_r + \left[g_0 - \omega^2\rho h\right] W = 0; \tag{4.118}$$

where $g_i = g_i\,(r)$ for $i = 0, 1, 2, 3$. Note that Equation (4.118) can be solved using the Galerkin method (Hagedorn & DasGupta, 2007, [70]). The Galerkin method is not discussed in this thesis and is left for future study.

4.6 NUMERICAL SOLUTIONS

In this section the eigenfunctions for the vibrating circular plate which correspond to the out-of-plane vibration of a thin disc gyroscope are calculated. To calculate the eigenfunctions, the boundary conditions given by Equations (4.64) and (4.65) with the analytical solution given by Equation (4.93) are used. To demonstrate the procedure, the disc in plate mode with both clamped and free edges is considered. The physical and geometrical characteristics of the plate are similar to the ones considered for in-plane vibrations as demonstrated in Chapter 3. In this section the in-plane vibrations are neglected and only transverse vibration is considered. The eigenvalues are

numerically calculated for the mode number $m = 3$. To speed up the calculation process CAS programmes such as MATHEMATICA® and MAPLE™ are used. The codes for all calculations are given in Appendix A.

The rules for the calculation of the first and second derivatives of the Bessel functions of the first and second kind as well as for the modified Bessel functions of the first and second kind are used to aid in symbolic calculations. Recall the identities:

$$\begin{aligned}
\frac{d}{dr}J_m(\alpha r) &= J'_m(\alpha r) = \frac{m}{r}J_m(\alpha r) - \alpha J_{m+1}(\alpha r);\\
\frac{d}{dr}Y_m(\alpha r) &= Y'_m(\alpha r) = \frac{m}{r}Y_m(\alpha r) - \alpha Y_{m+1}(\alpha r);\\
\frac{d}{dr}I_m(\alpha r) &= I'_m(\alpha r) = \frac{m}{r}I_m(\alpha r) + \alpha I_{m+1}(\alpha r); \text{ and}\\
\frac{d}{dr}K_m(\alpha r) &= K'_m(\alpha r) = \frac{m}{r}K_m(\alpha r) - \alpha K_{m+1}(\alpha r).
\end{aligned} \tag{4.119}$$

To solve for the constants A_1, A_2, A_3 and A_4, Equation (4.93) is substituted into the equations of each pair of boundary conditions given by Equations (4.64) and (4.65) and the resulting matrix equation is solved numerically to obtain the approximate eigenvalues. Once the approximate eigenvalues are obtained, the constants can be obtained using Cramer's rule for each respective boundary condition. In the subsections to follow, various types of boundary conditions of the plate are considered to approximate the eigenvalues and eigenfrequencies.

4.6.1 Solid circular plate clamped at its edge

For a solid plate clamped at its edge, the boundary conditions in explicit form can be obtained from Equations (4.64) and (4.65). Thus:

$$r = b \qquad W(r)|_{r=b} = 0; \text{ and } W'(r)|_{r=b} = 0. \tag{4.120}$$

Similar to the in-plane vibrations, the matrix equation can be obtained by substituting Equation (4.93) into Equations (4.64) and (4.65), respectively. The resulting matrix is a 2×2 because the Bessel functions Y_m and K_m are not bounded for $a = 0$. The resulting matrix equation has the form:

$$\underbrace{\begin{pmatrix} b_{11} & b_{12} \\ b_{21} & b_{22} \end{pmatrix}}_{\mathbf{N}_1} \begin{pmatrix} A_1 \\ A_3 \end{pmatrix} = 0; \tag{4.121}$$

where:

$$b_{11} = J_m(\beta r),\ b_{12} = I_m(\beta r); \tag{4.122}$$

$$b_{21} = \frac{1}{2}\beta\left[J_{m-1}(\beta b) - J_{m+1}(\beta b)\right];\ \text{and}\ b_{22} = \frac{1}{2}\beta\left[I_{m-1}(\beta b) + I_{m+1}(\beta b)\right]. \tag{4.123}$$

If $A_1 = 1$, then:

$$A_3 = -\frac{b_{11}(\omega_p)}{b_{12}(\omega_p)}; \tag{4.124}$$

where ω_p is the angular frequency of the out-of-plane vibration. For a non-trivial solution to Equation (4.121), the determinant of the coefficient matrix vanishes. That is:

$$\det(\mathbf{N}_1) = \det(DP) = 0. \tag{4.125}$$

Solving this transcendental characteristic equation yields, for each circumferential wave number m, *a sequence of eigenvalues* $\omega_{mp,k}$ $(k = 0, 1, 2, 3, \cdots)$ with:

$$\omega_{mp,0} < \omega_{mp,1} < \omega_{mp,2} < \cdots. \tag{4.126}$$

The eigenvalue $\omega_{mp,0}$ is called the *fundamental vibration eigenvalue* while $\omega_{mp,1}$ is called the *first overtone vibration eigenvalue*, and so forth. Results for the fundamental and the first five *overtone vibration eigenvalues* and the associated *eigenfrequencies* for the solid plate clamped at its edge for $m = 3$ are given in Table 4.1

Table 4.1: The fundamental and the first five overtone vibration eigenvalues and the associated eigenfrequencies of a clamped solid plate vibrating at $m = 3$

k	$\omega_{3p,k}\left(\mathrm{rad\,s^{-1}}\right)$	$f_{3p,k} = \frac{\omega_{3,k}}{2\pi}\,(\mathrm{Hz})$
0	765736.6	121870.8
1	1.665943×10^6	265143.1
2	2.855623×10^6	454486.6
3	4.339319×10^6	690624.1
4	6.118228×10^6	973746.2
5	8.192806×10^6	1.303926×10^6

To calculate the values of the eigenvalues and eigenfrequencies given in Table 4.1, the MATHEMATICA® function "*FindRoot"* is used. The first approximate values of both the eigenvalue and eigenfrequency are obtained from the graph of the logarithm of the modulus of the function given in Equation (4.125). The idea is that, the approximate values of the horizontal components of the coordinates of spikes correspond to the zeros of the characteristic equation given by Equation (4.125), thus the approximate coordinate of the first spike is $(758191.7321, 25.3912)$. Using "*FindRoot"* the more accurate value of the *fundamental vibration eigenvalue* is $\omega_{3p,0} = 765736.6\,\mathrm{rad\,s^{-1}}$. Its corresponding *fundamental eigenfrequency* is $f_{3p,0} = \dfrac{\omega_{3p,0}}{2\pi} \approx 121870.8\,\mathrm{Hz}$.

The subsequent eigenvalues and eigenfrequencies to the latter, in Table 4.1 are obtained using the same procedure. The graph of the normalised transverse eigenfunction for a clamped solid plate

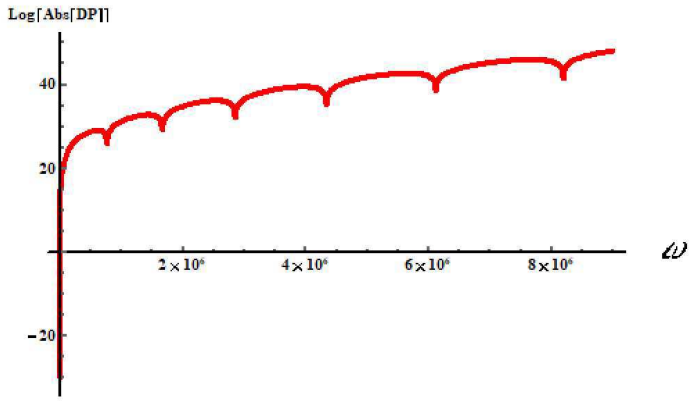

Figure 4.2: The graph used to estimate the eigenvalues and eigenfrequencies of a clamped solid plate

is presented in Figure 4.3. Due to the moment and edge forces at the clamped "sides" of the plate, the displacement is zero. The displacement of the plate is maximum at approximately half of the radius of the plate. The displacement is not necessarily zero at the centre of the plate.

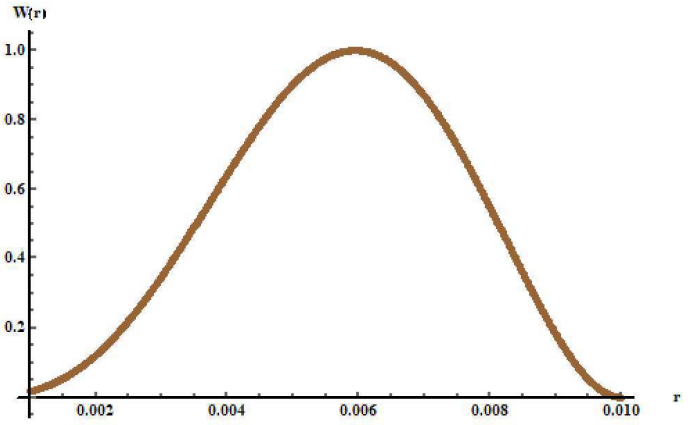

Figure 4.3: The normalised eigenfunction $W(r)$ corresponding to the eigenvalue $\omega_{3,0} = 765736.6\,\mathrm{rad.\,s^{-1}}$ for a solid aluminium disc in its plate form clamped at the edge

The normalised eigenfunction for the eigenvalue $\omega_{3p,1}$ is given in Figure 4.4. The deflection of the plate becomes zero around the clamped edge of the plate.

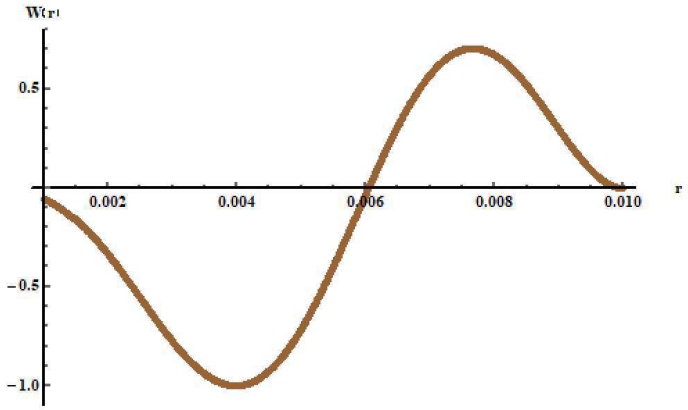

Figure 4.4: The normalised eigenfunction $W(r)$ corresponding to the eigenvalue $\omega_{3,1} = 1.665943 \times 10^6\,\mathrm{rad.s^{-1}}$ for a solid aluminium disc in its plate form clamped at the edge

4.6.2 Annular plate with free edges

This subsection presents the determination of eigenvalues, eigenfunctions and their nature for the annular plate, free at both edges. The explicit boundary conditions for the annular plate vibrating freely with mode number m are given by:

$$\left[W'''_{rrr} + \frac{1}{r}W''_{rr} - \frac{(2-\eta)\,m^2+1}{r^2}W'_r + \left(\frac{3-\eta}{r^3}\right)m^2 W\right]_{r=a,b} = 0; \tag{4.127}$$

and

$$\left[W''_{rr} + \frac{\eta}{r}W'_r + -\frac{\eta m^2}{r^2}W\right]_{r=a,b} = 0; \tag{4.128}$$

where W is a function of only radius of the plate. Similar procedures as those performed for the solid clamped plate are employed here for the determination of both the eigenvalues and eigenfrequencies. Substitution of Equation (4.93) into Equation (4.127) yields:

$$\begin{aligned}
&-A_1\frac{m}{a}\left(\left[\frac{(1-\eta)\,m\,(m-1)}{a^2}+\beta^2\right]J_m(\beta a)+\beta\left[\frac{(1-\eta)\,m^2}{a^2}+\beta^2\right]J_{m+1}(\beta a)\right)-\\
&A_2\frac{m}{a}\left(\left[\frac{(1-\eta)\,m\,(m-1)}{a^2}+\beta^2\right]Y_m(\beta a)+\beta\left[\frac{(1-\eta)\,m^2}{a^2}+\beta^2\right]Y_{m+1}(\beta a)\right)+\\
&A_3\frac{m}{a}\left(\left[-\frac{(1-\eta)\,m\,(m-1)}{a^2}+\beta^2\right]I_m(\beta a)+\beta\left[-\frac{(1-\eta)\,m^2}{a^2}+\beta^2\right]I_{m+1}(\beta a)\right)+\\
&A_4\frac{m}{a}\left(\left[-\frac{(1-\eta)\,m\,(m-1)}{a^2}+\beta^2\right]K_m(\beta a)+\beta\left[\frac{(1-\eta)\,m^2}{a^2}+\beta^2\right]K_{m+1}(\beta a)\right)\\
=\;&0.
\end{aligned} \tag{4.129}$$

The matrix form of Equation (4.129) is:

$$\begin{bmatrix} -\frac{m}{a}\left(\left[\frac{(1-\eta)\,m\,(m-1)}{a^2}+\beta^2\right]J_m(\beta a)+\beta\left[\frac{(1-\eta)\,m^2}{a^2}+\beta^2\right]J_{m+1}(\beta a)\right) \\ -\frac{m}{a}\left(\left[\frac{(1-\eta)\,m\,(m-1)}{a^2}+\beta^2\right]Y_m(\beta a)+\beta\left[\frac{(1-\eta)\,m^2}{a^2}+\beta^2\right]Y_{m+1}(\beta a)\right) \\ \frac{m}{a}\left(\left[-\frac{(1-\eta)\,m\,(m-1)}{a^2}+\beta^2\right]I_m(\beta a)+\beta\left[-\frac{(1-\eta)\,m^2}{a^2}+\beta^2\right]I_{m+1}(\beta a)\right) \\ \frac{m}{a}\left(\left[-\frac{(1-\eta)\,m\,(m-1)}{a^2}+\beta^2\right]K_m(\beta a)+\beta\left[\frac{(1-\eta)\,m^2}{a^2}+\beta^2\right]K_{m+1}(\beta a)\right) \end{bmatrix}^T \begin{bmatrix} A_1 \\ A_2 \\ A_3 \\ A_4 \end{bmatrix} = 0. \tag{4.130}$$

By a similar analogy, the second boundary condition given by Equation (4.65) for the free inner edge of the plate can be written as:

$$\begin{aligned} & A_1\frac{m}{a}\left(\left[\frac{(1-\eta)\,m\,(m-1)}{a^2}-\beta^2\right]J_m(\beta a)+\frac{(1-\eta)\,\beta}{a}J_{m+1}(\beta a)\right)+ \\ & A_2\frac{m}{a}\left(\left[\frac{(1-\eta)\,m\,(m-1)}{a^2}-\beta^2\right]Y_m(\beta a)+\frac{(1-\eta)\,\beta}{a}Y_{m+1}(\beta a)\right)+ \\ & A_3\frac{m}{a}\left(\left[-\frac{(1-\eta)\,m\,(m-1)}{a^2}+\beta^2\right]I_m(\beta a)-\frac{(1-\eta)\,\beta}{a}I_{m+1}(\beta a)\right)+ \\ & A_4\frac{m}{a}\left(\left[-\frac{(1-\eta)\,m\,(m-1)}{a^2}+\beta^2\right]K_m(\beta a)+\frac{(1-\eta)\,\beta}{a}K_{m+1}(\beta a)\right) \\ = \;& 0. \end{aligned} \tag{4.131}$$

The corresponding matrix format of Equation (4.131) is given by:

$$\begin{bmatrix} \frac{m}{a}\left(\left[\frac{(1-\eta)\,m\,(m-1)}{a^2}-\beta^2\right]J_m(\beta a)+\frac{(1-\eta)\,\beta}{a}J_{m+1}(\beta a)\right) \\ \frac{m}{a}\left(\left[\frac{(1-\eta)\,m\,(m-1)}{a^2}-\beta^2\right]Y_m(\beta a)+\frac{(1-\eta)\,\beta}{a}Y_{m+1}(\beta a)\right) \\ \frac{m}{a}\left(\left[-\frac{(1-\eta)\,m\,(m-1)}{a^2}+\beta^2\right]I_m(\beta a)-\frac{(1-\eta)\,\beta}{a}I_{m+1}(\beta a)\right) \\ \frac{m}{a}\left(\left[-\frac{(1-\eta)\,m\,(m-1)}{a^2}+\beta^2\right]K_m(\beta a)+\frac{(1-\eta)\,\beta}{a}K_{m+1}(\beta a)\right) \end{bmatrix}^T \begin{bmatrix} A_1 \\ A_2 \\ A_3 \\ A_4 \end{bmatrix} = 0. \tag{4.132}$$

Similarly, the boundary conditions for the free outer rim of the plate are used as shown next. The

first boundary condition (4.127), can be written as:

$$\begin{aligned}
&-A_1\frac{m}{b}\left(\left[\frac{(1-\eta)\,m\,(m-1)}{b^2}+\beta^2\right]J_m(\beta b)+\beta\left[\frac{(1-\eta)\,m^2}{b^2}+\beta^2\right]J_{m+1}(\beta b)\right)-\\
&A_2\frac{m}{b}\left(\left[\frac{(1-\eta)\,m\,(m-1)}{b^2}+\beta^2\right]Y_m(\beta b)+\beta\left[\frac{(1-\eta)\,m^2}{b^2}+\beta^2\right]Y_{m+1}(\beta b)\right)+\\
&A_3\frac{m}{b}\left(\left[-\frac{(1-\eta)\,m\,(m-1)}{b^2}+\beta^2\right]I_m(\beta b)+\beta\left[-\frac{(1-\eta)\,m^2}{b^2}+\beta^2\right]I_{m+1}(\beta b)\right)+\\
&A_4\frac{m}{b}\left(\left[-\frac{(1-\eta)\,m\,(m-1)}{b^2}+\beta^2\right]K_m(\beta b)+\beta\left[\frac{(1-\eta)\,m^2}{b^2}+\beta^2\right]K_{m+1}(\beta b)\right)\\
=\;&0. \qquad (4.133)
\end{aligned}$$

The matrix form of Equation (4.133) is:

$$\begin{bmatrix}
-\frac{m}{b}\left[\frac{(1-\eta)\,m\,(m-1)}{b^2}+\beta^2\right]J_m(\beta b)+\beta\left[\frac{(1-\eta)\,m^2}{b^2}+\beta^2\right]J_{m+1}(\beta b)\\
-\frac{m}{b}\left(\left[\frac{(1-\eta)\,m\,(m-1)}{b^2}+\beta^2\right]Y_m(\beta b)+\beta\left[\frac{(1-\eta)\,m^2}{b^2}+\beta^2\right]Y_{m+1}(\beta b)\right)\\
\frac{m}{b}\left(\left[-\frac{(1-\eta)\,m\,(m-1)}{b^2}+\beta^2\right]I_m(\beta b)+\beta\left[-\frac{(1-\eta)\,m^2}{b^2}+\beta^2\right]I_{m+1}(\beta b)\right)\\
\frac{m}{b}\left(\left[-\frac{(1-\eta)\,m\,(m-1)}{b^2}+\beta^2\right]K_m(\beta b)+\beta\left[\frac{(1-\eta)\,m^2}{b^2}+\beta^2\right]K_{m+1}(\beta b)\right)
\end{bmatrix}^T
\begin{bmatrix}A_1\\A_2\\A_3\\A_4\end{bmatrix}=0. \qquad (4.134)$$

The second boundary condition (4.65) for the free outer rim of the plate can be written as:

$$\begin{aligned}
&A_1\frac{m}{b}\left(\left[\frac{(1-\eta)\,m\,(m-1)}{b^2}-\beta^2\right]J_m(\beta b)+\frac{(1-\eta)\,\beta}{b}J_{m+1}(\beta b)\right)+\\
&A_2\frac{m}{b}\left(\left[\frac{(1-\eta)\,m\,(m-1)}{b^2}-\beta^2\right]Y_m(\beta b)+\frac{(1-\eta)\,\beta}{b}Y_{m+1}(\beta b)\right)+\\
&A_3\frac{m}{b}\left(\left[-\frac{(1-\eta)\,m\,(m-1)}{b^2}+\beta^2\right]I_m(\beta b)-\frac{(1-\eta)\,\beta}{b}I_{m+1}(\beta b)\right)+\\
&A_4\frac{m}{b}\left(\left[-\frac{(1-\eta)\,m\,(m-1)}{b^2}+\beta^2\right]K_m(\beta b)+\frac{(1-\eta)\,\beta}{b}K_{m+1}(\beta b)\right)\\
=\;&0. \qquad (4.135)
\end{aligned}$$

The corresponding matrix form of Equation (4.135) is given by:

$$\begin{bmatrix}
\frac{m}{b}\left(\left[\frac{(1-\eta)\,m\,(m-1)}{b^2}-\beta^2\right]J_m(\beta b)+\frac{(1-\eta)\,\beta}{b}J_{m+1}(\beta b)\right)\\
\frac{m}{b}\left(\left[\frac{(1-\eta)\,m\,(m-1)}{b^2}-\beta^2\right]Y_m(\beta b)+\frac{(1-\eta)\,\beta}{b}Y_{m+1}(\beta b)\right)\\
\frac{m}{b}\left(\left[-\frac{(1-\eta)\,m\,(m-1)}{b^2}+\beta^2\right]I_m(\beta b)-\frac{(1-\eta)\,\beta}{b}I_{m+1}(\beta b)\right)\\
\frac{m}{b}\left(\left[-\frac{(1-\eta)\,m\,(m-1)}{b^2}+\beta^2\right]K_m(\beta b)+\frac{(1-\eta)\,\beta}{b}K_{m+1}(\beta b)\right)
\end{bmatrix}^T
\begin{bmatrix}A_1\\A_2\\A_3\\A_4\end{bmatrix}=0. \qquad (4.136)$$

Equations (4.130), (4.132), (4.134) and (4.136) can be combined to give a system of homogeneous

linear equations with respect to A_1, A_2, A_3 and A_4. That is:

$$\underbrace{\begin{bmatrix} c_{11} & c_{12} & c_{13} & c_{14} \\ c_{21} & c_{22} & c_{23} & c_{24} \\ c_{31} & c_{32} & c_{33} & c_{34} \\ c_{41} & c_{42} & c_{43} & c_{44} \end{bmatrix}}\begin{bmatrix} A_1 & A_2 & A_3 & A_4 \end{bmatrix}^T = 0; \tag{4.137}$$

where $c_{ij} = c_{ij}(\beta) = c_{ij}(\omega)$,$\forall i,j = 0,1,2,3,4$ are the components of the 4×4 matrix. The components are given as follows:

$$\begin{aligned}
c_{11} &= -\frac{m}{a}\left[\frac{(1-\eta)\,m\,(m-1)}{a^2}+\beta^2\right]J_m(\beta a)+\beta\left[\frac{(1-\eta)\,m^2}{a^2}+\beta^2\right]J_{m+1}(\beta a);\\
c_{12} &= -\frac{m}{a}\left(\left[\frac{(1-\eta)\,m\,(m-1)}{a^2}+\beta^2\right]Y_m(\beta a)+\beta\left[\frac{(1-\eta)\,m^2}{a^2}+\beta^2\right]Y_{m+1}(\beta a)\right);\\
c_{13} &= \frac{m}{a}\left(\left[-\frac{(1-\eta)\,m\,(m-1)}{a^2}+\beta^2\right]I_m(\beta a)+\beta\left[-\frac{(1-\eta)\,m^2}{a^2}+\beta^2\right]I_{m+1}(\beta a)\right);\\
c_{14} &= \frac{m}{a}\left(\left[-\frac{(1-\eta)\,m\,(m-1)}{a^2}+\beta^2\right]K_m(\beta a)+\beta\left[\frac{(1-\eta)\,m^2}{a^2}+\beta^2\right]K_{m+1}(\beta a)\right);\\
c_{21} &= \frac{m}{a}\left(\left[\frac{(1-\eta)\,m\,(m-1)}{a^2}-\beta^2\right]J_m(\beta a)+\frac{(1-\eta)\,\beta}{a}J_{m+1}(\beta a)\right);\\
c_{22} &= \frac{m}{a}\left(\left[\frac{(1-\eta)\,m\,(m-1)}{a^2}-\beta^2\right]Y_m(\beta a)+\frac{(1-\eta)\,\beta}{a}Y_{m+1}(\beta a)\right);\\
c_{23} &= \frac{m}{a}\left(\left[-\frac{(1-\eta)\,m\,(m-1)}{a^2}+\beta^2\right]I_m(\beta a)-\frac{(1-\eta)\,\beta}{a}I_{m+1}(\beta a)\right);\\
c_{24} &= \frac{m}{a}\left(\left[-\frac{(1-\eta)\,m\,(m-1)}{a^2}+\beta^2\right]K_m(\beta a)+\frac{(1-\eta)\,\beta}{a}K_{m+1}(\beta a)\right);\\
c_{31} &= -\frac{m}{b}\left[\frac{(1-\eta)\,m\,(m-1)}{b^2}+\beta^2\right]J_m(\beta b)+\beta\left[\frac{(1-\eta)\,m^2}{b^2}+\beta^2\right]J_{m+1}(\beta b);\\
c_{32} &= \left(-\frac{m}{b}\left[\frac{(1-\eta)\,m\,(m-1)}{b^2}+\beta^2\right]Y_m(\beta b)+\beta\left[\frac{(1-\eta)\,m^2}{b^2}+\beta^2\right]Y_{m+1}(\beta b)\right);\\
c_{33} &= \frac{m}{b}\left(\left[-\frac{(1-\eta)\,m\,(m-1)}{b^2}+\beta^2\right]I_m(\beta b)+\beta\left[-\frac{(1-\eta)\,m^2}{b^2}+\beta^2\right]I_{m+1}(\beta b)\right);\\
c_{34} &= \frac{m}{b}\left(\left[-\frac{(1-\eta)\,m\,(m-1)}{b^2}+\beta^2\right]K_m(\beta b)+\beta\left[\frac{(1-\eta)\,m^2}{b^2}+\beta^2\right]K_{m+1}(\beta b)\right);\\
c_{41} &= \frac{m}{b}\left(\left[\frac{(1-\eta)\,m\,(m-1)}{b^2}-\beta^2\right]J_m(\beta b)+\frac{(1-\eta)\,\beta}{b}J_{m+1}(\beta b)\right);\\
c_{42} &= \frac{m}{b}\left(\left[\frac{(1-\eta)\,m\,(m-1)}{b^2}-\beta^2\right]Y_m(\beta b)+\frac{(1-\eta)\,\beta}{b}Y_{m+1}(\beta b)\right);\\
c_{43} &= \frac{m}{b}\left(\left[-\frac{(1-\eta)\,m\,(m-1)}{b^2}+\beta^2\right]I_m(\beta b)-\frac{(1-\eta)\,\beta}{b}I_{m+1}(\beta b)\right);\text{ and}\\
c_{44} &= \frac{m}{b}\left(\left[-\frac{(1-\eta)\,m\,(m-1)}{b^2}+\beta^2\right]K_m(\beta b)+\frac{(1-\eta)\,\beta}{b}K_{m+1}(\beta b)\right).
\end{aligned}$$

Note that the coefficient matrix in Equation (4.137) can be written as:

$$\mathbf{N}_2\left(\omega_p\right) = \begin{bmatrix} c_{11}\left(\omega_p\right) & c_{12}\left(\omega_p\right) & c_{13}\left(\omega_p\right) & c_{14}\left(\omega_p\right) \\ c_{21}\left(\omega_p\right) & c_{22}\left(\omega_p\right) & c_{23}\left(\omega_p\right) & c_{24}\left(\omega_p\right) \\ c_{31}\left(\omega_p\right) & c_{32}\left(\omega_p\right) & c_{33}\left(\omega_p\right) & c_{34}\left(\omega_p\right) \\ c_{41}\left(\omega_p\right) & c_{42}\left(\omega_p\right) & c_{43}\left(\omega_p\right) & c_{44}\left(\omega_p\right) \end{bmatrix}. \tag{4.138}$$

It is well-known from linear algebra that Equation (4.137) has a non-trivial solution if the determinant of Equation (4.138) is zero, that is:

$$\Delta_p(\omega_p) = \det \mathbf{N}_2(\omega_p) = 0. \tag{4.139}$$

Equation (4.139) is known as the *characteristic* equation of the BVP. Using a CAS to solve this transcendental characteristic equation yields, for each circumferential wave number m, *a sequence of eigenvalues* $\omega_{mp,k}$ $(k = 0, 1, 2, 3, \cdots)$ with:

$$\omega_{mp,0} < \omega_{mp,1} < \omega_{mp,2} < \cdots. \tag{4.140}$$

The eigenvalue $\omega_{m,0}$ is called the *fundamental vibration eigenvalue* while $\omega_{m,1}$ is called the *first*

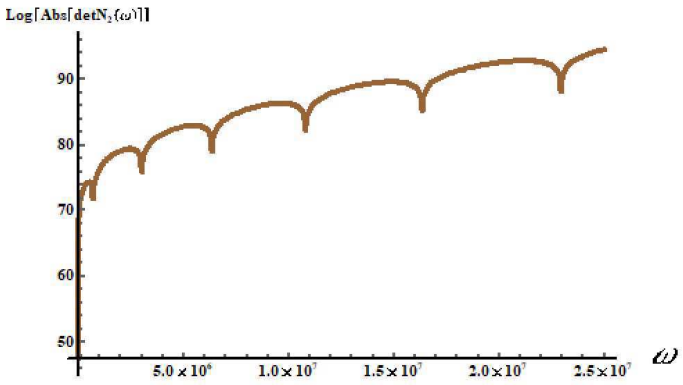

Figure 4.5: The graph used to estimate eigenvalues and eigenfrequencies of an annular plate free at both edges

overtone vibration eigenvalue, and so forth. A plot of the function $f(\omega_p) = \ln\left(|\Delta_p(\omega)|\right)$ appears in Figure 4.5 for an aluminium circular plate where the "spikes" point towards the roots of the function $\Delta_p(\omega)$. Note that the eigenvalues are not linearly spaced.

To solve for the constants, an integer k with $k \geq 0$ is fixed and the eigenvalue $\omega_{mp,k}$ is substituted back into Equation (4.137). Performing Gaussian elimination on the augmented matrix of Equation

Table 4.2: The fundamental and the first five overtone vibration eigenvalues and the associated eigenfrequencies of an annular plate free at the edges and vibrating at $m = 3$.

k	$\omega_{3p,k}\,(\mathrm{rad\,s^{-1}})$	$f_{3,k} = \frac{\omega_{3p,k}}{2\pi}\,(\mathrm{Hz})$
0	695335.3	110666.0
1	3.008646×10^6	478840.8
2	6.354535×10^6	1.011356×10^6
3	1.080587×10^7	1.719807×10^6
4	1.634623×107	2.601584×10^6
5	2.295467×10^7	3.653359×10^6

(4.137) indicates that any one of the A_1, A_2, A_3, A_4 can be chosen as being free, for example:

$$A_1 = \frac{\det\begin{pmatrix} -a_{14}A_4 & a_{12} & a_{13} \\ -a_{24}A_4 & a_{22} & a_{23} \\ -a_{34}A_4 & a_{32} & a_{33} \end{pmatrix}}{\det\begin{pmatrix} a_{11} & a_{12} & a_{13} \\ a_{21} & a_{22} & a_{23} \\ a_{31} & a_{32} & a_{33} \end{pmatrix}}. \tag{4.141}$$

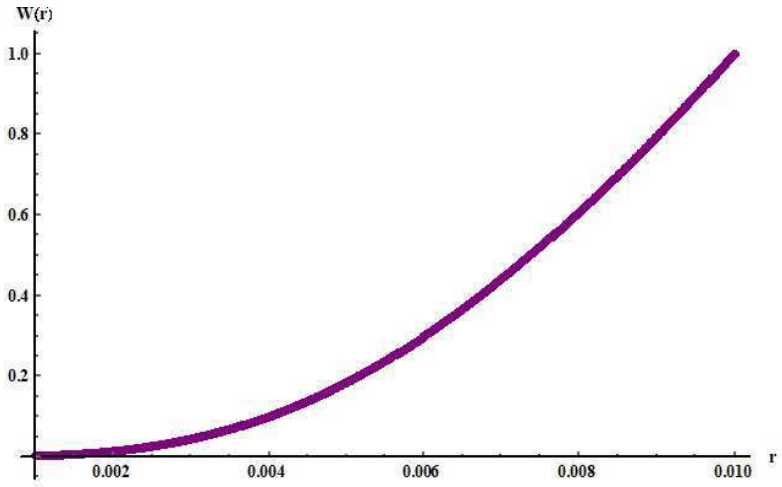

Figure 4.6: The normalised eigenfunction $W(r)$ corresponding to the eigenvalue $\omega_{3,0} = 695335.3\,\mathrm{rad.\,s^{-1}}$ for the annular aluminium disc in its plate form, free at the edges

Hence, choosing any non-zero value for A_4 (say $A_4 = 1$), the value of A_1 can be obtained using Cramer's rule, and similarly for A_2 and A_3. Consequently, with these values of $A_{i=1,2,3,4}$, the eigenfunction $W(r)$ corresponding to $\omega = \omega_{mp,k}$ can be calculated. These eigenfunctions are also referred to as the *form-factors* of the m-ω_p vibrating pattern or mode. A normalised eigenfunction $W(r)$ corresponding to the fundamental eigenvalue $\omega_{3p,0} = 695335.3\,\mathrm{rad.\,s^{-1}}$ for the annular aluminium circular plate and its out-of-plane vibration with free edges is shown in Figure 4.6.

4.7 CONCLUSION

The eigenfunctions and eigenvalues obtained numerically so far are considered only for the vibrating disc in Chapter 3 and and circular plates in Chapter 4, where rotation is neglected. Joubert, Shatalov and Fay (2014, [76]) have demonstrated that the eigenfunctions, for a vibrating structure that is not rotating, remain invariant if the structure is subjected to slow rotation. Consequently, the results obtained here are used in Chapter 5 where the vibrating disc gyroscope is subjected to slow 3D-rotation.

Chapter 5

THE DYNAMICS OF A TUNING DISC-VIBRATORY GYROSCOPE

5.1 INTRODUCTION

Chapters 3 and 4 independently dealt with the respective in-plane and out-of-plane vibratory dynamics of the disc gyroscope without rotation. This chapter incorporates the ideas of the previous two chapters with a slowly rotating disc to investigate the possibility of a 3D, tuned, disc-vibratory gyroscope. The equations of motion and the boundary conditions describing the dynamics of the 3D-tuned disc gyroscope are derived from the variational principle.

5.2 THE KINEMATICS OF THE 3D DISC-VIBRATORY GYROSCOPE

Consider two coordinate systems $0\xi\eta\zeta$ and $0xyz$, respectively as shown in Figure 5.1, where $0\xi\eta\zeta$ is connected to the disc and rotates with respect to any inertial coordinate system, whereas $0xyz$ is located at an angle φ from the 0ξ-axis of the $0\xi\eta\zeta$ system and characterises the location of the infinitesimal element $dm = \rho hrdrd\varphi$, as shown in Figure 5.1. Furthermore, assume that the 0ζ-axis of $0\xi\eta\zeta$ system and the $0z$-axis of the $0xyz$-system overlap and coincide with the axis of the disc as shown in Figure 5.1. Suppose that the disc is subjected to *slow three-dimensional rotation* with components Ω_ξ, Ω_η and Ω_ζ in the directions along the 0ξ-axis, 0η-axis and 0ζ-axis, respectively. Assume that the annular disc (of axial plate thickness h) has an inner radius a and outer radius b with r being the position of a point on the the disc, as shown in Figure 5.1. Let E be Young's modulus, ρ be the mass density, and η be the Poisson's ratio for the disc. Assume that $h << \min(a, b)$ and hence the "thin-plate theory" is used to simplify matters. The position vector of a vibrating element on the disc is thus given by $\vec{R} = \begin{pmatrix} r+u, & v, & w \end{pmatrix}^T$, where u, v and w are the displacements of the disc element in the radial, tangential and axial directions, respectively.

Let $\vec{\Omega}$ be the slow inertial angular rate of the vibrating system with its components given by $\begin{pmatrix} \Omega_x, & \Omega_y, & \Omega_z \end{pmatrix}^T$ in the $0xyz$-coordinate system. In this case, the components Ω_ξ, Ω_η and Ω_ζ are small and that the $O(\varepsilon^2)$ terms such as Ω_ξ^2, Ω_η^2, Ω_ζ^2, $\Omega_\xi\Omega_\eta$, $\Omega_\xi\Omega_\zeta$ and $\Omega_\zeta\Omega_\eta$ are neglected. Thus the absolute linear velocity of the disc element dm in Figure 5.1 is given by Euler's formula as

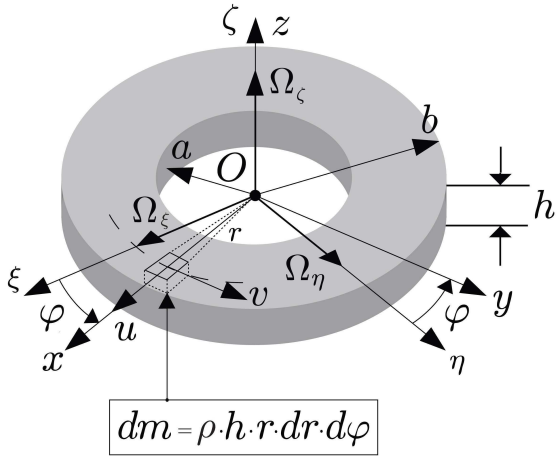

Figure 5.1: A thick disc, thin plate three dimensional vibratory gyroscope showing the three orthogonal axes with rotation rate components $\Omega_\zeta, \Omega_\eta$ and Ω_ξ

(Spiegel, 1982, [29]):

$$\vec{V} = \left(\begin{array}{cccc} \widetilde{\dot{u}}, & \widetilde{\dot{v}}, & \widetilde{\dot{w}} \end{array} \right)^T = \left(\begin{array}{cccc} \dot{u}, & \dot{v}, & \dot{w} \end{array} \right)^T + \varepsilon \vec{\Omega} \times \vec{R}; \tag{5.1}$$

where:

$$\vec{R} = \left(\begin{array}{cccc} r+u, & v, & w \end{array} \right)^T; \tag{5.2}$$

and

$$\vec{\Omega} = \varepsilon \left(\begin{array}{cccc} \Omega_x, & \Omega_y, & \Omega_z \end{array} \right)^T = \varepsilon \left(\begin{array}{c} \Omega_\xi \cos\varphi + \Omega_\eta \sin\varphi \\ \Omega_\eta \cos\varphi - \Omega_\xi \sin\varphi \\ \Omega_\zeta \end{array} \right). \tag{5.3}$$

The vector (cross) product of $\vec{\Omega}$ and $\vec{R}$ in matrix form is obtained as follows:

$$\begin{aligned} \vec{\Omega} \times \vec{R} &= \varepsilon \left| \begin{array}{ccc} \hat{\imath} & \hat{\jmath} & \hat{k} \\ (\Omega_\xi \cos\varphi + \Omega_\eta \sin\varphi) & (\Omega_\eta \cos\varphi - \Omega_\xi \sin\varphi) & \Omega_\zeta \\ r+u & v & w \end{array} \right| \\ &= \varepsilon \left(\begin{array}{c} (\Omega_\eta \cos\varphi - \Omega_\xi \sin\varphi) w - \Omega_\zeta v \\ (\Omega_\zeta (r+u) - (\Omega_\xi \cos\varphi + \Omega_\eta \sin\varphi) w) \\ \left(\begin{array}{c} (\Omega_\xi \cos\varphi + \Omega_\eta \sin\varphi) v + \\ (\Omega_\xi \sin\varphi - \Omega_\eta \cos\varphi)(r+u) \end{array} \right) \end{array} \right). \end{aligned} \tag{5.4}$$

Note that the components of the inertial rate on the $0xyz$-coordinate system are assumed to be $\left(\begin{array}{cccc} \Omega_x, & \Omega_y, & \Omega_z \end{array} \right)^T$. Substituting Equation (5.4) into Equation (5.1) gives:

$$\vec{V} = \left(\begin{array}{c} \widetilde{\dot{u}} \\ \widetilde{\dot{v}} \\ \widetilde{\dot{w}} \end{array} \right) = \left(\begin{array}{c} \dot{u} \\ \dot{v} \\ \dot{w} \end{array} \right) + \varepsilon \left(\begin{array}{c} (\Omega_\eta \cos\varphi - \Omega_\xi \sin\varphi) w - \Omega_\zeta v \\ \Omega_\zeta (r+u) - (\Omega_\xi \cos\varphi + \Omega_\eta \sin\varphi) w \\ (\Omega_\xi \cos\varphi + \Omega_\eta \sin\varphi) v + (\Omega_\xi \sin\varphi - \Omega_\eta \cos\varphi)(r+u). \end{array} \right). \tag{5.5}$$

5.3 ENERGY

In this section, both kinetic and potential energies of the disc vibratory gyroscope are discussed. The effects of rotary inertia are ignored. Thus the kinetic energy of the vibrating disc is influenced only by the absolute velocity of its centre (Joubert, Shatalov & Fay, 2009, [51]).

5.3.1 Kinetic energy

Assume that the components of the displacement of the vibrating disc are given by:

$$u[r,\varphi,t] = U(r)\left[C(t)\cos(m\varphi) + S(t)\sin(m\varphi)\right]; \tag{5.6}$$

$$v[r,\varphi,t] = V(r)\left[C(t)\sin(m\varphi) - S(t)\cos(m\varphi)\right]; \text{ and} \tag{5.7}$$

$$w[r,\varphi,t] = W(r)\left[A(t)\cos(m+1)\varphi + B(t)\sin(m+1)\varphi\right]; \tag{5.8}$$

where m is a vibration mode number, $U(r)$ and $V(r)$ are eigenfunctions of the in-plane vibrations and $W(r)$ is the eigenfunction of the out-of-plane vibration. Due to orthogonality of the trigonometric functions, the contributions of the components of the rotation rates to the total kinetic energy are non-zero if and only if $(m-n) = \pm 1$, where n and m are the in-plane and out-of-plane mode numbers, respectively. In what follows, the eigenfuctions can be calculated in terms of known functions using well-documented standard techniques (see Sections 3.4 and 4.6). On the other hand, the functions of time $C(t)$, $S(t)$, $A(t)$ and $B(t)$ can easily be determined numerically once the equations of motion (see Equations (5.62) to (5.65) below) have been established. In order to formulate the kinetic energy in terms of the time-dependent variables, Equations (5.6), (5.7) and (5.8) are differentiated with respect to time. Thus it follows that:

$$\dot{u} = U[\dot{C}\cos(m\varphi) + \dot{S}\sin(m\varphi)]; \tag{5.9}$$

$$\dot{v} = V[\dot{C}\sin(m\varphi) - \dot{S}\cos(m\varphi)]; \text{ and} \tag{5.10}$$

$$\dot{w} = W[\dot{A}\cos(m+1)\varphi + \dot{B}\sin(m+1)\varphi]. \tag{5.11}$$

The absolute velocity can thus be written as:

$$\vec{V} = \widetilde{\dot{u}}\hat{\imath} + \widetilde{\dot{v}}\hat{\jmath} + \widetilde{\dot{w}}\hat{k};$$

where, $\hat{\imath}$, $\hat{\jmath}$ and $\hat{k}$ are unit vectors in the increasing directions of x, y and z, respectively. Further-

more:

$$\widetilde{\dot{u}} = U\left[\dot{C}\cos(m\varphi) + \dot{S}\sin(m\varphi)\right] + \varepsilon\left(\left(\Omega_\eta\cos\varphi - \Omega_\xi\sin\varphi\right)w - \Omega_\zeta v\right), \tag{12}$$

$$\widetilde{\dot{v}} = V\left[\dot{C}\sin(m\varphi) + \dot{S}\cos(m\varphi)\right] + \varepsilon\left(\Omega_\zeta\left(r+u\right) - \left(\Omega_\xi\cos\varphi + \Omega_\eta\sin\varphi\right)w\right) \text{ and} \tag{13}$$

$$\widetilde{\dot{w}} = W[\dot{A}\cos(m+1)\varphi + \dot{B}\sin(m+1)\varphi] +$$
$$\varepsilon\left(\left(\Omega_\xi\cos\varphi + \Omega_\eta\sin\varphi\right)v + \left(\left(\Omega_\xi\sin\varphi - \Omega_\eta\cos\varphi\right)\left(r+u\right)\right)\right). \tag{14}$$

The kinetic energy for a disc gyroscope vibrating in its plane as well as out-of-plane can now be written from Equation (5.5) as:

$$\begin{aligned} E_k &= \frac{1}{2}\int_0^h\int_0^{2\pi}\int_a^b \rho\left(\vec{V}\cdot\vec{V}\right) r dr d\varphi dz; \text{ and} \\ E_k &\approx \int_0^{2\pi}\int_a^b \frac{\rho h r}{2}\left(\widetilde{\dot{u}}^2 + \widetilde{\dot{v}}^2 + \widetilde{\dot{w}}^2\right) dr d\varphi. \end{aligned} \tag{5.15}$$

Now $\widetilde{\dot{u}}^2$, $\widetilde{\dot{v}}^2$ and $\widetilde{\dot{w}}^2$ from Equations (5.12)-(5.14) are expanded using direct series expansion around $\varepsilon = 0$ and up to order $O(\varepsilon^2)$. Retaining terms proportional to $O(\varepsilon)$ and neglecting terms of order $O(\varepsilon^2)$ and higher, yields the following:

$$\widetilde{\dot{u}}^2 \approx \left\{\begin{array}{c} U^2\left(\dot{C}\cos(m\varphi) + \dot{S}\sin(m\varphi)\right)^2 - \\ 2U\left\{\begin{array}{c} \sin(\varphi)\cos((m+1)\varphi)\cos(m\varphi)\dot{C}\Omega_\xi AW + \\ \sin(\varphi)\cos((m+1)\varphi)\sin(m\varphi)\dot{S}\Omega_\xi AW + \\ \sin(\varphi)\sin((m+1)\varphi)\cos(m\varphi)\dot{C}\Omega_\xi BW + \\ \sin(\varphi)\sin((m+1)\varphi)\sin(m\varphi)\dot{S}\Omega_\xi BW - \\ \cos(\varphi)\cos((m+1)\varphi)\cos(m\varphi)\dot{C}\Omega_\eta AW - \\ \cos(\varphi)\cos((m+1)\varphi)\sin(m\varphi)\dot{S}\Omega_\eta AW - \\ \cos(\varphi)\sin((m+1)\varphi)\cos(m\varphi)\dot{C}\Omega_\eta BW - \\ \cos(\varphi)\sin((m+1)\varphi)\sin(m\varphi)\dot{S}\Omega_\eta BW - \\ \left(\cos(m\varphi)\right)^2\dot{C}\Omega_\zeta SV - \cos(m\varphi)\sin(m\varphi)\dot{S}\Omega_\zeta SV + \\ \cos(m\varphi)\sin(m\varphi)\dot{C}\Omega_\zeta CV - \left(\cos(m\varphi)\right)^2\dot{S}\Omega_\zeta CV + \dot{S}\Omega_\zeta CV \end{array}\right\} \end{array}\right\}; \tag{5.16}$$

$$\widetilde{\dot{v}}^2 \approx \left\{\begin{array}{c} V^2\left(\dot{S}\cos(m\varphi) - \dot{C}\sin(m\varphi)\right)^2 - \\ 2V\left\{\begin{array}{c} -\cos(m\varphi)\dot{S}\Omega_\xi A\cos(\varphi)\cos((m+1)\varphi)W + \\ \sin(m\varphi)\dot{C}\Omega_\xi A\cos(\varphi)\cos((m+1)\varphi)W - \\ \cos(m\varphi)\dot{S}\Omega_\xi B\cos(\varphi)\sin((m+1)\varphi)W + \\ \sin(m\varphi)\dot{C}\Omega_\xi B\cos(\varphi)\sin((m+1)\varphi)W - \\ \cos(m\varphi)\dot{S}\Omega_\eta A\sin(\varphi)\cos((m+1)\varphi)W + \\ \sin(m\varphi)\dot{C}\Omega_\eta A\sin(\varphi)\cos((m+1)\varphi)W - \\ \cos(m\varphi)\dot{S}\Omega_\eta B\sin(\varphi)\sin((m+1)\varphi)W + \\ \sin(m\varphi)\dot{C}\Omega_\eta B\sin(\varphi)\sin((m+1)\varphi)W + \\ \left(\cos(m\varphi)\right)^2\dot{S}\Omega_\zeta CU - \cos(m\varphi)\sin(m\varphi)\dot{C}\Omega_\zeta CU + \\ \cos(m\varphi)\sin(m\varphi)\dot{S}\Omega_\zeta SU + \left(\cos(m\varphi)\right)^2\dot{C}\Omega_\zeta SU - \\ \dot{C}\Omega_\zeta SU + \cos(m\varphi)\dot{S}\Omega_\zeta r - \sin(m\varphi)\dot{C}(t)\Omega_\zeta r \end{array}\right\} \end{array}\right\}; \tag{5.17}$$

and

$$\widetilde{\ddot{w}}^2 \approx \left\{ \begin{array}{c} W^2 \left(\dot{A} \cos\left((m+1)\,\varphi \right) + \dot{B} \sin\left((m+1)\,\varphi \right) \right)^2 + \\ 2W \left\{ \begin{array}{c} -\dot{B}\Omega_\eta \cos\left(\varphi\right) \sin\left((m+1)\,\varphi \right) r + \dot{B}\Omega_\xi \sin\left(\varphi\right) \sin\left((m+1)\,\varphi \right) r - \\ \dot{A}\Omega_\eta \cos\left(\varphi\right) \cos\left((m+1)\,\varphi \right) r + \dot{A}\Omega_\xi \sin\left(\varphi\right) \cos\left((m+1)\,\varphi \right) r - \\ \dot{B} \sin\left(m\,\varphi\right) \Omega_\eta S \cos\left(\varphi\right) \sin\left((m+1)\,\varphi \right) U + \\ \dot{B} \sin\left(m\,\varphi\right) \Omega_\eta C \sin\left(\varphi\right) \sin\left((m+1)\,\varphi \right) V + \\ \dot{B} \sin\left(m\,\varphi\right) \Omega_\xi S \sin\left(\varphi\right) \sin\left((m+1)\,\varphi \right) U + \\ \dot{B} \sin\left(m\,\varphi\right) \Omega_\xi C \cos\left(\varphi\right) \sin\left((m+1)\,\varphi \right) V - \\ \dot{B} \cos\left(m\,\varphi\right) \Omega_\eta S \sin\left(\varphi\right) \sin\left((m+1)\,\varphi \right) V - \\ \dot{B} \cos\left(m\,\varphi\right) \Omega_\eta C \cos\left(\varphi\right) \sin\left((m+1)\,\varphi \right) U - \\ \dot{B} \cos\left(m\,\varphi\right) \Omega_\xi S \cos\left(\varphi\right) \sin\left((m+1)\,\varphi \right) V + \\ \dot{B} \cos\left(m\,\varphi\right) \Omega_\xi C \sin\left(\varphi\right) \sin\left((m+1)\,\varphi \right) U - \\ \dot{A} \sin\left(m\,\varphi\right) \Omega_\eta S \cos\left(\varphi\right) \cos\left((m+1)\,\varphi \right) U + \\ \dot{A} \sin\left(m\,\varphi\right) \Omega_\eta C \sin\left(\varphi\right) \cos\left((m+1)\,\varphi \right) V + \\ \dot{A} \sin\left(m\,\varphi\right) \Omega_\xi S \sin\left(\varphi\right) \cos\left((m+1)\,\varphi \right) U + \\ \dot{A} \sin\left(m\,\varphi\right) \Omega_\xi C \cos\left(\varphi\right) \cos\left((m+1)\,\varphi \right) V - \\ \dot{A} \cos\left(m\,\varphi\right) \Omega_\eta S \sin\left(\varphi\right) \cos\left((m+1)\,\varphi \right) V - \\ \dot{A} \cos\left(m\,\varphi\right) \Omega_\eta C \cos\left(\varphi\right) \cos\left((m+1)\,\varphi \right) U - \\ \dot{A} \cos\left(m\,\varphi\right) \Omega_\xi S \cos\left(\varphi\right) \cos\left((m+1)\,\varphi \right) V + \\ \dot{A} \cos\left(m\,\varphi\right) \Omega_\xi C \sin\left(\varphi\right) \cos\left((m+1)\,\varphi \right) U. \end{array} \right\} \end{array} \right\}. \tag{5.18}$$

For all values of m the following integrals are observed:

$$\int_0^{2\pi} \sin^2\left(m\varphi\right) d\varphi = \int_0^{2\pi} \cos^2\left(m\varphi\right) d\varphi = \pi; \tag{5.19}$$

$$\int_0^{2\pi} \sin\left(m\varphi\right) \cos\left(m\varphi\right) d\varphi = 0; \tag{5.20}$$

$$\int_0^{2\pi} \sin\left((m+1)\,\varphi \right) \cos\left(m\varphi\right) d\varphi = 0; \tag{5.21}$$

$$\int_0^{2\pi} \cos\left((m+1)\,\varphi \right) \sin\left(m\varphi\right) d\varphi = 0; \tag{5.22}$$

$$\int_0^{2\pi} \cos\left((m+1)\,\varphi \right) \cos\left(m\varphi\right) d\varphi = 0; \text{ and} \tag{5.23}$$

$$\int_0^{2\pi} \sin\left(m\varphi\right) \sin\left(m+1\right) \varphi d\varphi = 0. \tag{5.24}$$

Integrating $\widetilde{\dot{u}}^2$, $\widetilde{\dot{v}}^2$ and $\widetilde{\dot{w}}^2$, respectively, over $[0,\ 2\pi]$, with respect to φ yields:

$$\begin{aligned}
\int_0^{2\pi} \widetilde{\dot{u}}^2 \, d\varphi &\approx \left\{ \begin{array}{c} U^2\pi \left(\left(\dfrac{dC}{dt} \right)^2 + \left(\dfrac{dS}{dt} \right)^2 \right) - \\ \pi U \left\{ \begin{array}{c} \dfrac{dC}{dt}\Omega_\xi BW - \dfrac{dC}{dt}\Omega_\eta AW - \\ 2\dfrac{dC}{dt}\Omega_\zeta SV - \dfrac{dS}{dt}\Omega_\xi AW - \\ -\dfrac{dS}{dt}\Omega_\eta BW + 2\dfrac{dS}{dt}\Omega_\zeta CV \end{array} \right\} \end{array} \right\} \\
&= U^2\pi \left(\dot{C}^2 + \dot{S}^2 \right) - \\
&\quad \pi U \left\{ \begin{array}{c} \dot{C}\Omega_\xi BW - \dot{C}\Omega_\eta AW - 2\dot{C}\Omega_\zeta SV - \\ \dot{S}\Omega_\xi AW - \dot{S}\Omega_\eta BW + 2\dot{S}\Omega_\zeta CV \end{array} \right\}; \qquad (5.25)
\end{aligned}$$

$$\begin{aligned}
\int_0^{2\pi} \widetilde{\dot{v}}^2 \, d\varphi &\approx \left\{ \begin{array}{c} V^2\pi \left(\left(\dfrac{dC}{dt} \right)^2 + \left(\dfrac{dS}{dt} \right)^2 \right) - \\ V\pi \left\{ \begin{array}{c} \dfrac{dC}{dt}\Omega_\xi BW - \dfrac{dC}{dt}\Omega_\eta AW - \\ 2\dfrac{dC}{dt}\Omega_\zeta SU - \dfrac{dS}{dt}\Omega_\xi AW - \\ \dfrac{dS}{dt}\Omega_\eta BW + 2\dfrac{dS}{dt}\Omega_\zeta CU \end{array} \right\} \end{array} \right\} \\
&= V^2\pi \left(\dot{C}^2 + \dot{S}^2 \right) - \\
&\quad V\pi \left\{ \begin{array}{c} \dot{C}\Omega_\xi BW - \dot{C}\Omega_\eta AW - 2\dot{C}\Omega_\zeta SU - \\ \dot{S}\Omega_\xi AW - \dot{S}\Omega_\eta BW + 2\dot{S}\Omega_\zeta CU \end{array} \right\}; \qquad (5.26)
\end{aligned}$$

and

$$\begin{aligned}
\int_0^{2\pi} \widetilde{\dot{w}}^2 \, d\varphi &\approx \left\{ \begin{array}{c} \pi W^2 \left(\left(\dfrac{dA}{dt} \right)^2 + \left(\dfrac{dB}{dt} \right)^2 \right) + \\ \pi W \left\{ \begin{array}{c} \dfrac{dB}{dt}\Omega_\xi CU + VC\Omega_\xi \dfrac{dB}{dt} - \\ \dfrac{dA}{dt}\Omega_\xi SU - \dfrac{dA}{dt}\Omega_\xi SV - \\ \dfrac{dA}{dt}\Omega_\eta CU - V\Omega_\eta C\dfrac{dA}{dt} - \\ \dfrac{dB}{dt}\Omega_\eta SU - \dfrac{dB}{dt}\Omega_\eta SV \end{array} \right\} \end{array} \right\} \\
&= \pi W^2 \left(\dot{A}^2 + \dot{B}^2 \right) + \\
&\quad \pi W \left\{ \begin{array}{c} \dot{B}\Omega_\xi CU + \dot{B}VC\Omega_\xi - \dot{A}\Omega_\xi SU - \dot{A}\Omega_\xi SV - \\ \dot{A}\Omega_\eta CU - \dot{A}V\Omega_\eta C - \dot{B}\Omega_\eta SU - \dot{B}\Omega_\eta SV \end{array} \right\}. \qquad (5.27)
\end{aligned}$$

Adding Equations (5.25), (5.26) and (5.27) yields:

$$\int_0^{2\pi} \left(\widetilde{\dot{u}}^2 + \widetilde{\dot{v}}^2 + \widetilde{\dot{w}}^2 \right) d\varphi \approx \left[\begin{array}{c} \pi \left(\dot{C}^2 + \dot{S}^2 \right) (U^2 + V^2) + 4\pi\Omega_\zeta \left(\dot{C}S - C\dot{S} \right) UV + \\ \pi\Omega_\eta \left(A\dot{C} - \dot{A}C + B\dot{S} - \dot{B}S \right) W(U+V) + \\ \pi\Omega_\xi \left(A\dot{S} - \dot{A}S + \dot{B}C - B\dot{C} \right) W(U+V) + \\ W^2\pi \left(\dot{A}^2 + \dot{B}^2 \right) \end{array} \right]. \qquad (5.28)$$

Substitution of Equation (5.28) into Equation (5.15) after simplification gives:

$$E_k = \int_a^b \frac{\rho h}{2} \left\{ \begin{array}{c} \pi\left(\dot{C}^2+\dot{S}^2\right)\left(U^2+V^2\right)+4\pi\Omega_\zeta\left(\dot{C}S-C\dot{S}\right)UV+ \\ \pi\Omega_\eta\left(A\dot{C}-\dot{A}C+B\dot{S}-\dot{B}S\right)W\left(U+V\right)+ \\ \pi\Omega_\xi\left(A\dot{S}-\dot{A}S+\dot{B}C-B\dot{C}\right)W\left(U+V\right)+W^2\pi\left(\dot{A}^2+\dot{B}^2\right) \end{array} \right\} rdr$$

$$= \left[\begin{array}{c} \pi\left(\dot{C}^2+\dot{S}^2\right)\frac{\rho h}{2}\int_a^b\left(U^2+V^2\right)rdr+2\pi\rho h\Omega_\zeta\left(\dot{C}S-C\dot{S}\right)\int_a^b UVrdr+ \\ \frac{\pi\rho h\Omega_\eta}{2}\left(A\dot{C}-\dot{A}C+B\dot{S}-\dot{B}S\right)\int_a^b\left(U+V\right)Wrdr+ \\ \frac{\pi\rho h\Omega_\xi}{2}\left(A\dot{S}-\dot{A}S+\dot{B}C-B\dot{C}\right)\int_a^b\left(U+V\right)Wrdr+ \\ \pi\left(\dot{A}^2+\dot{B}^2\right)\frac{\rho h}{2}\int_a^b W^2rdr. \end{array} \right] . \quad (5.29)$$

Thus the kinetic energy in terms of $C, S, \dot{C}, \dot{S}, A, B, \dot{A}$ and $\dot{B}$ in its compact form can now be written as:

$$E_k = K\left(C,S,\dot{C},\dot{S},A,B,\dot{A},\dot{B}\right)$$

$$= \pi \left[\begin{array}{c} 2\Omega_\zeta\left(\dot{C}S-C\dot{S}\right)I_1+I_3\Omega_\eta\left(A\dot{C}-\dot{A}C+B\dot{S}-\dot{B}S\right)+ \\ I_0\left(\dot{C}^2+\dot{S}^2\right)+I_3\Omega_\xi\left(A\dot{S}-\dot{A}S+\dot{B}C-B\dot{C}\right)+I_4\left(\dot{A}^2+\dot{B}^2\right) \end{array} \right] ; \quad (5.30)$$

with:

$$I_0 = \frac{\rho h}{2}\int_a^b\left(U^2+V^2\right)rdr, \quad I_1 = \rho h\int_a^b UVrdr; \text{ and}$$

$$I_3 = \frac{\rho h}{2}\int_a^b\left(U+V\right)Wrdr \quad I_4 = \frac{\rho h}{2}\int_a^b W^2rdr. \quad (5.31)$$

In Equation (5.15) it is assumed that the size of the angular rate of rotation $\vec{\Omega}$ is substantially smaller than the lowest eigenvalue $\omega_{\min}$ of the in-plane or out-of-plane vibration. Consequently, terms containing Ω_ξ^2, Ω_η^2, Ω_ζ^2, $\Omega_\zeta\Omega_\eta$, $\Omega_\eta\Omega_\xi$ and $\Omega_\xi\Omega_\zeta$ which have $O\left(\varepsilon^2\right)$ order of smallness are neglected (Joubert, Shatalov & Manzhirov, 2013, [53]).

5.3.2 Potential energy

The potential energy of deformation stored in the form of strain energy can be obtained as shown in Novozhilov (1970, [61]). The total strain energy of the disc is the sum of the strain energies of the in-plane and out-of-plane vibrations (Rourke, McWilliam & Fox, 2005, [63]). If σ_r, σ_φ, and $\sigma_{r\varphi}$, respectively (ϵ_r, ϵ_φ and $\epsilon_{r\varphi}$, respectively) are the usual tensile radial, tensile tangential and shear stresses (or strains, respectively) for in-plane vibrations, then the potential energy of the in-plane vibrations is (Redwood, 1960, [59]; Joubert, Shatalov & Fay, 2009, [51]):

$$E_{p,in} = \frac{Eh}{2(1-\eta^2)}\int_0^{2\pi}\int_a^b\left[\sigma_r\epsilon_r+\sigma_\varphi\epsilon_\varphi+\sigma_{r\varphi}\epsilon_{r\varphi}\right]rdrd\varphi = \pi I_2(C^2+S^2); \quad (5.32)$$

where I_2 (Joubert, Shatalov & Fay, 2009, [51]) is given by the definite integral:

$$I_2 = \frac{Eh}{2\left(1-\eta^2\right)} \left[\begin{array}{c} \int_a^b \left(U_r'\right)^2 + 2\eta U_r' \dfrac{(U+mV)}{r} + \left(\dfrac{U+mV}{r}\right)^2 + \\ \dfrac{1-\eta}{2}\left(V_r' - \dfrac{mU+V}{r}\right)^2 \end{array} \right]. \tag{5.33}$$

Using the assumptions of "thin plate theory", the potential energy for out-of plane vibrations is given by (see Novozhilov (1970, [61])):

$$E_{p,out} = \frac{Eh^3}{24\left(1-\eta^2\right)} \int_0^{2\pi} \int_a^b \left[\chi_1^2 + \chi_2^2 + 2\eta\chi_1\chi_2 + 2\left(1-\eta\right)\tilde{\tau}^2\right] r dr d\varphi; \tag{5.34}$$

with:

$$\chi_1 = -\frac{\partial^2 w}{\partial r^2}, \quad \chi_2 = -\frac{1}{r}\frac{\partial w}{\partial r} - \frac{1}{r^2}\frac{\partial^2 w}{\partial \varphi^2}, \quad \tilde{\tau} = -\frac{1}{r}\frac{\partial^2 w}{\partial r \partial \varphi} + \frac{1}{r^2}\frac{\partial w}{\partial \varphi}; \tag{5.35}$$

where:

$$w = W\left(r\right)\left[A\left(t\right)\cos\left(m+1\right)\varphi + B\left(t\right)\sin\left(m+1\right)\varphi\right].$$

As for kinetic energy, an expression for the potential energy in terms of C, S, A and B is obtained using MAPLE's symbolic computation. By substitution of Equation (5.35) into Equation (5.34) and integrating with respect to φ over the interval $[0, 2\pi]$ using MAPLE yields:

$$E_{p,out} = \tfrac{Eh^3}{24(1-\eta^2)} \int_a^b \left\{ \begin{array}{c} \frac{2\eta\pi\left(A^2+B^2\right)W_{rr}''W_r'}{r} + \pi\left(A^2+B^2\right)\left(W_{rr}''\right)^2 \\ -\frac{\left(2m^2\eta-2m^2+4m\eta-4m+2\eta-3\right)\pi\left(A^2+B^2\right)\left(W_r'\right)^2}{r^2} + \\ \frac{2\left(2m^2\eta-3m^2+4m\eta-6m+2\eta-3\right)\pi\left(A^2+B^2\right)WW_r'}{r^3} - \\ \left(\frac{2\eta\pi(m+1)^2}{r^2}\right)\left(A^2+B^2\right)WW_{rr}'' + \\ \pi\left(\frac{m^4+4m^3-2m^2\eta+8m^2--4m\eta+8m-2\eta+3}{r^4}\right)\pi\left(A^2+B^2\right) \end{array} \right\} r dr; \tag{5.36}$$

which can be written in compact form as:

$$E_{p,out} = I_5\pi\left(A^2+B^2\right); \tag{5.37}$$

with:

$$I_5 = \frac{Eh^3}{24\left(1-\eta^2\right)} \int_a^b \left\{ \begin{array}{c} \frac{2\eta W_r'W_{rr}''}{r} - \frac{\left(2(\eta-1)(m+1)^2-1\right)W_r'^2}{r^2} + \\ \left(\frac{(2\eta-3)(m+1)^2}{r^3}\right)WW_r' + r\left(W_{rr}''\right)^2 - \left(\frac{2\eta(m+1)^2}{r^2}\right)WW_{rr}'' \\ + \left(\frac{m^2\left(m^2+4m+8-2\eta\right)-2(\eta-2)(2m+1)-1}{r^4}\right)W^2 \end{array} \right\} r dr. \tag{5.38}$$

Here I_5 is a constant that is determined by the out-of-plane eigenfunctions and their derivatives. The total potential energy of the vibrating disc is obtained by summing up the strain energies of the in-plane and out-of-plane vibrations. Consequently:

$$\begin{aligned} E_p(C,S,A,S) &= E_{p,in} + E_{p,out} \\ &= \pi I_2(C^2+S^2) + I_5\pi\left(A^2+B^2\right). \end{aligned} \tag{5.39}$$

5.3.3 Lagrangian

The general form of the Lagrangian (Spiegel, 1967, [29]) for the system is defined as a difference between the kinetic energy and potential energy. Hence the Lagrangian of the m and $m+1$-vibrating patterns for the disc gyroscope is obtained from Equations (5.29) and (5.39) and can thus be written as:

$$\begin{aligned} L &= K\left(C, S, \dot{C}, \dot{S}, A, B, \dot{A}, \dot{B}\right) - P\left(C, S, A, B\right) \\ &= \pi \begin{bmatrix} I_0\left(\dot{C}^2 + \dot{S}^2\right) + 2\Omega_\zeta\left(\dot{C}S - C\dot{S}\right) I_1 + \\ I_3\Omega_\eta\left(A\dot{C} - \dot{A}C + B\dot{S} - \dot{B}S\right) + \\ I_3\Omega_\xi\left(A\dot{S} - \dot{A}S + \dot{B}C - B\dot{C}\right) + I_4\left(\dot{A}^2 + \dot{B}^2\right) - \\ \left[I_2(C^2 + S^2) + I_5\left(A^2 + B^2\right)\right] \end{bmatrix}. \end{aligned} \tag{5.40}$$

5.4 THE EULER-LAGRANGE EQUATIONS OF MOTION

The Euler-Lagrange equations of motion for a disc-vibratory gyroscope subjected to a slow 3D-rotation rate are derived in this section. The equations of motion for a disc gyroscope with free vibration and the disc gyroscope subjected to a small light isotropic damping are formulated.

5.4.1 Homogeneous equations of motion

In this subsection the equations governing the vibrating patterns of the disc gyroscope are derived under homogeneous conditions. It is assumed that the gyroscope operates under ideal conditions and hence any actions of non-conservative forces are neglected for now. In order to formulate the

governing equations, the following derivatives of the Lagrangian (L) are required:

$$\frac{\partial L}{\partial C} = \pi\left[I_3\Omega_\xi\dot{B} - 2\Omega_\zeta I_1\dot{S} - I_3\Omega_\eta\dot{A} - 2I_2C\right]; \tag{5.41a}$$

$$\frac{\partial L}{\partial \dot{C}} = \pi\left[2I_0\dot{C} + 2\Omega_\zeta I_1 S + I_3\Omega_\eta A - I_3\Omega_\xi B\right]; \tag{5.41b}$$

$$\frac{\partial L}{\partial S} = \pi\left[2I_1\Omega_\zeta\dot{C} - 2\Omega_\eta I_3\dot{B} - I_3\Omega_\xi\dot{A} - 2I_2S\right]; \tag{5.41c}$$

$$\frac{\partial L}{\partial \dot{S}} = \pi\left[2I_0\dot{S} - 2\Omega_\zeta I_1 C + I_3\Omega_\eta B + I_3\Omega_\xi A\right]; \tag{5.41d}$$

$$\frac{\partial L}{\partial A} = \pi\left[I_3\Omega_\eta\dot{C} + I_3\Omega_\xi\dot{S} - 2I_5A\right]; \tag{5.41e}$$

$$\frac{\partial L}{\partial \dot{A}} = \pi\left[2I_4\dot{A} - I_3\Omega_\eta C - I_3\Omega_\xi S\right]; \tag{5.41f}$$

$$\frac{\partial L}{\partial B} = \pi\left[I_3\Omega_\eta\dot{S} - I_3\Omega_\xi\dot{C} - 2I_5B\right]; \text{ and} \tag{5.41g}$$

$$\frac{\partial L}{\partial \dot{B}} = \pi\left[2I_4\dot{B} + I_3\Omega_\xi C - I_3\Omega_\eta S\right]. \tag{5.41h}$$

If non-conservative forces are neglected, the Euler-Lagrange equations for the generalised coordinates C, S, A and B (Goldstein, Poole & Safco, 2000, [64]) can be written as:

$$\frac{d}{dt}\left(\frac{\partial L}{\partial \dot{C}}\right) - \frac{\partial L}{\partial C} = 0; \tag{5.42a}$$

$$\frac{d}{dt}\left(\frac{\partial L}{\partial \dot{S}}\right) - \frac{\partial L}{\partial S} = 0; \tag{5.42b}$$

$$\frac{d}{dt}\left(\frac{\partial L}{\partial \dot{A}}\right) - \frac{\partial L}{\partial A} = 0; \text{ and} \tag{5.42c}$$

$$\frac{d}{dt}\left(\frac{\partial L}{\partial \dot{B}}\right) - \frac{\partial L}{\partial B} = 0. \tag{5.42d}$$

Differentiating Equation (5.41b) with respect to time yields:

$$\frac{d}{dt}\left(\frac{\partial L}{\partial \dot{C}}\right) = \pi\left[2I_0\ddot{C} + 2\dot{\Omega}_\zeta I_1 S + 2\Omega_\zeta I_1\dot{S} + I_3\Omega_\eta\dot{A} + I_3\dot{\Omega}_\eta A - I_3\dot{\Omega}_\xi B - I_3\Omega_\xi\dot{B}\right]. \tag{5.43}$$

Substitution of Equations (5.43) and (5.41a) into Equation (5.42a) leads to:

$$\pi\left[\begin{array}{c} 2I_0\ddot{C} + 2\dot{\Omega}_\zeta I_1 S + 2\Omega_\zeta I_1\dot{S} + I_3\Omega_\eta\dot{A} - I_3\dot{\Omega}_\xi B - I_3\Omega_\xi B - \\ \left[I_3\Omega_\xi\dot{B} - 2\Omega_\zeta I_1\dot{S} - I_3\Omega_\eta\dot{A} - 2I_2C\right] \end{array}\right] = 0; \text{ and} \tag{5.44a}$$

$$\pi\left[\begin{array}{c} 2I_0\ddot{C} + 4\Omega_\zeta I_1\dot{S} + 2\dot{\Omega}_\zeta I_1 S + 2I_3\Omega_\eta\dot{A} - 2I_3\Omega_\xi\dot{B} + I_3\dot{\Omega}_\eta A - \\ I_3\dot{\Omega}_\xi B + 2I_2C \end{array}\right] = 0. \tag{5.44b}$$

Dividing Equation (5.44b) throughout by $2I_0\pi$ yields:

$$\ddot{C} + 2\frac{I_1}{I_0}\Omega_\zeta\dot{S} + \dot{\Omega}_\zeta\frac{I_1}{I_0}S + \frac{I_3}{I_0}\left(\Omega_\eta\dot{A} - \Omega_\xi\dot{B}\right) + \frac{I_3}{2I_0}\left(\dot{\Omega}_\eta A - \dot{\Omega}_\xi B\right) + \frac{I_2}{I_0}C = 0; \text{ and}$$

$$\ddot{C} + 2\beta_1\Omega_\zeta\dot{S} + \dot{\Omega}_\zeta\beta_1 S + \omega_I^2 C + \beta_2\left[2\left(\Omega_\eta\dot{A} - \Omega_\xi\dot{B}\right) + \left(\dot{\Omega}_\eta A - \dot{\Omega}_\xi B\right)\right] = 0; \tag{5.45}$$

with:

$$\beta_1 = \frac{I_1}{I_0} = \frac{2\int_a^b UVrdr}{\int_a^b (U^2+V^2)\,rdr};\ \text{and} \tag{5.46}$$

$$\beta_2 = \frac{I_3}{2I_0} = \frac{\frac{1}{2}\int_a^b (U+V)\,Wrdr}{\int_a^b (U^2+V^2)\,rdr}; \tag{5.47}$$

and

$$\omega_I^2 = \frac{I_2}{I_0};\ \text{and}\quad \omega_I = \sqrt{\frac{I_2}{I_0}}. \tag{5.48}$$

Differentiating Equation (5.41d) with respect to time yields:

$$\frac{d}{dt}\left(\frac{\partial L}{\partial \dot{S}}\right) = \pi\left[2I_0\ddot{S} - 2\dot{\Omega}_\zeta I_1 C - 2\Omega_\zeta I_1\dot{C} + I_3\dot{\Omega}_\eta B + I_3\Omega_\eta\dot{B} + I_3\dot{\Omega}_\xi A + I_3\Omega_\xi\dot{A}\right]. \tag{5.49}$$

Thus, the equation in the generalised S coordinate can be obtained as shown here. Substitution of Equations (5.49) and (5.41c) into Equation (5.42b) leads to:

$$\pi\left[\begin{array}{c} 2I_0\ddot{S} - 2\dot{\Omega}_\zeta I_1 C - 2\Omega_\zeta I_1\dot{C} + I_3\dot{\Omega}_\eta B + I_3\Omega_\eta\dot{B} + I_3\dot{\Omega}_\xi A + \\ I_3\Omega_\xi\dot{A} - \left[2I_1\Omega_\zeta\dot{C} - \Omega_\eta I_3\dot{B} - I_3\Omega_\xi\dot{A} - 2I_2 S\right] \end{array}\right] = 0;\ \text{and} \tag{5.50a}$$

$$\pi\left[\begin{array}{c} 2I_0\ddot{S} - 4\Omega_\zeta I_1\dot{C} - 2\dot{\Omega}_\zeta I_1 C + 2I_3\Omega_\xi\dot{A} + 2I_3\Omega_\eta\dot{B} + I_3\dot{\Omega}_\xi A + \\ I_3\dot{\Omega}_\eta B + 2I_2 S \end{array}\right] = 0. \tag{5.50b}$$

Dividing Equation (5.50b) throughout by $2I_0\pi$ yields:

$$\begin{aligned} \ddot{S} - 2\frac{I_1}{I_0}\Omega_\zeta\dot{C} - \frac{I_1}{I_0}\dot{\Omega}_\zeta C + \frac{I_3}{I_0}\Omega_\xi\dot{A} + \frac{I_3}{I_0}\Omega_\eta\dot{B} + \frac{I_3}{2I_0}\dot{\Omega}_\xi A + \frac{I_3}{2I_0}\dot{\Omega}_\eta B + \frac{I_2}{I_0}S &= 0; \\ \ddot{S} - 2\beta_1\Omega_\zeta\dot{C} - \beta_1\dot{\Omega}_\zeta C + \beta_2\Omega_\xi\dot{A} + \beta_2\Omega_\eta\dot{B} + \frac{1}{2}\beta_2\dot{\Omega}_\xi A + \frac{1}{2}\beta_2\dot{\Omega}_\eta B + \omega_I^2 S &= 0;\ \text{and} \\ \ddot{S} - 2\beta_1\Omega_\zeta\dot{C} - \beta_1\dot{\Omega}_\zeta C + \omega_I^2 S + \beta_2\left[2\left(\Omega_\xi\dot{A} + \beta_2\Omega_\eta\dot{B}\right) + \dot{\Omega}_\xi A + \beta_2\dot{\Omega}_\eta B\right] &= 0; \end{aligned} \tag{5.51}$$

with β_1, β_2 and ω_I as defined in Equations (5.46), (5.47) and (5.48), respectively. Equations (5.45) and (5.51) describe the equations of motion of the in-plane vibrating pattern of the disc gyroscope. The equations of motion for the out-of-plane vibrating pattern are obtained using the Euler-Lagrange form and the Lagrangian:

$$L = E_k\left(C, S, \dot{C}, \dot{S}, A, B, \dot{A}, \dot{B}\right) = \pi\left[\begin{array}{c} I_0\left(\dot{C}^2 + \dot{S}^2\right) + 2\Omega_\zeta\left(\dot{C}S - C\dot{S}\right)I_1 + \\ I_3\Omega_\eta\left(A\dot{C} - \dot{A}C + B\dot{S} - \dot{B}S\right) + \\ I_3\Omega_\xi\left(A\dot{S} - \dot{A}S + \dot{B}C - B\dot{C}\right) + I_4\left(\dot{A}^2 + \dot{B}^2\right) - \\ \left[I_2(C^2+S^2) + I_5\left(A^2+B^2\right)\right] \end{array}\right].$$

Differentiating Equation (5.41f) with respect to time yields:

$$\frac{d}{dt}\left(\frac{\partial L}{\partial \dot{A}}\right) = \pi\left[2I_4\ddot{A} - I_3\Omega_\eta\dot{C} - I_3\Omega_\xi\dot{S} - I_3\dot{\Omega}_\eta C - I_3\dot{\Omega}_\xi S\right]. \tag{5.52}$$

Substituting Equations (5.52) and (5.41e) into Equation (5.42c) yields:

$$\pi\left[\begin{array}{c} 2I_4\ddot{A} - I_3\Omega_\eta\dot{C} - I_3\Omega_\xi\dot{S} - I_3\dot{\Omega}_\eta C - I_3\dot{\Omega}_\xi S - \\ \left[I_3\Omega_\eta\dot{C} + I_3\Omega_\xi\dot{S} - 2I_5 A\right] \end{array}\right] = 0;\ \text{and} \tag{5.53}$$

$$\pi\left[2I_4\ddot{A} - 2I_3\Omega_\eta\dot{C} - 2I_3\Omega_\xi\dot{S} - I_3\dot{\Omega}_\eta C - I_3\dot{\Omega}_\xi S + 2I_5 A\right] = 0. \tag{5.54}$$

Dividing Equation (5.54) throughout by $2I_4\pi$ results in:

$$\begin{aligned}
\ddot{A} - \frac{I_3}{I_4}\Omega_\eta\dot{C} - \frac{I_3}{I_4}\Omega_\xi\dot{S} - \frac{I_3}{2I_4}\dot{\Omega}_\eta C - \frac{I_3}{2I_4}\dot{\Omega}_\xi S + \frac{I_5}{I_4}A &= 0; \\
\ddot{A} - 2\beta_3\Omega_\eta\dot{C} - 2\beta_3\Omega_\xi\dot{S} - \beta_3\dot{\Omega}_\eta C - \beta_3\dot{\Omega}_\xi S + \omega_o^2 A &= 0; \text{ and} \\
\ddot{A} + \omega_o^2 A - \beta_3\left[2\left(\Omega_\eta\dot{C} + \Omega_\xi\dot{S}\right) + \left(\dot{\Omega}_\eta C + \dot{\Omega}_\xi S\right)\right] &= 0; \qquad (5.55)
\end{aligned}$$

with:

$$\beta_3 = \frac{I_3}{2I_4} = \frac{\frac{1}{2}\int_a^b (U+V)\,W r dr}{\int_a^b W^2 r dr}; \qquad (5.56)$$

and

$$\frac{I_5}{I_4} = \omega_o^2, \quad \omega_o = \sqrt{\frac{I_5}{I_4}}; \qquad (5.57)$$

where I_4 is given by Equation (5.31) while I_5 is given by Equation (5.38). By the same analogy, the equation for the other out-of-plane coordinate B can be obtained as follows. Differentiating Equation (5.41h) with respect to time gives:

$$\frac{d}{dt}\left(\frac{\partial L}{\partial \dot{B}}\right) = \pi\left[2I_4\ddot{B} + I_3\Omega_\xi\dot{C} + I_3\dot{\Omega}_\xi C - I_3\Omega_\eta\dot{S} - I_3\dot{\Omega}_\eta S\right]. \qquad (5.58)$$

Substituting Equations (5.58) and (5.41g) into Equation (5.42d) yields:

$$\begin{aligned}
\pi\left[\begin{array}{c} 2I_4\ddot{B} + I_3\Omega_\xi\dot{C} - I_3\Omega_\eta\dot{S} + I_3\dot{\Omega}_\xi C - I_3\dot{\Omega}_\eta S - \\ \left[I_3\Omega_\eta\dot{S} - I_3\Omega_\xi\dot{C} - 2I_5 B\right] \end{array}\right] &= 0; \text{ and} \qquad (5.59) \\
\pi\left[2I_4\ddot{B} + 2I_3\Omega_\xi\dot{C} - 2I_3\Omega_\eta\dot{S} + I_3\dot{\Omega}_\xi C - I_3\dot{\Omega}_\eta S + 2I_5 B\right] &= 0. \qquad (5.60)
\end{aligned}$$

Dividing Equation (5.60) throughout by $2I_4\pi$ gives:

$$\begin{aligned}
\ddot{B} + \frac{I_3}{I_4}\Omega_\xi\dot{C} - \frac{I_3}{I_4}\Omega_\eta\dot{S} + \frac{I_3}{2I_4}\dot{\Omega}_\xi C - \frac{I_3}{2I_4}\dot{\Omega}_\eta S + \frac{I_5}{I_4}B &= 0; \\
\ddot{B} + \omega_o^2 B + 2\beta_3\Omega_\xi\dot{C} - 2\beta_3\Omega_\eta\dot{S} + \beta_3\dot{\Omega}_\xi C - \beta_3\dot{\Omega}_\eta S &= 0; \text{ and} \\
\ddot{B} + \omega_o^2 B + \beta_3\left[2\left(\Omega_\xi\dot{C} - \beta_3\Omega_\eta\dot{S}\right) + \left(\dot{\Omega}_\xi C - \dot{\Omega}_\eta S\right)\right] &= 0. \qquad (5.61)
\end{aligned}$$

For the generalised coordinates C, S, A and B, a system of highly-coupled equations of motion for a rotating 3D-disc vibratory gyroscope is obtained. Thus the equations of motion for a vibratory-disc gyroscope in 3D can now be written as:

$$\begin{aligned}
\ddot{C} + 2\beta_1\Omega_\zeta\dot{S} + \dot{\Omega}_\zeta\beta_1 S + \omega_I^2 C + \beta_2\left[2\left(\Omega_\eta\dot{A} - \Omega_\xi\dot{B}\right) + \left(\dot{\Omega}_\eta A - \dot{\Omega}_\xi B\right)\right] &= 0; \qquad (5.62) \\
\ddot{S} - 2\beta_1\Omega_\zeta\dot{C} - \beta_1\dot{\Omega}_\zeta C + \omega_I^2 S + \beta_2\left[2\left(\Omega_\xi\dot{A} + \Omega_\eta\dot{B}\right) + \dot{\Omega}_\xi A + \dot{\Omega}_\eta B\right] &= 0; \qquad (5.63) \\
\ddot{A} + \omega_o^2 A - \beta_3\left[2\left(\Omega_\eta\dot{C} + \Omega_\xi\dot{S}\right) + \left(\dot{\Omega}_\eta C + \dot{\Omega}_\xi S\right)\right] &= 0; \text{ and} \qquad (5.64) \\
\ddot{B} + \omega_o^2 B + \beta_3\left[2\left(\Omega_\xi\dot{C} - \Omega_\eta\dot{S}\right) + \left(\dot{\Omega}_\xi C - \dot{\Omega}_\eta S\right)\right] &= 0. \qquad (5.65)
\end{aligned}$$

The equations of motion in matrix form can be written as:

$$\begin{bmatrix} \ddot{C} \\ \ddot{S} \\ \ddot{A} \\ \ddot{B} \end{bmatrix} + 2 \begin{bmatrix} 0 & \beta_1\Omega_\zeta & \beta_2\Omega_\eta & -\beta_2\Omega_\xi \\ -\beta_1\Omega_\zeta & 0 & \beta_2\Omega_\xi & \beta_2\Omega_\eta \\ -\beta_3\Omega_\eta & -\beta_3\Omega_\xi & 0 & 0 \\ \beta_3\Omega_\xi & -\beta_3\Omega_\eta & 0 & 0 \end{bmatrix} \begin{bmatrix} \dot{C} \\ \dot{S} \\ \dot{A} \\ \dot{B} \end{bmatrix} +$$
$$\begin{bmatrix} 0 & \beta_1\dot{\Omega}_\zeta & \beta_2\dot{\Omega}_\eta & -\beta_2\dot{\Omega}_\xi \\ -\beta_1\dot{\Omega}_\zeta & 0 & \beta_2\dot{\Omega}_\xi & \beta_2\dot{\Omega}_\eta \\ -\beta_3\dot{\Omega}_\eta & -\beta_3\dot{\Omega}_\xi & 0 & 0 \\ \beta_3\dot{\Omega}_\xi & -\beta_3\dot{\Omega}_\eta & 0 & 0 \end{bmatrix} \begin{bmatrix} C \\ S \\ A \\ B \end{bmatrix} +$$
$$\begin{bmatrix} \omega_I^2 & 0 & 0 & 0 \\ 0 & \omega_I^2 & 0 & 0 \\ 0 & 0 & \omega_o^2 & 0 \\ 0 & 0 & 0 & \omega_o^2 \end{bmatrix} \begin{bmatrix} C \\ S \\ A \\ B \end{bmatrix} = 0. \tag{5.66}$$

In Equations (5.62) to (5.65), the terms such as $2\beta_1\Omega_\zeta\dot{S}$, $2\beta_1\Omega_\zeta\dot{C}$, $2\beta_2\Omega_\eta\dot{A}$ and $2\beta_2\Omega_\xi\dot{B}$, and so forth, are the so-called "gyroscopic coupling forces" where as $\omega_I^2 C$, $\omega_I^2 S$, $\omega_o^2 A$ and $\omega_o^2 B$ are the elastic forces. It can be seen from these equations that the in-plane modes are gyroscopically coupled to each other and to the out-of-plane modes but there is no gyroscopic coupling between the out-of-plane modes. Note that gyroscopic coupling forces determine how the modes of vibration interact with each other.

If $\vec{\Omega} = (\Omega_x, \Omega_y, \Omega_z) = 0$, Equation (5.66) becomes fully uncoupled and gives:

$$\begin{bmatrix} \ddot{C} \\ \ddot{S} \\ \ddot{A} \\ \ddot{B} \end{bmatrix} + \begin{bmatrix} \omega_I^2 & 0 & 0 & 0 \\ 0 & \omega_I^2 & 0 & 0 \\ 0 & 0 & \omega_o^2 & 0 \\ 0 & 0 & 0 & \omega_o^2 \end{bmatrix} \begin{bmatrix} C \\ S \\ A \\ B \end{bmatrix} = 0; \tag{5.67}$$

which is a harmonic oscillator equation with four degrees of freedom. In this case the in-plane modes (C, S) have undamped natural frequency:

$$\omega_I = \sqrt{\frac{\frac{Eh}{2(1-\eta^2)} \begin{bmatrix} \int_a^b (U_r')^2 + 2\eta U_r' \dfrac{(U+mV)}{r} + \left(\dfrac{U+mV}{r}\right)^2 + \\ \dfrac{1-\eta}{2}\left(V_r' - \dfrac{mU+V}{r}\right)^2 \end{bmatrix}}{\int_a^b (U^2+V^2)\, r dr}}; \tag{5.68}$$

and the undamped out-of-plane natural frequency for the modes (A, B) is given by:

$$\omega_o = \sqrt{\frac{\frac{Eh^3}{24(1-\eta^2)}\int_a^b \left[\begin{array}{c} \frac{2\eta W_r' W_{rr}''}{r} - \frac{\left(2(\eta-1)(m+1)^2-1\right)W_r'^2}{r^2} + \\ \left(\frac{(2\eta-3)(m+1)^2}{r^3}\right) W W_r' + r\left(W_{rr}''\right)^2 - \left(\frac{2\eta(m+1)^2}{r^2}\right) W W_{rr}'' \\ + \left(\frac{m^2\left(m^2+4m+8-2\eta\right)-2(\eta-2)(2m+1)-1}{r^4}\right) W^2 \end{array}\right] r dr}{\frac{\rho h}{2}\int_a^b W^2 r dr}}. \tag{5.69}$$

5.4.2 Non-homogeneous equations of motion

In the previous sub-section the equations of motion for the ideal case was developed, where the external forces and dissipative forces were neglected. For the purposes of the present discussion, assume that there is an ever-present, light-isotropic linear damping, with damping factor δ for both in-plane and out-of-plane vibrations. Define Rayleigh's dissipation functions R as shown in Joubert, Shatalov and Manzhirov (2013, [53]), namely:

$$R = \pi\delta\left\{I_0\left(\dot{C}^2 + \dot{S}^2\right) + I_4\left(\dot{A}^2 + \dot{B}^2\right)\right\}. \tag{5.70}$$

By "small light damping" it is meant that δ is substantially smaller than the lowest eigenvalue $\omega_{\min}$ of either the in-plane or out-of-plane vibration. It has been demonstrated by Joubert, Shatalov and Manzhirov (2013, [53]) that the rotation rates of vibrating patterns are not affected by light isotropic damping.

Using Equations (5.30) and (5.39), the Lagrangian $L = E_k - E_p(E_{p,in} + E_{p,out}) + E_e$ is determined, where E_e is the electrical potential energy introduced to achieve electronic control of the gyroscope. The electrical potential energy E_e is chosen in such a manner that it produces a so-called *force-to-rebalance regime* (See Wang *et al.* (2011, [73]) for a similar setup) that drives only the C and S-channels (not the A and B-channels) of the gyroscope at an operational angular frequency ω close to the natural frequencies, respectively, ω_I and ω_o of in-plane and out-of-plane vibrations. As in Joubert, Shatalov and Spoelstra (2017, [74]), the Euler-Lagrange equations for the generalised coordinates C, S, A and B in the Lagrangian L is applied, obtaining the *coupled system of ODE of gyroscopic motion* for an isotropically-damped and externally-excited system that can be written as:

$$\ddot{C} + 2\delta\dot{C} + 2\beta_1\Omega_\zeta\dot{S} + \beta_1\dot{\Omega}_\zeta S + \omega_I^2 C + \beta_2\left[2\left(\Omega_\eta\dot{A} - \Omega_\xi\dot{B}\right) + \left(\dot{\Omega}_\eta A - \dot{\Omega}_\xi B\right)\right] = f\cos\left(\omega t + \psi\right); \tag{5.71}$$

$$\ddot{S} + 2\delta\dot{S} - 2\beta_1\Omega_\zeta\dot{C} - \beta_1\dot{\Omega}_\zeta C + \omega_I^2 S + \beta_2\left[2\left(\Omega_\xi\dot{A} + \Omega_\eta\dot{B}\right) + \left(\dot{\Omega}_\xi A + \dot{\Omega}_\eta B\right)\right] = F\cos\left(\omega t + \Psi\right); \tag{5.72}$$

$$\ddot{A} + 2\delta\dot{A} + \omega_o^2 A - \beta_3\left[2\left(\Omega_\eta\dot{C} + \Omega_\xi\dot{S}\right) + \left(\dot{\Omega}_\eta C + \dot{\Omega}_\xi S\right)\right] = 0; \text{ and} \tag{5.73}$$

$$\ddot{B} + 2\delta\dot{B} + \omega_o^2 B + \beta_3\left[2\left(\Omega_\xi\dot{C} - \Omega_\eta\dot{S}\right) + \left(\dot{\Omega}_\xi C - \dot{\Omega}_\eta S\right)\right] = 0. \tag{5.74}$$

In the above equations, ψ and Ψ are phase angles with:

$$\beta_1 = \frac{I_1}{I_0}; \quad \beta_2 = \frac{I_3}{2I_0}; \quad \beta_3 = \frac{I_3}{2I_4}; \quad \omega_I = \sqrt{\frac{I_2}{I_0}}; \quad \text{and } \omega_o = \sqrt{\frac{I_5}{I_4}}. \tag{5.75}$$

The constant β_1 is *Bryan's factor* (See Joubert, Shatalov and Spoelstra (2017, [74])) while β_2 and β_3 are *auxiliary Bryan's factors* (Sedebo, Joubert & Shatalov, 2018, [34]). The quantities ω_I and ω_o are the eigenvalues of the in-plane and out-of-plane vibrations, respectively.

5.5 THE OPERATION PRINCIPLE OF THE DISC GYROSCOPE

The disc gyroscope operates as a rate sensor when one of the C-channels is set to oscillate at a constant amplitude with an in-plane natural frequency. This self-excited oscillation is said to be "the primary motion of the gyroscope". The amplitude of the primary oscillation is kept constant by means of an amplitude control loop (Wang *et al.*, 2011, [73]). To demonstrate the operation principle, Equations (5.71 to 5.74) are used without any external forces. Suppose that the primary motion of the gyroscope via the C-channel is independent of the rotation rate and is given by:

$$C\left(t\right) = C_s\sin\left(\omega_I t\right). \tag{5.76}$$

The rotation rate $\vec{\Omega} = (\Omega_x, \Omega_y, \Omega_z)$ is significantly less than the lowest eigenvalue of the vibrating system. Thus, the cross-coupling terms with contributions of $O\left(\left(\frac{\Omega_\eta}{\omega_I}\right)^2 C_s\right)$, $O\left(\left(\frac{\Omega_\xi}{\omega_I}\right)^2 C_s\right)$ and $O\left(\left(\frac{\Omega_\zeta}{\omega_I}\right)^2 C_s\right)$ are neglected (Gallacher *et al.*, [75]). Furthermore, all the effects of centrifugal forces are negligible and thus angular accelerations are irrelevant. Equations (5.72) to (5.74) then reduce to:

$$\begin{gathered}\ddot{S} + 2\delta\dot{S} + \omega_I^2 S = 2\omega_I\beta_1\Omega_\zeta C_c\cos\left(\omega_I t\right); \\ \ddot{A} + 2\delta\dot{A} + \omega_o^2 A = 2\omega_o\beta_2\Omega_\eta C_c\cos\left(\omega_I t\right); \text{ and} \\ \ddot{B} + 2\delta\dot{B} + \omega_o^2 B = -2\omega_o\beta_2\Omega_\xi C_c\cos\left(\omega_I t\right).\end{gathered} \tag{5.77}$$

Solving equations in Equation (5.77), using the method of undetermined coefficients and neglecting the transient part of the solution yields an approximate solution for each channel as:

$$S(t) = \frac{\beta_1 \Omega_\zeta C_c \cos(\omega_I t)}{\delta \omega_I}; \tag{5.78}$$

$$A(t) = -\frac{2\beta_2 \Omega_\eta \omega_I C_c \cos(\omega_I t - \alpha)}{\sqrt{(\omega_o^2 - \omega_I^2)^2 + 4\delta^2 \omega_I^2 \omega_o^2}}; \tag{5.79}$$

and

$$B(t) = \frac{2\beta_2 \Omega_\xi \omega_I C_c \cos(\omega_I t - \alpha)}{\sqrt{(\omega_o^2 - \omega_I^2)^2 + 4\delta^2 \omega_I^2 \omega_o^2}}; \tag{5.80}$$

with:

$$\alpha = \tan^{-1}\left(\frac{2\delta \omega_I \omega_o}{\omega_o^2 - \omega_I^2}\right). \tag{5.81}$$

It is clear from Equations (5.78) to (5.80) that the components of the applied inertial rate $\vec{\Omega}$ can be obtained by means of the measurement of the respective secondary motions. The components of the inertial rate and Bryan's effect are presented in the next section.

5.6 INERTIAL ROTATION RATES AND BRYAN'S EFFECT

G.H. Bryan (1890, [13]) in his experiment at the end of the nineteenth century explained the beating of sound produced by a ringing wine glass placed on a turntable, and his work laid the foundation for the physics of present day hemispherical resonator gyroscopes (HRGs). For a fixed mode of vibration, Bryan made the following calculation for the constant of proportionality (known as Bryan's factor) or angular gain (Johari & Ayazi, 2007, [18]) given by

$$BF = \frac{\text{Rate of rotation of the vibrating pattern}}{\text{Inertial rate of rotation of the vibrating structure}}. \tag{5.82}$$

Now assume that the disc is subjected to slow three-dimensional rotation described by projections Ω_ξ, Ω_η and Ω_ζ of the inertial angular rate onto the coordinate system $0\xi\eta\zeta$ as in Figure 5.1. Further, assume that the angular rate is much less than the smallest eigenvalue of the vibrating system. Now consider that in-plane vibrations of the structure are realised at m-mode and that of out-of-plane or bending vibrations are realised at $(m+1)$-mode. If the corresponding eigenvalues of the in-plane and out-of-plane vibrations are ω_I and ω_o, respectively then the equations of the m-ω_I and $(m+1)$-ω_o vibration patterns can be used in Section 5.6.1.

5.6.1 Inertial rotation rates

The *control or excitation force* $f\cos(\omega t+\psi)$ in Equation (5.71) is used to keep the *vibration amplitude of the C-channel constant* with the phase shift ψ *chosen* in such a way that $C\left(t\right)=C_{c}\cos\left(\omega t\right)$. With an appropriate phase shift Ψ, the *rebalance force* $F\cos\left(\omega t+\Psi\right)$ in Equation (5.72) is used to obtain $S\left(t\right)=0$.

To demonstrate how β_1 and β_3 are *related to rotation rates,* the force-rebalance electronic array discussed in (Wang *et al.*, 2011, [73]) can be used and it is assumed that a steady-state solution for Equation (5.71) to Equation (5.74) is of the form:

$$C\left(t\right) = C_{c}\cos\left(\omega t\right); \tag{5.83}$$

$$S(t) = 0; \tag{5.84}$$

$$A\left(t\right) = A_{c}\cos\left(\omega t\right)+A_{s}\sin\left(\omega t\right); \text{ and} \tag{5.85}$$

$$B\left(t\right) = B_{c}\cos\left(\omega t\right)+B_{s}\sin\left(\omega t\right). \tag{5.86}$$

Owing to the slow inertial rotation rate $\vec{\Omega}$, the amplitudes A_c, A_s, B_c and B_s are *slowly varying time-dependent quantities* that are *assumed to be constant* in order to determine simplified expressions for the angular rates. The exact nature of these amplitudes is left for future study. It can be assumed that acceptable average estimations of these amplitudes could be measured experimentally.

Substituting Equations (5.83) to (5.86) into Equations (5.71) to (5.74) yields the equations for the angular velocities $\Omega_{\zeta},\Omega_{\eta},\Omega_{\xi}$ and angular accelerations $\dot{\Omega}_{\zeta},\dot{\Omega}_{\eta},\dot{\Omega}_{\xi}$ as follows:

$$\begin{aligned}
\Omega_{\zeta} &= -\frac{F\sin\Psi}{2\omega C_{c}\beta_{1}};\ \Omega_{\eta}=\frac{1}{2}\left(\frac{2A_{c}\delta\omega+A_{s}\omega^{2}-A_{s}\omega_{o}^{2}}{C_{c}\,\beta_{3}\,\omega}\right);\text{ and}\\
\Omega_{\xi} &= -\frac{1}{2}\left(\frac{2B_{c}\,\delta\omega+B_{s}\omega^{2}-B_{s}\omega_{o}^{2}}{C_{c}\beta_{3}\omega}\right).
\end{aligned} \tag{5.87}$$

$$\begin{aligned}
\dot{\Omega}_{\zeta} &= -\frac{F\cos\Psi}{C_{c}\beta_{1}};\ \dot{\Omega}_{\eta}=-\left(\frac{A_{c}\omega^{2}-A_{c}\omega_{o}^{2}-2A_{s}\delta\omega}{C_{c}\beta_{3}}\right);\ \text{ and}\\
\dot{\Omega}_{\xi} &= \frac{B_{c}\omega^{2}-B_{c}\omega_{o}^{2}-2B_{s}\delta\omega}{C_{c}\beta_{3}}.
\end{aligned} \tag{5.88}$$

If the frequency split is introduced by a difference between the in-plane angular frequencies and the out-of-plane angular frequencies, the gyroscope can be “tuned” by varying the radial and/or axial thickness, thus $\omega_I=\omega_o=\omega$ for all practical purposes. It has been verified in Section 5.7 that this “tuning” is possible by conducting a numerical experiment. This "tuning” yields the following

simplified equations:

$$F\sin\Psi = -2\omega C_c\beta_1\Omega_\zeta;\quad A_c = \frac{C_c\beta_3}{\delta}\Omega_\eta;\quad B_c = \frac{-C_c\,\beta_3\Omega_\xi}{\delta}; \tag{5.89}$$

$$F\cos\Psi = -C_c\beta_1\dot{\Omega}_\zeta;\quad A_s = \frac{C_c\beta_3}{2\delta\omega}\dot{\Omega}_\eta;\quad B_s = -\frac{C_c\beta_3}{2\delta\omega}\dot{\Omega}_\xi. \tag{5.90}$$

The first equation in (5.89) demonstrates that the axial inertial rotation rate Ω_ζ is directly proportional to the amplitude F of the rebalance force. This result is *essentially* the same as that reported for the axial rotation rate of a HVG operating under the force-to-rebalance regime (see Wang *et al.* (2011, [73])). The amplitude F and phase angle Ψ of the rebalance force, the operational angular frequency ω as well as the amplitudes A_c, B_c and C_c should all be experimentally measurable.

5.6.2 Bryan's factors

The factors:

$$\beta_1 = \frac{I_1}{I_0} = \frac{2\int_a^b UVrdr}{\int_a^b (U^2+V^2)\,rdr};$$

$$\beta_2 = \frac{I_3}{2I_0} = \frac{\frac{1}{2}\int_a^b (U+V)\,Wrdr}{\int_a^b (U^2+V^2)\,rdr};$$

and

$$\beta_3 = \frac{I_3}{2I_4} = \frac{\frac{1}{2}\int_a^b (U+V)\,Wrdr}{\int_a^b W^2rdr};$$

from Equations (5.46), (5.47) and (5.56), respectively, are *Bryan's factor* (See Joubert, Shatalov & Spoelstra (2017, [74])) and what this study refers to as *auxiliary Bryan's factors* (Sedebo, Joubert & Shatalov, 2018, [34]). It was demonstrated in Joubert, Shatalov and Fay (2014, [76]) that the eigenfunctions (form-factors) of a vibrating structure that is not rotating remain invariant for a slowly rotating structure. Consequently, it is assumed that a small inertial rotation $\varepsilon\Omega$ takes place with $\varepsilon\Omega << \omega_{\min}$ where $\omega_{\min}$ is the minimum eigenvalue of the vibrating disc. Then, keeping in mind the remarks made above, Bryan's factor is calculated using the eigenfunctions already calculated. The quantities ω_I and ω_o are the eigenvalues or angular rates of the in-plane and out-of-plane vibrations, respectively. All the integrals I_0, I_1, I_2, I_3, I_4 and I_5 can be determined once the eigenfunctions U, V and W have been obtained in terms of Bessel's functions.

It has been shown by Shatalov, Fedotov and Joubert (2006, [77]) that Bryan's factor β_1 has values in the range $-1 \leq \beta_1 \leq 1$. Furthermore, β_1 varies with the geometric parameters, amongst others, for example, with the radius of the disc. It also varies with parameters like the mass density of the disc ρ and the modulus of elasticity E. It should also be noted that Bryan's factor depends

on the particular mode eigenfunctions. Bryan's factors β_1, β_2 and β_3 can be calculated from the formulae in Equation (5.75), once the eigenfunctions $U(r)$, $V(r)$ and $W(r)$ have been calculated as outlined in Sections 3.4 and 4.6, respectively. In Tables 5.2 and 5.4, the negative Bryan's factor β_1 indicates that, for in-plane-vibrations, the vibration pattern is rotating in the opposite direction to the direction of the inertial axial rotation rate. As the annulus decreases in thickness (inner radius increases), so Bryan's factor β_1 and the auxiliary Bryan's factor β_2 appear to increase in size, whereas the auxiliary Bryan's factor β_3 decreases in size.

5.7 TUNING

For this first approximation theory of a 3D-tuning, disc-vibratory gyroscope, a numerical experiment is provided, which demonstrates that it may well be possible to tune and design a TDVG. Consider an aluminium disc with Young's modulus $E = 7 \times 10^{10}\,\mathrm{N.m^{-2}}$, density $\rho = 2700\,\mathrm{kg.m^{-3}}$ and Poisson's ratio $\eta = 0.33$. With reference to Figure 5.1, the outer radius is kept constant at $b = 100\,\mathrm{mm}$, while the inner radius a and the height h are varied. Figure 5.2 illustrates how the estimate for tuned values of angular frequencies of in-plane and out-of-plane vibrations for $m = 2$ and $m = 3$, respectively, of an aluminium disc is obtained.

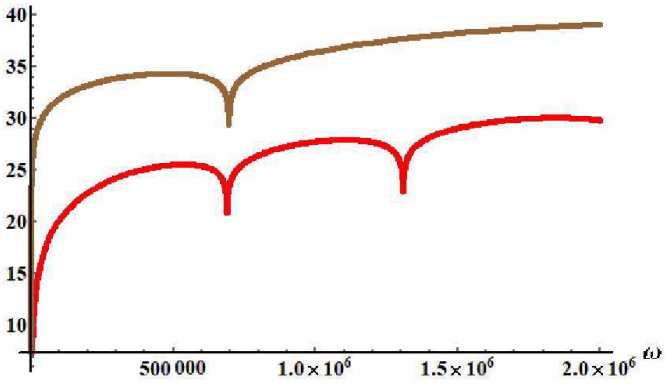

Figure 5.2: The graph used to estimate the tuned angular frequencies of in-plane and out-of-plane vibrations for $m = 2$ and $m = 3$, respectively, of an aluminium disc with inner radius $a = 42\ \mathrm{mm}$, outer radius $b = 100\ \mathrm{mm}$, density $\rho = 2.7 \times 10^3\ \mathrm{kg.m^{-3}}$, Young's modulus $E = 7 \times 10^{10}\ \mathrm{Pa}$ and Poisson's ratio $\upsilon = \frac{1}{3}$. The brown curve spike is used to approximate the out-of-plane eigenvalues and the red curve spikes are used to approximate the in-plane eigenvalues. Both eigenvalues are tuned approximately at $\omega \approx 688949.1598\ \mathrm{rad\,s^{-1}}$

Tables 5.1, 5.2, 5.3 and 5.4 were generated using Equation (5.75) and the computer algebra system

Maple 18 at standard working precision. In Table 5.3, with $h = 4.824\,\mathrm{mm}$ and $b = 100\,\mathrm{mm}$, the inner radius in each case is approximately $a = 40\,\mathrm{mm}$. Hence the thickness T of the annular disc is $T = b - a \approx 60\,\mathrm{mm}$ for each inner radius, and so the value of the ratio $\dfrac{T}{h} \approx 12$ lies in the interval defined for a "thin plate" in Section 1.1.3 of Venstel and Krauthammer (2001, [68]). Consequently, the values used in all the tables are commensurate with the theory developed above. With an inner radius of $42.51\,\mathrm{mm}$, it appears that it is feasible to "tune" the gyroscope and achieve a frequency split $\Delta f \approx 0\,\mathrm{kHz}$ (to four significant figures of accuracy).

Table 5.1: Eigenfrequencies for an aluminium vibratory disc gyroscope for a fixed outer radius of b = 100 mm and inner radius of a=42.51 mm for various values of thickness

$h\,(\mathrm{mm})$	$f_{in} = \frac{\omega_I}{2\pi}\,(\mathrm{kHz})$	$f_{out} = \frac{\omega_o}{2\pi}\,(\mathrm{kHz})$	$\Delta f = \lvert f_I - f_o \rvert\,(\mathrm{kHz})$
4.4240	5.7521	5.2749	0.4772
4.5240	5.7521	5.3941	0.3580
4.6240	5.7521	5.5133	0.2380
4.7240	5.7521	5.6323	0.1195
4.8240	5.7521	5.7518	0.0003

Table 5.2: Bryan's factor and auxiliary Bryan's factors for an aluminium vibratory-disc gyroscope for a fixed outer radius of b = 100 mm and inner radius of a = 42.51 mm, for various values of thickness h

$h\,(\mathrm{mm})$	β_1	β_2	β_3
4.4240	−0.7516	−0.1064	−0.0032
4.5240	−0.7516	−0.1064	−0.0032
4.6240	−0.7516	−0.1064	−0.0032
4.7240	−0.7516	−0.1064	−0.0032
4.8240	−0.7516	−0.1064	−0.0032

Table 5.3: Eigenfrequencies for an aluminium vibratory-disc gyroscope for a fixed outer radius of b = 100 mm and thickness of h = 4.824 mm for various values of inner radius a

$a\,(\mathrm{mm})$	$f_{in} = \frac{\omega_I}{2\pi}\,(\mathrm{kHz})$	$f_{out} = \frac{\omega_o}{2\pi}\,(\mathrm{kHz})$	$\Delta f = \lvert f_I - f_o \rvert\,(\mathrm{kHz})$
38.51	6.3233	5.8616	0.4617
39.51	6.1778	5.8329	0.3449
40.51	6.0341	5.8049	0.2293
41.51	5.8922	5.7777	0.1145
42.51	5.7521	5.7518	0.0003

Table 5.4: Bryan's factor and auxiliary Bryan's factors for an aluminium vibratory disc gyroscope with a fixed outer radius of b = 100 mm and thickness of h = 4.824 mm, for various values of inner radius a

$a\,(\mathrm{mm})$	β_1	β_2	β_3
38.51	−0.7515	−0.1008	−0.0072
39.51	−0.7513	−0.1037	−0.0060
40.51	−0.7513	−0.1057	−0.0050
41.51	−0.7514	−0.1067	−0.0040
42.51	−0.7516	−0.1064	−0.0032

5.8 EIGENFUNCTIONS FOR VARIOUS FREQUENCIES

Considering in-plane vibration with mode number $m = 2$ and out-of plane vibration with mode number $m+1 = 3$, and assuming free boundaries on the tuning, disc-vibratory gyroscope (TDVG), the eigenfunctions are calculated as outlined in Sections 3.4 and 4.6, respectively. The normalised eigenfunctions for various boundary conditions and values of eigenfrequencies are determined numerically and presented graphically in Figures 5.3 through 5.7. Salient properties are given in the captions. The $U_{2,0}$ $V_{2,0}$ and etcetera in Figures 5.5 and 5.6, respectively, are the radial and tengential eigenfunctions corresponding to the fundamental eigenfrequency, while $U_{2,1}$ $V_{2,1}$ and etcetera, respectively, are the radial and tangential eigenfunctions corresponding to the first overtone eigenfrequency. Similarly, in Figure 5.7, the $W_{3,0}, W_{3,1}$ and etcetera represent the axial eigenfunctions corresponding to the fundamental, first overtone and etcetera eigenfrequencies.

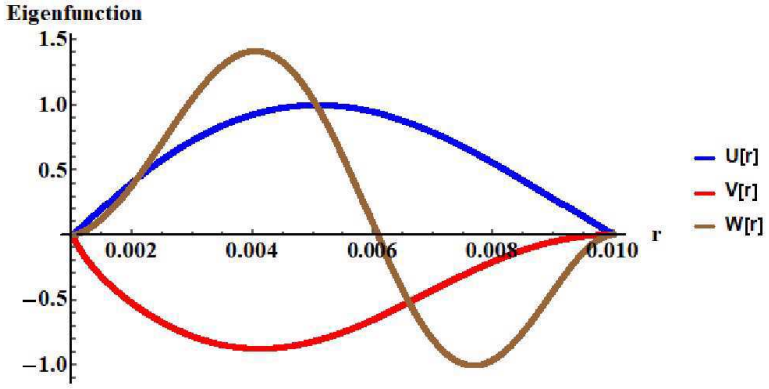

Figure 5.3: The normalised eigenfunctions U (blue curve), V (red curve) and W (brown curve) for an annular disc with clamped edges and scaled by their maximum modulus such that U and V are determined for mode number $m = 2$ while W is determined for mode number $m = 3$ and $\omega \approx 1.681977 \times 10^6\ \mathrm{rad\,s^{-1}}$

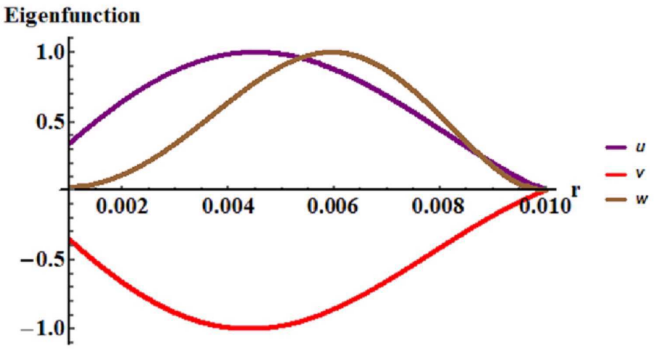

Figure 5.4: The normalised eigenfunctions U (purple curve), V (red curve) and W (brown curve) for a clamped solid disc and scaled by their maximum modulus such that U and V are determined for mode number $m = 2$ while W is determined for mode number $m = 3$ and $\omega \approx 1.362852 \times 10^6$ $\mathrm{rad\,s^{-1}}$

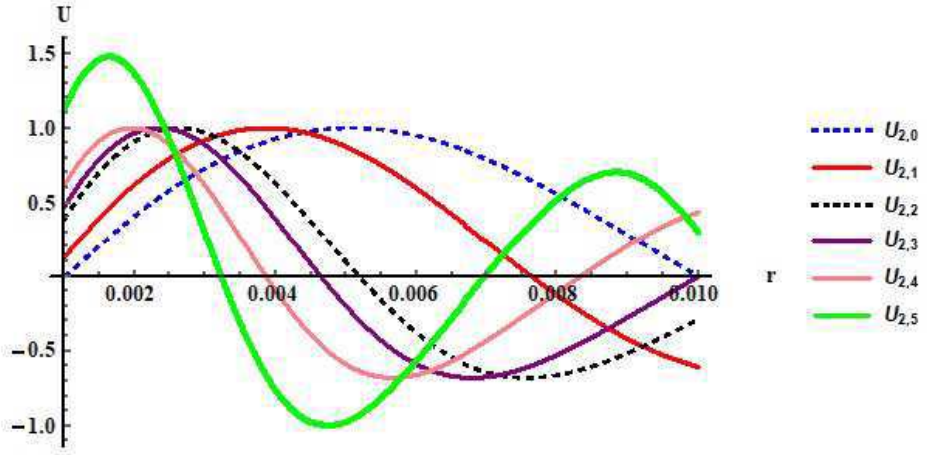

Figure 5.5: The first five normalised radial eigenfunctions corresponding the first five eigenfrequencies for an annular-disc gyroscope clamped at both edges

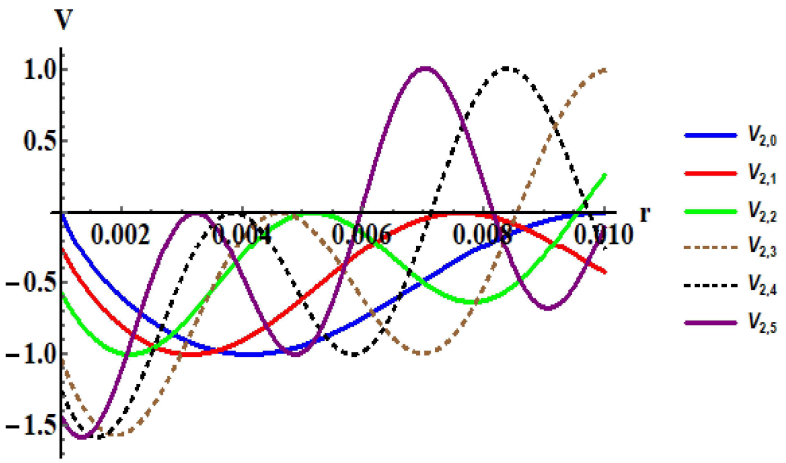

Figure 5.6: The first five normalised tangential eigenfunctions corresponding the first five eigenfrequencies for an annular-disc gyroscope clamped at both edges

5.9 CONCLUSION

In this chapter it was demonstrated that the model of the disc gyroscope can be developed in such a way that it measures three mutually-perpendicular rates of rotation along its different axes. The work presented here is new and it describes the dynamics of a 3D, disc-vibratory gyroscope. The equations of motion were derived using Hamilton's variational principle. The natural and geometric boundary conditions were set up using previous chapters. The eigenvalues and eigenfunctions of the vibrating disc for both in-plane and out-of-plane vibrations were incorporated with 3D rotations and fully described using Bryan's effect and inertial rotations. The eigenvalues and/or eigenfrequencies of both in-plane and out-of-plane vibrations were tuned to guarantee an optimum sensing capability of the proposed disc sensor. Eigenfunctions of both modes were obtained numerically to demonstrate how the deformations inside the disc gyroscope behave. The eigenfunctions demonstrated how the waves within the prescribed boundaries are guided. The natural frequencies of in-plane vibrations and out-of-plane vibrations were tuned by selecting appropriate thickness and radius of the disc. An approximate theory for an essentially ideal-tuning, disc-vibratory gyroscope (TDVG) rotating at a slow inertial angular rate in three dimensions was developed. Under various mild assumptions, the equations of motion of the TDVG were derived. Under a force-rebalance regime, assuming a steady-state solution, approximate expressions for the

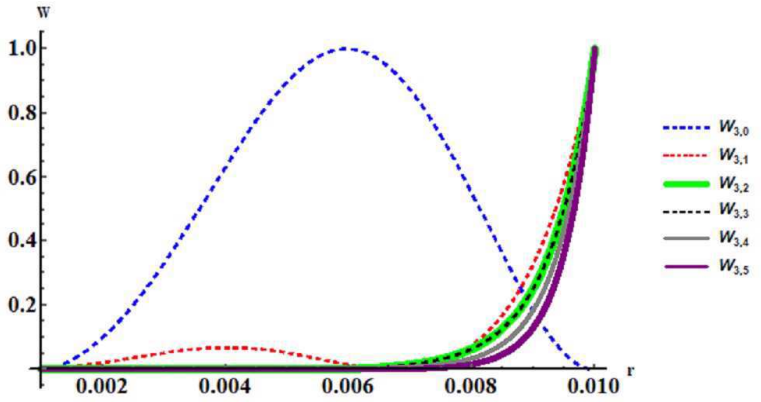

Figure 5.7: The first six normalised axial eigenfunctions corresponding to the first five eigenfrequencies for an annular-disc gyroscope clamped at both edges

angular rotation rate along each orthogonal rotation axis as well as the corresponding angular accelerations were formulated. The expression derived in this work for the axial inertial angular rate agrees with known results for a single axis of rotation, hemispherical, vibratory gyroscope. A numerical experiment using the first approximation theory was conducted to illustrate how it might be feasible to build and tune a three-dimensional (3D) TDVG.

Chapter 6

MASS IMPERFECTION IN A THREE-DIMENSIONAL, DISC-VIBRATORY GYROSCOPE

6.1 INTRODUCTION

The investigations of the disc gyroscope so far did not consider imperfections. Imperfections resulting from fabrication processes are the major sources of limitation of the performance of disc-vibratory gyroscopes (Lynch, 1995, [78]). The presence of imperfections in these gyroscopes causes deviations from ideal mass, stiffness and damping distributions and hence affects the dynamics of the resonator (Coetzee, 2008, [15]). The most common and easily observable consequences of imperfections in a resonator designed to operate in degenerate modes are : Natural frequency mismatch; localised mode shapes; and explicitly different damping factors associated with each mode (Ngungu, 2014, [79]).

Structural imperfections such as mass imperfections are discussed in the literature at length. Gallacher *et al*. (2005, [80]) studied procedures for identifying both mass and stiffness imperfections which result from fabrication variances in a microring gyroscope. They used electrostatic "tuning" because of its advantages over the usual trimming techniques to correct these perturbations. Control schemes to reduce structural imperfections in "whole angle" or "rate integrating" ring-vibratory gyroscope were investigated by Bowles *et al.* (2015, [81]). The authors provided an experimental validation to substantiate the theoretical study of the control scheme they investigated. A vibratory gyroscope with stiffness and damping imperfections was studied by Friedland and Hutton (1978, [82]), where they transformed the differential equations into the fourth order of linear systems in terms of average energy and momentum. A micromachined, silicon disc gyroscope with stiffness imperfections was investigated for analytical formulation of modal frequency split by Wei and Seshia in (2014, [46]). The theoretical study conducted for the elliptical mode was in good agreement with the finite element simulation.

In this study only mass anisotropy is considered, that is, anisotropies resulting from stiffness, Poisson's ratio and Young's modulus are left for future study. The derivation and analysis of mass imperfection in the disc-vibratory gyroscope are discussed in the sections that follow.

6.2 ENERGY AND THE LAGRANGIAN

In this section the expressions for kinetic energy, potential energy and the Lagrangian for a disc gyroscope with mass imperfections are derived. Similar to the perfect disc, the effects of rotary inertia are neglected. Hence, the kinetic energy of the disc will only be influenced by the absolute velocity of the centre of mass.

6.2.1 Kinetic energy

The approximate kinetic energy of a perfect disc gyroscope vibrating in its plane as well as out-of-plane is given by Equation (5.15), that is:

$$E_k \approx \int_0^{2\pi}\int_a^b \frac{\rho h r}{2}\left(\widetilde{\dot{u}}^2 + \widetilde{\dot{v}}^2 + \widetilde{\dot{w}}^2\right) dr d\varphi; \tag{6.1}$$

where ρ is the mass density of the disc. Now assume that the latter density of the disc varies circumferentially with respect to the orbital angle φ. Further assume that all the properties of light mass-imperfections that are needed to be addressed are explained by the φ dependence of the mass density. Due to the periodicity of the mass density along the circumference of the disc, it can be expanded using Fourier-series expansion as:

$$\rho(\varphi) = \rho_0\left(1 + \varepsilon\sum_{k=1}^{\infty}\left(\rho_{kc}\cos(k\varphi) + \rho_{ks}\sin(k\varphi)\right)\right); \tag{6.2}$$

where $\varepsilon > 0$ is a measure of smallness and hence characterises the variation of mass density with the circumferential angle φ. Further, ρ_0 is the fundamental component of the Fourier series or the average density of the disc and ρ_{kc} and ρ_{ks} are the coefficients of the k^{th}- harmonic component of the Fourier series. Taking mass-anisotropy into account Equation (6.1) can now be rewritten as:

$$\mathbb{K} \approx \frac{h}{2}\int_0^{2\pi}\int_a^b \rho(\varphi)\left(\widetilde{\dot{u}}^2 + \widetilde{\dot{v}}^2 + \widetilde{\dot{w}}^2\right) r dr d\varphi. \tag{6.3}$$

It should be kept in mind that:

$$u[r,\varphi,t] = U(r)\left[C(t)\cos(m\varphi) + S(t)\sin(m\varphi)\right]; \tag{6.4}$$

$$v[r,\varphi,t] = V(r)\left[C(t)\sin(m\varphi) - S(t)\cos(m\varphi)\right]; \text{ and} \tag{6.5}$$

$$w[r,\varphi,t] = W(r)\left[A(t)\cos(m+1)\varphi + B(t)\sin(m+1)\varphi\right]; \tag{6.6}$$

and further, the following integrals for all values of m should be recalled:

$$\int_0^{2\pi}\sin^2(m\varphi)\,d\varphi = \int_0^{2\pi}\cos^2(m\varphi)\,d\varphi = \pi;$$

$$
\begin{aligned}
\int_0^{2\pi} \sin(m\varphi)\cos(m\varphi)\,d\varphi &= 0;\\
\int_0^{2\pi} \sin((m+1)\varphi)\cos(m\varphi)\,d\varphi &= 0;\\
\int_0^{2\pi} \cos((m+1)\varphi)\sin(m\varphi)\,d\varphi &= 0;\ \text{and}\\
\int_0^{2\pi} \cos((m+1)\varphi)\cos(m\varphi)\,d\varphi &= 0.
\end{aligned}
$$

Thus it can be seen that only the $2m^{th}$ and $2(m+1)^{th}$ harmonics are important in the calculation of the kinetic energy of the system.

As explained in previous chapters the vibration modes which are investigated in this study are the $m = 2$ and the $(m+1)$-modes, respectively. Consequently only the 4^{th} and 6^{th} harmonics are crucial in the Fourier-series expansion. Now $\rho(\varphi) \times \widetilde{\dot{u}}^2$, $\rho(\varphi) \times \widetilde{\dot{v}}^2$ and $\rho(\varphi) \times \widetilde{\dot{w}}^2$ are expanded in Equation (6.3) using direct series expansion around $\varepsilon = 0$ and up to order $O(\varepsilon^2)$ (calculation details are given in the Appendices). Retaining terms proportional to $O(\varepsilon)$ and integrating the result with respect to φ on $[0,\, 2\pi]$ for each term, respectively, yields:

$$
\int_0^{2\pi} \rho(\varphi) \times \widetilde{\dot{u}}^2 d\varphi \approx \left\{ \begin{array}{c} U^2\pi\rho_0 \left(\left(\frac{dC}{dt}\right)^2 + \left(\frac{dS}{dt}\right)^2 \right) + \\ \pi\varepsilon \left\{ \begin{array}{c} \frac{U^2\rho_0}{2}\left(\frac{dC}{dt}\right)^2 \rho_{4c} - \frac{U^2\rho_0}{2}\left(\frac{dS}{dt}\right)^2 \rho_{4c} + \\ -2U\rho_0 \frac{dS}{dt}\Omega_\zeta CV + 2U\rho_0 \frac{dC}{dt}\Omega_\zeta SV + \\ -U\rho_0 \frac{dC}{dt}\Omega_\xi BW + U\rho_0 \frac{dS}{dt}\Omega_\xi AW + \\ U\rho_0 \frac{dS}{dt}\Omega_\eta BW + U\rho_0 \frac{dC}{dt}\Omega_\eta AW + \\ U^2\rho_0 \frac{dC}{dt}\frac{dS}{dt}\rho_{4s} \end{array} \right\} \end{array} \right\}; \qquad (6.7)
$$

$$
\int_0^{2\pi} \rho(\varphi) \times \widetilde{\dot{v}}^2 d\varphi \approx \left\{ \begin{array}{c} V^2\pi\rho_0 \left(\left(\frac{dC}{dt}\right)^2 + \left(\frac{dS}{dt}\right)^2 \right) + \\ \varepsilon\pi \left\{ \begin{array}{c} -2U\rho_0 \frac{dS}{dt}\Omega_\zeta CV + 2U\rho_0 \frac{dC}{dt}\Omega_\zeta SV + \\ \frac{V^2\rho_0}{2}\left(\frac{dS}{dt}\right)^2 \rho_{4c} - \frac{V^2\rho_0}{2}\left(\frac{dC}{dt}\right)^2 \rho_{4c} + \\ -V^2\rho_0 \frac{dC}{dt}\frac{dS}{dt}\rho_{4s} - V\rho_0 \frac{dC}{dt}\Omega_\xi BW + \\ V\rho_0 \frac{dS}{dt}\Omega_\xi AW + V\rho_0 \frac{dS}{dt}\Omega_\eta BW + \\ V\rho_0 \frac{dC}{dt}\Omega_\eta AW \end{array} \right\} \end{array} \right\}; \qquad (6.8)
$$

and

$$\int_0^{2\pi} \rho(\varphi) \times \widetilde{\dot{w}}^2 d\varphi \approx \left\{ \begin{array}{c} \pi W^2 \rho_0 \left(\left(\frac{dA}{dt} \right)^2 + \left(\frac{dB}{dt} \right)^2 \right) + \\ \pi W \left\{ \begin{array}{c} \frac{W^2 \rho_0}{2} \left(\frac{dA}{dt} \right)^2 \rho_{6c} - \frac{W^2 \rho_0}{2} \left(\frac{dB}{dt} \right)^2 \rho_{6c} + \\ W^2 \rho_0 \frac{dA}{dt} \frac{dB}{dt} \rho_{6s} + W \rho_0 \Omega_\xi C \frac{dB}{dt} V + \\ -W \rho_0 \Omega_\xi S \frac{dA}{dt} V - W \rho_0 \Omega_\eta C \frac{dA}{dt} V + \\ -W \rho_0 \Omega_\eta S \frac{dB}{dt} V - W \rho_0 \Omega_\eta C \frac{dA}{dt} U + \\ -W \rho_0 \Omega_\eta S \frac{dB}{dt} U + W \rho_0 \Omega_\xi C \frac{dB}{dt} U + \\ -W \rho_0 \Omega_\xi S \frac{dA}{dt} U \end{array} \right\} \end{array} \right\}. \quad (6.9)$$

Substitution of the expressions given by Equations (6.7), (6.8) and (6.9) into Equation (6.3) yields the approximate kinetic energy of disc gyroscope with mass imperfection vibrating in the $m = 2$ for in-plane and $m = 3$ for out-of-plane vibration modes. Using dot notation for derivatives with respect to time yields the following expression for kinetic energy:

$$\begin{aligned} \mathbb{K} &= \pi \left(\dot{C}^2 + \dot{S}^2 \right) \frac{\rho_0 h}{2} \int_a^b \left(U^2 + V^2 \right) r dr + 2\pi\varepsilon\Omega_\zeta \dot{C} S \rho_0 h \int_a^b UV r dr + \\ & \pi\varepsilon\rho_{4s} \dot{C}\dot{S} \frac{\rho_0 h}{2} \int_a^b (U - V)(U + V) r dr - 2\pi\varepsilon\Omega_\zeta C \dot{S} \rho_0 h \int_a^b UV r dr + \\ & + \varepsilon\pi\rho_{4c} \left(\dot{C}^2 - \dot{S}^2 \right) \frac{\rho_0 h}{4} \int_a^b (U - V)(U + V) r dr + \dot{A}\dot{B}\pi\varepsilon\rho_{6s} \frac{\rho_0 h}{2} \int_a^b W^2 r dr + \\ & \varepsilon\pi\dot{C} (A\Omega_\eta - B\Omega_\xi) \frac{\rho_0 h}{2} \int_a^b W (U + V) r dr + \varepsilon\pi\dot{S} (A\Omega_\xi + B\Omega_\eta) \frac{\rho_0 h}{2} \int_a^b W (U + V) r dr - \\ & \dot{A}\pi\varepsilon (S\Omega_\xi + C\Omega_\eta) \frac{\rho_0 h}{2} \int_a^b W (U + V) r dr + \dot{B}\pi\varepsilon (C\Omega_\xi - S\Omega_\eta) \frac{\rho_0 h}{2} \int_a^b W (U + V) r dr + \\ & \left(\dot{A}^2 - \dot{B}^2 \right) \pi\varepsilon\rho_{6c} \frac{\rho_0 h}{4} \int_a^b W^2 r dr + \pi \left(\dot{A}^2 + \dot{B}^2 \right) \frac{\rho_0 h}{2} \int_a^b W^2 r dr. \end{aligned} \quad (6.10)$$

Assuming that the eigenfunctions U, V and W of Equations (6.4)-(6.6) are known and replacing the density with the average density, the following definite integrals can be obtained:

$$I_0 = \frac{\rho_0 h}{2} \int_a^b \left(U^2 + V^2 \right) r dr,\ I_1 = \rho_0 h \int_a^b UV r dr; \quad (6.11)$$

$$I_3 = \frac{\rho_0 h}{2} \int_a^b W (U + V) r dr,\ I_4 = \frac{\rho_0 h}{2} \int_a^b W^2 r dr; \text{ and} \quad (6.12)$$

$$I_6 = \frac{\rho_0 h}{4} \int_a^b \left(U^2 - V^2 \right) r dr. \quad (6.13)$$

Thus, substituting the expressions given for the definite integrals in Equations (6.11), (6.12) and (6.13) into Equation (6.10), the kinetic energy of the disc gyroscope with mass imperfection in

terms of C, S, $\dot{C}$, $\dot{S}$, A, B, $\dot{A}$ and $\dot{B}$ in compact form can now be written as:

$$\begin{aligned}\mathbb{K} &= \pi\left(\dot{C}^2+\dot{S}^2\right)I_0+\varepsilon\pi\rho_{4c}\left(\dot{C}^2-\dot{S}^2\right)I_6+2\pi\varepsilon\rho_{4s}\dot{C}\dot{S}I_6+2\pi\varepsilon\Omega_\zeta\dot{C}SI_1- \\ &\quad 2\pi\varepsilon\Omega_\zeta C\dot{S}I_1+\varepsilon\pi\dot{C}\left(A\Omega_\eta-B\Omega_\xi\right)I_3+\varepsilon\pi\dot{S}\left(A\Omega_\xi+B\Omega_\eta\right)I_3- \\ &\quad \dot{A}\pi\varepsilon\left(S\Omega_\xi+C\Omega_\eta\right)I_3+\dot{B}\pi\varepsilon\left(C\Omega_\xi-S\Omega_\eta\right)I_3+\dot{A}\dot{B}\pi\varepsilon\rho_{6s}I_4+ \\ &\quad \frac{1}{2}\left(\dot{A}^2-\dot{B}^2\right)\pi\varepsilon\rho_{6c}I_4+\pi\left(\dot{A}^2+\dot{B}^2\right)I_4. \end{aligned} \tag{6.14}$$

In Equation (6.14), terms of order $O\left(\varepsilon^2\right)$, such as Ω_ξ^2, Ω_η^2, Ω_ζ^2, $\Omega_\zeta\Omega_\eta$, $\Omega_\eta\Omega_\xi$ and $\Omega_\xi\Omega_\zeta$ are neglected, because the lowest eigenvalue of the vibrating system is assumed to be much larger than the angular rotation rate $\vec{\Omega}$. It should be noted here that the time dependence of $\vec{\Omega}=(\Omega_x,\ \Omega_y,\ \Omega_z)$ is suppressed in this chapter for the purpose of simplification of the model.

6.2.2 Potential energy

The disc gyroscope under investigation is assumed to be a perfectly elastic structure and hence when the structure deforms the potential energy is stored in the form of strain energy. In this study pre-stresses which stipulate the stiffness imperfections are ignored. Consequently, stiffness imperfections are not considered. Similar to the previous model, the total potential energy of the disc is given by the sum of the in-plane potential energy and out-of-plane potential energy. Thus the potential energy of the disc gyroscope is assumed to be the same as the potential energy of the perfect disc gyroscope discussed in Subsection 5.3.2 as given in Equation (5.39).

6.2.3 Lagrangian

The Lagrangian $(\mathcal{L})$ of the disc with mass imperfections is given as the difference between the kinetic and potential energies (Spiegel, 1982, [29]). Using Equation (6.10) for the kinetic energy and Equation (5.39) for the potential energy, the expression of the Lagrangian for the disc gyroscope with mass imperfection is given by:

$$\begin{aligned}\mathcal{L} &= \pi\left(\dot{C}^2+\dot{S}^2\right)I_0+\varepsilon\pi\rho_{4c}\left(\dot{C}^2-\dot{S}^2\right)I_6+2\pi\varepsilon\rho_{4s}\dot{C}\dot{S}I_6+2\pi\varepsilon\Omega_\zeta\dot{C}SI_1- \\ &\quad 2\pi\varepsilon\Omega_\zeta C\dot{S}I_1+\varepsilon\pi\dot{C}\left(A\Omega_\eta-B\Omega_\xi\right)I_3+\varepsilon\pi\dot{S}\left(A\Omega_\xi+B\Omega_\eta\right)I_3- \\ &\quad \dot{A}\pi\varepsilon\left(S\Omega_\xi+C\Omega_\eta\right)I_3+\dot{B}\pi\varepsilon\left(C\Omega_\xi-S\Omega_\eta\right)I_3+\dot{A}\dot{B}\pi\varepsilon\rho_{6s}I_4+ \\ &\quad \frac{1}{2}\left(\dot{A}^2-\dot{B}^2\right)\pi\varepsilon\rho_{6c}I_4+\pi\left(\dot{A}^2+\dot{B}^2\right)I_4- \\ &\quad I_2\pi\left(C^2+S^2\right)-I_5\pi\left(A^2+B^2\right). \end{aligned} \tag{6.15}$$

6.3 THE EULER-LAGRANGE EQUATIONS OF MOTION FOR A DISC GYROSCOPE WITH MASS IMPERFECTIONS

To formulate the governing equations of motion for a disc gyroscope with mass imperfections the generalised coordinates C, S, A and B are used. The following derivatives are required to derive the equations of motion:

$$\frac{\partial \mathcal{L}}{\partial C} = \pi\left\{-2\varepsilon\Omega_\zeta \dot{S} I_1 - \dot{A}\varepsilon\Omega_\eta I_3 + \dot{B}\varepsilon\Omega_\xi I_3 - 2I_2 C\right\}; \tag{6.16}$$

$$\frac{\partial \mathcal{L}}{\partial \dot{C}} = \pi\left\{2I_0\dot{C} + 2\varepsilon\rho_{4c}\dot{C}I_6 + 2\varepsilon\rho_{4s}\dot{S}I_6 + 2\varepsilon\Omega_\zeta S I_1 + \varepsilon\left(A\Omega_\eta - B\Omega_\xi\right) I_3\right\}; \tag{6.17}$$

$$\frac{d}{dt}\left(\frac{\partial \mathcal{L}}{\partial \dot{C}}\right) = \pi\left\{\begin{array}{c} 2I_0\ddot{C} + 2\varepsilon\rho_{4c}\ddot{C}I_6 + 2\varepsilon\rho_{4s}\ddot{S}I_6 + 2\varepsilon\Omega_\zeta\dot{S}I_1 + \\ \varepsilon\left(\dot{A}\Omega_\eta - \dot{B}\Omega_\xi\right) I_3 \end{array}\right\}; \tag{6.18}$$

$$\frac{\partial \mathcal{L}}{\partial S} = \pi\left\{-\dot{A}\varepsilon\Omega_\xi I_3 - \dot{B}\varepsilon\Omega_\eta I_3 + 2\varepsilon\Omega_\zeta\dot{C}I_1 - 2I_2 S\right\}; \tag{6.19}$$

$$\frac{\partial \mathcal{L}}{\partial \dot{S}} = \pi\left\{2I_0\dot{S} - 2\varepsilon\rho_{4c}I_6\dot{S} + 2\varepsilon\rho_{4s}\dot{C}I_6 - 2\varepsilon\Omega C I_1 + \varepsilon\left(A\Omega_\xi + B\Omega_\eta\right) I_3\right\}; \tag{6.20}$$

$$\frac{d}{dt}\left(\frac{\partial \mathcal{L}}{\partial \dot{S}}\right) = \pi\left\{2I_0\ddot{S} - 2\varepsilon\rho_{4c}I_6\ddot{S} + 2\varepsilon\rho_{4s}\ddot{C}I_6 - 2\varepsilon\Omega\dot{C}I_1 + \varepsilon\left(\dot{A}\Omega_\xi + \dot{B}\Omega_\eta\right) I_3\right\}; \tag{6.21}$$

$$\frac{\partial \mathcal{L}}{\partial A} = \pi\left\{\varepsilon\dot{C}\Omega_\eta I_3 + \dot{S}\varepsilon\Omega_\xi I_3 - 2I_5 A,\right\}, \tag{6.22}$$

$$\frac{\partial \mathcal{L}}{\partial \dot{A}} = \pi\left\{2\dot{A}I_4 + 2\dot{A}\varepsilon\rho_{6c}I_4 - \varepsilon\left(S\Omega_\xi + C\Omega_\eta\right) I_3 + \dot{B}\varepsilon\rho_{6s}I_4\right\}, \tag{6.23}$$

$$\frac{d}{dt}\left(\frac{\partial \mathcal{L}}{\partial \dot{A}}\right) = \pi\left\{2\ddot{A}I_4 + 2\ddot{A}\varepsilon\rho_{6c}I_4 - \varepsilon\left(\dot{S}\Omega_\xi + \dot{C}\Omega_\eta\right) I_3 + \varepsilon\ddot{B}\rho_{6s}I_4\right\}, \tag{6.24}$$

$$\frac{\partial \mathcal{L}}{\partial B} = \pi\left\{-\varepsilon\Omega_\xi\dot{C}I_3 + \varepsilon\Omega_\eta\dot{S}I_3 - 2I_5 B\right\}; \tag{6.25}$$

$$\frac{\partial \mathcal{L}}{\partial \dot{B}} = \pi\left\{2\dot{B}I_4 - 2\dot{B}\varepsilon\rho_{6c}I_4 + \dot{A}\varepsilon\rho_{6c}I_4 + \varepsilon\left(C\Omega_\xi - S\Omega_\eta\right) I_3\right\}; \text{ and} \tag{6.26}$$

$$\frac{d}{dt}\left(\frac{\partial \mathcal{L}}{\partial \dot{B}}\right) = \pi\left\{2\ddot{B}I_4 - 2\ddot{B}\varepsilon\rho_{6c}I_4 + \ddot{A}\varepsilon\rho_{6c}I_4 + \varepsilon\left(\dot{C}\Omega_\xi - \dot{S}\Omega_\eta\right) I_3\right\}. \tag{6.27}$$

The governing equations of motion for the disc gyroscope vibrating in the m^{th} and $(m+1)^{th}$ vibration modes are obtained in terms of the generalised coordinates (C, S, A, S) (Goldstein, Poole & Safco, 2000, [64]) as:

$$\frac{d}{dt}\left(\frac{\partial L}{\partial \dot{C}}\right) - \frac{\partial L}{\partial C} = 0; \tag{6.28a}$$

$$\frac{d}{dt}\left(\frac{\partial L}{\partial \dot{S}}\right) - \frac{\partial L}{\partial S} = 0; \tag{6.28b}$$

$$\frac{d}{dt}\left(\frac{\partial L}{\partial \dot{A}}\right) - \frac{\partial L}{\partial A} = 0; \text{ and} \tag{6.28c}$$

$$\frac{d}{dt}\left(\frac{\partial L}{\partial \dot{B}}\right) - \frac{\partial L}{\partial B} = 0. \tag{6.28d}$$

Assume that there is ever-present light isotropic, linear damping, with damping factors δ_1 for in-plane and δ_2 for out-of-plane vibrations, respectively. Now Rayleigh's dissipation function $\mathcal{D}$ is defined as (see Joubert *et al.* (2017, [83])):

$$\mathcal{D} = \pi\varepsilon \left\{ I_0\delta_1 \left(\dot{C}^2 + \dot{S}^2 \right) + I_4\delta_2 \left(\dot{A}^2 + \dot{B}^2 \right) \right\}. \tag{6.29}$$

Including light isotropic damping into Equations (6.28a)-(6.28d) the following are obtained:

$$\frac{d}{dt}\left(\frac{\partial \mathcal{L}}{\partial \dot{C}}\right) - \frac{\partial \mathcal{L}}{\partial C} = -\frac{\partial \mathcal{D}}{\partial \dot{C}}; \tag{6.30a}$$

$$\frac{d}{dt}\left(\frac{\partial \mathcal{L}}{\partial \dot{S}}\right) - \frac{\partial \mathcal{L}}{\partial S} = -\frac{\partial \mathcal{D}}{\partial \dot{S}}; \tag{6.30b}$$

$$\frac{d}{dt}\left(\frac{\partial \mathcal{L}}{\partial \dot{A}}\right) - \frac{\partial \mathcal{L}}{\partial A} = -\frac{\partial \mathcal{D}}{\partial \dot{A}}; \text{ and} \tag{6.30c}$$

$$\frac{d}{dt}\left(\frac{\partial \mathcal{L}}{\partial \dot{B}}\right) - \frac{\partial \mathcal{L}}{\partial B} = -\frac{\partial \mathcal{D}}{\partial \dot{B}}. \tag{6.30d}$$

Substituting Equations (6.16)-(6.18) into Equation (6.30a) after simplifications yields:

$$\left(1 + \varepsilon\rho_{4c}\gamma_1\right)\ddot{C} + \varepsilon\rho_{4s}\gamma_1\ddot{S} + 2\varepsilon\Omega_\zeta\beta_1\dot{S} + 2\beta_2\varepsilon\left(\dot{A}\Omega_\eta - \dot{B}\Omega_\xi\right) + \omega_I^2 C = -2\varepsilon\delta_1\dot{C}; \tag{6.31}$$

where:

$$\gamma_1 = \frac{I_6}{I_0},\ \beta_2 = \frac{I_3}{2I_0}, \beta_1 = \frac{I_1}{I_0}, \omega_I^2 = \frac{I_2}{I_0}. \tag{6.32}$$

Similarly, for the generalised coordinate S, substitution of Equations (6.19) to (6.21) into Equation (6.30b) leads to:

$$\varepsilon\rho_{4s}\ddot{C}\gamma_1 + \left(1 - \varepsilon\rho_{4c}\gamma_1\right)\ddot{S} - 2\varepsilon\Omega_\zeta\beta_1\dot{C} + 2\beta_2\varepsilon\left(\dot{A}\Omega_\xi + \dot{B}\Omega_\eta\right) + \omega_I^2 S = -2\varepsilon\delta_1\dot{S}. \tag{6.33}$$

Equations (6.31) and (6.33) describe the in-plane vibration of the disc gyroscope with mass imperfections and vibrating at mode number $m = 2$.

The equations of motion which describe the out-of-plane vibrations of the disc gyroscope with a mode number $m = 3$ can be derived in a similar way. Consequently, substitution of Equations (6.22) to (6.24) into Equation (6.30c) simplifies to:

$$\left(1 + \varepsilon\rho_{6c}\gamma_2\right)\ddot{A} + \varepsilon\rho_{6s}\gamma_2\ddot{B} - 2\beta_3\varepsilon\left(\dot{C}\Omega_\eta + \dot{S}\Omega_\xi\right) + \omega_o^2 A = -2\varepsilon\delta_2\dot{A}; \tag{6.34}$$

where:

$$\gamma_2 = \frac{I_4}{2I_4}, \beta_3 = \frac{I_3}{2I_4}, \omega_o^2 = \frac{I_5}{I_4}. \tag{6.35}$$

For the generalised coordinate B, substituting Equations (6.25) to (6.27) into Equation (6.30d) yields:

$$\varepsilon\rho_{6s}\gamma_2\ddot{A} + \left(1 - \varepsilon\rho_{6c}\gamma_2\right)\ddot{B} + 2\beta_3\varepsilon\left(\dot{C}\Omega_\xi - \dot{S}\Omega_\eta\right) + \omega_o^2 B = -2\varepsilon\delta_2\dot{B}. \tag{6.36}$$

The Euler-Lagrange equations for the generalised coordinates C, S, A and B in the Lagrangian $\mathcal{L}$, for the isotropically-damped disc gyroscope with mass imperfections leads to a *coupled system of*

ODEs of gyroscopic motion :

$$(1+\varepsilon\rho_{4c}\gamma_1)\,\ddot{C}+\varepsilon\rho_{4s}\gamma_1\ddot{S}+2\varepsilon\Omega_\zeta\beta_1\dot{S}+2\beta_2\varepsilon\left(\dot{A}\Omega_\eta-\dot{B}\Omega_\xi\right)+\omega_I^2C = -2\varepsilon\delta_1\dot{C} \quad (6.37)$$

$$\varepsilon\rho_{4s}\gamma_1\ddot{C}+(1-\varepsilon\rho_{4c}\gamma_1)\,\ddot{S}-2\varepsilon\Omega_\zeta\beta_1\dot{C}+2\beta_2\varepsilon\left(\dot{A}\Omega_\xi+\dot{B}\Omega_\eta\right)+\omega_I^2S = -2\varepsilon\delta_1\dot{S} \quad (6.38)$$

$$(1+\varepsilon\rho_{6c}\gamma_2)\,\ddot{A}+\varepsilon\rho_{6s}\gamma_2\ddot{B}-2\beta_3\varepsilon\left(\dot{C}\Omega_\eta+\dot{S}\Omega_\xi\right)+\omega_o^2A = -2\varepsilon\delta_2\dot{A} \quad (6.39)$$

$$\varepsilon\rho_{6s}\gamma_2\ddot{A}+(1-\varepsilon\rho_{6c}\gamma_2)\,\ddot{B}+2\beta_3\varepsilon\left(\dot{C}\Omega_\xi-\dot{S}\Omega_\eta\right)+\omega_o^2B = -2\varepsilon\delta_2\dot{B}. \quad (6.40)$$

In Equations (6.37) to (6.40), β_1 is Bryan's factor whereas β_2 and β_3 are the auxiliary (secondary) Bryan's factors (Sedebo, Joubert & Shatalov, 2018, [34]). Note that $-1 \leq \beta_1 \leq \dfrac{I_1}{I_0} \leq 1$.

6.4 FREQUENCY SPLIT

It is common that structural imperfections such as mass imperfections resulting from manufacturing processes perturb the system from the ideal isotropic mass (Gallachar *et al.*, 2005, [80]). Due to mass imperfection the symmetry of the disc gyroscope breaks and that results in a frequency split. In this section this frequency mismatch is shown for both in-plane and out-of-plane vibration modes. As an example, the frequency split between the two in-plane modes and the out-of-plane modes is shown as below.

The matrix form of Equations (6.37) and (6.38) can be written as:

$$\begin{pmatrix} 1+\varepsilon\rho_{CI} & \varepsilon\rho_{SI} \\ \varepsilon\rho_{SI} & 1-\varepsilon\rho_{CI} \end{pmatrix}\begin{pmatrix} \ddot{C} \\ \ddot{S} \end{pmatrix}+\begin{pmatrix} 0 & 2\varepsilon\Omega_\zeta\beta_1 \\ -2\varepsilon\Omega_\zeta\beta_1 & 0 \end{pmatrix}\begin{pmatrix} \dot{C} \\ \dot{S} \end{pmatrix}+ \begin{pmatrix} 2\varepsilon\Omega_\eta\beta_2 & -2\varepsilon\Omega_\xi\beta_2 \\ 2\varepsilon\Omega_\xi\beta_2 & 2\varepsilon\Omega_\eta\beta_2 \end{pmatrix}\begin{pmatrix} \dot{A} \\ \dot{B} \end{pmatrix}+\omega_I^2\begin{pmatrix} 1 & 0 \\ 0 & 1 \end{pmatrix}\begin{pmatrix} C \\ S \end{pmatrix} \quad ; \quad (6.41)$$
$$= \begin{pmatrix} -2\varepsilon\delta_1 & 0 \\ 0 & -2\varepsilon\delta_1 \end{pmatrix}\begin{pmatrix} \dot{C} \\ \dot{S} \end{pmatrix}$$

where:

$$\rho_{4c}\gamma_1 = \rho_{CI};\ \text{and}\ \rho_{4s}\gamma_1 = \rho_{SI}.$$

The determinant Δ_1 of the leading coefficient matrix after neglecting terms proportional to $O(\varepsilon^2)$ gives:

$$\Delta_1 = \det\begin{pmatrix} 1+\varepsilon\rho_{CI} & \varepsilon\rho_{SI} \\ \varepsilon\rho_{SI} & 1-\varepsilon\rho_{CI} \end{pmatrix} \approx 1. \quad (6.42)$$

Thus, the inverse of the leading coefficient matrix is given by:

$$\frac{1}{\Delta_1}\begin{pmatrix} 1-\varepsilon\rho_{CI} & -\varepsilon\rho_{SI} \\ -\varepsilon\rho_{SI} & 1+\varepsilon\rho_{CI} \end{pmatrix} = \begin{pmatrix} 1-\varepsilon\rho_{CI} & -\varepsilon\rho_{SI} \\ -\varepsilon\rho_{SI} & 1+\varepsilon\rho_{CI} \end{pmatrix}. \quad (6.43)$$

Consequently, multiplication on the left of Equation (6.41) by Equation (6.43) and again neglecting

$O(\varepsilon^2)$ terms yields:

$$\left\{ \begin{array}{c} \begin{pmatrix} \ddot{C} \\ \ddot{S} \end{pmatrix} + \begin{pmatrix} 0 & 2\varepsilon\Omega_\zeta\beta_1 \\ -2\varepsilon\Omega_\zeta\beta_1 & 0 \end{pmatrix} \begin{pmatrix} \dot{C} \\ \dot{S} \end{pmatrix} + \\ \omega_I^2 \begin{pmatrix} 1-\varepsilon\rho_{CI} & -\varepsilon\rho_{SI} \\ -\varepsilon\rho_{SI} & 1+\varepsilon\rho_{CI} \end{pmatrix} \begin{pmatrix} C \\ S \end{pmatrix} + \\ \begin{pmatrix} 2\varepsilon\Omega_\eta\beta_2 & -2\varepsilon\Omega_\xi\beta_2 \\ 2\varepsilon\Omega_\xi\beta_2 & 2\varepsilon\Omega_\eta\beta_2 \end{pmatrix} \begin{pmatrix} \dot{A} \\ \dot{B} \end{pmatrix} \\ = \begin{pmatrix} -2\varepsilon\delta_1 & 0 \\ 0 & -2\varepsilon\delta_1 \end{pmatrix} \begin{pmatrix} \dot{C} \\ \dot{S} \end{pmatrix}. \end{array} \right\}. \tag{6.44}$$

The eigenvalues:

$$\omega_I^2\left(1+\varepsilon\sqrt{\rho_{CI}^2+\rho_{SI}^2}\right);\ \text{and}\ \omega_I^2\left(1-\varepsilon\sqrt{\rho_{CI}^2+\rho_{SI}^2}\right); \tag{6.45}$$

of the matrix:

$$\omega_I^2 \begin{pmatrix} 1-\varepsilon\rho_{CI} & -\varepsilon\rho_{SI} \\ -\varepsilon\rho_{SI} & 1+\varepsilon\rho_{CI} \end{pmatrix};$$

indicate that the mass imperfection causes a frequency splitting (beats) in the in-plane vibration mode. Thus it is clear that there are two waves operating with frequencies:

$$f_1 = \frac{\omega_I}{2\pi}\sqrt{1+\varepsilon\sqrt{\rho_{CI}^2+\rho_{SI}^2}}; \tag{6.46}$$

and

$$f_2 = \frac{\omega_I}{2\pi}\sqrt{1-\varepsilon\sqrt{\rho_{CI}^2+\rho_{SI}^2}}; \tag{6.47}$$

respectively. Direct series expansions of $\sqrt{1+\varepsilon\sqrt{\rho_{CI}^2+\rho_{SI}^2}}$ and $\sqrt{1-\varepsilon\sqrt{\rho_{CI}^2+\rho_{SI}^2}}$, neglecting terms proportional to $O(\varepsilon^2)$ and higher yields:

$$\sqrt{1+\varepsilon\sqrt{\rho_{CI}^2+\rho_{SI}^2}} = 1+\frac{1}{2}\varepsilon\sqrt{\rho_{CI}^2+\rho_{SI}^2}+O\left(\varepsilon^2\right); \tag{6.48}$$

and

$$\sqrt{1-\varepsilon\sqrt{\rho_{CI}^2+\rho_{SI}^2}} = 1-\frac{1}{2}\varepsilon\sqrt{\rho_{CI}^2+\rho_{SI}^2}+O\left(\varepsilon^2\right). \tag{6.49}$$

Approximate values for the two frequencies can be written as:

$$f_1 \approx \frac{\omega_I}{2\pi}\left(1+\frac{1}{2}\varepsilon\sqrt{\rho_{CI}^2+\rho_{SI}^2}\right); \tag{6.50}$$

and

$$f_2 \approx \frac{\omega_I}{2\pi}\left(1-\frac{1}{2}\varepsilon\sqrt{\rho_{CI}^2+\rho_{SI}^2}\right). \tag{6.51}$$

Thus the frequency of the beats of the in-plane vibration is:

$$\Delta f_I = |f_1 - f_2| = \frac{\omega_I\varepsilon\sqrt{\rho_{CI}^2+\rho_{SI}^2}}{2\pi}. \tag{6.52}$$

Using similar reasoning it can be shown that the mass imperfection can cause a frequency split or beats between the out-of-plane modes. Accordingly, the frequency of beats between the two

out-of-plane modes is:

$$\Delta f_o = \frac{\omega_o \varepsilon \sqrt{\rho_{Co}^2 + \rho_{So}^2}}{2\pi}; \tag{6.53}$$

where:

$$\rho_{Co} = \rho_{6c}\gamma_2; \text{ and } \rho_{So} = \rho_{6s}\gamma_2.$$

Mechanisms of control and compensation of frequency split either between the two in-plane modes or the two out-of-plane modes or between the in-plane and out-of-plane modes are not considered in this study and are left for future study.

6.5 THEORETICAL ANALYTICAL DISCUSSION

The coupled equations of gyroscopic motion given in Equations (6.37) to (6.40) which are subjected to light isotropic damping and mass imperfections are used for theoretical analysis of operation principles and light imperfections of the disc gyroscope. The cosine signal (A) and sine signal (B) of the out-of-plane vibration of the disc-vibratory gyroscope are demodulated into in-phase $(A_s,\ B_s)$ and in-quadrature $(A_c,\ B_c)$ components as follows:

$$A(t) = A_c \cos(\omega t) + A_s \sin(\omega t); \tag{6.54}$$

and

$$B(t) = B_c \cos(\omega t) + B_s \sin(\omega t); \tag{6.55}$$

with the phase of demodulating signal being:

$$\phi_1 = \omega t. \tag{6.56}$$

Here $\omega = \omega_o$ is the operational frequency of the disc gyroscope and t is dimensionless time. Thus the original variables A, B $\dot{A}$, and $\dot{B}$ are transformed into the new variables, these being A_c, A_s, B_c and B_s. A theoretical analysis using the new variables is presented in the subsections that follow.

6.5.1 Non-averaged solution

Consider the matrix form of Equations (6.39) and (6.40), which can be rewritten as:

$$\begin{pmatrix} 1+\varepsilon\rho_{6c}\gamma_2 & \varepsilon\rho_{6s}\gamma_2 \\ \varepsilon\rho_{6s}\gamma_2 & 1-\varepsilon\rho_{6c}\gamma_2 \end{pmatrix} \begin{pmatrix} \ddot{A} \\ \ddot{B} \end{pmatrix} = \begin{pmatrix} F_A \\ F_B \end{pmatrix} - \begin{pmatrix} -2\varepsilon\delta_2\dot{A} \\ -2\varepsilon\delta_2\dot{B} \end{pmatrix}; \tag{6.57}$$

where:

$$\begin{pmatrix} F_A \\ F_B \end{pmatrix} = 2\varepsilon\beta_3 \begin{pmatrix} \Omega_\eta & \Omega_\xi \\ -\Omega_\xi & \Omega_\eta \end{pmatrix} \begin{pmatrix} \dot{C} \\ \dot{S} \end{pmatrix} - \omega_o^2 \begin{pmatrix} A \\ B \end{pmatrix}. \tag{6.58}$$

Since:

$$\det \begin{pmatrix} 1+\varepsilon\rho_{6c}\gamma_2 & \varepsilon\rho_{6s}\gamma_2 \\ \varepsilon\rho_{6s}\gamma_2 & 1-\varepsilon\rho_{6c}\gamma_2 \end{pmatrix} \approx 1; \tag{6.59}$$

neglecting $O(\varepsilon^2)$ and higher, and then using Cramer's rule and solving for $\ddot{A}$ and $\ddot{B}$, respectively, yields:

$$\ddot{A} + \omega^2 A = \omega^2 \varepsilon \gamma_2 \left(A\rho_{6\mathrm{c}} + B\rho_{6\mathrm{s}} \right) + 2\beta_3 \varepsilon \left(\dot{C}\Omega_\eta + \dot{S}\Omega_\xi \right) - 2\varepsilon\delta_2 \dot{A}; \tag{6.60}$$

and

$$\ddot{B} + \omega^2 B = \omega^2 \varepsilon \gamma_2 \left(A\rho_{6\mathrm{s}} - B\rho_{6\mathrm{c}} \right) - 2\beta_3 \varepsilon \left(\dot{C}\Omega_\xi - \dot{S}\Omega_\eta \right) - 2\varepsilon\delta_2 \dot{B}. \tag{6.61}$$

By letting:

$$2\beta_3 \left(\dot{C}\Omega_\eta + \dot{S}\Omega_\xi \right) = \tilde{F}_A; \tag{6.62}$$

and

$$-2\beta_3 \left(\dot{C}\Omega_\xi - \dot{S}\Omega_\eta \right) = \tilde{F}_B; \tag{6.63}$$

for Equations (6.60) and (6.61), respectively, the following is obtained:

$$\ddot{A} + \omega^2 A = \varepsilon \left(\omega^2 \gamma_2 A\rho_{6\mathrm{c}} + \omega^2 \gamma_2 B\rho_{6\mathrm{s}} + \tilde{F}_A \right) - 2\varepsilon\delta_2 \dot{A}; \tag{6.64}$$

and

$$\ddot{B} + \omega^2 B = \varepsilon \left(\omega^2 \gamma_2 A\rho_{6\mathrm{s}} - \omega^2 \gamma_2 B\rho_{6\mathrm{c}} + \tilde{F}_B \right) - 2\varepsilon\delta_2 \dot{B}. \tag{6.65}$$

Now consider the demodulated signal $A(t)$ given by Equation (6.54). Taking the first derivative of $A(t)$ with respect to t yields:

$$\dot{A} = \dot{A}_c \cos(\omega t) + \dot{A}_s \sin(\omega t) + \omega \left[-A_c \sin(\omega t) + A_s \cos(\omega t) \right]; \tag{6.66}$$

and imposing the condition that:

$$\dot{A}_c \cos(\omega t) + \dot{A}_s \sin(\omega t) = 0; \tag{6.67}$$

then yields:

$$\ddot{A} + \omega^2 A = \omega \left[-\dot{A}_c \sin(\omega t) + \dot{A}_s \cos(\omega t) \right]. \tag{6.68}$$

Further, comparing Equation (6.64) with Equation (6.68) leads to:

$$-\dot{A}_c \sin(\omega t) + \dot{A}_s \cos(\omega t) = \frac{\varepsilon}{\omega} \left[\tilde{F}_A + \omega^2 \gamma_2 A\rho_{6\mathrm{c}} + \omega^2 \gamma_2 B\rho_{6\mathrm{s}} - 2\varepsilon\delta_2 \dot{A} \right]. \tag{6.69}$$

Keeping Equations (6.66) and (6.67) in mind and using the new variables leads to:

$$-\dot{A}_c \sin(\omega t) + \dot{A}_s \cos(\omega t) = \frac{\varepsilon}{\omega} \left[\begin{array}{c} \tilde{F}_A + \omega^2 \gamma_2 \rho_{6\mathrm{c}} \left[A_c \cos(\omega t) + A_s \sin(\omega t) \right] + \\ \omega^2 \gamma_2 \rho_{6\mathrm{s}} \left[B_c \cos(\omega t) + B_s \sin(\omega t) \right] - \\ 2\varepsilon\delta_2 \omega \left[-A_c \sin(\omega t) + A_s \cos(\omega t) \right] \end{array} \right]. \tag{6.70}$$

Solving Equations (6.67) and (6.70) simultaneously for $\dot{A}_c$ and $\dot{A}_s$, respectively, yields:

$$\dot{A}_c = -\frac{\varepsilon}{\omega} \left\{ \begin{array}{c} \tilde{F}_A \sin(\omega t) + \dfrac{\omega^2 \gamma_2 \rho_{6\mathrm{c}}}{2} \left[A_c \sin(2\omega t) + A_s \left(1 - \cos(2\omega t) \right) \right] + \\ \dfrac{\omega^2 \gamma_2 \rho_{6\mathrm{s}}}{2} \left[B_c \sin(2\omega t) + B_s \left(1 - \cos(2\omega t) \right) \right] - \\ \delta_2 \omega \left[-A_c \left(1 - \cos(2\omega t) \right) + A_s \sin(2\omega t) \right] \end{array} \right\}; \tag{6.71}$$

and

$$\dot{A}_s = \frac{\varepsilon}{\omega}\left\{\begin{array}{c} \tilde{F}_A\cos(\omega t) + \frac{\omega^2\gamma_2\rho_{6c}}{2}\left[A_c\left(1+\cos(2\omega t)\right) + A_s\sin(2\omega t)\right] + \\ \frac{\omega^2\gamma_2\rho_{6s}}{2}\left[B_c\left(1+\cos(2\omega t)\right) + B_s\sin(2\omega t)\right] - \\ \delta_2\omega\left[-A_c\sin(2\omega t) + A_s\left(1+\cos(2\omega t)\right)\right] \end{array}\right\}. \tag{6.72}$$

The first derivative of $B(t)$ with respect to t yields:

$$\dot{B} = \dot{B}_c\cos(\omega t) + \dot{B}_s\sin(\omega t) + \omega\left[-B_c\sin(\omega t) + B_s\cos(\omega t)\right]; \tag{6.73}$$

and again imposing the condition that:

$$\dot{B}_c\cos(\omega t) + \dot{B}_s\sin(\omega t) = 0; \tag{6.74}$$

and differentiating Equation (6.73) with respect to time (t) yields:

$$\ddot{B} + \omega^2 B = \omega\left[-\dot{B}_c\sin(\omega t) + \dot{B}_s\cos(\omega t)\right]. \tag{6.75}$$

Comparing Equation (6.65) with Equation (6.75) simplifies to:

$$-\dot{B}_c\sin(\omega t) + \dot{B}_s\cos(\omega t) = \frac{\varepsilon}{\omega}\left[\tilde{F}_B + \omega^2\gamma_2 A\rho_{6s} - \omega^2\gamma_2 B\rho_{6c} - 2\varepsilon\delta_2\dot{B}\right]. \tag{6.76}$$

Solving Equations (6.74) and (6.75) simultaneously for $\dot{B}_c$ and $\dot{B}_s$, respectively yields:

$$\dot{B}_c = -\frac{\varepsilon}{\omega}\left\{\begin{array}{c} \tilde{F}_B\sin(\omega t) + \frac{\omega^2\gamma_2\rho_{6s}}{2}\left[A_c\sin(2\omega t) + A_s\left(1-\cos(2\omega t)\right)\right] - \\ \frac{\omega^2\gamma_2\rho_{6c}}{2}\left[B_c\sin(2\omega t) + B_s\left(1-\cos(2\omega t)\right)\right] - \\ \delta_2\omega\left[-B_c\left(1-\cos(2\omega t)\right) + B_s\sin(2\omega t)\right] \end{array}\right\}; \tag{6.77}$$

and

$$\dot{B}_s = \frac{\varepsilon}{\omega}\left\{\begin{array}{c} \tilde{F}_B\cos(\omega t) + \frac{\omega^2\gamma_2\rho_{6s}}{2}\left[A_c\left(1+\cos(2\omega t)\right) + A_s\sin(2\omega t)\right] - \\ \frac{\omega^2\gamma_2\rho_{6c}}{2}\left[B_c\left(1+\cos(2\omega t)\right) + B_s\sin(2\omega t)\right] - \\ \delta_2\omega\left[-B_c\sin(2\omega t) + B_s\left(1+\cos(2\omega t)\right)\right] \end{array}\right\}. \tag{6.78}$$

6.5.2 Averaging

Averaging is an effective method that is used to suppress quadrature error imperfections (Lynch, 1995, [78]). Averaging is used here to do the theoretical analysis using the first approximation. Consequently the first-order derivatives of the in-phase $(A_s,\ B_s)$ and quadrature $(A_c,\ B_c)$ components of the cosine and sine signals of the out-of-plane vibrations are determined. The main objective of averaging is to obtain an equation which can be more easily used to draw inferences about the dynamics of the unaveraged system after having obtained the equations for the averaged system.

If f is a continuous function of t on $[0, 2\pi]$ and has a period $T = 2\pi$, then the averaged form of

the function f is given by:

$$\langle f \rangle = \frac{1}{2\pi} \int_0^{2\pi} f(t)\, dt.$$

Now by applying the method of averaging to Equations (6.71), (6.72), (6.77) and (6.78), the following is obtained:

$$\begin{aligned}
\left\langle \dot{A}_c \right\rangle &= -\frac{\varepsilon}{2\pi\omega} \left\{ \int_0^{2\pi} \left[\begin{array}{c} \tilde{F}_A \sin\phi_1 + \frac{\omega^2 \gamma_2 \rho_{6c}}{2} \left[A_c \sin 2\phi_1 + A_s \left(1 - \cos 2\phi_1 \right) \right] + \\ \frac{\omega^2 \gamma_2 \rho_{6s}}{2} \left[B_c \sin 2\phi_1 + B_s \left(1 - \cos 2\phi_1 \right) \right] - \\ \delta_2 \omega \left[-A_c \left(1 - \cos 2\phi_1 \right) + A_s \sin 2\phi_1 \right] \end{array} \right] d\phi_1 \right\} \\
&= -\frac{\varepsilon\omega}{2} \left[\rho_{6c} A_s + \rho_{6s} B_s \right] - \varepsilon \delta_2 A_c; \qquad (6.79) \\
\left\langle \dot{A}_s \right\rangle &= \frac{\varepsilon}{2\pi\omega} \left\{ \int_0^{2\pi} \left[\begin{array}{c} \tilde{F}_A \cos\phi_1 + \frac{\omega^2 \gamma_2 \rho_{6c}}{2} \left[A_c \left(1 + \cos 2\phi_1 \right) + A_s \sin 2\phi_1 \right] + \\ \frac{\omega^2 \gamma_2 \rho_{6s}}{2} \left[B_c \left(1 + \cos 2\phi_1 \right) + B_s \sin 2\phi_1 \right] - \\ \delta_2 \omega \left[-A_c \sin 2\phi_1 + A_s \left(1 + \cos 2\phi_1 \right) \right] \end{array} \right] d\phi_1 \right\} \\
&= \frac{\varepsilon\omega}{2} \left[\rho_{6c} A_c + \rho_{6s} B_c \right] - \varepsilon \delta_2 A_s; \qquad (6.80) \\
\left\langle \dot{B}_c \right\rangle &= -\frac{\varepsilon}{2\pi\omega} \left\{ \int_0^{2\pi} \left[\begin{array}{c} \tilde{F}_B \sin\phi_1 + \frac{\omega^2 \gamma_2 \rho_{6s}}{2} \left[A_c \sin 2\phi_1 + A_s \left(1 - \cos 2\phi_1 \right) \right] - \\ \frac{\omega^2 \gamma_2 \rho_{6c}}{2} \left[B_c \sin 2\phi_1 + B_s \left(1 - \cos 2\phi_1 \right) \right] - \\ \delta_2 \omega \left[-B_c \left(1 - \cos 2\phi_1 \right) + B_s \sin 2\phi_1 \right] \end{array} \right] d\phi_1 \right\} \\
&= -\frac{\varepsilon\omega}{2} \left[\rho_{6s} A_s - \rho_{6c} B_s \right] - \varepsilon \delta_2 B_c; \qquad (6.81)
\end{aligned}$$

and

$$\begin{aligned}
\left\langle \dot{B}_s \right\rangle &= \frac{\varepsilon}{2\pi\omega} \left\{ \int_0^{2\pi} \left[\begin{array}{c} \tilde{F}_B \cos\phi_1 + \frac{\omega^2 \gamma_2 \rho_{6s}}{2} \left[A_c \left(1 + \cos 2\phi_1 \right) + A_s \sin 2\phi_1 \right] - \\ \frac{\omega^2 \gamma_2 \rho_{6c}}{2} \left[B_c \left(1 + \cos 2\phi_1 \right) + B_s \sin 2\phi_1 \right] - \\ \delta_2 \omega \left[-B_c \sin 2\phi_1 + B_s \left(1 + \cos 2\phi_1 \right) \right] \end{array} \right] d\phi_1 \right\} \\
&= \frac{\varepsilon\omega}{2} \left[\rho_{6s} A_c - \rho_{6c} B_c \right] - \varepsilon \delta_2 B_s. \qquad (6.82)
\end{aligned}$$

6.6 CONCLUSION

It is possible to make qualitative inferences based on both the non-averaged and averaged systems of ordinary differential equations as given in Equations (6.71) to (6.78) and (6.79) to (6.82). Both systems of ODEs can be solved using the "NDSolve" routine in Mathematica but that is left for future investigation. In Equations (6.79) to (6.82) it appears that the rate of change of amplitudes of in-phase and quadrature components are not influenced by the inertial angular rates. But for the case of the non-averaged systems given in Equations (6.71) to (6.78) the time rate of change of

both amplitudes is influenced by the inertial angular rates. The time rate of change of quadrature amplitudes of both signals is out-of-phase with respect to each amplitude. The drift caused by mass imperfections to the quadrature amplitudes is more significant than the drift caused to the in-phase amplitudes. If mass anisotropy is absent in both the in-phase and quadrature components of both sine and cosine signals then the only amplitude suppression comes from light isotropic damping.

Chapter 7

FINAL CONCLUSIONS AND RECOMMENDATIONS

7.1 SUMMARY OF CONCLUSIONS

In this study, the disc gyroscope subjected to a 3D rotation rate was studied and various boundary conditions were formulated. Implicit equations of motion for both in-plane and out-of-plane vibrations of the disc gyroscope were derived using Hamilton's variational principle. For this study, the disc under investigation was assumed to be perfectly elastic and thus obeyed Hooke's law. In determining the potential energy of the deformation of the disc, the potential energy of in-plane vibrations and the potential energy of out-of-plane vibrations were assumed to be independent provided that the disc is "thin". The potential energy of in-plane vibrations comes from extension and shear while the potential energy out-of-plane vibrations comes from bending and torsion. The Lagrangian and Euler-Lagrange equations of motion were derived for a disc gyroscope using polar coordinate systems. A coupled system of gyroscopic equations in terms of the generalised coordinates was obtained for a free as well as lightly, isotropically-damped disc gyroscope.

Analytical determination of the components of the rotation rate was performed and their dependence on the amplitudes of the secondary motion was calculated. Expressions for the solutions of the angular accelerations of each axis were determined. The ratio of the rate of rotation of the vibrating pattern to the rate of rotation of the disc was obtained as the ratio of the integrals of the eigenfunctions. The relationship between the rate of rotation of the vibrating pattern and the rate of rotation of the disc was described by Bryan's factor. Apart from the well-known Bryan's factor, the so-called "auxiliary Bryan's factors" or "secondary Bryan's factors" were identified due to the inclusion of the bending vibrations. The auxiliary Bryan's factors were described by the ratios of sums and/or products of the integrals of the eigenfunctions. Various magnitudes of the eigenvalues and eigenfrequencies were calculated for both the $m = 2$ and $m = 3$ modes. The eigenfrequencies of the in-plane mode with the out-of-plane mode were tuned by varying the radial and\or axial thickness. By conducting a numerical experiment, it was verified that this tuning was achieved . The disc gyroscope operating under tuned natural frequencies was shown to have improved sensitivity (Bryan's factor) to the applied rotation rates. Note that a 3D-disc vi-

bratory gyroscope realisation is still possible even if the modal frequencies are not tuned, but at reduced sensitivity. Numerical solutions of the normalised displacements were obtained for various in-plane and out-of-plane frequencies. In this study, MATHEMATICA 11 was used to solve the equations numerically.

Analysis of the dynamics of the in-plane vibration of the disc-vibratory gyroscope made up the core of Chapter 3. The equations of motion for the in-plane vibration of the disc gyroscope were derived using Hamilton's variational principle. Boundary conditions for both a solid and annular disc vibrating in its plane were obtained from the Lagrangian density. The eigenvalues for various boundary conditions of both the solid and annular disc gyroscope were obtained numerically from the frequency equations. Normalised values of the eigenfunctions for the in-plane vibration of the disc were numerically obtained. In Chapter 4, the out-of-plane vibration of the disc gyroscope was modelled using the transverse vibration of a circular plate. The Lagrangian density for the vibrating circular plate was obtained implicitly and used in the derivation of the equation of motion using Hamiliton's principle. As it was done for in-plane disc vibration in Chapter 3, an analytical solutions for a non-rotating disc in terms of Bessel and modified Bessel functions were calculated. The frequency equations for a non-rotating circular plate for various boundary conditions were formulated. Numerical values of the eigenvalues and the eigenfrequencies were also included in Chapter 4. Normalised values of the out-of-plane eigenfunctions for various boundary conditions were presented graphically.

Chapter 5 constituted novel work that investigated and discussed the 3D-tuning, disc-vibratory gyroscope. In the literature, single axis and dual axis gyroscopes were well-documented but multi-axis gyroscopes were not addressed adequately. Hence this study aimed to investigate the possibility of a disc gyroscope that is capable of sensing rotation rates around three, mutually-perpendicular axes. The equations of motion for a disc gyroscope subjected to a slow rotation were derived in terms of the generalised coordinates. A coupled homogeneous system of gyroscopic equations that describe the dynamics of the disc gyroscope was obtained. A non-homogeneous system of coupled gyroscopic equations, where the rebalance and excitation forces were included to set the gyroscope at primary oscillation and for control purposes, respectively, was formulated. The operation principle of the 3D-disc vibratory gyroscope was briefly discussed and formulated. The components of the rotation rates as well as the components of angular acceleration were calculated for the disc-vibratory gyroscope, initially set to vibrate at constant amplitude in one of its

in-plane modes. Bryan's factor and auxiliary Bryan's factors were calculated and tabulated for various geometric values of the disc-vibratory gyroscope. Section 5.7 discussed the tuning of in-plane natural frequencies to the out-of-plane natural frequencies by varying the thickness of the disc. Hence an approximate frequency split between the in-plane vibration modes and the out-of-plane vibration modes was small. The normalised eigenfunctions for the 3D-disc vibratory gyroscope for various boundary conditions were determined numerically. Graphical representation of the normalised eigenfunctions were determined for various frequency overtones.

In Chapter 6, mass imperfections were incorporated in order to study the structural anisotropies. It was assumed that the mass density of the disc varies circumferentially and that it models the mass imperfections. The frequency splitting caused by mass imperfection between the in-plane vibration modes was shown. Qualitative analysis was done for averaged an non-averaged equations of motion.

7.2 RECOMMENDATIONS FOR FURTHER STUDY

The research covered in this study is purely of a theoretical-applied mathematics. Thus the theory developed here has to be verified via experiments and therefore actual observations need to be set up to validate the theoretical findings. Future investigation should explore prototype production and development of appropriate circuitry for a separate detection and demodulation of the rotation rates. This study did not consider anisotropies such as stiffness imperfections, Poisson's ratio imperfections and Young's modulus imperfections, nor anisotropic non-linear damping. Thus a future study should consider anisotropies such as those resulting from non-linear damping, stiffness imperfections, Poisson's ratio imperfections and Young's modulus imperfections.

REFERENCES

[1] ANANDARAJAH, A. 2010. *Computational methods in elasticity and plasticity: Solids and porous media.* New York: Springer.

[2] RAO, S.S. 2011. *Mechanical vibrations.* New Jersey: Prentice Hall.

[3] ACAR, C. & SHKEL, A. 2009. *MEMS vibratory gyroscopes: Structural approaches to improve robustness.* New York: Springer.

[4] LAWRENCE, A. 1998. *Modern inertial technology: Navigation, guidance and control*. New York: Springer-Verlag.

[5] COOPER, G. 1996. The design, simulation and fabrication of microengineered silicon gyroscopes. Ph.D. thesis. University of Durham.

[6] SABAGEH, I. 2010. Design and modeling of decoupled and tunable bandwidth (40-330 Hz) MEMS vibratory gyroscopes. M.Sc. thesis. Delft University of Technology.

[7] PARK, S, HOROWITZ, R. & TAN, C. 2008. Dynamics and control of a MEMS, angle-measuring gyroscope. *Sensors and Actuators A*, **144:** 56–63.

[8] VINEELAL, V., RAMA, R.B., MADHUR, N.T. & SRINIVASA, K.R. 2014. Design and simulation of MEMS piezoelectric gyroscopes. *European Journal of Applied Engineering and Scientific Research*, **3(2)**: 8–12.

[9] LOVEDAY, P.W. 1999. Analysis and compensation of imperfection effects in piezoelectric vibratory gyroscopes. Ph.D. thesis. Virginia Polytechnic Institute and State University, Blacksburg.

[10] SCARBOROUGH, J.B. 1958. *The gyroscope: Theory and applications.* New York: Interscience Publishers.

[11] ZHANG, F. 2015. Control and self-calibration of microscale-rate integrating gyroscopes. Ph.D. dissertation, University of California, Berkeley.

[12] AZGIN, K. 2007. High performance MEMS gyroscopes. M.Sc. thesis. Middle-East Technical University, Ankara.

[13] BRYAN, G.H. 1890. On the beats in the vibrations of a revolving cylinder or bell. *Proceedings of the Cambridge Philosophical Soc. Math. Phys. Sci.,* **7:** 101–114.

[14] SHATALOV, M.Y., JOUBERT, S.V., COETZEE, C.E. & FEDOTOV I.A. 2009. Free vibration of rotating hollow spheres containing acoustic media. *Journal of Sound and Vibration*, **322**: 1038–1047.

[15] COETZEE, C.E. 2008. Gyroscopic effects in vibrating and rotating spherical bodies. D.Tech.

thesis. TUT, Pretoria.

[16] JOUBERT, S.V., SHATALOV, M.Y. & COETZEE, C.E. 2014. Using Fourier series to analyse mass imperfections in vibratory gyroscopes. *Journal of Symbolic Computation*, **61 & 62**: 116–127.

[17] LOVEDAY, P.W. & ROGERS, C.A. 1998. Free vibrations of elastically-supported, thin cylinders including gyroscopic effects. *Journal of Sound Vibration*, **217(3)**: 547–562.

[18] JOHARI, H. & AYAZI, F. 2007. High-frequency capacitive disk gyroscopes in (100) and (111) silicon. *Proceedings of MEMS.* Held in Japan on 21-25 January, 2007. Kobe: IEEE.

[19] ROZELLE, D.M. 2009. The hemispherical resonator gyro: From wineglass to the planets. *Proceedings of the Space Flight Mechanics Meeting.* Held in the USA on 8-12 February, 2009. Savannah, Georgia, United States: 19th AAS/AIAA.

[20] ROSSING, T.D. 1994. Acoustics of the glass harmonica. *Journal of the Acoustic Society of America,* **95(2)**: 1106–1111.

[21] RAYLEIGH, J.W.S. 1894. *The theory of sound, volume I.* 2nd edition. London: MacMillan and Company.

[22] SHARMA, M. 2013. Non-linear amplification techniques for inertial MEMS sensors. Ph.D. thesis. The University of British Columbia, Vancouver.

[23] DREYER, A.C. 2008. Modelling of MEMS vibratory gyroscopes utilizing phase detection. M.Sc. thesis. University of Stellenbosch.

[24] ARMENISE, M.N., CIMINELLI, C., DELLÒLIO, F. & PASSARO, V.M.N. 2010. *Advances in gyroscope technologies.* Berlin: Springer-Verlag.

[25] HYVÖNEN, H. 2011. Thermo-mechanical and mechanical characterization of a 3-axial MEMS gyroscope. M.Sc. thesis. Aalto University, Espoo.

[26] JOHARI, H. 2008. Micro-machined capacitive silicon bulk acoustic wave gyroscopes. Ph.D. dissertation. Georgia Institute of Technology, Atlanta.

[27] ANSARI, M. 2008. Modeling and vibration analysis of a rocking–mass gyroscope system. M.Sc. thesis. University of Ontario Institute of Technology.

[28] SHKEL, A., ACAR, C. & PAINTER, C. 2005. Two types of micro-machined vibratory gyroscopes. *IEEE Sensors*: 531–536.

[29] SPIEGEL, M. 1982. *Theoretical mechanics*. New York: Schaum Publishing.

[30] BURDESS, J.S. & WREN, T. 1986. The theory of a piezoelectric-disc gyroscope. *IEEE Transactions on Aerospace and Electronic Systems,* **22(4)**: 110–118.

[31] TSAI, N. & SUE, C. 2008. Design and analysis of a tri-axis gyroscope micro-machined by

surface fabrication. *IEEE Sensor Journal*, **8(12)**: 1933–1940.

[32] SUNG, W.K. 2013. High-frequency, tri-axial resonant gyroscopes. Ph.D. thesis. Georgia Institute of Technology, Atlanta.

[33] JOHARI, H., SHAH, J. & AYAZI, F. 2008. High frequency XYZ-axis single disk silicon gyroscope. *Proceedings of MEMS.* Held in USA on 13-17 January, 2008. Tucson, AZ: IEEE.

[34] SEDEBO, G.T., JOUBERT, S.V. & SHATALOV, M.Y. 2018. An analytical theory for a three-dimensional thick-disc, thin-plate vibratory gyroscope. *Journal of Physics: Conf. Series*, **991(1)**: 1–8.

[35] LOVE, A.E.H. 1893. *A Treatise on the mathematical theory of elasticity*. London: Cambridge University Press.

[36] BASHMAL, S., BHAT, R. & RAKHEJA, S. 2011. In-plane free vibration analysis of an annular disk with point elastic support. *Shock and Vibration*, **18**: 627–640.

[37] TIMOSHENKO, S. & WOINOWSKY-KRIEGER, S. 1959. *Theory of plates and shells*. New York: McGraw-Hill Company.

[38] LEISSA, A.W. 1969. *Vibration of plates-NASA SP-160*. Washington, D.C.: US Government Printing Office.

[39] LEISSA, A.W. & QATU, M.S. 2011. *Vibrations of continuous systems*. New York: McGraw-Hill.

[40] JIA, S.H., CHUN, S.B. & LEE, C.W. 1997. Evaluation of the longitudinal coupled vibrations in rotating flexible disks/spindle systems. *Journal of Sound and Vibration*, **208(2)**: 175–187.

[41] OUYANG, H., MOTTERSHEAD, J. E., BROOKFIELD, D. J., JAMES, S. & CARTMELL, M. P. 2000. A methodology for the determination of dynamic instabilities in a car disc brake. *International Journal of Vehicle Design*, **23(3–4)**: 241–262.

[42] SINGH, A.K. & GORAIN, U.K. 2004. Development of vibrating-disc piezoelectric gyroscope. *Defence Science Journal*, **54(3)**: 387–393.

[43] HAO, Z., POURKAMALI, S. & AYAZI, F. 2004. VHF single-crystal silicon elliptic bulk-mode capacitive disk resonators — Part I: Design and modeling. *Journal of Microelectromechanical Systems*, **13(6):** 1043–1053.

[44] TSAI, N.C., LIOU, J.S., LIN, C.C. & LI, T. 2010. Design of micro-electromagnetic drive on reciprocally rotating disc used for micro-gyroscopes. *Sensors and Actuators A: Physical*, **157**: 68–76.

[45] POURKAMALI, S., HAO, Z. & AYAZI, F. 2004. VHF single crystal silicon capacitive elliptic bulk-mode disk resonators — Part II: Implementation and characterization. *Journal of Microelectromechanical Systems*, **13(6):** 1054–1062.

[46] WEI, X., & SESHIA, A.A. 2014. Analytical formulation of modal frequency split in the elliptical mode of SCS micromechanical disk resonators. *Journal of Micromechanics and Microengineering*, **24**: 1–7.

[47] TSAI, N.C. & SUE, C.Y. 2010. Experimental analysis and characterization of electrostatic-drive, tri-axis, micro-gyroscope, *Sensors and Actuators A,* **158**: 231–239.

[48] GALLACHER, B.J, NEASHAM, J.A., BURDESS, J.S. & HARRIS, A.J. 2006. Initial test results from a 3-axis vibrating- ring gyroscope. *Journal of Physics: Conference Series*, **34**: 662–667.

[49] SUNG, W.K., DALAL, M. & AYAZI, F. 2011. A mode-matched 0.9 MHZ single proof-mass, dual-axis gyroscope. *Proceedings of Transducers. Held in China on 5-9 June, 2011. Beijing: IEEE.*

[50] VOGES, E.L. 2006. Free surface waves in a cylinder with a vibrating lateral side. D.Tech. thesis, TUT, Pretoria.

[51] JOUBERT, S.V., SHATALOV, M.Y. & FAY, T.H. 2009. Rotating structures and Bryan's effect. *American Journal of Physics*, **77(6)**: 520–525.

[52] PRETORIUS, W.E. 2007. Gyroscopic effects in a thin vibrating circular disc subjected to inertial rotation. M.Tech. dissertation, TUT, Pretoria.

[53] JOUBERT, S.V., SHATALOV, M.Y. & MANZHIROV, A.V. 2013. Bryan's effect and isotropic non-linear damping. *Journal of Sound and Vibration,* **332**: 6169–6176.

[54] SADD, M.H. 2009. *Elasticity: Theory, applications, and numerics*. Oxford: Elsevier Inc.

[55] ACHENBACH, J.D. 1973. *Wave propagation in elastic solid*s. Amsterdam: North-Holland Publishers.

[56] FAN, T. 2011. *Mathematical theory of elasticity of quasicrystals and its applications*. Berlin: Springer-Verlag.

[57] YENWONG-FAI, A.S. 2008. Wave propagation in a homogeneous piezoelectric solid cylinder of transversely isotropic material. M.Sc. dissertation. Johannesburg, University of the Witwatersrand.

[58] REDDY, J.N. 2004. *Mechanics of laminated composite plates and shells: Theory and analysis.* London: CRC.

[59] REDWOOD, M. 1960. *Mechanical waveguides*. Oxford: Pergamon Press.

[60] LEISSA, A.W. 1993. *Vibration of shells*. New York: Acoustical Society of America.

[61] NOVOZHILOV, V.V. 1970. *The theory of thin shells*. Groningen, The Netherlands: Wolters-Noordhoff.

[62] SOEDEL, W. 2004. *Vibrations of shells and plates*. New York: Marcel Dekker Inc.

[63] ROURKE, A.K., MCWILLIAM, S. & FOX, C.H.J. 2005. Frequency trimming of a vibrating ring-based multi-axis rate sensor. *Journal of Sound and Vibration,* **280**: 495–530.

[64] GOLDSTEIN, H., POOLE, C.P. & SAFKO, J.L. 2000. *Classical mechanics.* New York: Addison-Wesley.

[65] LANDAU, L.D. & LIFSHITZ, E.M. 1975. *Theory of elasticity*. Oxford: Pergamon Press.

[66] ASMAR, N.H. 2005. *Partial differential equations with Fourier series and boundary value problems.* New Jersey: Pearson Education Inc.

[67] O'NEIL, P.V. 2007. *Advanced engineering mathematics*. Toronto, Canada: Thomson.

[68] VENSTEL, E. & KRAUTHAMMER, T. 2001. *Thin plates and shells: Theory, analysis, and applications.* New York: Marcel Dekker, Inc.

[69] SPOELSTRA, H. 2015. Controlling mass imperfections in a vibratory-disk gyroscope. MTech. dissertation. TUT, Pretoria.

[70] HAGEDORN, P. & DASGUPTA, A. 2007. *Vibrations and waves in continuous mechanical systems*. Chichester, United Kingdom: Wiley.

[71] ZILL, D.G. & CULLEN, M.R. 2009. *Differential equations with boundary-value problems*. New York: Brooks and Cole.

[72] STROUD, K.A. & BOOTH, D.J. 2009. *Advanced engineering mathematics*. Hampshire: Palgrave MacMillan.

[73] WANG, X., WU, B.W., LUO, Z., F., Y. LI, Y. & JIANG, Q. 2011. Force to rebalance control of HRG and suppression of its errors on the basis of FPGA. *Sensors*, **11**: 11761–11773.

[74] JOUBERT, S.V., SHATALOV, M.Y & SPOELSTRA, H. 2017. On electronically restoring an imperfect vibratory gyroscope to an ideal state. In *Mechanics for Materials and Technologies* (H. Altenbach, R. V. Goldstein, and E. Murashkin, eds.), pp. 231–256, Cham: Springer International Publishing.

[75] GALLACHER, B.J., BURDESS, J.S., HARRIS, A.J. & MCNIE, M.E. 2001. Principles of a Three-Axis Vibrating Gyroscope. *IEEE Transactions on Aerospace and Electronic Systems,* **37(4)**: 1333–1343.

[76] JOUBERT, S.V., SHATALOV, M.Y. & FAY, T.H. 2014. On numerically solving an eigenvalue problem arising in a resonator gyroscope. *Applied Mathematics and Computation*, **246**: 561–571.

[77] SHATALOV, M.Y., FEDOTOV, I. & JOUBERT, S.V. 2006. Resonant vibrations and acoustic radiation of rotating spherical structures. *Proceedings of the Thirteenth International Congress on Sound and Vibration* (ICSV13), Vienna, Austria.

[78] LYNCH, D.D. 1995. Vibratory gyro analysis by the method of averaging. *Proceedings of the*

2nd Saint Petersburg International Conference on Integrated Navigation Systems. Russia, Saint Petersburg.

[79] NGUNGU, M.N. 2014. Imperfections in a cylindrical vibratory gyroscope. M. Tech. dissertation. TUT, Pretoria.

[80] GALLACHER, B.J., HEDLEY, J., BURDESS, J.S., HARRIS, A.J., RICKARD, A. & KING, D.O. 2005. Electrostatic of structural imperfections present in a micro-ring gyroscope. *Journal of Microelectromechanical Systems*, **14(2):** 221–234.

[81] BOWLES, S.R., GALLACHER, B.J., HU, Z. XU., FELL, C.P., & TOWNSEND, K. 2015. Control scheme to reduce the effect of structural imperfections in a rate integrating MEMS gyroscope. *IEEE Sensors Journal*, **15(1)**: 552–560.

[82] FRIEDLAND, B. & HUTTON, M.F. 1978. Theory and error analysis of vibrating-member gyroscope. *IEEE Transactions on Automatic Control*, **23(4)**: 545–556.

[83] JOUBERT, S.V., SHATALOV, M.Y., FAY, T.H. & SEDEBO, G.T. 2017. On Bryan's law and anisotropic non-linear damping. *Proceedings of the 24th International Congress on Sound and Vibration, UK, London.*

MATHEMATICA CODE FOR ANNULAR DISC CLAMPED AT BOTH EDGES

```
WP = 60
```

```
60
```

```
w[r, φ, t] := W[r] Cos[m φ] e^(i ω t);
```

```
Collect[w[r, φ, t], Cos[m φ] Cos[ω t + Θ], Simplify];
```

```
Collect[(∂r w[r, φ, t]), Cos[m φ] e^(i ω t), Simplify];
```

```
W[r_] := A1 BesselJ[m, β r] + A2 BesselY[m, β r] + A3 BesselI[m, β r] + A4 BesselK[m, β r]
Collect[w[r, φ, t], Cos[m φ] Cos[ω t + Θ], Simplify];
a11 = Simplify[W[r], Factor] /. {r -> a, A1 -> 1, A2 -> 0, A3 -> 0, A4 -> 0};
a12 = Simplify[W[r], Factor] /. {r -> a, A1 -> 0, A2 -> 1, A3 -> 0, A4 -> 0};
a13 = Simplify[W[r], Factor] /. {r -> a, A1 -> 0, A2 -> 0, A3 -> 1, A4 -> 0};
a14 = Simplify[W[r], Factor] /. {r -> a, A1 -> 0, A2 -> 0, A3 -> 0, A4 -> 1};
a21 = Simplify[W'[r], Factor] /. {r -> a, A1 -> 1, A2 -> 0, A3 -> 0, A4 -> 0};
a22 = Simplify[W'[r], Factor] /. {r -> a, A1 -> 0, A2 -> 1, A3 -> 0, A4 -> 0};
a23 = Simplify[W'[r], Factor] /. {r -> a, A1 -> 0, A2 -> 0, A3 -> 1, A4 -> 0};
a24 = Simplify[W'[r], Factor] /. {r -> a, A1 -> 0, A2 -> 0, A3 -> 0, A4 -> 1};

a31 = Simplify[W[r], Factor] /. {r -> b, A1 -> 1, A2 -> 0, A3 -> 0, A4 -> 0};
a32 = Simplify[W[r], Factor] /. {r -> b, A1 -> 0, A2 -> 1, A3 -> 0, A4 -> 0};
a33 = Simplify[W[r], Factor] /. {r -> b, A1 -> 0, A2 -> 0, A3 -> 1, A4 -> 0};
a34 = Simplify[W[r], Factor] /. {r -> b, A1 -> 0, A2 -> 0, A3 -> 0, A4 -> 1};
a41 = Simplify[W'[r], Factor] /. {r -> b, A1 -> 1, A2 -> 0, A3 -> 0, A4 -> 0};
a42 = Simplify[W'[r], Factor] /. {r -> b, A1 -> 0, A2 -> 1, A3 -> 0, A4 -> 0};
a43 = Simplify[W'[r], Factor] /. {r -> b, A1 -> 0, A2 -> 0, A3 -> 1, A4 -> 0};
a44 = Simplify[W'[r], Factor] /. {r -> b, A1 -> 0, A2 -> 0, A3 -> 0, A4 -> 1};
```

```
Φ[r, φ, t] := (B1 BesselJ[n, k1 r] + B2 BesselY[n, k1 r]) Cos[n φ] Cos[ω t + ϕ];
Ψ[r, φ, t] := (B3 BesselJ[n, k2 r] + B4 BesselY[n, k2 r]) Sin[n φ] Cos[ω t + ϕ];
```

$$u[r, \varphi, t] := \partial_r \Phi[r, \varphi, t] + \frac{1}{r} \partial_\varphi \Psi[r, \varphi, t];$$

$$v[r, \varphi, t] := \frac{1}{r} \partial_\varphi \Phi[r, \varphi, t] - \partial_r \Psi[r, \varphi, t];$$

```
Collect[u[r, φ, t], Cos[n φ] Cos[t ω]];
```

```
U[r_] := SetPrecision[ ((1/2) B1 k1 (BesselJ[-1 + n, k1 r] - BesselJ[1 + n, k1 r]) +
      (1/r) n (B3 BesselJ[n, k2 r] + B4 BesselY[n, k2 r]) +
      (1/2) B2 k1 (BesselY[-1 + n, k1 r] - BesselY[1 + n, k1 r])), WP]

Collect[v[r, φ, t], Sin[n φ] Cos[t ω]];

V[r_] := SetPrecision[ (-(1/2) B3 k2 (BesselJ[-1 + n, k2 r] - BesselJ[1 + n, k2 r]) -
      (1/r) n (B1 BesselJ[n, k1 r] + B2 BesselY[n, k1 r]) -
      (1/2) B4 k2 (BesselY[-1 + n, k2 r] - BesselY[1 + n, k2 r])), WP];

b11 = Simplify[ U[r], Factor] /.{r → a, B1 → 1, B2 → 0, B3 → 0, B4 → 0};
b12 = Simplify[U[r], Factor] /.{r → a, B1 → 0, B2 → 1, B3 → 0, B4 → 0};
b13 = Simplify[ U[r], Factor] /.{r → a, B1 → 0, B2 → 0, B3 → 1, B4 → 0};
b14 = Simplify[ U[r], Factor] /.{r → a, B1 → 0, B2 → 0, B3 → 0, B4 → 1};
b21 = Simplify[V[r], Factor] /.{r → a, B1 → 1, B2 → 0, B3 → 0, B4 → 0};
b22 = Simplify[V[r], Factor] /.{r → a, B1 → 0, B2 → 1, B3 → 0, B4 → 0};
b23 = Simplify[V[r], Factor] /.{r → a, B1 → 0, B2 → 0, B3 → 1, B4 → 0};
b24 = Simplify[V[r], Factor] /.{r → a, B1 → 0, B2 → 0, B3 → 0, B4 → 1};

b31 = Simplify[ U[r], Factor] /.{r → b, B1 → 1, B2 → 0, B3 → 0, B4 → 0};
b32 = Simplify[U[r], Factor] /.{r → b, B1 → 0, B2 → 1, B3 → 0, B4 → 0};
b33 = Simplify[ U[r], Factor] /.{r → b, B1 → 0, B2 → 0, B3 → 1, B4 → 0};
b34 = Simplify[ U[r], Factor] /.{r → b, B1 → 0, B2 → 0, B3 → 0, B4 → 1};
b41 = Simplify[V[r], Factor] /.{r → b, B1 → 1, B2 → 0, B3 → 0, B4 → 0};
b42 = Simplify[V[r], Factor] /.{r → b, B1 → 0, B2 → 1, B3 → 0, B4 → 0};
b43 = Simplify[V[r], Factor] /.{r → b, B1 → 0, B2 → 0, B3 → 1, B4 → 0};
b44 = Simplify[V[r], Factor] /.{r → b, B1 → 0, B2 → 0, B3 → 0, B4 → 1};
```

Set the WorkingPrecision WP for further use.

Now We two systems of system of four simultaneous equations with unknowns A1 , A2, A3 and A4 for out-of-plane vibrations and with unknowns B1, B2, B3 and B4 for in-plane vibrations:

$$\begin{pmatrix} a11 & a12 & a13 & a14 \\ a21 & a22 & a23 & a24 \\ a31 & a32 & a33 & a34 \\ a41 & a42 & a43 & a44 \end{pmatrix} \begin{pmatrix} A1 \\ A2 \\ A3 \\ A4 \end{pmatrix} = \begin{pmatrix} 0 \\ 0 \\ 0 \\ 0 \end{pmatrix}$$

$$\begin{pmatrix} b11 & b12 & b13 & b14 \\ b21 & b22 & b23 & b24 \\ b31 & b32 & b33 & b34 \\ b41 & b42 & b43 & b44 \end{pmatrix} \begin{pmatrix} B1 \\ B2 \\ B3 \\ B4 \end{pmatrix} = \begin{pmatrix} 0 \\ 0 \\ 0 \\ 0 \end{pmatrix}$$

Hence define as follows:

```
WP = 60
```

```
60
```

```
Clear[DP, ω]
```

```
Clear[DD, ω]
```

```
a = 1/1000
N[a]
b = 1/100;
N[b]
m = 3;
n = 2;
μ = 1/3;
h = 38.5/40 000;
N[h]
ρ = 2700;
EE = 70 × 10^9;
β = SetPrecision[Sqrt[ω/h Sqrt[12 ρ (1 - μ^2)/EE]], WP];
k1 = SetPrecision[ω Sqrt[ρ (1 - μ^2)/EE], WP];
k2 = SetPrecision[ω Sqrt[2 ρ (1 + μ)/EE], WP];
```

$$\frac{1}{1000}$$

```
0.001
0.01
0.0009625
SetPrecision[Det[{{a11, a12, a13, a14}, {a21, a22, a23, a24}, {a31, a32, a33, a34}, {a41, a42, a43, a44}}], WP];
DP = SetPrecision[Det[{{a11, a12, a13, a14}, {a21, a22, a23, a24}, {a31, a32, a33, a34}, {a41, a42, a43, a44}}], WP];
SetPrecision[Det[{{b11, b12, b13, b14}, {b21, b22, b23, b24}, {b31, b32, b33, b34}, {b41, b42, b43, b44}}], WP];
```

```
DD = SetPrecision[Det[{{b11, b12, b13, b14}, {b21, b22, b23, b24}, {b31, b32, b33, b34}, {b41, b42, b43, b44}}], WP];
```

```
Plot[DP, {ω, 0, 100000}, PlotRange → All]
```

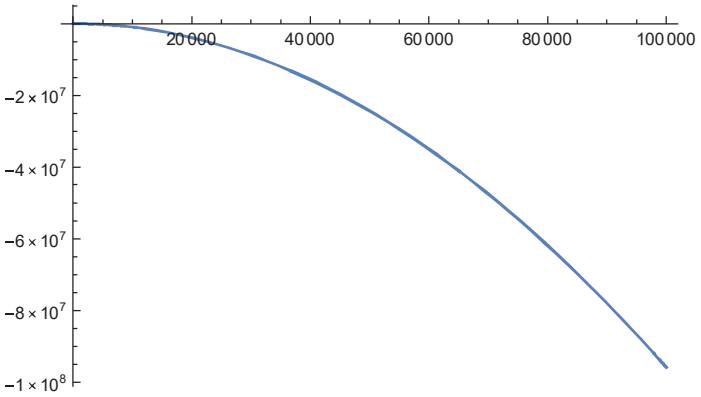


```
Plot[DD, {ω, 0, 1000000}, PlotRange → All]
```

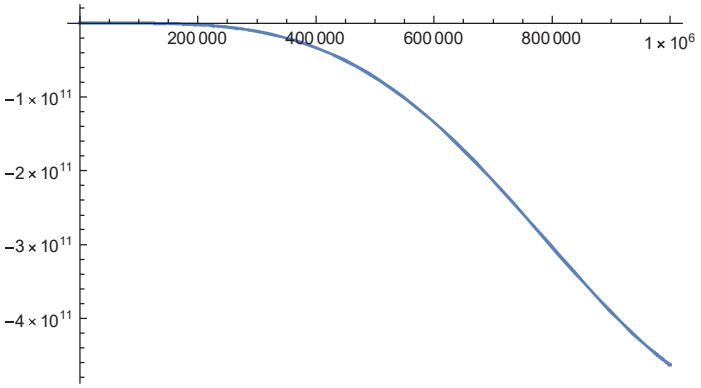


```
Plot[Log[Abs[DP]], {ω, 0, 2000000}, PlotRange → All]
```

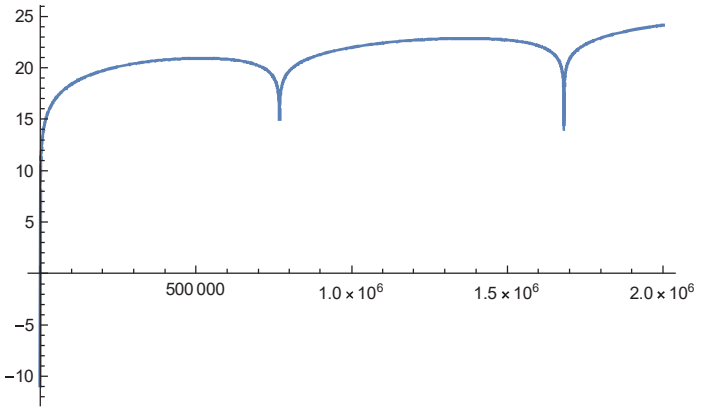

```
Plot[Log[Abs[DD]], {ω, 0, 2000000}, PlotRange → All]
```

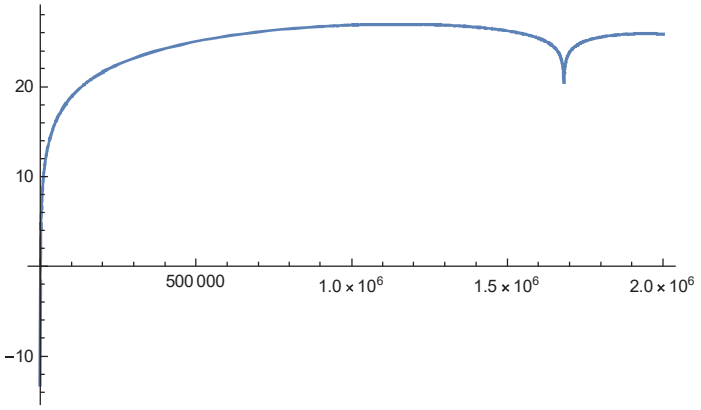


```
Plot[{Log[Abs[DD]], Log[Abs[DP]]}, {ω, 0, 4000000},
 PlotLegends → "Expressions", AxesLabel → {" ω", " Log[Abs[Det Eqn]]"},
 LabelStyle → Directive[Bold, Black], BaseStyle → {FontFamily → "Times", FontSize → 12},
 PlotStyle → {{Purple, Thickness[0.01]}, {Red, Thickness[0.01]}},
 AxesStyle → Thick, PlotTheme → "Default"]
```

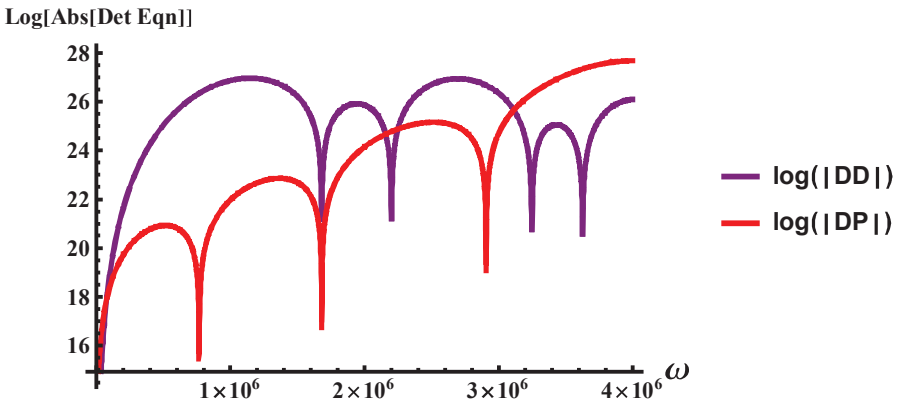

```
Plot[Log[Abs[DD]], {ω, 0, 2000000}, PlotRange → All,
 AxesLabel → {" ω", " f(ω)"}, LabelStyle → Directive[Bold, Black],
 AxesStyle → Thick, PlotStyle → {{Black, Thickness[0.01]}},
 BaseStyle → {FontFamily → "Times", FontSize → 12}]
```

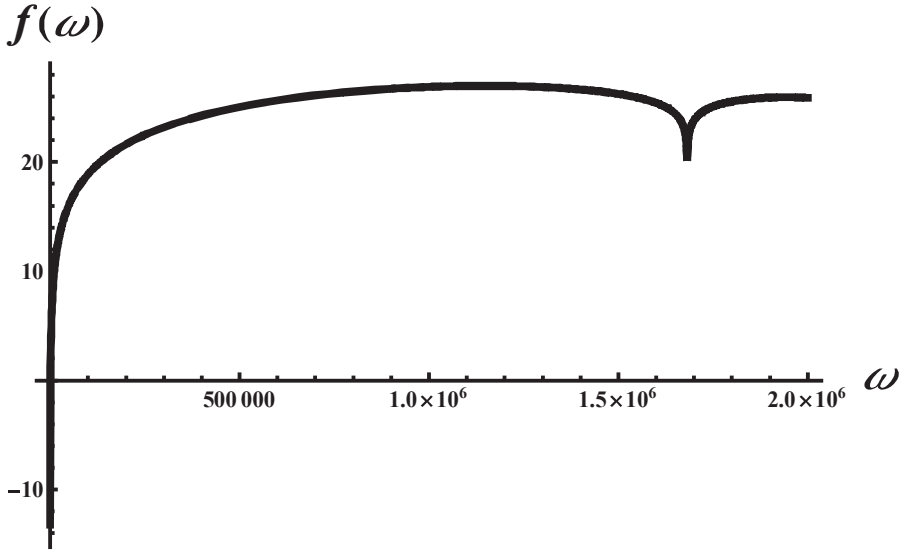


```
Plot[Log[Abs[DP]], {ω, 0, 2000000}, PlotRange → All, AxesLabel → {" ω", "F(ω)"},
 LabelStyle → Directive[Bold, Black], AxesStyle → Thick,
 PlotStyle → {{Black, Thickness[0.01]}}, BaseStyle → {FontFamily → "Times", FontSize → 12}]
```

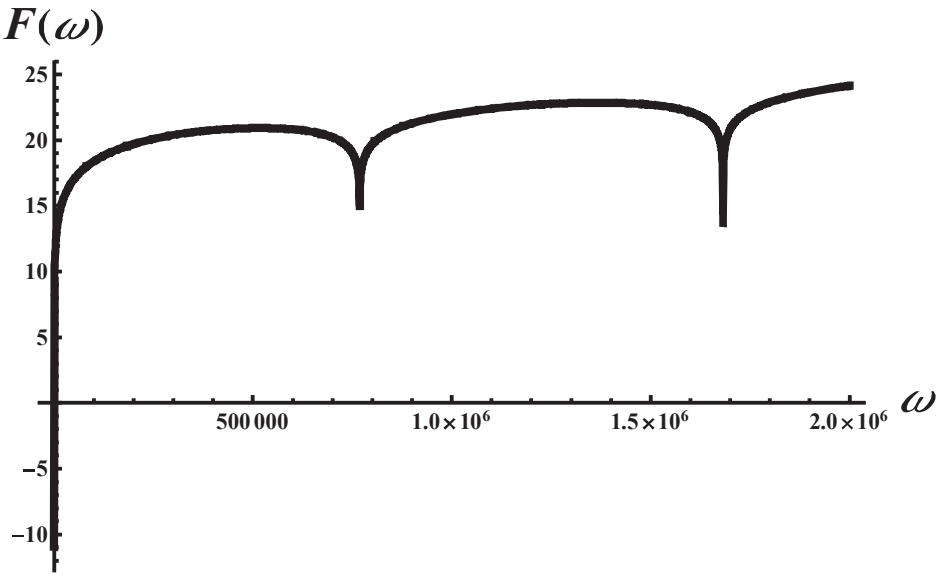

```
P1 = {{1.6851522842639596`*^6, 20.60561826844721}};
P2 = {{1.3095975232198145`*^6, 23.296681166870727`}};
P3 = {{2.182662538699691*^6, 24.37049483671059}};
P4 = {{2.7770897832817347`*^6, 25.137504600881936`}};
PP = Join[P1, P2, P3, P4]
```

$$\{\{1.68515\times10^6, 20.6056\}, \{1.3096\times10^6, 23.2967\},\ \{2.18266\times10^6, 24.3705\}, \{2.77709\times10^6, 25.1375\}\}$$

Right - click on the graphs above to get coordinates of a spike to use as a first approximation for $\omega_{m,n,0}$ (m declared above and n = 0,1,2,3...) using FindRoot. Note that at ω = 0 there is no spike; indeed, the curve has the vertical axis as an asymptote and so 0 is not an eigenvalue.

```
ωn,0,0 = PP[[1]][[1]]
ωn,0 := SetPrecision[FindRoot[DD, {ω, ωn,0,0}, WorkingPrecision → WP][[1]][[2]], 7]
ωn,0
% / (2 Pi)
```

1.68515×10^6

1.681977×10^6

$267\,695.0$

```
ωn,1,0 := PP[[2]][[1]];
ωn,1 := SetPrecision[FindRoot[DD, {ω, ωn,1,0}, WorkingPrecision → WP][[1]][[2]], WP]
ωn,1
% / (2 Pi)
```

$1.681977257748357094481636341727740050147442059484940701262 89\times10^6$

$267\,694.994738801946572282071255962007170664658144036299870988$

```
ωn,2,0 := PP[[3]][[1]];
ωn,2 := SetPrecision[FindRoot[DD, {ω, ωn,2,0}, WorkingPrecision → WP][[1]][[2]], WP]
ωn,2
% / (2 Pi)
```

$2.202228852768019592874038066102976533518923530660447458776 97\times10^6$

$350\,495.607737624110391791580487982549979304189007751631670098$

```
ω_{n,3,0} := PP[[4]][[1]];
ω_{n,3} := SetPrecision[FindRoot[DD, {ω, ω_{n,3,0}}, WorkingPrecision → WP][[1]][[2]], WP]
ω_{n,3}
% / (2 Pi)
```

$3.628087553873895648142202329440914299143664643590780500172 28 \times 10^{6}$

577 428.068169213615030170068245246581799246041199921764582646

Use RowReduce to determine the nature of B1, B2, B3 and B4 :

```
Clear[ω]
ω = ω_{n,0}
MatrixForm[RowReduce[
  {{b11, b12, b13, b14}, {b21, b22, b23, b24}, {b31, b32, b33, b34}, {b41, b42, b43, b44}}]]
```

1.681977×10^{6}

$$\begin{pmatrix} 1 & 0 & 0 & -8.09 \\ 0 & 1 & 0 & -0.3416 \\ 0 & 0 & 1 & -4.227 \\ 0 & 0 & 0 & 0 \end{pmatrix}$$

Clearly B4 is free, so choose a value for B4 that yields values for U and V on the boundaries that are feasible, say of order mm or μm. Then calculate B1, B2 and B3, using Cramer' s rule :

```
B4 = 1
```

$$B1 = \text{SetPrecision}\left[\frac{\text{Det}\left[\begin{pmatrix} -b14\,B4 & b12 & b13 \\ -b24\,B4 & b22 & b23 \\ -b34\,B4 & b32 & b33 \end{pmatrix}\right]}{\text{Det}\left[\begin{pmatrix} b11 & b12 & b13 \\ b21 & b22 & b23 \\ b31 & b32 & b33 \end{pmatrix}\right]}, WP + 10\right]$$

$$B2 = \text{SetPrecision}\left[\frac{\text{Det}\left[\begin{pmatrix} b11 & -b14\,B4 & b13 \\ b21 & -b24\,B4 & b23 \\ b31 & -b34\,B4 & b33 \end{pmatrix}\right]}{\text{Det}\left[\begin{pmatrix} b11 & b12 & b13 \\ b21 & b22 & b23 \\ b31 & b32 & b33 \end{pmatrix}\right]}, WP + 10\right]$$

$$B3 = \text{SetPrecision}\left[\frac{\text{Det}\left[\begin{pmatrix} b11 & b12 & -b14\,B4 \\ b21 & b22 & -b24\,B4 \\ b31 & b32 & -b34\,B4 \end{pmatrix}\right]}{\text{Det}\left[\begin{pmatrix} b11 & b12 & b13 \\ b21 & b22 & b23 \\ b31 & b32 & b33 \end{pmatrix}\right]}, WP + 10\right]$$

```
1
```

```
8.085163033040209773841255902482316741952672600746154785156250000000000
```

```
0.341629728121929244826979199523009356198599562048912048339843750000000000
```

```
4.226591755743599976844534354958327071472012903541326522827148437500000
```

Test the boundary conditions :

```
U[a]
V[a]
U[b]
W[a]
W[b]
W'[a]
```

```
0
```

```
0
```

```
0
```

$$0. \times 10^{-6}$$

$$0. \times 10^{-6}$$

$$0. \times 10^{-2}$$

```
MaxU = FindMaxValue[{Abs[U[r]], a ≤ r ≤ b}, {r, a}]
MU = %
```

```
1384.58
```

```
1384.58
```

```
MaxV = FindMaxValue[{Abs[V[r]], a ≤ r ≤ b}, {r, a}]
MV = %
```

```
1206.22
```

```
1206.22
```

```
p1 = Plot[{U[r]/MU}, {r, a, b}, PlotRange → All, DisplayFunction → Identity,
    PlotPoints → 10000, PlotStyle → {{Blue, Thickness[0.011]}, GrayLevel[0]}];
```

```
p2 = Plot[{V[r]/MV}, {r, a, b}, PlotRange → All, DisplayFunction → Identity,
    PlotPoints → 1000, PlotStyle → {{Red, Thickness[0.011]}, GrayLevel[0]}];
```

```
Show[p1, AxesStyle → Thick, AxesLabel → {"        r   ", " U(r)"},
 LabelStyle → Directive[Bold, Black], DisplayFunction → $DisplayFunction,
 BaseStyle → {FontFamily → "Times", FontSize → 15}]
Show[p2, AxesStyle → Thick, AxesLabel → {"        r   ", "V(r)"},
 LabelStyle → Directive[Bold, Black], DisplayFunction → $DisplayFunction,
 BaseStyle → {FontFamily → "Times", FontSize → 15}]
Show[p1, p2, AxesStyle → Thick, AxesLabel → {"     r   ", "Eigenfunctions"},
 LabelStyle → Directive[Bold, Black], DisplayFunction → $DisplayFunction,
 BaseStyle → {FontFamily → "Times", FontSize → 15}]
```

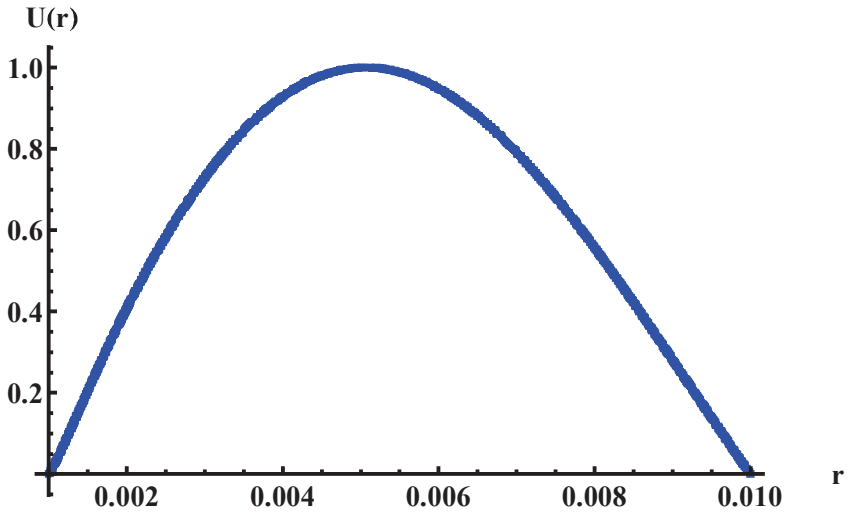

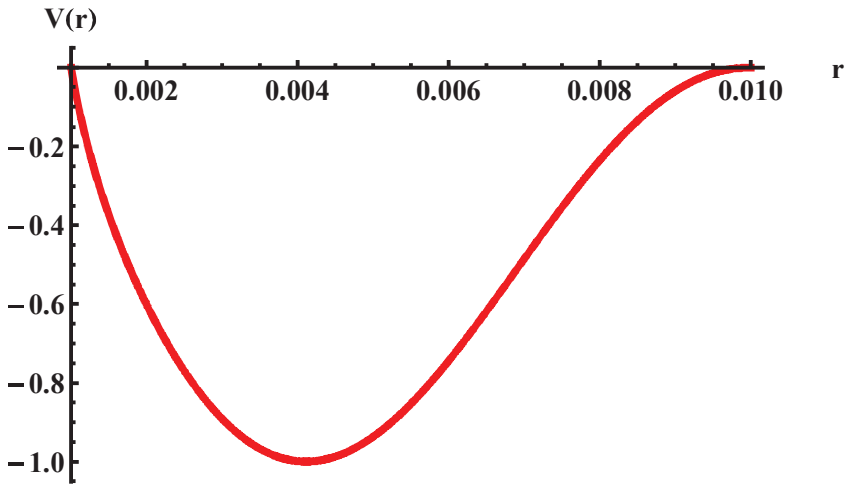

Eigenfunctions

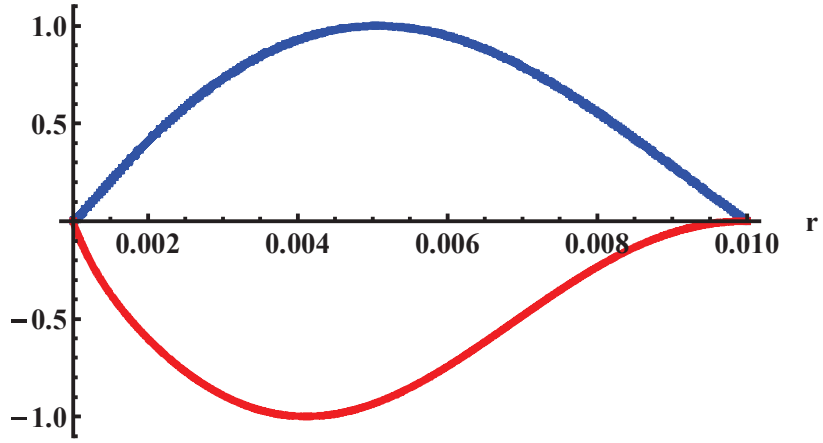


```
q1 = {{768993.231810491, 14.712066415255986`}};
q2 = {{3.0159744461243777`*^6, 77.95116372958098}};
q3 = {{6.389776363189273*^6, 80.56996132026089}};
q4 = {{1.0837060708411181`*^7, 83.36936564133254}};
qq = Join[q1, q2, q3, q4]
```

$$\{\{768993., 14.7121\}, \{3.01597 \times 10^6, 77.9512\}, \{6.38978 \times 10^6, 80.57\}, \{1.08371 \times 10^7, 83.3694\}\}$$

```
MaxW = FindMaxValue[{Abs[W[r]], a ≤ r ≤ b}, {r, a}]
MW = %
```

8.10746

8.10746

```
p3 = Plot[{W[r]/MW}, {r, a, b}, PlotRange → All, DisplayFunction → Identity,
  PlotPoints → 1000, PlotStyle → {{Brown, Thickness[0.011]}, GrayLevel[0]}]
```

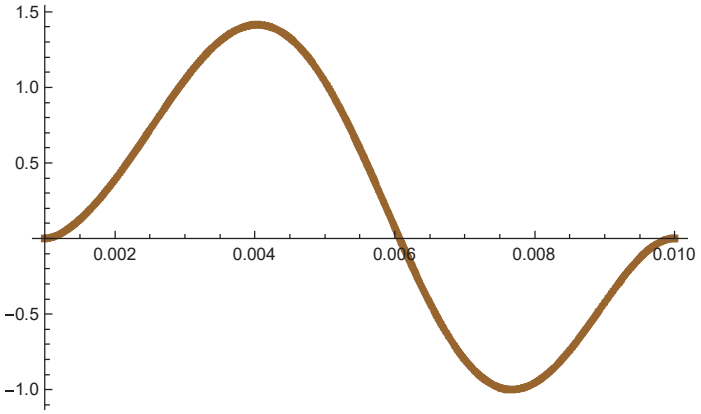


```
Show[p3, AxesStyle → Thick, AxesLabel → {"        r   ", "W(r)"},
 LabelStyle → Directive[Bold, Black], DisplayFunction → $DisplayFunction,
 BaseStyle → {FontFamily → "Times", FontSize → 15}]
```

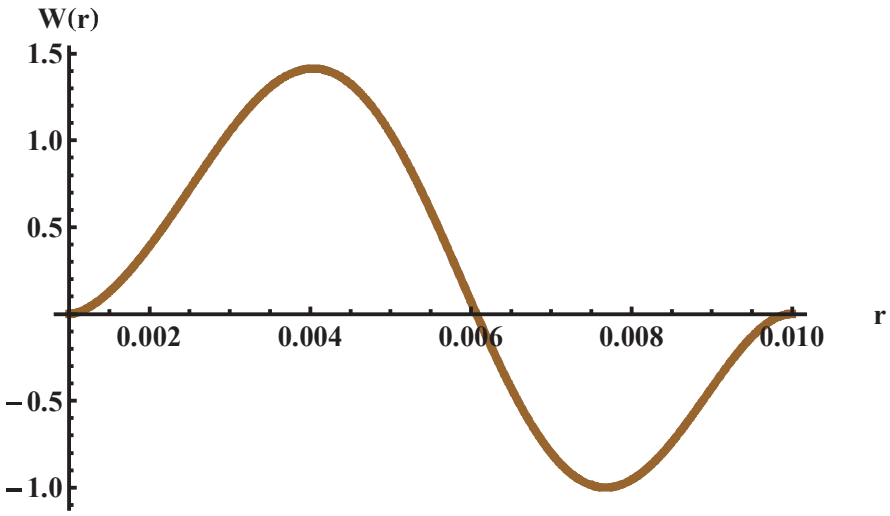

```
Plot[{U[r]/MU, V[r]/MV, W[r]/MW}, {r, a, b}, PlotRange → All, DisplayFunction → Identity,
 PlotPoints → 10000, AxesStyle → Thick, LabelStyle → Directive[Bold, Black],
 DisplayFunction → $DisplayFunction, BaseStyle → {FontFamily → "Times", FontSize → 15},
 PlotStyle → {{Blue, Thickness[0.01]}, {Red, Thickness[0.01]}, {Brown, Thickness[0.01]}},
 AxesLabel → {"        r  ", " Eigenfunction"}, PlotLegends → {"U[r]", "V[r]", "W[r]"}]
```

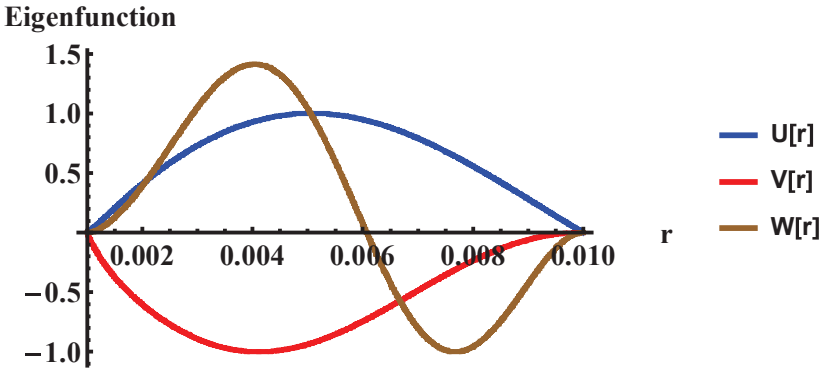


```
Plot[{U[r]/MU, V[r]/MV, W[r]/MW}, {r, a, b}, PlotStyle →
  {{Black, Thickness[0.008] }, {Gray, Thickness[0.008]}, {Black, Dashing[Large]}},
 PlotRange → All, DisplayFunction → Identity, PlotPoints → 10000,
 AxesStyle → Thickness[Large], LabelStyle → Directive[Bold, GrayLevel[0]],
 BaseStyle → {FontFamily → "Times", FontSize → 15},
 AxesLabel → {"        r  ", " Eigenfunction"}, PlotLegends → {"U[r]", "V[r]", "W[r]"}]
```

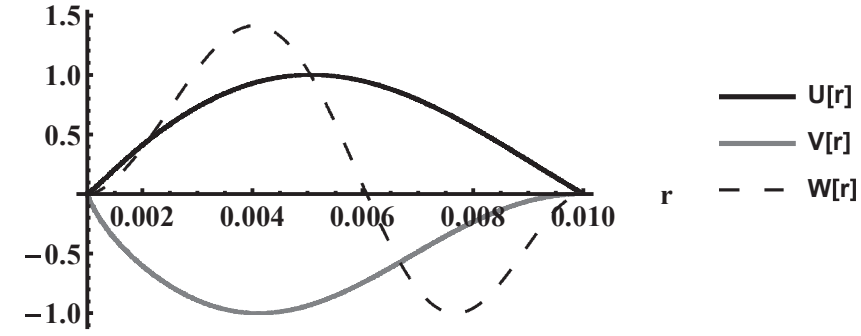

Mathematica code for the first five normalised eigenfunctions for annular disc gyroscope clamped at both edges

```
WP = 60
```

```
60
```

```
w[r, φ, t] := W[r] Cos[m φ] e^(i ω t);
```

```
Collect[w[r, φ, t], Cos[m φ] Cos[ω t + Θ], Simplify];
```

```
Collect[(∂r w[r, φ, t]), Cos[m φ] e^(i ω t), Simplify];
```

```
W[r_] := A1 BesselJ[m, β r] + A2 BesselY[m, β r] + A3 BesselI[m, β r] + A4 BesselK[m, β r]
Collect[w[r, φ, t], Cos[m φ] Cos[ω t + Θ], Simplify];
a11 = Simplify[W[r], Factor] /. {r -> a, A1 -> 1, A2 -> 0, A3 -> 0, A4 -> 0};
a12 = Simplify[W[r], Factor] /. {r -> a, A1 -> 0, A2 -> 1, A3 -> 0, A4 -> 0};
a13 = Simplify[W[r], Factor] /. {r -> a, A1 -> 0, A2 -> 0, A3 -> 1, A4 -> 0};
a14 = Simplify[W[r], Factor] /. {r -> a, A1 -> 0, A2 -> 0, A3 -> 0, A4 -> 1};
a21 = Simplify[W'[r], Factor] /. {r -> a, A1 -> 1, A2 -> 0, A3 -> 0, A4 -> 0};
a22 = Simplify[W'[r], Factor] /. {r -> a, A1 -> 0, A2 -> 1, A3 -> 0, A4 -> 0};
a23 = Simplify[W'[r], Factor] /. {r -> a, A1 -> 0, A2 -> 0, A3 -> 1, A4 -> 0};
a24 = Simplify[W'[r], Factor] /. {r -> a, A1 -> 0, A2 -> 0, A3 -> 0, A4 -> 1};

a31 = Simplify[W[r], Factor] /. {r -> b, A1 -> 1, A2 -> 0, A3 -> 0, A4 -> 0};
a32 = Simplify[W[r], Factor] /. {r -> b, A1 -> 0, A2 -> 1, A3 -> 0, A4 -> 0};
a33 = Simplify[W[r], Factor] /. {r -> b, A1 -> 0, A2 -> 0, A3 -> 1, A4 -> 0};
a34 = Simplify[W[r], Factor] /. {r -> b, A1 -> 0, A2 -> 0, A3 -> 0, A4 -> 1};
a41 = Simplify[W'[r], Factor] /. {r -> b, A1 -> 1, A2 -> 0, A3 -> 0, A4 -> 0};
a42 = Simplify[W'[r], Factor] /. {r -> b, A1 -> 0, A2 -> 1, A3 -> 0, A4 -> 0};
a43 = Simplify[W'[r], Factor] /. {r -> b, A1 -> 0, A2 -> 0, A3 -> 1, A4 -> 0};
a44 = Simplify[W'[r], Factor] /. {r -> b, A1 -> 0, A2 -> 0, A3 -> 0, A4 -> 1};
```

```
Φ[r, φ, t] := (B1 BesselJ[n, k1 r] + B2 BesselY[n, k1 r]) Cos[n φ] Cos[ω t + ϕ];
Ψ[r, φ, t] := (B3 BesselJ[n, k2 r] + B4 BesselY[n, k2 r]) Sin[n φ] Cos[ω t + ϕ];
```

$$u[r, \varphi, t] := \partial_r \Phi[r, \varphi, t] + \frac{1}{r} \partial_\varphi \Psi[r, \varphi, t];$$

$$v[r, \varphi, t] := \frac{1}{r} \partial_\varphi \Phi[r, \varphi, t] - \partial_r \Psi[r, \varphi, t];$$

```
Collect[u[r, φ, t], Cos[n φ] Cos[t ω]];
```

```
U[r_] := SetPrecision[ ((1/2) B1 k1 (BesselJ[-1 + n, k1 r] - BesselJ[1 + n, k1 r]) +
     (1/r) n (B3 BesselJ[n, k2 r] + B4 BesselY[n, k2 r]) +
     (1/2) B2 k1 (BesselY[-1 + n, k1 r] - BesselY[1 + n, k1 r])), WP]

Collect[v[r, φ, t], Sin[n φ] Cos[t ω]];

V[r_] := SetPrecision[ (-(1/2) B3 k2 (BesselJ[-1 + n, k2 r] - BesselJ[1 + n, k2 r]) -
     (1/r) n (B1 BesselJ[n, k1 r] + B2 BesselY[n, k1 r]) -
     (1/2) B4 k2 (BesselY[-1 + n, k2 r] - BesselY[1 + n, k2 r])), WP];

b11 = Simplify[ U[r], Factor] /.{r → a, B1 → 1, B2 → 0, B3 → 0, B4 → 0};
b12 = Simplify[U[r], Factor] /.{r → a, B1 → 0, B2 → 1, B3 → 0, B4 → 0};
b13 = Simplify[ U[r], Factor] /.{r → a, B1 → 0, B2 → 0, B3 → 1, B4 → 0};
b14 = Simplify[ U[r], Factor] /.{r → a, B1 → 0, B2 → 0, B3 → 0, B4 → 1};
b21 = Simplify[V[r], Factor] /.{r → a, B1 → 1, B2 → 0, B3 → 0, B4 → 0};
b22 = Simplify[V[r], Factor] /.{r → a, B1 → 0, B2 → 1, B3 → 0, B4 → 0};
b23 = Simplify[V[r], Factor] /.{r → a, B1 → 0, B2 → 0, B3 → 1, B4 → 0};
b24 = Simplify[V[r], Factor] /.{r → a, B1 → 0, B2 → 0, B3 → 0, B4 → 1};

b31 = Simplify[ U[r], Factor] /.{r → b, B1 → 1, B2 → 0, B3 → 0, B4 → 0};
b32 = Simplify[U[r], Factor] /.{r → b, B1 → 0, B2 → 1, B3 → 0, B4 → 0};
b33 = Simplify[ U[r], Factor] /.{r → b, B1 → 0, B2 → 0, B3 → 1, B4 → 0};
b34 = Simplify[ U[r], Factor] /.{r → b, B1 → 0, B2 → 0, B3 → 0, B4 → 1};
b41 = Simplify[V[r], Factor] /.{r → b, B1 → 1, B2 → 0, B3 → 0, B4 → 0};
b42 = Simplify[V[r], Factor] /.{r → b, B1 → 0, B2 → 1, B3 → 0, B4 → 0};
b43 = Simplify[V[r], Factor] /.{r → b, B1 → 0, B2 → 0, B3 → 1, B4 → 0};
b44 = Simplify[V[r], Factor] /.{r → b, B1 → 0, B2 → 0, B3 → 0, B4 → 1};

WP = 60
60

Clear[DP, ω]

Clear[DD, ω]
```

```
a = 1/1000
N[a]
b = 1/100;
N[b]
m = 3;
n = 2;
μ = 1/3;
h = 38.5/40000;
N[h]
ρ = 2700;
EE = 70 × 10^9;
β = SetPrecision[Sqrt[ω/h Sqrt[12 ρ (1 - μ^2)/EE]], WP];
k1 = SetPrecision[ω Sqrt[ρ (1 - μ^2)/EE], WP];
k2 = SetPrecision[ω Sqrt[2 ρ (1 + μ)/EE], WP];
```

$$\frac{1}{1000}$$

```
0.001
0.01
0.0009625
SetPrecision[Det[{{a11, a12, a13, a14}, {a21, a22, a23, a24}, {a31, a32, a33, a34}, {a41, a42, a43, a44}}], WP];
DP = SetPrecision[Det[{{a11, a12, a13, a14}, {a21, a22, a23, a24}, {a31, a32, a33, a34}, {a41, a42, a43, a44}}], WP];
SetPrecision[Det[{{b11, b12, b13, b14}, {b21, b22, b23, b24}, {b31, b32, b33, b34}, {b41, b42, b43, b44}}], WP];
```

```
DD = SetPrecision[Det[{{b11, b12, b13, b14}, {b21, b22, b23, b24}, {b31, b32, b33, b34}, {b41, b42, b43, b44}}], WP];
```

```
Plot[DP, {ω, 0, 100000}, PlotRange → All]
```

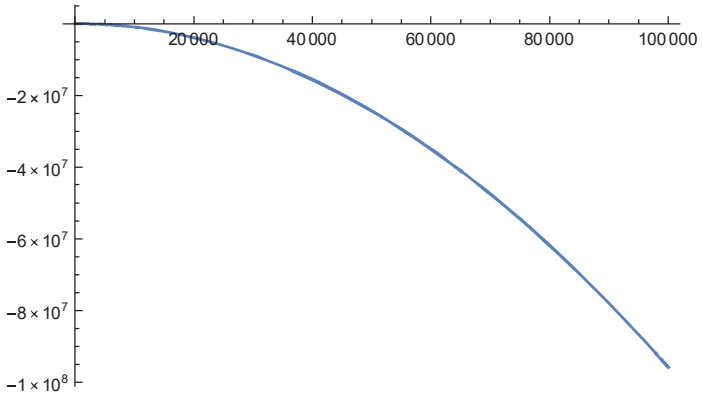


```
Plot[DD, {ω, 0, 1000000}, PlotRange → All]
```

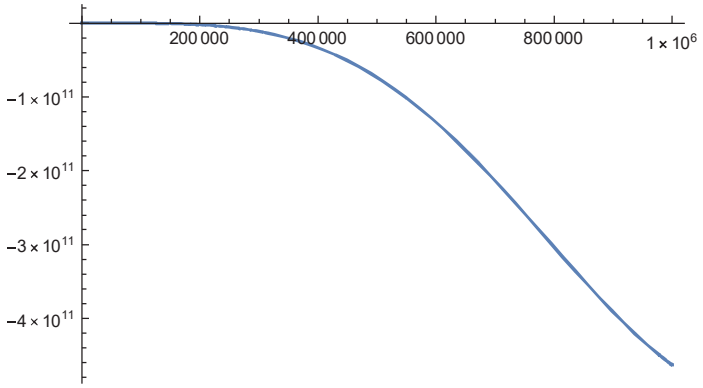


```
Plot[Log[Abs[DP]], {ω, 0, 2000000}, PlotRange → All]
```

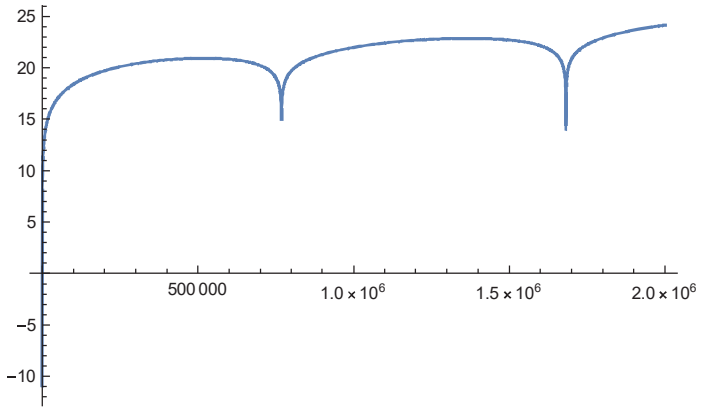

```
Plot[Log[Abs[DD]], {ω, 0, 6000000}, PlotRange → All]
```

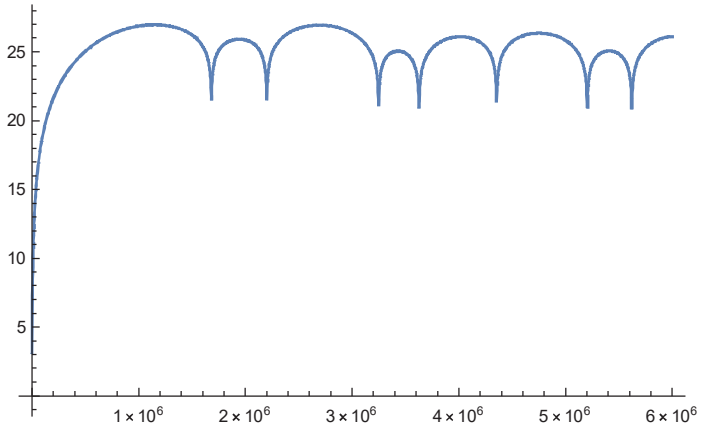


```
Plot[{Log[Abs[DD]], Log[Abs[DP]]}, {ω, 0, 3000000},
 PlotLegends → "Expressions", AxesLabel → {" ω", " Log[Abs[Det Eqn]]"},
 LabelStyle → Directive[Bold, Black], BaseStyle → {FontFamily → "Times", FontSize → 12},
 PlotStyle → {{Black, Thickness[0.01]}, {Gray, Thickness[0.01]}},
 AxesStyle → Thick, PlotTheme → "Default"]
```

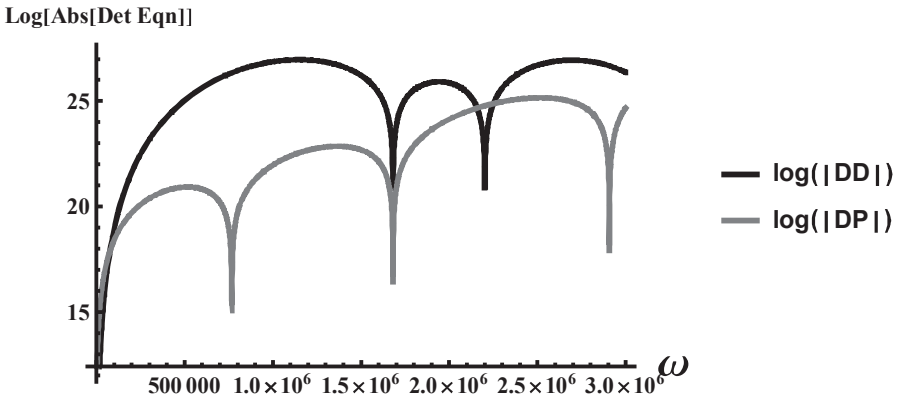

```
Plot[Log[Abs[DD]], {ω, 0, 6000000}, PlotRange → All,
 AxesLabel → {"        ω",  "        f(ω)"}, LabelStyle → Directive[Bold, Black],
 AxesStyle → Thick, PlotStyle → {{Black, Thickness[0.01]}},
 BaseStyle → {FontFamily → "Times", FontSize → 12}]
```

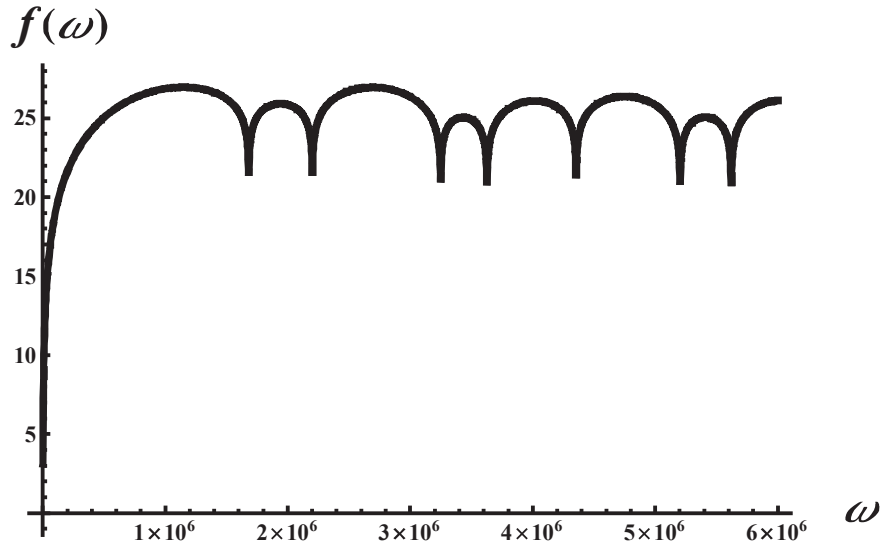


```
Plot[Log[Abs[DP]], {ω, 0, 9000000}, PlotRange → All,
 AxesLabel → {"        ω",  "F(ω)"}, LabelStyle → Directive[Bold, Black],
 AxesStyle → Thick, PlotStyle → {{Black, Thickness[0.01]}},
 BaseStyle → {FontFamily → "Times", FontSize → 12}]
```

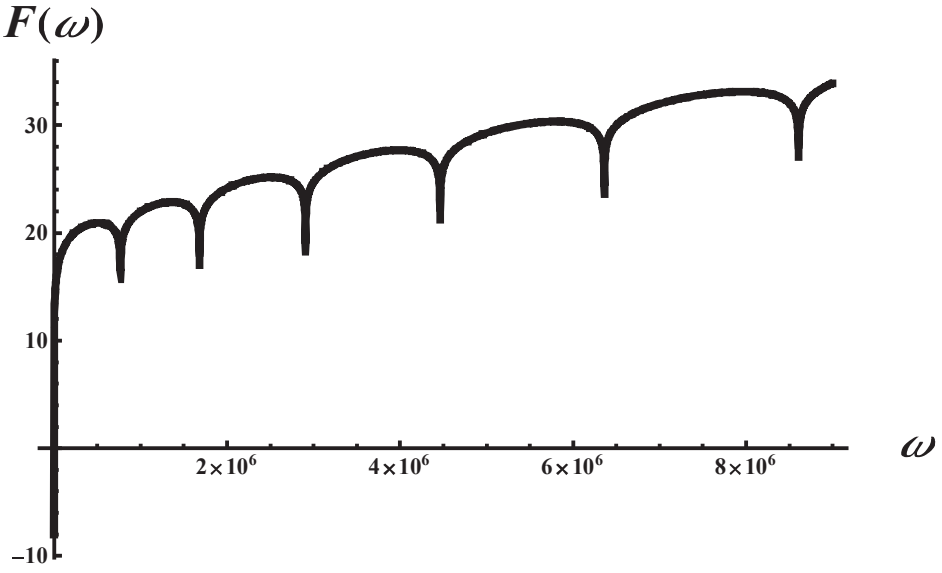

Right - click on the graphs above to get coordinates of a spike to use as a first approximation for $\omega_{m,n,0}$ (m declared above and n = 0,1,2,3...) using FindRoot. Note that at $\omega = 0$ there is no spike; indeed, the curve has the vertical axis as an asymptote and so 0 is not an eigenvalue.

```
P1 = {{1.679054019787645*^6, 21.24193288108749}};
P2 = {{2.1835585139961387`*^6, 20.99742988740663}};
P3 = {{3.255630564189189*^6, 21.119681384247063`}};
P4 = {{3.6340089348455593`*^6, 20.997429887406625`}};
p5 = {{4.374999910714285*^6, 21.241932881087486`}};
p6 = {{5.210585479247103*^6, 20.752926893725782`}};
PP = Join[P1, P2, P3, P4, p5, p6]
```

$$\{\{1.67905\times10^6, 21.2419\}, \{2.18356\times10^6, 20.9974\}, \{3.25563\times10^6, 21.1197\},\ \{3.63401\times10^6, 20.9974\}, \{4.375\times10^6, 21.2419\}, \{5.21059\times10^6, 20.7529\}\}$$

```
q1 = {{768993.231810491, 14.712066415255986`}};
q2 = {{3.0159744461243777`*^6, 77.95116372958098}};
q3 = {{6.389776363189273*^6, 80.56996132026089}};
q4 = {{1.0837060708411181`*^7, 83.36936564133254}};
qq = Join[q1, q2, q3, q4]
```

$$\{\{768993., 14.7121\}, \{3.01597\times10^6, 77.9512\},\ \{6.38978\times10^6, 80.57\}, \{1.08371\times10^7, 83.3694\}\}$$

```
ωn,0,0 = PP[[1]][[1]]
ωn,0 := SetPrecision[FindRoot[DD, {ω, ωn,0,0}, WorkingPrecision → WP]][[1]][[2]], 7]
ωn,0
% / (2 Pi)
```

1.67905×10^6

1.681977×10^6

267695.0

```
ω_{n,1,0} := PP[[2]][[1]];
ω_{n,1} := SetPrecision[FindRoot[DD, {ω, ω_{n,1,0}}, WorkingPrecision → WP][[1]][[2]], 7]
ω_{n,1}
% / (2 Pi)
```

2.202229×10^6

350 495.6

```
ω_{n,2,0} := PP[[3]][[1]];
ω_{n,2} := SetPrecision[FindRoot[DD, {ω, ω_{n,2,0}}, WorkingPrecision → WP][[1]][[2]], 7]
ω_{n,2}
% / (2 Pi)
```

3.249287×10^6

517 140.1

```
ω_{n,3,0} := PP[[4]][[1]];
ω_{n,3} := SetPrecision[FindRoot[DD, {ω, ω_{n,3,0}}, WorkingPrecision → WP][[1]][[2]], 7]
ω_{n,3}
% / (2 Pi)
```

3.628088×10^6

577 428.1

```
ω_{n,4,0} := PP[[5]][[1]];
ω_{n,4} := SetPrecision[
  FindRoot[DD, {ω, 4.374999910714285`*^6}, WorkingPrecision → WP][[1]][[2]], 7]
ω_{n,4}
% / (2 Pi)
```

4.355487×10^6

693 197.3

```
ω_{n,5,0} := PP[[6]][[1]];
ω_{n,5} := SetPrecision[
  FindRoot[DD, {ω, 5.210585479247103`*^6}, WorkingPrecision → WP][[1]][[2]], 7]
ω_{n,5}
% / (2 Pi)
```

5.204516×10^6

828 324.4

Use RowReduce to determine the nature of B1, B2, B3 and B4 :

```
Clear[ω]
ω = ω_{n,0}
MatrixForm[RowReduce[
  {{b11, b12, b13, b14}, {b21, b22, b23, b24}, {b31, b32, b33, b34}, {b41, b42, b43, b44}}]]
```

1.681977×10^6

$$\begin{pmatrix} 1 & 0 & 0 & -8.09 \\ 0 & 1 & 0 & -0.3416 \\ 0 & 0 & 1 & -4.227 \\ 0 & 0 & 0 & 0 \end{pmatrix}$$

Clearly B4 is free, so choose a value for B4 that yields values for U and V on the boundaries that are feasible, say of order mm or μm. Then calculate B1, B2 and B3, using Cramer' s rule :

```
B4 = 1
```

$$B1 = \text{SetPrecision}\left[\frac{\text{Det}\left[\begin{pmatrix} -b14\,B4 & b12 & b13 \\ -b24\,B4 & b22 & b23 \\ -b34\,B4 & b32 & b33 \end{pmatrix}\right]}{\text{Det}\left[\begin{pmatrix} b11 & b12 & b13 \\ b21 & b22 & b23 \\ b31 & b32 & b33 \end{pmatrix}\right]}, WP + 10\right]$$

$$B2 = \text{SetPrecision}\left[\frac{\text{Det}\left[\begin{pmatrix} b11 & -b14\,B4 & b13 \\ b21 & -b24\,B4 & b23 \\ b31 & -b34\,B4 & b33 \end{pmatrix}\right]}{\text{Det}\left[\begin{pmatrix} b11 & b12 & b13 \\ b21 & b22 & b23 \\ b31 & b32 & b33 \end{pmatrix}\right]}, WP + 10\right]$$

$$B3 = \text{SetPrecision}\left[\frac{\text{Det}\left[\begin{pmatrix} b11 & b12 & -b14\,B4 \\ b21 & b22 & -b24\,B4 \\ b31 & b32 & -b34\,B4 \end{pmatrix}\right]}{\text{Det}\left[\begin{pmatrix} b11 & b12 & b13 \\ b21 & b22 & b23 \\ b31 & b32 & b33 \end{pmatrix}\right]}, WP + 10\right]$$

```
1

8.085163033040209773841255902482316741952672600746154785156250000000000

0.341629728121929244826979199523009356198599562048912048339843750000000000

4.226591755743599976844534354958327071472012903541326522827148437500000
```

Test the boundary conditions :

```
U[a]
V[a]
U[b]

0

0

0

MaxU = FindMaxValue[{Abs[U[r]], a ≤ r ≤ b}, {r, a}]
MU = %

1384.58

1384.58
```

```
MaxV = FindMaxValue[{Abs[V[r]], a ≤ r ≤ b}, {r, a}]
MV = %
```

```
1206.22
```

```
1206.22
```

```
p1 = Plot[{U[r]/MU}, {r, a, b}, PlotRange → All, DisplayFunction → Identity,
    PlotPoints → 10000, PlotStyle → {{Blue, Thickness[0.011]}, GrayLevel[0]}];
```

```
p2 = Plot[{V[r]/MU}, {r, a, b}, PlotRange → All, DisplayFunction → Identity,
    PlotPoints → 1000, PlotStyle → {{Red, Thickness[0.011]}, GrayLevel[0]}];
```

```
Show[p1, AxesStyle → Thick, AxesLabel → {"        r   ", " U(r)"},
 LabelStyle → Directive[Bold, Black], DisplayFunction → $DisplayFunction,
 BaseStyle → {FontFamily → "Times", FontSize → 15}]
Show[p2, AxesStyle → Thick, AxesLabel → {"        r   ", "V(r)"},
 LabelStyle → Directive[Bold, Black], DisplayFunction → $DisplayFunction,
 BaseStyle → {FontFamily → "Times", FontSize → 15}]
Show[p1, p2, AxesStyle → Thick, AxesLabel → {"        r   ", " U(r)  V(r)"},
 LabelStyle → Directive[Bold, Black], DisplayFunction → $DisplayFunction,
 BaseStyle → {FontFamily → "Times", FontSize → 15}]
```

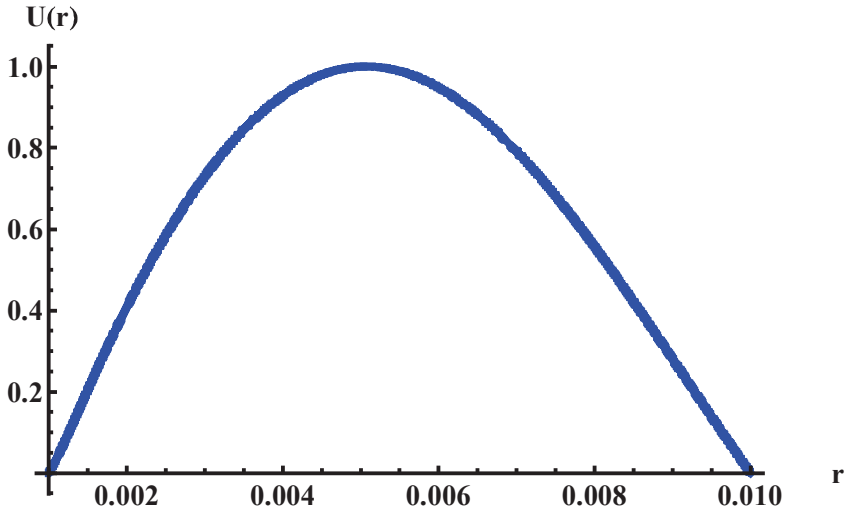

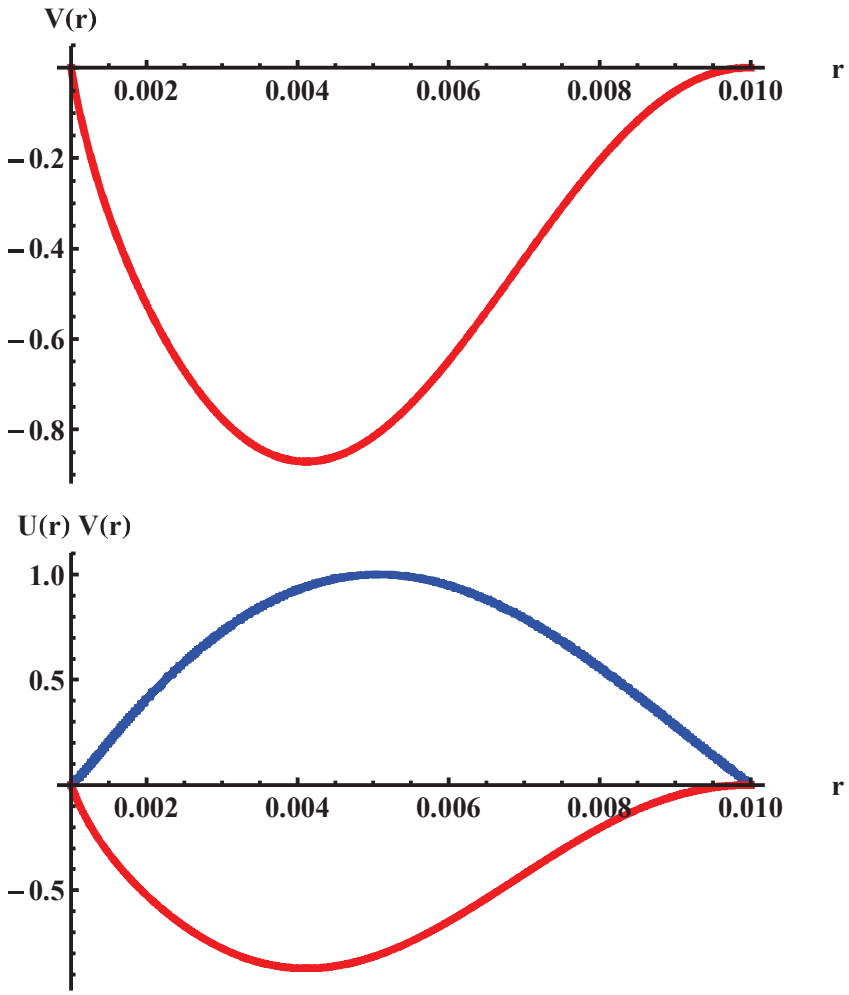


```
q1 = {{768993.231810491, 14.712066415255986`}};
q2 = {{3.0159744461243777`*^6, 77.95116372958098}};
q3 = {{6.389776363189273*^6, 80.56996132026089}};
q4 = {{1.0837060708411181`*^7, 83.36936564133254}};
qq = Join[q1, q2, q3, q4]
```

$$\{\{768993., 14.7121\}, \{3.01597 \times 10^6, 77.9512\}, \{6.38978 \times 10^6, 80.57\}, \{1.08371 \times 10^7, 83.3694\}\}$$

```
Clear[ω1]
```

```
ω1 =
 1.681977257748357094481636341727740050147442059484940701262891423944440831888152561756`60.
  .*^6
```

$$1.681977257748357094481636341727740050147442059484940701262891 \times 10^6$$

```
A4 = 1
```

$$\text{A1} = \text{SetPrecision}\left[\frac{\text{Det}\left[\begin{pmatrix} -\text{a14}\,\text{A4} & \text{a12} & \text{a13} \\ -\text{a24}\,\text{A4} & \text{a22} & \text{a23} \\ -\text{a34}\,\text{A4} & \text{a32} & \text{a33} \end{pmatrix}\right]}{\text{Det}\left[\begin{pmatrix} \text{a11} & \text{a12} & \text{a13} \\ \text{a21} & \text{a22} & \text{a23} \\ \text{a31} & \text{a32} & \text{a33} \end{pmatrix}\right]}, \text{WP} + 10\right]$$

$$\text{A2} = \text{SetPrecision}\left[\frac{\text{Det}\left[\begin{pmatrix} \text{a11} & -\text{a14}\,\text{A4} & \text{a13} \\ \text{a21} & -\text{a24}\,\text{A4} & \text{a23} \\ \text{a31} & -\text{a34}\,\text{A4} & \text{a33} \end{pmatrix}\right]}{\text{Det}\left[\begin{pmatrix} \text{a11} & \text{a12} & \text{a13} \\ \text{a21} & \text{a22} & \text{a23} \\ \text{a31} & \text{a32} & \text{a33} \end{pmatrix}\right]}, \text{WP} + 10\right]$$

$$\text{A3} = \text{SetPrecision}\left[\frac{\text{Det}\left[\begin{pmatrix} \text{a11} & \text{a12} & -\text{a14}\,\text{A4} \\ \text{a21} & \text{a22} & -\text{a24}\,\text{A4} \\ \text{a31} & \text{a32} & -\text{a34}\,\text{A4} \end{pmatrix}\right]}{\text{Det}\left[\begin{pmatrix} \text{a11} & \text{a12} & \text{a13} \\ \text{a21} & \text{a22} & \text{a23} \\ \text{a31} & \text{a32} & \text{a33} \end{pmatrix}\right]}, \text{WP} + 10\right]$$

```
1
```

```
26.635717479119986233484455168118998358295357320457696914672851562500000
```

```
1.305536512343436932113809045841179568014922551810741424560546875000000
```

```
-0.001428477400966389964601793716170163861534092575311660766601562500000000
```

```
MaxW = FindMaxValue[{Abs[W[r]], a ≤ r ≤ b}, {r, a}]
MW = %
```

```
8.10746
```

```
8.10746
```

```
p3 = Plot[{W[r]/MW}, {r, a, b}, PlotRange → All, DisplayFunction → Identity,
  PlotPoints → 1000, PlotStyle → {{Brown, Thickness[0.011]}, GrayLevel[0]}]
```

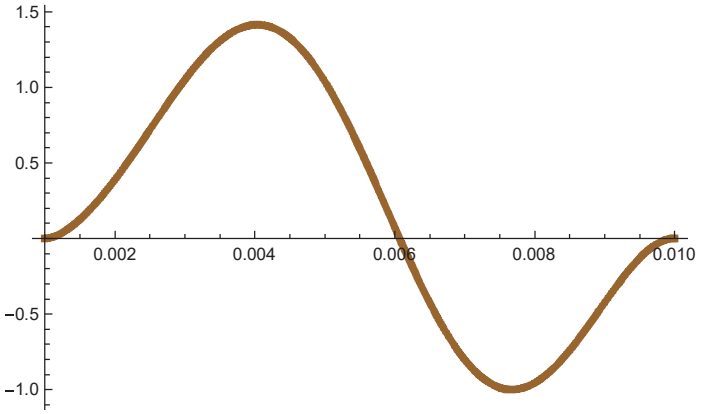


```
Show[p3, AxesStyle → Thick, AxesLabel → {"        r   ", "W(r)"},
 LabelStyle → Directive[Bold, Black], DisplayFunction → $DisplayFunction,
 BaseStyle → {FontFamily → "Times", FontSize → 15}]
```

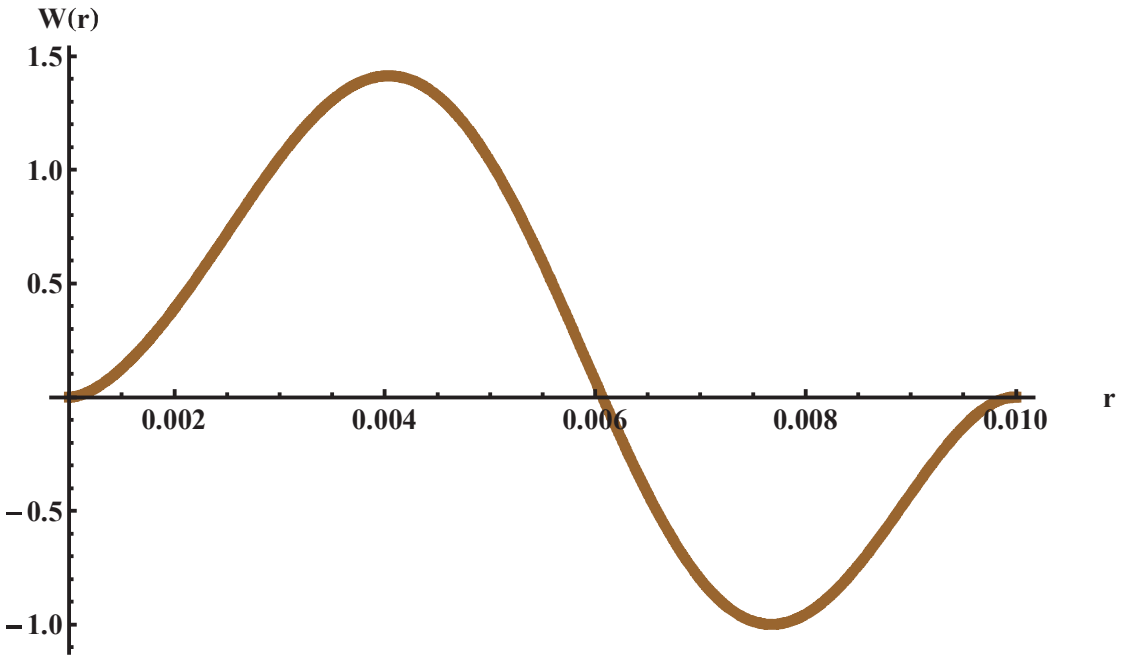

```
Plot[{U[r]/MU, V[r]/MV, W[r]/MW}, {r, a, b}, PlotRange → All, DisplayFunction → Identity,
 PlotPoints → 10000, AxesStyle → Thick, LabelStyle → Directive[Bold, Black],
 DisplayFunction → $DisplayFunction, BaseStyle → {FontFamily → "Times", FontSize → 15},
 PlotStyle → {{Blue, Thickness[0.01]}, {Red, Thickness[0.01]}, {Brown, Thickness[0.01]}},
 AxesLabel → {"        r  ", " Eigenfunction"}, PlotLegends → {u, v, w}]
```

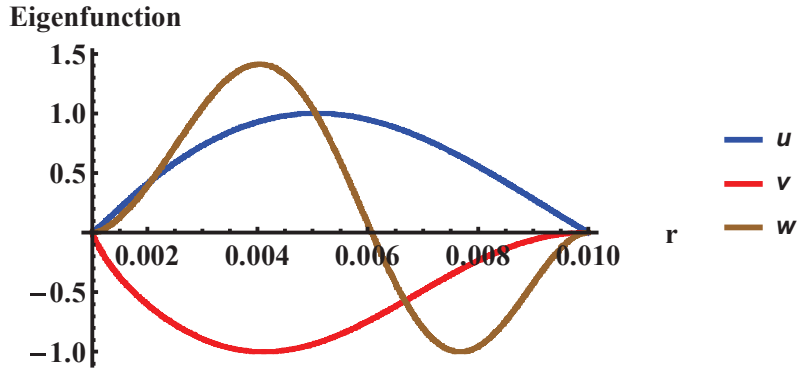


```
Plot[{U[r]/MU, V[r]/MV, W[r]/MW}, {r, a, b}, PlotStyle →
  {{Black, Thickness[0.008] }, {Gray, Thickness[0.008]}, {Black, Dashing[Large]}},
 PlotRange → All, DisplayFunction → Identity, PlotPoints → 10000,
 AxesStyle → Thickness[Large], LabelStyle → Directive[Bold, GrayLevel[0]],
 BaseStyle → {FontFamily → "Times", FontSize → 15},
 AxesLabel → {"        r  ", " Eigenfunction"}, PlotLegends → {"U[r]", "V[r]", "W[r]"}]
```

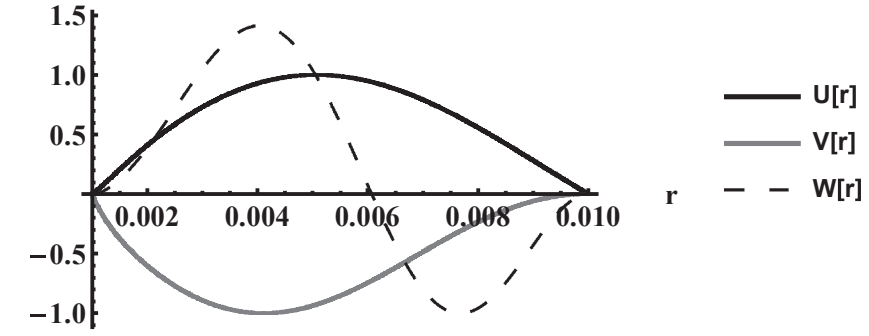


```
Z[r_] := A1 BesselJ[m, α r] + A2 BesselY[m, α r] + A3 BesselI[m, α r] + A4 BesselK[m, α r]

X[r_] := SetPrecision[((1/2) B1 c1 (BesselJ[-1 + n, c1 r] - BesselJ[1 + n, c1 r]) +
      (1/r) n (B3 BesselJ[n, c2 r] + B4 BesselY[n, c2 r]) +
      (1/2) B2 c1 (BesselY[-1 + n, c1 r] - BesselY[1 + n, c1 r])), WP];
```

```
Y[r_] := SetPrecision[ (-1/2 B3 c2 (BesselJ[-1 + n, c2 r] - BesselJ[1 + n, c2 r]) -
      1/r n (B1 BesselJ[n, c1 r] + B2 BesselY[n, c1 r]) -
      1/2 B4 c2 (BesselY[-1 + n, c2 r] - BesselY[1 + n, c2 r])), WP];
```

$$\alpha = \text{SetPrecision}\left[\sqrt{\frac{\gamma}{h}\sqrt{\frac{12\rho\left(1-\mu^2\right)}{EE}}}\,, \text{WP}\right];$$

$$c1 = \text{SetPrecision}\left[\gamma\sqrt{\frac{\rho\left(1-\mu^2\right)}{EE}}\,, \text{WP}\right];$$

$$c2 = \text{SetPrecision}\left[\gamma\sqrt{\frac{2\rho\,(1+\mu)}{EE}}\,, \text{WP}\right];$$

```
γ = 2.202228852768019592874038l`7.*^6
```

2.202229×10^{6}

```
Maxx = FindMaxValue[{Abs[X[r]], a ≤ r ≤ b}, {r, b}]
MX = %
```

1812.84

1812.84

```
Maxy = FindMaxValue[{Abs[Y[r]], a ≤ r ≤ b}, {r, b}]
MY = %
```

1579.32

1579.32

```
FindMaxValue[{Abs[Y[r]], a ≤ r ≤ b}, {r, b}]
```

1579.32

```
Maxz = FindMaxValue[{Abs[Z[r]], a ≤ r ≤ b}, {r, b}]
MZ = %
```

15.5778

15.5778

```
p4 = Plot[{X[r]/MX}, {r, 0.001, b}, PlotRange → All, DisplayFunction → Identity,
   PlotPoints → 10000, PlotStyle → {{Green, Thickness[0.011]}, GrayLevel[0]}]
```

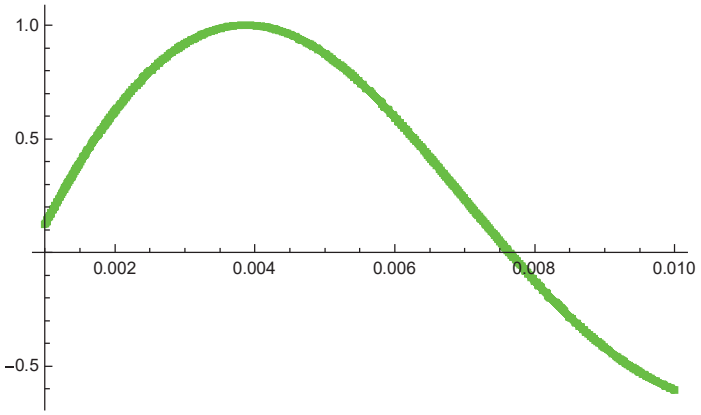


```
p5 = Plot[{Y[r]/MX}, {r, 0.001, b}, PlotRange → All, DisplayFunction → Identity,
    PlotPoints → 10000, PlotStyle → {{Pink, Thickness[0.011]}, GrayLevel[0]}];
p6 = Plot[{Z[r]/MZ}, {r, 0.001, b}, PlotRange → All, DisplayFunction → Identity,
    PlotPoints → 10000, PlotStyle → {{Purple, Thickness[0.011]}, GrayLevel[0]}];
```

```
Show[p4, AxesStyle → Thick, AxesLabel → {"        r   ", " U2,1(r)"},
 LabelStyle → Directive[Bold, Black], DisplayFunction → $DisplayFunction,
 BaseStyle → {FontFamily → "Times", FontSize → 12}]
Show[p5, AxesStyle → Thick, AxesLabel → {"        r   ", "V2,1(r)"},
 LabelStyle → Directive[Bold, Black], DisplayFunction → $DisplayFunction,
 BaseStyle → {FontFamily → "Times", FontSize → 12}]
```

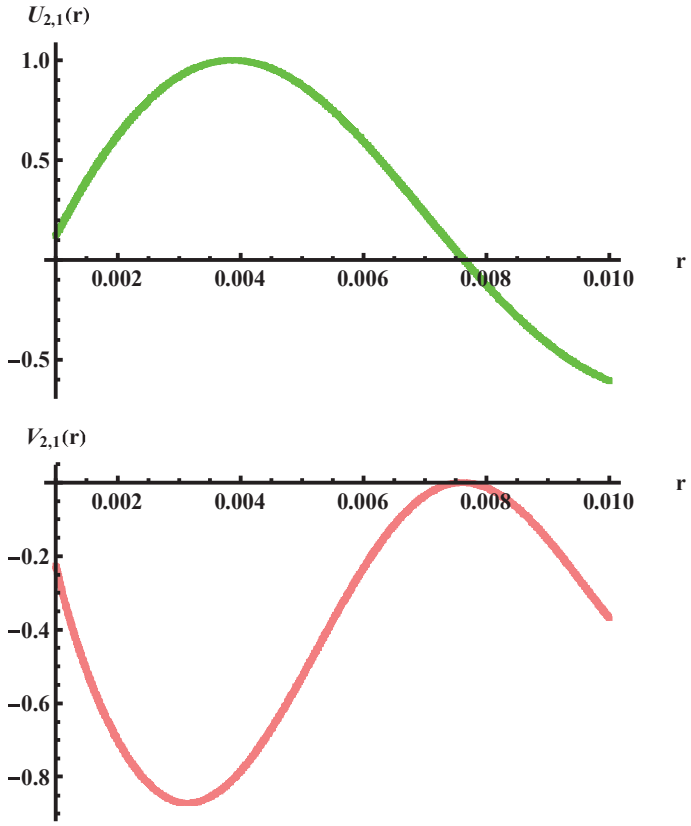


```
Show[p6, AxesStyle → Thick, AxesLabel → {"        r   ", "W3,1(r)"},
 LabelStyle → Directive[Bold, Black], DisplayFunction → $DisplayFunction,
 BaseStyle → {FontFamily → "Times", FontSize → 12}]
```

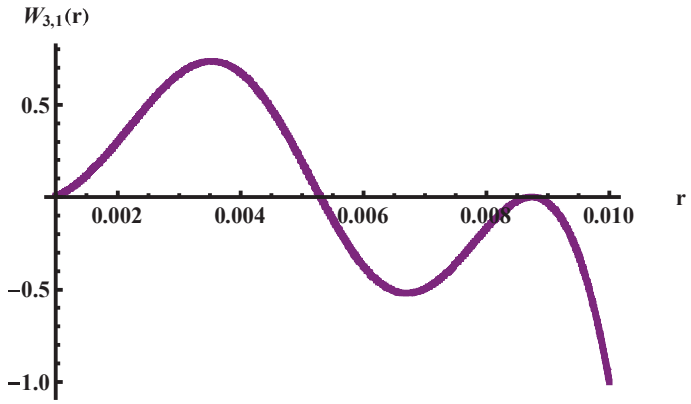

```
Plot[{U[r]/MU, V[r]/MU, W[r]/MU, X[r]/MX, Y[r]/MX, Z[r]/MZ}, {r, 0.001, b}, PlotRange → All,
 DisplayFunction → Identity, PlotPoints → 10000, AxesStyle → Thick,
 LabelStyle → Directive[Bold, Black], DisplayFunction → $DisplayFunction,
 BaseStyle → {FontFamily → "Times", FontSize → 12}, PlotStyle →
  {{Blue, Thickness[0.01`]}, {Red, Thickness[0.01`]}, {Brown, Thickness[0.01`]},
   {Green , Thickness[0.01`]}, {Pink, Thickness[0.01`]}, {Purple, Thickness[0.01`]},},
 AxesLabel → {"        r   ", " Eigenfunction"}, PlotLegends → {U2,0, V2,0, W3,0, U2,1, V2,1, W3,1}]
```

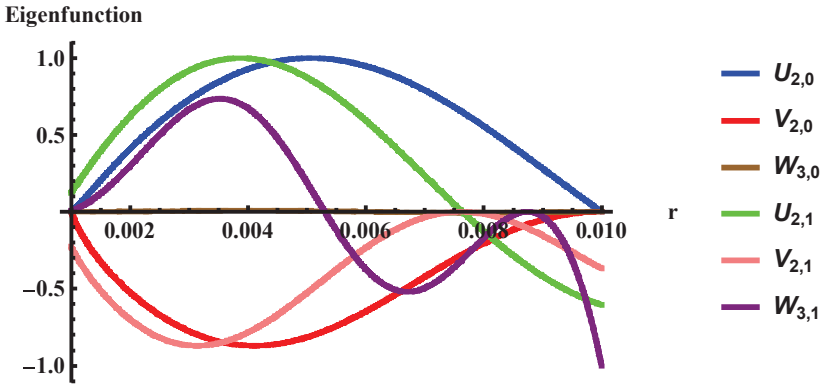


```
Z11[r_] := A1 BesselJ[m, δ r] + A2 BesselY[m, δ r] + A3 BesselI[m, δ r] + A4 BesselK[m, δ r]

X1[r_] := SetPrecision[((1/2) B1 d1 (BesselJ[-1 + n, d1 r] - BesselJ[1 + n, d1 r]) +
      (1/r) n (B3 BesselJ[n, d2 r] + B4 BesselY[n, d2 r]) +
      (1/2) B2 d1 (BesselY[-1 + n, d1 r] - BesselY[1 + n, d1 r])), WP];

Y1[r_] := SetPrecision[(-(1/2) B3 d2 (BesselJ[-1 + n, d2 r] - BesselJ[1 + n, d2 r]) -
      (1/r) n (B1 BesselJ[n, d1 r] + B2 BesselY[n, d1 r]) -
      (1/2) B4 d2 (BesselY[-1 + n, d2 r] - BesselY[1 + n, d2 r])), WP];

δ = SetPrecision[Sqrt[(λ/h) Sqrt[12 ρ (1 - μ^2)/EE]], WP];

d1 = SetPrecision[λ Sqrt[ρ (1 - μ^2)/EE], WP];

d2 = SetPrecision[λ Sqrt[2 ρ (1 + μ)/EE], WP];
```

```
λ = 3.24928732043530425127723 4`7.*^6
```

$$3.249287 \times 10^6$$

```
Z2[r_] := A1 BesselJ[m, η r] + A2 BesselY[m, η r] + A3 BesselI[m, η r] + A4 BesselK[m, η r]

X2[r_] := SetPrecision[((1/2) B1 m1 (BesselJ[-1 + n, m1 r] - BesselJ[1 + n, m1 r]) +
      (1/r) n (B3 BesselJ[n, m2 r] + B4 BesselY[n, m2 r]) +
      (1/2) B2 m1 (BesselY[-1 + n, m1 r] - BesselY[1 + n, m1 r])), WP];

Y2[r_] := SetPrecision[(-(1/2) B3 m2 (BesselJ[-1 + n, m2 r] - BesselJ[1 + n, m2 r]) -
      (1/r) n (B1 BesselJ[n, m1 r] + B2 BesselY[n, m1 r]) -
      (1/2) B4 m2 (BesselY[-1 + n, m2 r] - BesselY[1 + n, m2 r])), WP];

η = SetPrecision[Sqrt[(κ/h) Sqrt[12 ρ (1 - μ^2)/EE]], WP];

m1 = SetPrecision[κ Sqrt[ρ (1 - μ^2)/EE], WP];

m2 = SetPrecision[κ Sqrt[2 ρ (1 + μ)/EE], WP];

κ = 3.62808755387389564814220 23`7.*^6
```

$$3.628088 \times 10^6$$

```
Z3[r_] := A1 BesselJ[m, τ r] + A2 BesselY[m, τ r] + A3 BesselI[m, τ r] + A4 BesselK[m, τ r]

X3[r_] := SetPrecision[((1/2) B1 s1 (BesselJ[-1 + n, s1 r] - BesselJ[1 + n, s1 r]) +
      (1/r) n (B3 BesselJ[n, s2 r] + B4 BesselY[n, s2 r]) +
      (1/2) B2 s1 (BesselY[-1 + n, s1 r] - BesselY[1 + n, s1 r])), WP];

Y3[r_] := SetPrecision[(-(1/2) B3 s2 (BesselJ[-1 + n, s2 r] - BesselJ[1 + n, s2 r]) -
      (1/r) n (B1 BesselJ[n, s1 r] + B2 BesselY[n, s1 r]) -
      (1/2) B4 s2 (BesselY[-1 + n, s2 r] - BesselY[1 + n, s2 r])), WP];
```

```
τ = SetPrecision[Sqrt[(Θ/h) Sqrt[12 ρ (1 - μ^2)/EE]], WP];

s1 = SetPrecision[Θ Sqrt[ρ (1 - μ^2)/EE], WP];

s2 = SetPrecision[Θ Sqrt[2 ρ (1 + μ)/EE], WP];

Θ = 4.3554872473059969172974369`7.*^6
```

4.355487×10^6

```
Z4[r_] := A1 BesselJ[m, ψ r] + A2 BesselY[m, ψ r] + A3 BesselI[m, ψ r] + A4 BesselK[m, ψ r]

X4[r_] := SetPrecision[((1/2) B1 f1 (BesselJ[-1 + n, f1 r] - BesselJ[1 + n, f1 r]) +
      (1/r) n (B3 BesselJ[n, f2 r] + B4 BesselY[n, f2 r]) +
      (1/2) B2 f1 (BesselY[-1 + n, f1 r] - BesselY[1 + n, f1 r])), WP];

Y4[r_] := SetPrecision[(-(1/2) B3 f2 (BesselJ[-1 + n, f2 r] - BesselJ[1 + n, f2 r]) -
      (1/r) n (B1 BesselJ[n, f1 r] + B2 BesselY[n, f1 r]) -
      (1/2) B4 f2 (BesselY[-1 + n, f2 r] - BesselY[1 + n, f2 r])), WP];

ψ = SetPrecision[Sqrt[(Ω/h) Sqrt[12 ρ (1 - μ^2)/EE]], WP];

f1 = SetPrecision[Ω Sqrt[ρ (1 - μ^2)/EE], WP];

f2 = SetPrecision[Ω Sqrt[2 ρ (1 + μ)/EE], WP];

Ω = 5.2045155656928513917385405`7.*^6
```

5.204516×10^6

```
MaxX1 = FindMaxValue[{Abs[X1[r]], a ≤ r ≤ b}, {r, b}]
MX1 = %
```

2674.76

2674.76

```
MaxY1 = FindMaxValue[{Abs[Y1[r]], a ≤ r ≤ b}, {r, b}]
MY1 = %
```

2330.21

2330.21

```
MaxZ11 = FindMaxValue[{Abs[Z11[r]], a ≤ r ≤ b}, {r, b}]
MZ11 = %
```

274.345

274.345

```
MaxX2 = FindMaxValue[{Abs[X2[r]], a ≤ r ≤ b}, {r, b}]
MX2 = %
```

2986.58

2986.58

```
MaxY2 = FindMaxValue[{Abs[Y2[r]], a ≤ r ≤ b}, {r, b}]
MY2 = %
```

1663.18

1663.18

```
MaxZ2 = FindMaxValue[{Abs[Z2[r]], a ≤ r ≤ b}, {r, b}]
MZ2 = %
```

615.86

615.86

```
MaxX3 = FindMaxValue[{Abs[X3[r]], a ≤ r ≤ b}, {r, b}]
MX3 = %
```

3585.37

3585.37

```
MaxY3 = FindMaxValue[{Abs[Y3[r]], a ≤ r ≤ b}, {r, b}]
MY3 = %
```

3123.52

3123.52

```
MaxZ3 = FindMaxValue[{Abs[Z3[r]], a ≤ r ≤ b}, {r, b}]
MZ3 = %
```

2653.89

2653.89

```
MaxX4 = FindMaxValue[{Abs[X4[r]], a ≤ r ≤ b}, {r, b}]
MX4 = %
```

2909.32

2909.32

```
MaxY4 = FindMaxValue[{Abs[Y4[r]], a ≤ r ≤ b}, {r, b}]
MY4 = %
```

2365.64

2365.64

```
MaxZ4 = FindMaxValue[{Abs[Z4[r]], a ≤ r ≤ b}, {r, b}]
MZ4 = %
```

12 708.1

12 708.1

```
Plot[{U[r]/MU, X[r]/MX, X1[r]/MX1, X2[r]/MX2, X3[r]/MX3, X4[r]/MX4}, {r, 0.001, b},
 PlotRange → All, DisplayFunction → Identity, PlotPoints → 10 000,
 AxesStyle → Thick, LabelStyle → Directive[Bold, Black],
 DisplayFunction → $DisplayFunction, BaseStyle → {FontFamily → "Times", FontSize → 15},
 PlotStyle → {{Blue, Dashing[0.01`]}, {Red, Thickness[0.008`]}, {Black, Dashing[0.01`]},
   {Purple , Thickness[0.008`]}, {Pink, Thickness[0.008`]}, {Green, Thickness[0.01`]}},
 AxesLabel → {"        r   ", " U"}, PlotLegends → {U2,0, U2,1, U2,2, U2,3, U2,4, U2,5}]
```

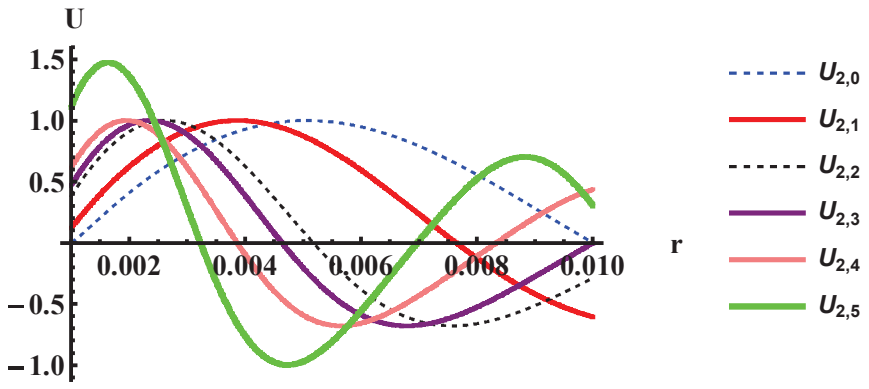

```
Plot[{V[r]/MV, Y[r]/MY, Y1[r]/MX1, Y2[r]/MX2, Y3[r]/MX3, Y4[r]/MX4}, {r, 0.001, b},
 PlotRange → All, DisplayFunction → Identity, PlotPoints → 10000, AxesStyle → Thick,
 LabelStyle → Directive[Bold, Black], DisplayFunction → $DisplayFunction,
 BaseStyle → {FontFamily → "Times", FontSize → 15}, PlotStyle →
  {{Blue, Thickness[0.008`]}, {Red, Thickness[0.008`]}, {Green, Thickness[0.008`]},
   {Brown , Dashing[0.01`]}, {Black, Dashing[0.01`]}, {Purple, Thickness[0.008`]}},
 AxesLabel → {"        r  ", " V"}, PlotLegends → {V2,0, V2,1, V2,2, V2,3, V2,4, V2,5}]
```

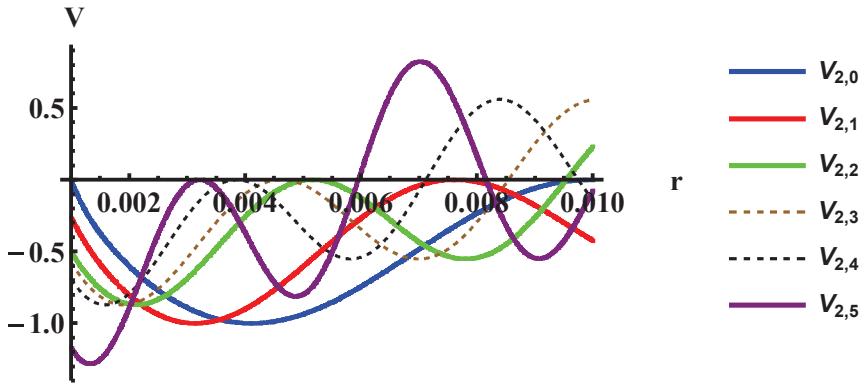

MAPLE CODE FOR ANNULAR DISC GYROSCOPE FREE AT THE EDGES

$\Phi\Phi = \Phi$ and $\psi\psi = \psi$, in the body of thesis. The constants C1, C2, C3 and C4 are arbitrary constants as defined in the relevant sections.

$$0 \tag{1}$$

$$\Phi\Phi := (C1 \cdot \mathrm{BesselJ}(n, k1(\omega l)\cdot r) + C2 \cdot \mathrm{BesselY}(n, k1(\omega l)\cdot r)) \cdot \cos(n\cdot\varphi)$$

$$(C1\ \mathrm{BesselJ}(n, k1(\omega l)\ r) + C2\ \mathrm{BesselY}(n, k1(\omega l)\ r))\ \cos(n\ \varphi) \tag{2}$$

$$\Psi\Psi := (C3 \cdot \mathrm{BesselJ}(n, k2(\omega l)\cdot r) + C4 \cdot \mathrm{BesselY}(n, k2(\omega l)\cdot r)) \cdot \sin(n\cdot\varphi)$$

$$(C3\ \mathrm{BesselJ}(n, k2(\omega l)\ r) + C4\ \mathrm{BesselY}(n, k2(\omega l)\ r))\ \sin(n\ \varphi) \tag{3}$$

$$uu := collect\left(\left(diff(\Phi\Phi, r) + \frac{1}{r}\cdot diff(\Psi\Psi, \varphi)\right), [\cos, C1, C2, C3, C4]\right)$$

$$\left(C1\left(-\mathrm{BesselJ}(n+1, k1(\omega l)\ r) + \frac{n\ \mathrm{BesselJ}(n, k1(\omega l)\ r)}{k1(\omega l)\ r}\right) k1(\omega l) + C2\left(-\mathrm{BesselY}(n\right.\right. \tag{4}$$

$$+1, k1(\omega l)\ r) + \frac{n\ \mathrm{BesselY}(n, k1(\omega l)\ r)}{k1(\omega l)\ r}\Bigg) k1(\omega l) + \frac{\mathrm{BesselJ}(n, k2(\omega l)\ r)\ n\ C3}{r}$$

$$\left.\left. + \frac{C4\ \mathrm{BesselY}(n, k2(\omega l)\ r)\ n}{r}\right)\cos(n\ \varphi)\right)$$

0

$$0 \tag{5}$$

$$vv := collect\left(\left(\frac{1}{r}\cdot diff(\Phi\Phi, \varphi) - diff(\Psi\Psi, r)\right), [\sin, C1, C2, C3, C4]\right)$$

$$\left(-\frac{\mathrm{BesselJ}(n, k1(\omega l)\ r)\ n\ C1}{r} - \frac{C2\ \mathrm{BesselY}(n, k1(\omega l)\ r)\ n}{r} - C3\left(-\mathrm{BesselJ}(n+1,\right.\right.$$

$$k2(\omega l)\ r) + \frac{n\ \mathrm{BesselJ}(n, k2(\omega l)\ r)}{k2(\omega l)\ r}\Bigg) k2(\omega l) - C4\left(-\mathrm{BesselY}(n+1, k2(\omega l)\ r)\right.$$

$$\left.\left. + \frac{n\ \mathrm{BesselY}(n, k2(\omega l)\ r)}{k2(\omega l)\ r}\right) k2(\omega l)\right)\sin(n\ \varphi)$$

$$\left(-\frac{\mathrm{BesselJ}(n, k1(\omega l)\ r)\ n\ C1}{r} - \frac{C2\ \mathrm{BesselY}(n, k1(\omega l)\ r)\ n}{r} - C3\left(-\mathrm{BesselJ}(n+1,\right.\right. \tag{7}$$

$$k2(\omega l)\ r) + \frac{n\ \mathrm{BesselJ}(n, k2(\omega l)\ r)}{k2(\omega l)\ r}\Bigg) k2(\omega l) - C4\left(-\mathrm{BesselY}(n+1, k2(\omega l)\ r)\right.$$

$$+\frac{n\,\mathrm{BesselY}(n,k2(\omega I)\,r)}{k2(\omega I)\,r}\Bigg)k2(\omega I)\Bigg)\sin(n\,\varphi)$$

Both uu and vv are respectively, given in the text as "u" and " v", respectively.

$$BC1 := collect\left(simplify\left(\frac{\left(diff(uu,r)+\frac{\mu}{r}\cdot(diff(vv,\varphi)+uu)\right)}{\cos(n\,\varphi)}\right),[C1,C2,C3,C4,\mathrm{BesselJ},\mathrm{BesselY},r],factor\right)$$

$$\left(\left(-k1(\omega I)^2-\frac{n\,(n-1)\,(\mu-1)}{r^2}\right)\mathrm{BesselJ}(n,k1(\omega I)\,r)-\frac{k1(\omega I)\,(\mu-1)\,\mathrm{BesselJ}(n+1,k1(\omega I)\,r)}{r}\right)C1+\left(\left(-k1(\omega I)^2-\frac{n\,(n-1)\,(\mu-1)}{r^2}\right)\mathrm{BesselY}(n,k1(\omega I)\,r)-\frac{k1(\omega I)\,(\mu-1)\,\mathrm{BesselY}(n+1,k1(\omega I)\,r)}{r}\right)C2+\left(-\frac{n\,(n-1)\,(\mu-1)\,\mathrm{BesselJ}(n,k2(\omega I)\,r)}{r^2}+\frac{k2(\omega I)\,n\,(\mu-1)\,\mathrm{BesselJ}(n+1,k2(\omega I)\,r)}{r}\right)C3+\left(-\frac{n\,(n-1)\,(\mu-1)\,\mathrm{BesselY}(n,k2(\omega I)\,r)}{r^2}+\frac{k2(\omega I)\,n\,(\mu-1)\,\mathrm{BesselY}(n+1,k2(\omega I)\,r)}{r}\right)C4 \tag{8}$$

$$BC2 := collect\left(simplify\left(\frac{\left(diff(vv,r)+\frac{1}{r}\cdot(diff(uu,\varphi)-vv)\right)}{\sin(n\,\varphi)}\right),[C1,C2,C3,C4,\mathrm{BesselJ},\mathrm{BesselY},r],factor\right)$$

$$\left(-\frac{2\,n\,(n-1)\,\mathrm{BesselJ}(n,k1(\omega I)\,r)}{r^2}+\frac{2\,\mathrm{BesselJ}(n+1,k1(\omega I)\,r)\,k1(\omega I)\,n}{r}\right)C1+\left(-\frac{2\,n\,(n-1)\,\mathrm{BesselY}(n,k1(\omega I)\,r)}{r^2}+\frac{2\,\mathrm{BesselY}(n+1,k1(\omega I)\,r)\,k1(\omega I)\,n}{r}\right)C2+\left(\left(k2(\omega I)^2-\frac{2\,n\,(n-1)}{r^2}\right)\mathrm{BesselJ}(n,k2(\omega I)\,r)\right. \tag{9}$$

$$-\frac{2\,\mathrm{BesselJ}(n+1,k2(\omega l)\,r)\,k2(\omega l)}{r}\Bigg)C3+\Bigg(\Bigg(k2(\omega l)^2-\frac{2\,n\,(n-1)}{r^2}\Bigg)\mathrm{BesselY}(n,$$

$$k2(\omega l)\,r)-\frac{2\,\mathrm{BesselY}(n+1,k2(\omega l)\,r)\,k2(\omega l)}{r}\Bigg)C4$$

$$BC3:=\Bigg(\Bigg(-k1(\omega l)^2-\frac{n\,(-1+n)\,(\mu-1)}{rr^2}\Bigg)\mathrm{BesselJ}(n,k1(\omega l)\,rr)$$

$$-\frac{k1(\omega l)\,(\mu-1)\,\mathrm{BesselJ}(n+1,k1(\omega l)\,rr)}{rr}\Bigg)C1+\Bigg(\Bigg(-k1(\omega l)^2$$

$$-\frac{n\,(-1+n)\,(\mu-1)}{rr^2}\Bigg)\mathrm{BesselY}(n,k1(\omega l)\,rr)$$

$$-\frac{k1(\omega l)\,(\mu-1)\,\mathrm{BesselY}(n+1,k1(\omega l)\,rr)}{rr}\Bigg)C2+\Bigg($$

$$-\frac{n\,(-1+n)\,(\mu-1)\,\mathrm{BesselJ}(n,k2(\omega l)\,rr)}{rr^2}+\frac{k2(\omega l)\,n\,(\mu-1)\,\mathrm{BesselJ}(n+1,k2(\omega l)\,rr)}{rr}\Bigg)$$

$$C3+\Bigg(-\frac{n\,(-1+n)\,(\mu-1)\,\mathrm{BesselY}(n,k2(\omega l)\,rr)}{rr^2}$$

$$+\frac{k2(\omega l)\,n\,(\mu-1)\,\mathrm{BesselY}(n+1,k2(\omega l)\,rr)}{rr}\Bigg)C4$$

$$\Bigg(\Bigg(-k1(\omega l)^2-\frac{n\,(n-1)\,(\mu-1)}{rr^2}\Bigg)\mathrm{BesselJ}(n,k1(\omega l)\,rr) \tag{10}$$

$$-\frac{k1(\omega l)\,(\mu-1)\,\mathrm{BesselJ}(n+1,k1(\omega l)\,rr)}{rr}\Bigg)C1+\Bigg(\Bigg(-k1(\omega l)^2$$

$$-\frac{n\,(n-1)\,(\mu-1)}{rr^2}\Bigg)\mathrm{BesselY}(n,k1(\omega l)\,rr)$$

$$-\frac{k1(\omega l)\,(\mu-1)\,\mathrm{BesselY}(n+1,k1(\omega l)\,rr)}{rr}\Bigg)C2+\Bigg($$

$$-\frac{n\,(n-1)\,(\mu-1)\,\mathrm{BesselJ}(n,k2(\omega l)\,rr)}{rr^2}$$

$$+\frac{k2(\omega l)\,n\,(\mu-1)\,\mathrm{BesselJ}(n+1,k2(\omega l)\,rr)}{rr}\Bigg)C3+\Bigg($$

$$-\frac{n\,(n-1)\,(\mu-1)\,\mathrm{BesselY}(n,k2(\omega l)\,rr)}{rr^2}$$

$$+\frac{k2(\omega l)\,n\,(\mu-1)\,\mathrm{BesselY}(n+1,k2(\omega l)\,rr)}{rr}\Bigg)C4$$

$$BC4:=\Bigg(-\frac{2\,n\,(-1+n)\,\mathrm{BesselJ}(n,k1(\omega l)\,rr)}{rr^2}+\frac{2\,k1(\omega l)\,\mathrm{BesselJ}(n+1,k1(\omega l)\,rr)\,n}{rr}\Bigg)C1+\Bigg($$

$$-\frac{2\,n\,(-1+n)\,\mathrm{BesselY}(n, k1(\omega l)\,rr)}{rr^2}+\frac{2\,k1(\omega l)\,\mathrm{BesselY}(n+1, k1(\omega l)\,rr)\,n}{rr}\Bigg)\,C2$$
$$+\left(\left(k2(\omega l)^2-\frac{2\,n\,(-1+n)}{rr^2}\right)\mathrm{BesselJ}(n, k2(\omega l)\,rr)\right.$$
$$\left.-\frac{2\,\mathrm{BesselJ}(n+1, k2(\omega l)\,rr)\,k2(\omega l)}{rr}\right)C3+\left(\left(k2(\omega l)^2-\frac{2\,n\,(-1+n)}{rr^2}\right)\mathrm{BesselY}(n,$$
$$k2(\omega l)\,rr)-\frac{2\,\mathrm{BesselY}(n+1, k2(\omega l)\,rr)\,k2(\omega l)}{rr}\Bigg)\,C4$$
$$\left(-\frac{2\,n\,(n-1)\,\mathrm{BesselJ}(n, k1(\omega l)\,rr)}{rr^2}+\frac{2\,k1(\omega l)\,\mathrm{BesselJ}(n+1, k1(\omega l)\,rr)\,n}{rr}\right)C1+\Bigg(\tag{11}$$
$$-\frac{2\,n\,(n-1)\,\mathrm{BesselY}(n, k1(\omega l)\,rr)}{rr^2}+\frac{2\,k1(\omega l)\,\mathrm{BesselY}(n+1, k1(\omega l)\,rr)\,n}{rr}\Bigg)\,C2$$
$$+\left(\left(k2(\omega l)^2-\frac{2\,n\,(n-1)}{rr^2}\right)\mathrm{BesselJ}(n, k2(\omega l)\,rr)\right.$$
$$\left.-\frac{2\,\mathrm{BesselJ}(n+1, k2(\omega l)\,rr)\,k2(\omega l)}{rr}\right)C3+\left(\left(k2(\omega l)^2-\frac{2\,n\,(n-1)}{rr^2}\right)\mathrm{BesselY}(n,$$
$$k2(\omega l)\,rr)-\frac{2\,\mathrm{BesselY}(n+1, k2(\omega l)\,rr)\,k2(\omega l)}{rr}\Bigg)\,C4$$

BC1 is the first boundary condition at r=a, BC2 is the second boundary condition at r=a, BC3 is the frist boundary condition at r=b and BC4 is the second boundary condition at r=b for in-plane vibration of the disc.
ww in this Maple code corresponds to "w" in the text of the thesis.

$$ww := (A1\cdot\mathrm{BesselJ}(m, \beta(\omega o)\cdot r)+A2\cdot\mathrm{BesselY}(m, \beta(\omega o)\cdot r)+A3\cdot\mathrm{BesselI}(m, \beta(\omega o)\cdot r)+A4$$
$$\cdot\mathrm{BesselK}(m, \beta(\omega o)\cdot r))\cdot\cos(m\cdot\varphi)$$
$$(A1\,\mathrm{BesselJ}(m, \beta(\omega o)\,r)+A2\,\mathrm{BesselY}(m, \beta(\omega o)\,r)+A3\,\mathrm{BesselI}(m, \beta(\omega o)\,r) \tag{12}$$
$$+A4\,\mathrm{BesselK}(m, \beta(\omega o)\,r))\,\cos(m\,\varphi)$$
$$BCP1 := collect\left(\frac{1}{\cos(m\cdot\varphi)}\left(diff(ww, r, r, r)+\frac{1}{r}\cdot diff(ww, r, r)-\frac{1}{r^2}\cdot diff(ww, r)+\frac{(2-\mu)}{r^2}\right.\right.$$
$$\left.\left.\cdot diff(ww, r, \varphi, \varphi)-\frac{(3-\mu)}{r^3}\cdot diff(ww, \varphi, \varphi)\right), [A1, A2, A3, A4, \mathrm{BesselJ}, \mathrm{BesselY}, \mathrm{BesselI},$$
$$\mathrm{BesselK}, r], factor\right)$$

$$\left(\left(-\frac{\beta(\omega o)^2\,m}{r}+\frac{m^2\,(\mu-1)\,(m-1)}{r^3}\right)\mathrm{BesselJ}(m, \beta(\omega o)\,r)+\left(\beta(\omega o)^3\right.\right. \tag{13}$$
$$\left.\left.-\frac{\beta(\omega o)\,m^2\,(\mu-1)}{r^2}\right)\mathrm{BesselJ}(m+1, \beta(\omega o)\,r)\right)A1+\left(\left(-\frac{\beta(\omega o)^2\,m}{r}\right.\right.$$

$$+\frac{m^2(\mu-1)(m-1)}{r^3}\Bigg)\,\mathrm{BesselY}(m,\beta(\omega o)\,r)+\Bigg(\beta(\omega o)^3$$
$$-\frac{\beta(\omega o)\,m^2(\mu-1)}{r^2}\Bigg)\,\mathrm{BesselY}(m+1,\beta(\omega o)\,r)\Bigg)\,A2+\Bigg(\Bigg(\frac{\beta(\omega o)^2 m}{r}$$
$$+\frac{m^2(\mu-1)(m-1)}{r^3}\Bigg)\,\mathrm{BesselI}(m,\beta(\omega o)\,r)+\Bigg(\beta(\omega o)^3$$
$$+\frac{\beta(\omega o)\,m^2(\mu-1)}{r^2}\Bigg)\,\mathrm{BesselI}(m+1,\beta(\omega o)\,r)\Bigg)\,A3+\Bigg(\Bigg(\frac{\beta(\omega o)^2 m}{r}$$
$$+\frac{m^2(\mu-1)(m-1)}{r^3}\Bigg)\,\mathrm{BesselK}(m,\beta(\omega o)\,r)+\Bigg(-\beta(\omega o)^3$$
$$-\frac{\beta(\omega o)\,m^2(\mu-1)}{r^2}\Bigg)\,\mathrm{BesselK}(m+1,\beta(\omega o)\,r)\Bigg)\,A4$$

$$BCP2 := collect\left(\frac{\left(diff(ww,r,r)+\frac{\mu}{r}\cdot\left(diff(ww,r)+\frac{1}{r}\cdot diff(ww,\varphi,\varphi)\right)\right)}{\cos(m\cdot\varphi)},\,[A1,A2,A3,A4,\right.$$
$$\left.\mathrm{BesselJ},\mathrm{BesselY},\mathrm{BesselI},\mathrm{BesselK},r],factor\right)$$

$$\Bigg(\Bigg(-\beta(\omega o)^2-\frac{m(m-1)(\mu-1)}{r^2}\Bigg)\,\mathrm{BesselJ}(m,\beta(\omega o)\,r) \tag{14}$$
$$-\frac{\beta(\omega o)(\mu-1)\,\mathrm{BesselJ}(m+1,\beta(\omega o)\,r)}{r}\Bigg)\,A1+\Bigg(\Bigg(-\beta(\omega o)^2$$
$$-\frac{m(m-1)(\mu-1)}{r^2}\Bigg)\,\mathrm{BesselY}(m,\beta(\omega o)\,r)$$
$$-\frac{\beta(\omega o)(\mu-1)\,\mathrm{BesselY}(m+1,\beta(\omega o)\,r)}{r}\Bigg)\,A2+\Bigg(\Bigg(\beta(\omega o)^2$$
$$-\frac{m(m-1)(\mu-1)}{r^2}\Bigg)\,\mathrm{BesselI}(m,\beta(\omega o)\,r)$$
$$+\frac{\beta(\omega o)(\mu-1)\,\mathrm{BesselI}(m+1,\beta(\omega o)\,r)}{r}\Bigg)\,A3+\Bigg(\Bigg(\beta(\omega o)^2$$
$$-\frac{m(m-1)(\mu-1)}{r^2}\Bigg)\,\mathrm{BesselK}(m,\beta(\omega o)\,r)$$
$$-\frac{\beta(\omega o)(\mu-1)\,\mathrm{BesselK}(m+1,\beta(\omega o)\,r)}{r}\Bigg)\,A4$$

0

$$0 \tag{15}$$

0

$$0 \tag{16}$$

0

$$0 \tag{17}$$

$$BCP3 := \left(\left(-\frac{\beta(\omega o)^2 m}{rr} + \frac{m^2(\mu-1)(-1+m)}{rr^3}\right)\text{BesselJ}(m, \beta(\omega o)\, rr) + \left(\beta(\omega o)^3 - \frac{\beta(\omega o)\, m^2(\mu-1)}{rr^2}\right)\text{BesselJ}(m+1, \beta(\omega o)\, rr)\right) A1 + \left(\left(-\frac{\beta(\omega o)^2 m}{rr} + \frac{m^2(\mu-1)(-1+m)}{rr^3}\right)\text{BesselY}(m, \beta(\omega o)\, rr) + \left(\beta(\omega o)^3 - \frac{\beta(\omega o)\, m^2(\mu-1)}{rr^2}\right)\text{BesselY}(m+1, \beta(\omega o)\, rr)\right) A2 + \left(\left(\frac{\beta(\omega o)^2 m}{rr} + \frac{m^2(\mu-1)(-1+m)}{rr^3}\right)\text{BesselI}(m, \beta(\omega o)\, rr) + \left(\beta(\omega o)^3 + \frac{\beta(\omega o)\, m^2(\mu-1)}{rr^2}\right)\text{BesselI}(m+1, \beta(\omega o)\, rr)\right) A3 + \left(\left(\frac{\beta(\omega o)^2 m}{rr} + \frac{m^2(\mu-1)(-1+m)}{rr^3}\right)\text{BesselK}(m, \beta(\omega o)\, rr) + \left(-\beta(\omega o)^3 - \frac{\beta(\omega o)\, m^2(\mu-1)}{rr^2}\right)\text{BesselK}(m+1, \beta(\omega o)\, rr)\right) A4$$

$$\left(\left(-\frac{\beta(\omega o)^2 m}{rr} + \frac{m^2(\mu-1)(m-1)}{rr^3}\right)\text{BesselJ}(m, \beta(\omega o)\, rr) + \left(\beta(\omega o)^3 - \frac{\beta(\omega o)\, m^2(\mu-1)}{rr^2}\right)\text{BesselJ}(m+1, \beta(\omega o)\, rr)\right) A1 + \left(\left(-\frac{\beta(\omega o)^2 m}{rr} + \frac{m^2(\mu-1)(m-1)}{rr^3}\right)\text{BesselY}(m, \beta(\omega o)\, rr) + \left(\beta(\omega o)^3 - \frac{\beta(\omega o)\, m^2(\mu-1)}{rr^2}\right)\text{BesselY}(m+1, \beta(\omega o)\, rr)\right) A2 + \left(\left(\frac{\beta(\omega o)^2 m}{rr} + \frac{m^2(\mu-1)(m-1)}{rr^3}\right)\text{BesselI}(m, \beta(\omega o)\, rr) + \left(\beta(\omega o)^3 + \frac{\beta(\omega o)\, m^2(\mu-1)}{rr^2}\right)\text{BesselI}(m+1, \beta(\omega o)\, rr)\right) A3 + \left(\left(\frac{\beta(\omega o)^2 m}{rr} + \frac{m^2(\mu-1)(m-1)}{rr^3}\right)\text{BesselK}(m, \beta(\omega o)\, rr) + \left(-\beta(\omega o)^3 - \frac{\beta(\omega o)\, m^2(\mu-1)}{rr^2}\right)\text{BesselK}(m+1, \beta(\omega o)\, rr)\right) A4 \tag{18}$$

$$BCP4 := \left(\left(-\beta(\omega o)^2 - \frac{m(-1+m)(\mu-1)}{rr^2}\right)\text{BesselJ}(m, \beta(\omega o)\, rr) - \frac{\beta(\omega o)(\mu-1)\,\text{BesselJ}(m+1, \beta(\omega o)\, rr)}{rr}\right) A1 + \left(\left(-\beta(\omega o)^2 - \frac{m(-1+m)(\mu-1)}{rr^2}\right)\text{BesselY}(m, \beta(\omega o)\, rr) - \frac{\beta(\omega o)(\mu-1)\,\text{BesselY}(m+1, \beta(\omega o)\, rr)}{rr}\right) A2 + \left(\left(\beta(\omega o)^2 - \frac{m(-1+m)(\mu-1)}{rr^2}\right)\text{BesselI}(m, \beta(\omega o)\, rr) + \frac{\beta(\omega o)(\mu-1)\,\text{BesselI}(m+1, \beta(\omega o)\, rr)}{rr}\right) A3 + \left(\left(\beta(\omega o)^2 - \frac{m(-1+m)(\mu-1)}{rr^2}\right)\text{BesselK}(m, \beta(\omega o)\, rr) - \frac{\beta(\omega o)(\mu-1)\,\text{BesselK}(m+1, \beta(\omega o)\, rr)}{rr}\right) A4$$

$$\left(\left(-\beta(\omega o)^2 - \frac{m(m-1)(\mu-1)}{rr^2}\right)\text{BesselJ}(m, \beta(\omega o)\, rr) - \frac{\beta(\omega o)(\mu-1)\,\text{BesselJ}(m+1, \beta(\omega o)\, rr)}{rr}\right) A1 + \left(\left(-\beta(\omega o)^2 - \frac{m(m-1)(\mu-1)}{rr^2}\right)\text{BesselY}(m, \beta(\omega o)\, rr) - \frac{\beta(\omega o)(\mu-1)\,\text{BesselY}(m+1, \beta(\omega o)\, rr)}{rr}\right) A2 + \left(\left(\beta(\omega o)^2 - \frac{m(m-1)(\mu-1)}{rr^2}\right)\text{BesselI}(m, \beta(\omega o)\, rr) + \frac{\beta(\omega o)(\mu-1)\,\text{BesselI}(m+1, \beta(\omega o)\, rr)}{rr}\right) A3 + \left(\left(\beta(\omega o)^2 - \frac{m(m-1)(\mu-1)}{rr^2}\right)\text{BesselK}(m, \beta(\omega o)\, rr) - \frac{\beta(\omega o)(\mu-1)\,\text{BesselK}(m+1, \beta(\omega o)\, rr)}{rr}\right) A4 \quad \textbf{(19)}$$

BCP1 is the first boundary condition at r=a, BCP2 is the second boundary condition at r=a, BCP3 is the frist boundary condition at r=b and BCP4 is the second boundary condition at r=b for out-of-plane vibration of the disc.

$$c11 := coeff(BC1, C1)$$

$$\left(-k1(\omega l)^2-\frac{n\,(n-1)\,(\mu-1)}{r^2}\right)\mathrm{BesselJ}(n,k1(\omega l)\,r)-\frac{k1(\omega l)\,(\mu-1)\,\mathrm{BesselJ}(n+1,k1(\omega l)\,r)}{r} \tag{20}$$

$c12 := coeff(BC1, C2)$

$$\left(-k1(\omega l)^2-\frac{n\,(n-1)\,(\mu-1)}{r^2}\right)\mathrm{BesselY}(n,k1(\omega l)\,r)-\frac{k1(\omega l)\,(\mu-1)\,\mathrm{BesselY}(n+1,k1(\omega l)\,r)}{r} \tag{21}$$

$c13 := coeff(BC1, C3)$

$$-\frac{n\,(n-1)\,(\mu-1)\,\mathrm{BesselJ}(n,k2(\omega l)\,r)}{r^2}+\frac{k2(\omega l)\,n\,(\mu-1)\,\mathrm{BesselJ}(n+1,k2(\omega l)\,r)}{r} \tag{22}$$

$c14 := coeff(BC1, C4)$

$$-\frac{n\,(n-1)\,(\mu-1)\,\mathrm{BesselY}(n,k2(\omega l)\,r)}{r^2}+\frac{k2(\omega l)\,n\,(\mu-1)\,\mathrm{BesselY}(n+1,k2(\omega l)\,r)}{r} \tag{23}$$

$c21 := coeff(BC2, C1)$

$$-\frac{2\,n\,(n-1)\,\mathrm{BesselJ}(n,k1(\omega l)\,r)}{r^2}+\frac{2\,\mathrm{BesselJ}(n+1,k1(\omega l)\,r)\,k1(\omega l)\,n}{r} \tag{24}$$

$c22 := coeff(BC2, C2)$

$$-\frac{2\,n\,(n-1)\,\mathrm{BesselY}(n,k1(\omega l)\,r)}{r^2}+\frac{2\,\mathrm{BesselY}(n+1,k1(\omega l)\,r)\,k1(\omega l)\,n}{r} \tag{25}$$

$c23 := coeff(BC2, C3)$

$$\left(k2(\omega l)^2-\frac{2\,n\,(n-1)}{r^2}\right)\mathrm{BesselJ}(n,k2(\omega l)\,r)-\frac{2\,\mathrm{BesselJ}(n+1,k2(\omega l)\,r)\,k2(\omega l)}{r} \tag{26}$$

$c24 := coeff(BC2, C4)$

$$\left(k2(\omega l)^2-\frac{2\,n\,(n-1)}{r^2}\right)\mathrm{BesselY}(n,k2(\omega l)\,r)-\frac{2\,\mathrm{BesselY}(n+1,k2(\omega l)\,r)\,k2(\omega l)}{r} \tag{27}$$

$c31 := coeff(BC3, C1)$

$$\left(-k1(\omega l)^2-\frac{n\,(n-1)\,(\mu-1)}{rr^2}\right)\mathrm{BesselJ}(n,k1(\omega l)\,rr)-\frac{k1(\omega l)\,(\mu-1)\,\mathrm{BesselJ}(n+1,k1(\omega l)\,rr)}{rr} \tag{28}$$

$c32 := coeff(BC3, C2)$

$$\left(-k1(\omega l)^2-\frac{n\,(n-1)\,(\mu-1)}{rr^2}\right)\mathrm{BesselY}(n,k1(\omega l)\,rr)-\frac{k1(\omega l)\,(\mu-1)\,\mathrm{BesselY}(n+1,k1(\omega l)\,rr)}{rr}$$

$$\left(-k1(\omega)^2-\frac{n\,(n-1)\,(\mu-1)}{rr^2}\right)\mathrm{BesselY}(n,k1(\omega)\,rr)-\frac{k1(\omega)\,(\mu-1)\,\mathrm{BesselY}(n+1,k1(\omega)\,rr)}{rr} \tag{30}$$

$c33 := coeff(BC3, C3)$

$$-\frac{n\,(n-1)\,(\mu-1)\,\mathrm{BesselJ}(n,k2(\omega I)\,rr)}{rr^2}+\frac{k2(\omega I)\,n\,(\mu-1)\,\mathrm{BesselJ}(n+1,k2(\omega I)\,rr)}{rr} \tag{31}$$

$c34 := coeff(BC3, C4)$

$$-\frac{n\,(n-1)\,(\mu-1)\,\mathrm{BesselY}(n,k2(\omega I)\,rr)}{rr^2}+\frac{k2(\omega I)\,n\,(\mu-1)\,\mathrm{BesselY}(n+1,k2(\omega I)\,rr)}{rr} \tag{32}$$

$c41 := coeff(BC4, C1)$

$$-\frac{2\,n\,(n-1)\,\mathrm{BesselJ}(n,k1(\omega I)\,rr)}{rr^2}+\frac{2\,k1(\omega I)\,\mathrm{BesselJ}(n+1,k1(\omega I)\,rr)\,n}{rr} \tag{33}$$

$c42 := coeff(BC4, C2)$

$$-\frac{2\,n\,(n-1)\,\mathrm{BesselY}(n,k1(\omega I)\,rr)}{rr^2}+\frac{2\,k1(\omega I)\,\mathrm{BesselY}(n+1,k1(\omega I)\,rr)\,n}{rr} \tag{34}$$

$c43 := coeff(BC4, C3)$

$$\left(k2(\omega I)^2-\frac{2\,n\,(n-1)}{rr^2}\right)\mathrm{BesselJ}(n,k2(\omega I)\,rr)-\frac{2\,\mathrm{BesselJ}(n+1,k2(\omega I)\,rr)\,k2(\omega I)}{rr} \tag{35}$$

$c44 := coeff(BC4, C4)$

$$\left(k2(\omega I)^2-\frac{2\,n\,(n-1)}{rr^2}\right)\mathrm{BesselY}(n,k2(\omega I)\,rr)-\frac{2\,\mathrm{BesselY}(n+1,k2(\omega I)\,rr)\,k2(\omega I)}{rr} \tag{36}$$

$d11 := coeff(BCP1, A1)$

$$\left(-\frac{\beta(\omega o)^2\,m}{r}+\frac{m^2\,(\mu-1)\,(m-1)}{r^3}\right)\mathrm{BesselJ}(m,\beta(\omega o)\,r)+\left(\beta(\omega o)^3-\frac{\beta(\omega o)\,m^2\,(\mu-1)}{r^2}\right)\mathrm{BesselJ}(m+1,\beta(\omega o)\,r) \tag{37}$$

$d12 := coeff(BCP1, A2)$

$$\left(-\frac{\beta(\omega o)^2\,m}{r}+\frac{m^2\,(\mu-1)\,(m-1)}{r^3}\right)\mathrm{BesselY}(m,\beta(\omega o)\,r)+\left(\beta(\omega o)^3-\frac{\beta(\omega o)\,m^2\,(\mu-1)}{r^2}\right)\mathrm{BesselY}(m+1,\beta(\omega o)\,r) \tag{38}$$

$d13 := coeff(BCP1, A3)$

$$\left(\frac{\beta(\omega o)^2\,m}{r}+\frac{m^2\,(\mu-1)\,(m-1)}{r^3}\right)\mathrm{BesselI}(m,\beta(\omega o)\,r)+\left(\beta(\omega o)^3\right. \tag{39}$$

$$+\frac{\beta(\omega o)\,m^2\,(\mu-1)}{r^2}\Bigg)\,\mathrm{BesselI}(m+1,\beta(\omega o)\,r)$$

$d14 := coeff(BCP1, A4)$

$$\left(\frac{\beta(\omega o)^2\,m}{r}+\frac{m^2\,(\mu-1)\,(m-1)}{r^3}\right)\mathrm{BesselK}(m,\beta(\omega o)\,r)+\left(-\beta(\omega o)^3\right. \tag{40}$$
$$\left.-\frac{\beta(\omega o)\,m^2\,(\mu-1)}{r^2}\right)\mathrm{BesselK}(m+1,\beta(\omega o)\,r)$$

$d21 := coeff(BCP2, A1)$

$$\left(-\beta(\omega o)^2-\frac{m\,(m-1)\,(\mu-1)}{r^2}\right)\mathrm{BesselJ}(m,\beta(\omega o)\,r) \tag{41}$$
$$-\frac{\beta(\omega o)\,(\mu-1)\,\mathrm{BesselJ}(m+1,\beta(\omega o)\,r)}{r}$$

$d22 := coeff(BCP2, A2)$

$$\left(-\beta(\omega o)^2-\frac{m\,(m-1)\,(\mu-1)}{r^2}\right)\mathrm{BesselY}(m,\beta(\omega o)\,r) \tag{42}$$
$$-\frac{\beta(\omega o)\,(\mu-1)\,\mathrm{BesselY}(m+1,\beta(\omega o)\,r)}{r}$$

$d23 := coeff(BCP2, A3)$

$$\left(\beta(\omega o)^2-\frac{m\,(m-1)\,(\mu-1)}{r^2}\right)\mathrm{BesselI}(m,\beta(\omega o)\,r) \tag{43}$$
$$+\frac{\beta(\omega o)\,(\mu-1)\,\mathrm{BesselI}(m+1,\beta(\omega o)\,r)}{r}$$

$d24 := coeff(BCP2, A4)$

$$\left(\beta(\omega o)^2-\frac{m\,(m-1)\,(\mu-1)}{r^2}\right)\mathrm{BesselK}(m,\beta(\omega o)\,r) \tag{44}$$
$$-\frac{\beta(\omega o)\,(\mu-1)\,\mathrm{BesselK}(m+1,\beta(\omega o)\,r)}{r}$$

$d31 := coeff(BCP3, A1)$

$$\left(-\frac{\beta(\omega o)^2\,m}{rr}+\frac{m^2\,(\mu-1)\,(m-1)}{rr^3}\right)\mathrm{BesselJ}(m,\beta(\omega o)\,rr)+\left(\beta(\omega o)^3\right. \tag{45}$$
$$\left.-\frac{\beta(\omega o)\,m^2\,(\mu-1)}{rr^2}\right)\mathrm{BesselJ}(m+1,\beta(\omega o)\,rr)$$

$d32 := coeff(BCP3, A2)$

$$\left(-\frac{\beta(\omega o)^2\,m}{rr}+\frac{m^2\,(\mu-1)\,(m-1)}{rr^3}\right)\mathrm{BesselY}(m,\beta(\omega o)\,rr)+\left(\beta(\omega o)^3\right. \tag{46}$$
$$\left.-\frac{\beta(\omega o)\,m^2\,(\mu-1)}{rr^2}\right)\mathrm{BesselY}(m+1,\beta(\omega o)\,rr)$$

$d33 := coeff(BCP3, A3)$

$$\left(\frac{\beta(\omega o)^2 m}{rr}+\frac{m^2(\mu-1)(m-1)}{rr^3}\right)\mathrm{BesselI}(m,\beta(\omega o)\,rr)+\left(\beta(\omega o)^3+\frac{\beta(\omega o)\,m^2(\mu-1)}{rr^2}\right)\mathrm{BesselI}(m+1,\beta(\omega o)\,rr) \tag{47}$$

$d34 := coeff(BCP3, A4)$

$$\left(\frac{\beta(\omega o)^2 m}{rr}+\frac{m^2(\mu-1)(m-1)}{rr^3}\right)\mathrm{BesselK}(m,\beta(\omega o)\,rr)+\left(-\beta(\omega o)^3-\frac{\beta(\omega o)\,m^2(\mu-1)}{rr^2}\right)\mathrm{BesselK}(m+1,\beta(\omega o)\,rr) \tag{48}$$

$d41 := coeff(BCP4, A1)$

$$\left(-\beta(\omega o)^2-\frac{m(m-1)(\mu-1)}{rr^2}\right)\mathrm{BesselJ}(m,\beta(\omega o)\,rr)-\frac{\beta(\omega o)(\mu-1)\,\mathrm{BesselJ}(m+1,\beta(\omega o)\,rr)}{rr}$$

$$\left(-\beta(\omega o)^2-\frac{m(m-1)(\mu-1)}{rr^2}\right)\mathrm{BesselJ}(m,\beta(\omega o)\,rr)-\frac{\beta(\omega o)(\mu-1)\,\mathrm{BesselJ}(m+1,\beta(\omega o)\,rr)}{rr} \tag{50}$$

$d42 := coeff(BCP4, A2)$

$$\left(-\beta(\omega o)^2-\frac{m(m-1)(\mu-1)}{rr^2}\right)\mathrm{BesselY}(m,\beta(\omega o)\,rr)-\frac{\beta(\omega o)(\mu-1)\,\mathrm{BesselY}(m+1,\beta(\omega o)\,rr)}{rr} \tag{51}$$

$d43 := coeff(BCP4, A3)$

$$\left(\beta(\omega o)^2-\frac{m(m-1)(\mu-1)}{rr^2}\right)\mathrm{BesselI}(m,\beta(\omega o)\,rr)+\frac{\beta(\omega o)(\mu-1)\,\mathrm{BesselI}(m+1,\beta(\omega o)\,rr)}{rr} \tag{52}$$

$d44 := coeff(BCP4, A4)$

$$\left(\beta(\omega o)^2-\frac{m(m-1)(\mu-1)}{rr^2}\right)\mathrm{BesselK}(m,\beta(\omega o)\,rr)-\frac{\beta(\omega o)(\mu-1)\,\mathrm{BesselK}(m+1,\beta(\omega o)\,rr)}{rr} \tag{53}$$

$with(LinearAlgebra):$

$M := Matrix([[c11, c12, c13, c14], [c21, c22, c23, c24], [c31, c32, c33, c34], [c41, c42, c43, c44]])$

$$\left[\left[\left(-k1(\omega I)^2-\frac{n(n-1)(\mu-1)}{r^2}\right)\mathrm{BesselJ}(n,k1(\omega I)\,r)\right.\right. \tag{54}$$

$$
-\frac{k1(\omega I)\ (\mu-1)\ \mathrm{BesselJ}(n+1,k1(\omega I)\ r)}{r},\left(-k1(\omega I)^2\right.
$$

$$
\left.-\frac{n\ (n-1)\ (\mu-1)}{r^2}\right)\mathrm{BesselY}(n,k1(\omega I)\ r)
$$

$$
-\frac{k1(\omega I)\ (\mu-1)\ \mathrm{BesselY}(n+1,k1(\omega I)\ r)}{r},
$$

$$
-\frac{n\ (n-1)\ (\mu-1)\ \mathrm{BesselJ}(n,k2(\omega I)\ r)}{r^2}
$$

$$
+\frac{k2(\omega I)\ n\ (\mu-1)\ \mathrm{BesselJ}(n+1,k2(\omega I)\ r)}{r},
$$

$$
-\frac{n\ (n-1)\ (\mu-1)\ \mathrm{BesselY}(n,k2(\omega I)\ r)}{r^2}
$$

$$
+\frac{k2(\omega I)\ n\ (\mu-1)\ \mathrm{BesselY}(n+1,k2(\omega I)\ r)}{r}\Bigg],
$$

$$
\Bigg[-\frac{2\ n\ (n-1)\ \mathrm{BesselJ}(n,k1(\omega I)\ r)}{r^2}+\frac{2\ \mathrm{BesselJ}(n+1,k1(\omega I)\ r)\ k1(\omega I)\ n}{r},
$$

$$
-\frac{2\ n\ (n-1)\ \mathrm{BesselY}(n,k1(\omega I)\ r)}{r^2}+\frac{2\ k1(\omega I)\ \mathrm{BesselY}(n+1,k1(\omega I)\ r)\ n}{r},\left(k2(\omega I)^2\right.
$$

$$
\left.-\frac{2\ n\ (n-1)}{r^2}\right)\mathrm{BesselJ}(n,k2(\omega I)\ r)-\frac{2\ \mathrm{BesselJ}(n+1,k2(\omega I)\ r)\ k2(\omega I)}{r},\left(k2(\omega I)^2\right.
$$

$$
\left.-\frac{2\ n\ (n-1)}{r^2}\right)\mathrm{BesselY}(n,k2(\omega I)\ r)-\frac{2\ \mathrm{BesselY}(n+1,k2(\omega I)\ r)\ k2(\omega I)}{r}\Bigg],
$$

$$
\Bigg[\left(-k1(\omega I)^2-\frac{n\ (n-1)\ (\mu-1)}{rr^2}\right)\mathrm{BesselJ}(n,k1(\omega I)\ rr)
$$

$$
-\frac{k1(\omega I)\ (\mu-1)\ \mathrm{BesselJ}(n+1,k1(\omega I)\ rr)}{rr},\left(-k1(\omega I)^2\right.
$$

$$
\left.-\frac{n\ (n-1)\ (\mu-1)}{rr^2}\right)\mathrm{BesselY}(n,k1(\omega I)\ rr)
$$

$$
-\frac{k1(\omega I)\ (\mu-1)\ \mathrm{BesselY}(n+1,k1(\omega I)\ rr)}{rr},
$$

$$
-\frac{n\ (n-1)\ (\mu-1)\ \mathrm{BesselJ}(n,k2(\omega I)\ rr)}{rr^2}
$$

$$
+\frac{k2(\omega I)\ n\ (\mu-1)\ \mathrm{BesselJ}(n+1,k2(\omega I)\ rr)}{rr},
$$

$$
-\frac{n\ (n-1)\ (\mu-1)\ \mathrm{BesselY}(n,k2(\omega I)\ rr)}{rr^2}
$$

$$+\frac{k2(\omega I)\ n\ (\mu-1)\ \mathrm{BesselY}(n+1,k2(\omega I)\ rr)}{rr}\Bigg],$$

$$\Bigg[-\frac{2\ n\ (n-1)\ \mathrm{BesselJ}(n,k1(\omega I)\ rr)}{rr^2}+\frac{2\ k1(\omega I)\ \mathrm{BesselJ}(n+1,k1(\omega I)\ rr)\ n}{rr},$$

$$-\frac{2\ n\ (n-1)\ \mathrm{BesselY}(n,k1(\omega I)\ rr)}{rr^2}+\frac{2\ k1(\omega I)\ \mathrm{BesselY}(n+1,k1(\omega I)\ rr)\ n}{rr},$$

$$\left(k2(\omega I)^2-\frac{2\ n\ (n-1)}{rr^2}\right)\mathrm{BesselJ}(n,k2(\omega I)\ rr)$$

$$-\frac{2\ \mathrm{BesselJ}(n+1,k2(\omega I)\ rr)\ k2(\omega I)}{rr},\left(k2(\omega I)^2-\frac{2\ n\ (n-1)}{rr^2}\right)\mathrm{BesselY}(n,$$

$$k2(\omega I)\ rr)-\frac{2\ \mathrm{BesselY}(n+1,k2(\omega I)\ rr)\ k2(\omega I)}{rr}\Bigg]\Bigg]$$

$$\begin{matrix}0\\0\end{matrix}$$

$$\begin{matrix}0\\0\end{matrix} \tag{55}$$

$$\begin{matrix}0\\0\end{matrix} \tag{56}$$

$MP := Matrix([[d11, d12, d13, d14], [d21, d22, d23, d24], [d31, d32, d33, d34], [d41, d42, d43, d44]])$

$$\Bigg[\Bigg[\left(-\frac{\beta(\omega o)^2\ m}{r}+\frac{m^2\ (\mu-1)\ (m-1)}{r^3}\right)\mathrm{BesselJ}(m,\beta(\omega o)\ r)+\left(\beta(\omega o)^3\right. \tag{57}$$

$$\left.-\frac{\beta(\omega o)\ m^2\ (\mu-1)}{r^2}\right)\mathrm{BesselJ}(m+1,\beta(\omega o)\ r),\left(-\frac{\beta(\omega o)^2\ m}{r}\right.$$

$$\left.+\frac{m^2\ (\mu-1)\ (m-1)}{r^3}\right)\mathrm{BesselY}(m,\beta(\omega o)\ r)+\left(\beta(\omega o)^3\right.$$

$$\left.-\frac{\beta(\omega o)\ m^2\ (\mu-1)}{r^2}\right)\mathrm{BesselY}(m+1,\beta(\omega o)\ r),\left(\frac{\beta(\omega o)^2\ m}{r}\right.$$

$$\left.+\frac{m^2\ (\mu-1)\ (m-1)}{r^3}\right)\mathrm{BesselI}(m,\beta(\omega o)\ r)+\left(\beta(\omega o)^3\right.$$

$$\left.+\frac{\beta(\omega o)\ m^2\ (\mu-1)}{r^2}\right)\mathrm{BesselI}(m+1,\beta(\omega o)\ r),\left(\frac{\beta(\omega o)^2\ m}{r}\right.$$

$$\left.+\frac{m^2\ (\mu-1)\ (m-1)}{r^3}\right)\mathrm{BesselK}(m,\beta(\omega o)\ r)+\left(-\beta(\omega o)^3\right.$$

$$\left.-\frac{\beta(\omega o)\ m^2\ (\mu-1)}{r^2}\right)\mathrm{BesselK}(m+1,\beta(\omega o)\ r)\Bigg],$$

$$\Bigg[\left(-\beta(\omega o)^2-\frac{m\ (m-1)\ (\mu-1)}{r^2}\right)\mathrm{BesselJ}(m,\beta(\omega o)\ r)$$

$$
-\frac{\beta(\omega o)\ (\mu-1)\ \text{BesselJ}(m+1,\beta(\omega o)\ r)}{r},\left(-\beta(\omega o)^2\right.
$$

$$
\left.-\frac{m\ (m-1)\ (\mu-1)}{r^2}\right)\text{BesselY}(m,\beta(\omega o)\ r)
$$

$$
-\frac{\beta(\omega o)\ (\mu-1)\ \text{BesselY}(m+1,\beta(\omega o)\ r)}{r},\left(\beta(\omega o)^2\right.
$$

$$
\left.-\frac{m\ (m-1)\ (\mu-1)}{r^2}\right)\text{BesselI}(m,\beta(\omega o)\ r)
$$

$$
+\frac{\beta(\omega o)\ (\mu-1)\ \text{BesselI}(m+1,\beta(\omega o)\ r)}{r},\left(\beta(\omega o)^2\right.
$$

$$
\left.-\frac{m\ (m-1)\ (\mu-1)}{r^2}\right)\text{BesselK}(m,\beta(\omega o)\ r)
$$

$$
\left.-\frac{\beta(\omega o)\ (\mu-1)\ \text{BesselK}(m+1,\beta(\omega o)\ r)}{r}\right],
$$

$$
\left[\left(-\frac{\beta(\omega o)^2\ m}{rr}+\frac{m^2\ (\mu-1)\ (m-1)}{rr^3}\right)\text{BesselJ}(m,\beta(\omega o)\ rr)+\left(\beta(\omega o)^3\right.\right.
$$

$$
\left.-\frac{\beta(\omega o)\ m^2\ (\mu-1)}{rr^2}\right)\text{BesselJ}(m+1,\beta(\omega o)\ rr),\left(-\frac{\beta(\omega o)^2\ m}{rr}\right.
$$

$$
\left.+\frac{m^2\ (\mu-1)\ (m-1)}{rr^3}\right)\text{BesselY}(m,\beta(\omega o)\ rr)+\left(\beta(\omega o)^3\right.
$$

$$
\left.-\frac{\beta(\omega o)\ m^2\ (\mu-1)}{rr^2}\right)\text{BesselY}(m+1,\beta(\omega o)\ rr),\left(\frac{\beta(\omega o)^2\ m}{rr}\right.
$$

$$
\left.+\frac{m^2\ (\mu-1)\ (m-1)}{rr^3}\right)\text{BesselI}(m,\beta(\omega o)\ rr)+\left(\beta(\omega o)^3\right.
$$

$$
\left.+\frac{\beta(\omega o)\ m^2\ (\mu-1)}{rr^2}\right)\text{BesselI}(m+1,\beta(\omega o)\ rr),\left(\frac{\beta(\omega o)^2\ m}{rr}\right.
$$

$$
\left.+\frac{m^2\ (\mu-1)\ (m-1)}{rr^3}\right)\text{BesselK}(m,\beta(\omega o)\ rr)+\left(-\beta(\omega o)^3\right.
$$

$$
\left.-\frac{\beta(\omega o)\ m^2\ (\mu-1)}{rr^2}\right)\text{BesselK}(m+1,\beta(\omega o)\ rr)\Bigg],
$$

$$
\left[\left(-\beta(\omega o)^2-\frac{m\ (m-1)\ (\mu-1)}{rr^2}\right)\text{BesselJ}(m,\beta(\omega o)\ rr)\right.
$$

$$
\left.-\frac{\beta(\omega o)\ (\mu-1)\ \text{BesselJ}(m+1,\beta(\omega o)\ rr)}{rr},\left(-\beta(\omega o)^2\right.\right.
$$

$$- \frac{m\,(m-1)\,(\mu-1)}{rr^2}\Bigg)\,\mathrm{BesselY}(m,\beta(\omega o)\,rr) - \frac{\beta(\omega o)\,(\mu-1)\,\mathrm{BesselY}(m+1,\beta(\omega o)\,rr)}{rr},\Bigg(\beta(\omega o)^2 - \frac{m\,(m-1)\,(\mu-1)}{rr^2}\Bigg)\,\mathrm{BesselI}(m,\beta(\omega o)\,rr) + \frac{\beta(\omega o)\,(\mu-1)\,\mathrm{BesselI}(m+1,\beta(\omega o)\,rr)}{rr},\Bigg(\beta(\omega o)^2 - \frac{m\,(m-1)\,(\mu-1)}{rr^2}\Bigg)\,\mathrm{BesselK}(m,\beta(\omega o)\,rr) - \frac{\beta(\omega o)\,(\mu-1)\,\mathrm{BesselK}(m+1,\beta(\omega o)\,rr)}{rr}\Bigg]\Bigg]$$

0

$$0 \tag{58}$$

0

$$0 \tag{59}$$

$m := 3$

$$3 \tag{60}$$

$n := m - 1$

$$2 \tag{61}$$

$r := \frac{1}{100} \cdot \frac{4251}{1000}$

$$\frac{4251}{100000} \tag{62}$$

$a := r$

$rr := \frac{1}{10}$

$$\frac{1}{10} \tag{63}$$

$b := rr$

$$b = rr \tag{64}$$

$h := 0.004824$

$$0.004824 \tag{65}$$

$E := 70 \cdot 10^9$

$$70000000000 \tag{66}$$

$\rho := 2700$

$$2700 \tag{67}$$

$\mu := \frac{1}{3}$

$$\frac{1}{3} \tag{68}$$

0

$$0 \tag{69}$$

0

$$0 \tag{70}$$

$$k1(\omega I) := evalf[17]\left(\omega I \cdot \mathrm{sqrt}\left(\frac{\rho\cdot\left(1-\mu^2\right)}{E}\right)\right)$$

$$\omega I \to evalf_{17}\left(\omega I \sqrt{\frac{\rho\left(-\mu^2+1\right)}{E}}\right)$$

$$\omega I \to evalf_{17}\left(\omega I \sqrt{\frac{\rho\left(-\mu^2+1\right)}{E}}\right) \tag{72}$$

$$k2(\omega I) := evalf[17]\left(\omega I \cdot \mathrm{sqrt}\left(\frac{2\cdot\rho\cdot\left(1+\mu\right)}{E}\right)\right)$$

$$\omega I \to evalf_{17}\left(\omega I \sqrt{\frac{2\,\rho\left(1+\mu\right)}{E}}\right) \tag{73}$$

$$\beta(\omega o) := evalf[17]\left(\mathrm{sqrt}\left(\frac{\omega o}{h}\cdot\mathrm{sqrt}\left(\frac{12\cdot\rho\cdot\left(1-\mu^2\right)}{E}\right)\right)\right)$$

$$\omega o \to evalf_{17}\left(\sqrt{\frac{\omega o\sqrt{\frac{12\,\rho\left(-\mu^2+1\right)}{E}}}{h}}\right) \tag{74}$$

$$plot\left([\log[10]((\ \mathrm{abs}(Determinant(M))\ ))\ ],\ \omega I = 10\cdot 10^3 ..50\cdot 10^3,\ numpoints = 100\right)$$

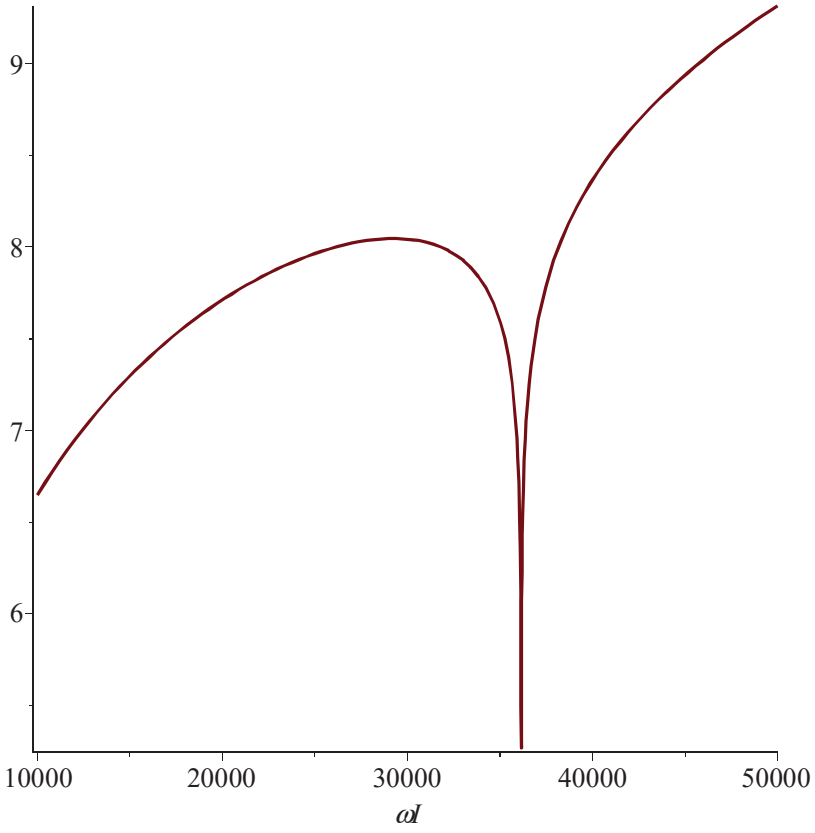

$$plot\left([\ \log[10]((\ \mathrm{abs}(Determinant(MP)))) - 7],\ \omega o = 10\cdot 10^{3}..50\cdot 10^{3},\ numpoints = 100 \right)$$

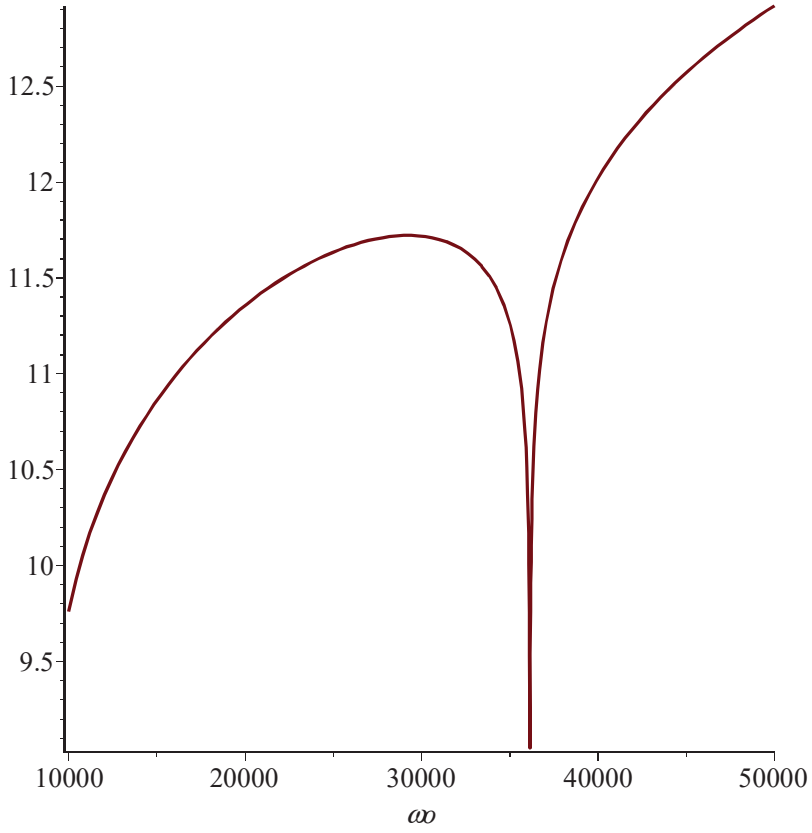

$evalf(h)$

$$0.004824 \quad \textbf{(75)}$$

$evalf(rr)$

$$0.1000000000 \quad \textbf{(76)}$$

$evalf(r)$

$$0.04251000000 \quad \textbf{(77)}$$

$$\frac{36132.79859817449}{34336.66468118740}$$

$$1.052309505 \quad \textbf{(78)}$$

$$\omega D := evalf[16]\left(fsolve\left(\left\{ Determinant(M) \cdot 10^{-14} = 0 \right\}, \left\{ \omega I = 10 \cdot 10^{3} ..100 \cdot 10^{3} \right\} \right) \right)[1]$$

$$\omega I = 36141.54818193475 \quad \textbf{(79)}$$

$$\omega P := evalf[16]\left(fsolve\left(\left\{ Determinant(MP) \cdot 10^{-25} = 0 \right\}, \left\{ \omega o = 10 \cdot 10^{3} ..50 \cdot 10^{3} \right\} \right) \right)[1]$$

$$\omega o = 36139.78695872854 \quad \textbf{(80)}$$

$evalf[16](\omega D - \omega P)$

$$\omega I - 1.\ \omega o = 1.76122320621 \quad \textbf{(81)}$$

$$evalf[16]\left(\frac{\omega D-\omega P}{2\cdot \mathrm{Pi}\cdot 1000}\right)$$

$$0.0001591549430918954\ \omega I-0.0001591549430918954\ \omega o=0.0002803073791564780 \tag{82}$$

$$evalf\left(\frac{\omega D}{2\cdot \mathrm{Pi}\cdot 1000}\right)$$

$$0.0001591549430\ \omega I=5.752106042 \tag{83}$$

$$evalf\left(\frac{\omega P}{2\cdot \mathrm{Pi}\cdot 1000}\right)$$

$$0.0001591549430\ \omega o=5.751825735 \tag{84}$$

$$\omega I := evalf[16](36141.54818193475)$$

$$36141.54818193475 \tag{85}$$

0

$$0 \tag{86}$$

$$MM := \langle\langle c12, c22, c32\rangle|\langle c13, c23, c33\rangle|\langle c14, c24, c34\rangle|\langle -c11, -c21, -c31\rangle\rangle$$

$$\begin{bmatrix} -34586.75324 & 21.05013857 & 11836.31291 & -7.013937018 \\ -1.051613512\ 10^{5} & -63.17079083 & 35570.10606 & 21.94105380 \\ -1086.916806 & 15.38113189 & 430.0616817 & -5.045436859 \end{bmatrix} \tag{87}$$

$$SolMM := LinearSolve(MM)$$

$$\begin{bmatrix} 0.00642419830312352 \\ -0.402371015828906 \\ 0.0188950893574095 \end{bmatrix} \tag{88}$$

$$U := \left(C1\left(-\mathrm{BesselJ}(n+1, k1(\omega I)\cdot R)+\frac{n\ \mathrm{BesselJ}(n, k1(\omega I)\cdot R)}{k1(\omega I)\cdot R}\right)k1(\omega I)+C2\left(-\mathrm{BesselY}(n+1, k1(\omega I)\cdot R)+\frac{n\ \mathrm{BesselY}(n, k1(\omega I)\cdot R)}{k1(\omega I)\cdot R}\right)k1(\omega I)+\frac{\mathrm{BesselJ}(n, k2(\omega I)\cdot R)\ n\ C3}{R}+\frac{C4\ \mathrm{BesselY}(n, k2(\omega I)\cdot R)\ n}{R}\right)$$

$$6.6921143487466615\ C1\left(-\mathrm{BesselJ}(3, 6.6921143487466615\ R)+\frac{0.2988592089\ \mathrm{BesselJ}(2, 6.6921143487466615\ R)}{R}\right)+6.6921143487466615\ C2\left(-\mathrm{BesselY}(3, 6.6921143487466615\ R)+\frac{0.2988592089\ \mathrm{BesselY}(2, 6.6921143487466615\ R)}{R}\right)+\frac{2\ \mathrm{BesselJ}(2, 11.591082062089926\ R)\ C3}{R}+\frac{2\ C4\ \mathrm{BesselY}(2, 11.591082062089926\ R)}{R}$$

$$5.8313176620302085\ C1\left(-\text{BesselJ}(3,\ 5.8313176620302085\ R)+\frac{0.3429756559\ \text{BesselJ}(2,\ 5.8313176620302085\ R)}{R}\right)+5.8313176620302085\ C2\left(-\text{BesselY}(3,\ 5.8313176620302085\ R)+\frac{0.3429756559\ \text{BesselY}(2,\ 5.8313176620302085\ R)}{R}\right)+\frac{2\ \text{BesselJ}(2,\ 10.100138465710080\ R)\ C3}{R}+\frac{2\ C4\ \text{BesselY}(2,\ 10.100138465710080\ R)}{R} \tag{90}$$

$$V:=\left(-\frac{\text{BesselJ}(n,\ k1(\omega I)\cdot R)\ n\ C1}{R}-\frac{C2\ \text{BesselY}(n,\ k1(\omega I)\cdot R)\ n}{R}-C3\left(-\text{BesselJ}(n+1,\ k2(\omega I)\cdot R)+\frac{n\ \text{BesselJ}(n,\ k2(\omega I)\cdot R)}{k2(\omega I)\cdot R}\right)k2(\omega I)-C4\left(-\text{BesselY}(n+1,\ k2(\omega I)\cdot R)+\frac{n\ \text{BesselY}(n,\ k2(\omega I)\cdot R)}{k2(\omega I)\cdot R}\right)k2(\omega I)\right)$$

$$-\frac{2\ \text{BesselJ}(2,\ 6.6921143487466615\ R)\ C1}{R}-\frac{2\ C2\ \text{BesselY}(2,\ 6.6921143487466615\ R)}{R}-11.591082062089926\ C3\left(-\text{BesselJ}(3,\ 11.591082062089926\ R)+\frac{0.1725464447\ \text{BesselJ}(2,\ 11.591082062089926\ R)}{R}\right)-11.591082062089926\ C4\left(-\text{BesselY}(3,\ 11.591082062089926\ R)+\frac{0.1725464447\ \text{BesselY}(2,\ 11.591082062089926\ R)}{R}\right) \tag{91}$$

$C1 := 1.$

$$1. \tag{92}$$

$C2 := SolMM[1]$

$$0.00642419830312352 \tag{93}$$

$C3 := SolMM[2]$

$$-0.402371015828906 \tag{94}$$

$C4 := SolMM[3]$

$$0.0188950893574095 \tag{95}$$

0

$$0 \tag{96}$$

0

$$0 \tag{97}$$

$\omega o := evalf[16](36139.7869587285)$

$$36139.7869587285 \tag{98}$$

$MMP := \langle\langle d12, d22, d32\rangle|\langle d13, d23, d33\rangle|\langle d14, d24, d34\rangle|\langle -d11, -d21, -d31\rangle\rangle$

$$\begin{bmatrix} -2.607882155\ 10^{5} & 1.941837104\ 10^{5} & -10329.16393 & 77952.14169 \\ 410.858567 & 5946.287666 & 1293.968136 & 640.5039265 \\ 62344.91268 & 2.429563497\ 10^{7} & -274.4451435 & -89294.60527 \end{bmatrix} \quad (99)$$

$SolMMP := LinearSolve(MMP)$

$$\begin{bmatrix} -0.325231175366365 \\ -0.00283385607619319 \\ 0.611281562954837 \end{bmatrix} \quad (100)$$

$W := (A1 \cdot \mathrm{BesselJ}(m, \beta(\omega o) \cdot R) + A2 \cdot \mathrm{BesselY}(m, \beta(\omega o) \cdot R) + A3 \cdot \mathrm{BesselI}(m, \beta(\omega o) \cdot R) + A4 \cdot \mathrm{BesselK}(m, \beta(\omega o) \cdot R))$

$$A1\ \mathrm{BesselJ}(3, 69.320670766679665\ R) + A2\ \mathrm{BesselY}(3, 69.320670766679665\ R) + A3\ \mathrm{BesselI}(3, 69.320670766679665\ R) + A4\ \mathrm{BesselK}(3, 69.320670766679665\ R) \quad (101)$$

$A1 := 1.$

$$1. \quad (102)$$

$A2 := SolMMP[1]$

$$-0.325231175366365 \quad (103)$$

$A3 := SolMMP[2]$

$$-0.00283385607619319 \quad (104)$$

$A4 := SolMMP[3]$

$$0.611281562954837 \quad (105)$$

$plot(1^{-1} \cdot [U], R = r..rr)$

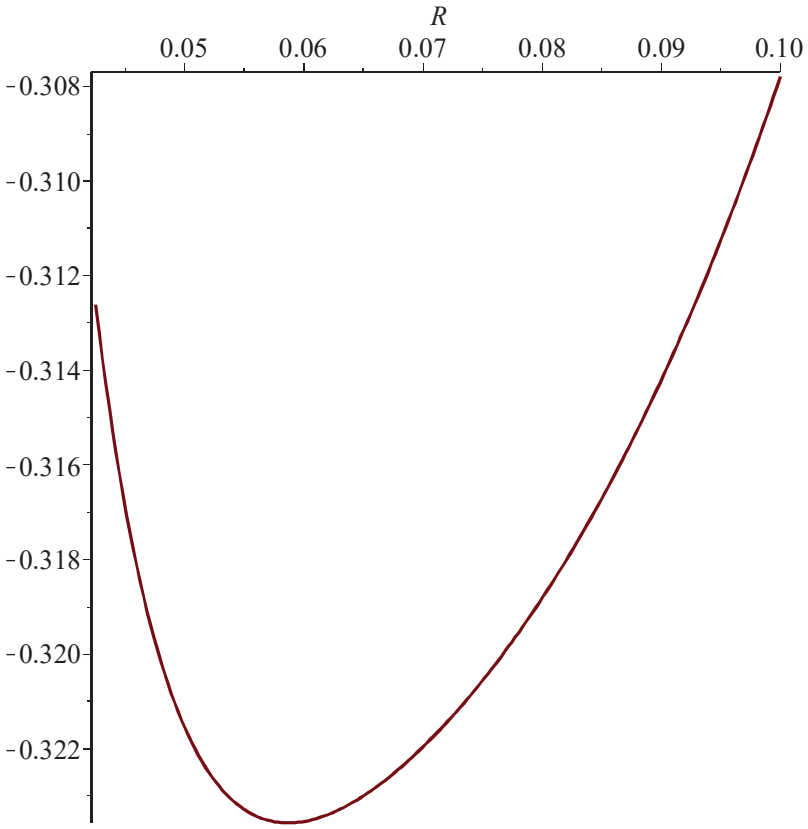

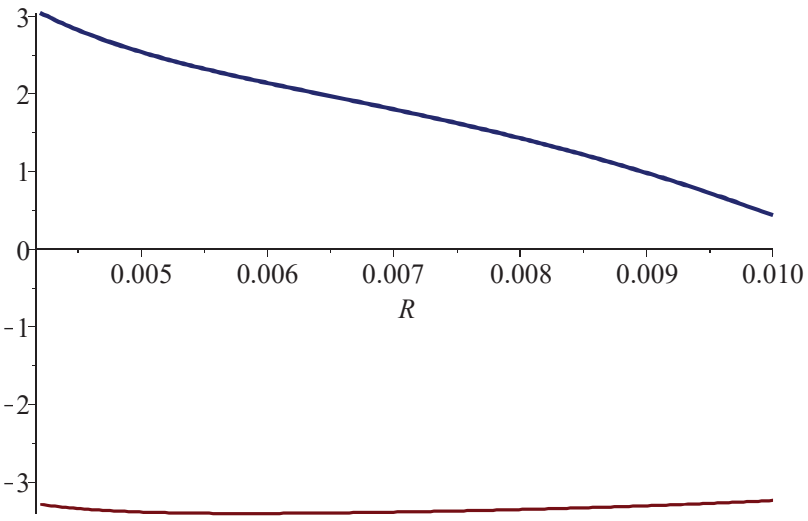

$plot([1^{-1} \cdot V], R = r..rr)$

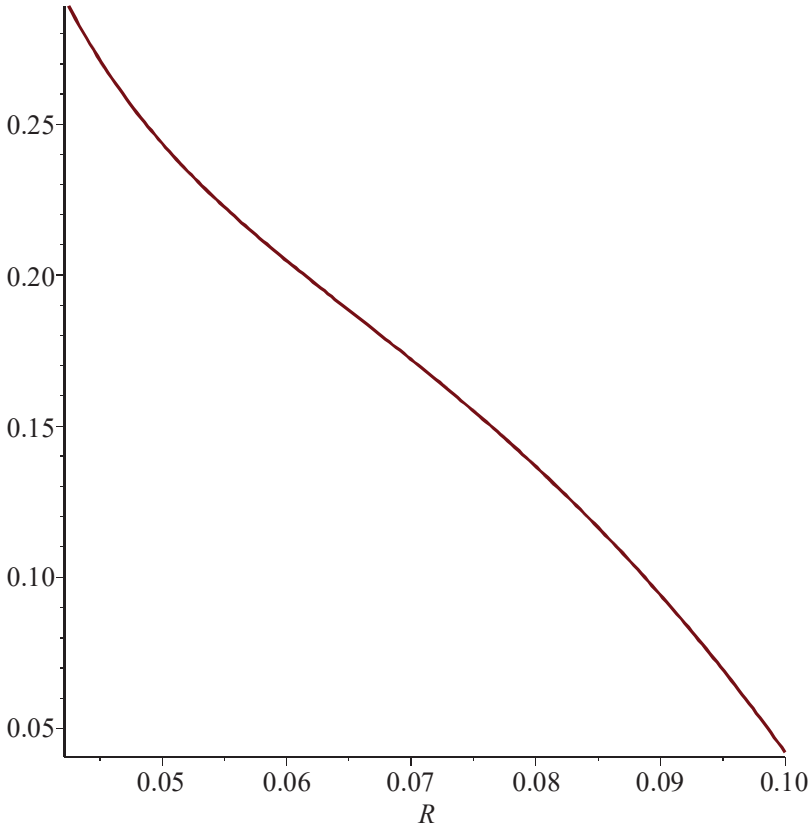

$plot([1^{-1}\cdot W, 0], R = r..rr)$

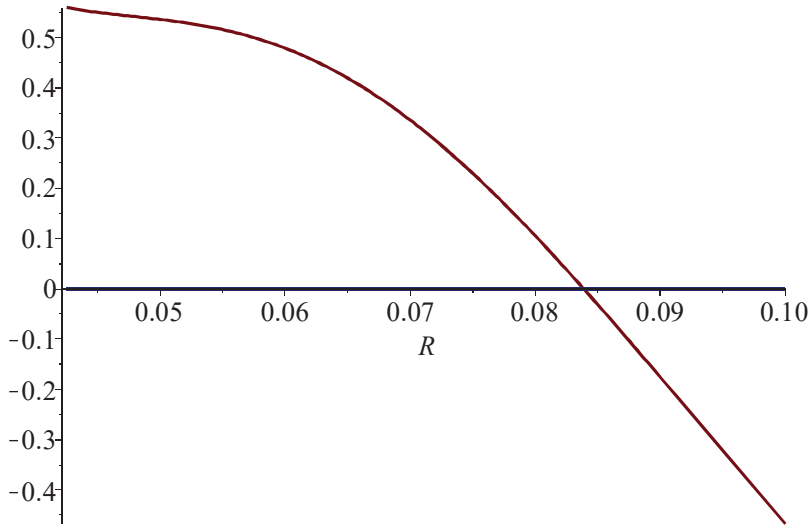

$$evalf\left(\frac{\omega I}{2\cdot \mathrm{Pi}\cdot 10^{3}}\right)$$

$$5.752106042$$

$$58.23353366 \tag{107}$$

$$evalf\left(\frac{\omega o}{2\cdot \mathrm{Pi}\cdot 10^{3}}\right)$$

$$5.751825735 \tag{108}$$

0

$$0 \tag{109}$$

U

$$-6.692114349\,\mathrm{BesselJ}(3, 6.6921143487466615\,R) + \frac{2.000000000\,\mathrm{BesselJ}(2, 6.6921143487466615\,R)}{R} - 0.0429914696451544\,\mathrm{BesselY}(3, 6.6921143487466615\,R) + \frac{0.0128483966075992\,\mathrm{BesselY}(2, 6.6921143487466615\,R)}{R} - \frac{0.804742031657812\,\mathrm{BesselJ}(2, 11.591082062089926\,R)}{R} + \frac{0.0377901787148191\,\mathrm{BesselY}(2, 11.591082062089926\,R)}{R} \tag{110}$$

W

$$1.\,\mathrm{BesselJ}(3, 69.320670766679665\,R) - 0.325231175366365\,\mathrm{BesselY}(3, 69.320670766679665\,R) - 0.00283385607619319\,\mathrm{BesselI}(3, 69.320670766679665\,R) + 0.611281562954837\,\mathrm{BesselK}(3, 69.320670766679665\,R) \tag{111}$$

0

$$0 \tag{112}$$

0

$$0 \tag{113}$$

$$U := 3.23548485861240^{-1}\cdot U$$

$$-2.068349766\,\mathrm{BesselJ}(3, 6.6921143487466615\,R) + \frac{0.6181453746\,\mathrm{BesselJ}(2, 6.6921143487466615\,R)}{R} - 0.0132874890542042\,\mathrm{BesselY}(3, 6.6921143487466615\,R) + \frac{0.00397108846700689\,\mathrm{BesselY}(2, 6.6921143487466615\,R)}{R} - \frac{0.248723782307741\,\mathrm{BesselJ}(2, 11.591082062089926\,R)}{R} + \frac{0.0116799120889364\,\mathrm{BesselY}(2, 11.591082062089926\,R)}{R} \tag{114}$$

$$V := 3.23548485861240^{-1}\cdot V$$

$$-\frac{0.6181453746\,\mathrm{BesselJ}(2, 6.6921143487466615\,R)}{R} - \frac{0.00397108846658897\,\mathrm{BesselY}(2, 6.6921143487466615\,R)}{R} \tag{115}$$

$$-1.44148888550130\ \mathrm{BesselJ}(3, 11.591082062089926\ R) + \frac{0.248723782267815\ \mathrm{BesselJ}(2, 11.591082062089926\ R)}{R} + 0.0676914097382238\ \mathrm{BesselY}(3, 11.591082062089926\ R) - \frac{0.0116799120870615\ \mathrm{BesselY}(2, 11.591082062089926\ R)}{R}$$

$$W := 0.559139410005858^{-1} \cdot W$$

$$1.788462738\ \mathrm{BesselJ}(3, 69.320670766679665\ R) - 0.581663838378688\ \mathrm{BesselY}(3, 69.320670766679665\ R) - 0.00506824599712640\ \mathrm{BesselI}(3, 69.320670766679665\ R) + 1.09325429777113\ \mathrm{BesselK}(3, 69.320670766679665\ R) \quad \textbf{(116)}$$

$plot([U, V, W], R = r..rr)$

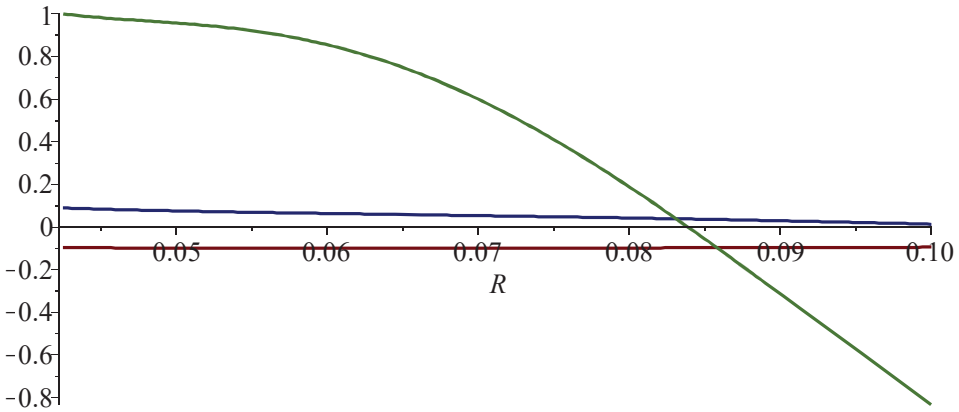

$$\beta 1 := \frac{2 \cdot evalf(int(U \cdot V \cdot R, R = r..rr))}{evalf\left(int\left(\left(U^2 + V^2\right) \cdot R, R = r..rr\right)\right)}$$

$$-0.7515544830 \quad \textbf{(117)}$$

$$\beta 2 := \frac{evalf(int((U + V) \cdot W \cdot R, R = r..rr))}{2 \cdot evalf\left(int\left(\left(U^2 + V^2\right) \cdot R, R = r..rr\right)\right)}$$

$$-0.1063962520 \quad \textbf{(118)}$$

$$\beta 3 := \frac{evalf(int((U + V) \cdot W \cdot R, R = r..rr))}{2 \cdot evalf\left(int\left((W)^2 \cdot R, R = r..rr\right)\right)}$$

$$-0.003233973327 \quad \textbf{(119)}$$

$$\mathrm{sqrt}(\mathrm{abs}(\beta 4 \cdot \beta 5))$$

$$0.01854946471 \quad \textbf{(120)}$$

$$\mathrm{sqrt}\left(\frac{0.464633987642163}{0.132676119506226}\right)$$

$$1.871367604 \quad \textbf{(121)}$$

MAPLE CODE FOR KINETIC ENERGY FOR A DISC GYROSCOPE WITH MASS IMPERFECTIONS

$$0 \tag{1}$$

$assume(m, integer)$

$$0 \tag{2}$$

$m := 2$

$$2 \tag{3}$$

$u := U\cdot(C(t)\cdot\cos(m\cdot\varphi) + S(t)\cdot\sin(m\cdot\varphi))$

$$U\,(C(t)\,\cos(2\,\varphi) + S(t)\,\sin(2\,\varphi)) \tag{4}$$

$v := V\cdot(C(t)\cdot\sin(m\cdot\varphi) - S(t)\cdot\cos(m\cdot\varphi))$

$$V\,(C(t)\,\sin(2\,\varphi) - S(t)\,\cos(2\,\varphi)) \tag{5}$$

$w := W\cdot(A(t)\cdot\cos((m+1)\cdot\varphi) + B(t)\cdot\sin((m+1)\cdot\varphi))$

$$W\,(A(t)\,\cos(3\,\varphi) + B(t)\,\sin(3\,\varphi)) \tag{6}$$

$du := diff(u, t)$

$$U\left(\left(\frac{\mathrm{d}}{\mathrm{d}t}\,C(t)\right)\cos(2\,\varphi) + \left(\frac{\mathrm{d}}{\mathrm{d}t}\,S(t)\right)\sin(2\,\varphi)\right) \tag{7}$$

$dv := diff(v, t)$

$$V\left(\left(\frac{\mathrm{d}}{\mathrm{d}t}\,C(t)\right)\sin(2\,\varphi) - \left(\frac{\mathrm{d}}{\mathrm{d}t}\,S(t)\right)\cos(2\,\varphi)\right) \tag{8}$$

$dw := diff(w, t)$

$$W\left(\left(\frac{\mathrm{d}}{\mathrm{d}t}\,A(t)\right)\cos(3\,\varphi) + \left(\frac{\mathrm{d}}{\mathrm{d}t}\,B(t)\right)\sin(3\,\varphi)\right) \tag{9}$$

$dut := du + \varepsilon\cdot\left(\left(-\Omega\xi(t)\cdot\sin(\varphi) + \Omega\eta(t)\cdot\cos(\varphi)\right)\cdot w - \Omega\zeta(t)\cdot v\right)$

$$U\left(\left(\frac{\mathrm{d}}{\mathrm{d}t}\,C(t)\right)\cos(2\,\varphi) + \left(\frac{\mathrm{d}}{\mathrm{d}t}\,S(t)\right)\sin(2\,\varphi)\right) + \varepsilon\,\left(\left(-\Omega\xi(t)\,\sin(\varphi) + \Omega\eta(t)\,\cos(\varphi)\right)\,W\,(A(t)\,\cos(3\,\varphi) + B(t)\,\sin(3\,\varphi)) - \Omega\zeta(t)\,V\,(C(t)\,\sin(2\,\varphi) - S(t)\,\cos(2\,\varphi))\right) \tag{10}$$

$dvt := dv + \varepsilon\cdot\left(-\left(\Omega\xi(t)\cdot\cos(\varphi) + \Omega\eta(t)\cdot\sin(\varphi)\right)\cdot w + \Omega\zeta(t)\cdot(r+u)\right)$

$$V\left(\left(\frac{\mathrm{d}}{\mathrm{d}t}\,C(t)\right)\sin(2\,\varphi) - \left(\frac{\mathrm{d}}{\mathrm{d}t}\,S(t)\right)\cos(2\,\varphi)\right) + \varepsilon\,\left(-\left(\Omega\xi(t)\,\cos(\varphi) + \Omega\eta(t)\,\sin(\varphi)\right)\,W\,(A(t)\,\cos(3\,\varphi) + B(t)\,\sin(3\,\varphi)) + \Omega\zeta(t)\,(r + U\,(C(t)\,\cos(2\,\varphi) + S(t)\,\sin(2\,\varphi)))\right) \tag{11}$$

$dwt := dw + \varepsilon\cdot\left(\left(\Omega\xi(t)\cdot\cos(\varphi) + \Omega\eta(t)\cdot\sin(\varphi)\right)\cdot v - \left(-\Omega\xi(t)\,\sin(\varphi) + \Omega\eta(t)\,\cos(\varphi)\right)\cdot(r+u)\right)$

$$W\left(\left(\frac{\mathrm{d}}{\mathrm{d}t}\,A(t)\right)\cos(3\,\varphi) + \left(\frac{\mathrm{d}}{\mathrm{d}t}\,B(t)\right)\sin(3\,\varphi)\right) + \varepsilon\,\left(\left(\Omega\xi(t)\,\cos(\varphi) + \Omega\eta(t)\,\sin(\varphi)\right)\,V\,(C(t)\,\sin(2\,\varphi) - S(t)\,\cos(2\,\varphi)) - \left(-\Omega\xi(t)\,\sin(\varphi) + \Omega\eta(t)\,\cos(\varphi)\right)\,(r + U\,(C(t)\,\cos(2\,\varphi) + S(t)\,\sin(2\,\varphi)))\right) \tag{12}$$

0

$$0 \tag{13}$$

0

$$0 \tag{14}$$

$$L1 := collect\left(convert\left(series\left(int\left(\frac{1}{2}\cdot\frac{1}{2\cdot \mathrm{Pi}}\cdot\left(dut^2+dvt^2+dwt^2\right),\ \varphi=0..2\cdot \mathrm{Pi}\right),\ \varepsilon=0,2\right),polynom\right),\ [diff, C, S], factor\right)$$

$$\begin{aligned}&\frac{1}{4}\left(\frac{d}{dt}A(t)\right)^2 W^2+\left(-\frac{1}{4}W\Omega\eta(t)\ (V+U)\ \varepsilon\ C(t)-\frac{1}{4}W\Omega\xi(t)\ (V\right.\\&\left.+U)\ \varepsilon\ S(t)\right)\left(\frac{d}{dt}A(t)\right)+\frac{1}{4}\left(\frac{d}{dt}B(t)\right)^2 W^2+\left(\frac{1}{4}W\Omega\xi(t)\ (V+U)\ \varepsilon\ C(t)\right.\\&\left.-\frac{1}{4}W\Omega\eta(t)\ (V+U)\ \varepsilon\ S(t)\right)\left(\frac{d}{dt}B(t)\right)+\left(\frac{1}{4}U^2+\frac{1}{4}V^2\right)\left(\frac{d}{dt}C(t)\right)^2\\&+\left(V\Omega\zeta(t)\ U\varepsilon\ S(t)-\frac{1}{4}W(V+U)\left(\Omega\xi(t)\ B(t)-\Omega\eta(t)\ A(t)\right)\varepsilon\right)\left(\frac{d}{dt}C(t)\right)\\&+\left(\frac{1}{4}U^2+\frac{1}{4}V^2\right)\left(\frac{d}{dt}S(t)\right)^2+\left(-V\Omega\zeta(t)\ U\varepsilon\ C(t)+\frac{1}{4}W(V+U)\left(\Omega\xi(t)\ A(t)\right.\right.\\&\left.\left.+\Omega\eta(t)\ B(t)\right)\varepsilon\right)\left(\frac{d}{dt}S(t)\right)\end{aligned} \tag{15}$$

$$\rho := \rho 0+\rho 0\cdot\varepsilon\cdot sum\left(\rho C[k]\cdot\cos(k\cdot\varphi)+\rho S[k]\cdot\sin(k\cdot\varphi),\ k=1..6\right)$$

$$\begin{aligned}&\rho 0+\rho 0\,\varepsilon\left(\rho C_1\cos(\varphi)+\rho S_1\sin(\varphi)+\rho C_2\cos(2\varphi)+\rho S_2\sin(2\varphi)+\rho C_3\cos(3\varphi)\right.\\&+\rho S_3\sin(3\varphi)+\rho C_4\cos(4\varphi)+\rho S_4\sin(4\varphi)+\rho C_5\cos(5\varphi)+\rho S_5\sin(5\varphi)\\&\left.+\rho C_6\cos(6\varphi)+\rho S_6\sin(6\varphi)\right)\end{aligned} \tag{16}$$

dut^2

$$\begin{aligned}&\left(U\left(\left(\frac{d}{dt}C(t)\right)\cos(2\varphi)+\left(\frac{d}{dt}S(t)\right)\sin(2\varphi)\right)+\varepsilon\left(\left(-\Omega\xi(t)\sin(\varphi)\right.\right.\right.\\&\left.+\Omega\eta(t)\cos(\varphi)\right)W(A(t)\cos(3\varphi)+B(t)\sin(3\varphi))-\Omega\zeta(t)\ V(C(t)\sin(2\varphi)\\&\left.\left.\left.-S(t)\cos(2\varphi))\right)\right)^2\end{aligned} \tag{17}$$

dvt^2

$$\begin{aligned}&\left(V\left(\left(\frac{d}{dt}C(t)\right)\sin(2\varphi)-\left(\frac{d}{dt}S(t)\right)\cos(2\varphi)\right)+\varepsilon\left(-\left(\Omega\xi(t)\cos(\varphi)\right.\right.\right.\\&\left.+\Omega\eta(t)\sin(\varphi)\right)W(A(t)\cos(3\varphi)+B(t)\sin(3\varphi))+\Omega\zeta(t)\ (r+U(C(t)\cos(2\varphi)\\&\left.\left.\left.+S(t)\sin(2\varphi)))\right)\right)^2\end{aligned} \tag{18}$$

dwt^2

$$\begin{aligned}&\left(W\left(\left(\frac{d}{dt}A(t)\right)\cos(3\varphi)+\left(\frac{d}{dt}B(t)\right)\sin(3\varphi)\right)+\varepsilon\left(\left(\Omega\xi(t)\cos(\varphi)\right.\right.\right.\\&\left.+\Omega\eta(t)\sin(\varphi)\right)V(C(t)\sin(2\varphi)-S(t)\cos(2\varphi))-\left(-\Omega\xi(t)\sin(\varphi)\right.\\&\left.\left.\left.+\Omega\eta(t)\cos(\varphi)\right)(r+U(C(t)\cos(2\varphi)+S(t)\sin(2\varphi)))\right)\right)^2\end{aligned} \tag{19}$$

$$Ue := \int_0^{2\cdot\pi} dut^2 \, d\varphi$$

$$U^2\,\rho 0\left(\frac{d}{dt}C(t)\right)^2\pi + U^2\,\rho 0\left(\frac{d}{dt}S(t)\right)^2\pi + \left(\frac{1}{2}U^2\,\rho 0\left(\frac{d}{dt}C(t)\right)^2\rho C_4\,\pi\right. \tag{20}$$
$$-\frac{1}{2}U^2\,\rho 0\left(\frac{d}{dt}S(t)\right)^2\rho C_4\,\pi - 2\,U\,\rho 0\left(\frac{d}{dt}S(t)\right)\Omega\zeta(t)\,C(t)\,V\pi$$
$$+2\,U\,\rho 0\left(\frac{d}{dt}C(t)\right)\Omega\zeta(t)\,S(t)\,V\pi - U\,\rho 0\left(\frac{d}{dt}C(t)\right)\Omega\xi(t)\,B(t)\,W\pi$$
$$+U\,\rho 0\left(\frac{d}{dt}S(t)\right)\Omega\xi(t)\,A(t)\,W\pi + U\,\rho 0\left(\frac{d}{dt}S(t)\right)\Omega\eta(t)\,B(t)\,W\pi$$
$$\left.+U\,\rho 0\left(\frac{d}{dt}C(t)\right)\Omega\eta(t)\,A(t)\,W\pi + U^2\,\rho 0\left(\frac{d}{dt}C(t)\right)\left(\frac{d}{dt}S(t)\right)\rho S_4\,\pi\right)\varepsilon + O\left(\varepsilon^2\right)$$

$$Ve := \int_0^{2\cdot Pi} dvt^2 \, d\varphi$$

$$V^2\,\rho 0\left(\frac{d}{dt}C(t)\right)^2\pi + V^2\,\rho 0\left(\frac{d}{dt}S(t)\right)^2\pi + \left(-2\,U\,\rho 0\left(\frac{d}{dt}S(t)\right)\Omega\zeta(t)\,C(t)\,V\pi\right. \tag{21}$$
$$+2\,U\,\rho 0\left(\frac{d}{dt}C(t)\right)\Omega\zeta(t)\,S(t)\,V\pi + \frac{1}{2}V^2\,\rho 0\left(\frac{d}{dt}S(t)\right)^2\rho C_4\,\pi$$
$$-\frac{1}{2}V^2\,\rho 0\left(\frac{d}{dt}C(t)\right)^2\rho C_4\,\pi - V^2\,\rho 0\left(\frac{d}{dt}C(t)\right)\left(\frac{d}{dt}S(t)\right)\rho S_4\,\pi$$
$$-V\,\rho 0\left(\frac{d}{dt}C(t)\right)\Omega\xi(t)\,B(t)\,W\pi + V\,\rho 0\left(\frac{d}{dt}S(t)\right)\Omega\xi(t)\,A(t)\,W\pi$$
$$\left.+V\,\rho 0\left(\frac{d}{dt}S(t)\right)\Omega\eta(t)\,B(t)\,W\pi + V\,\rho 0\left(\frac{d}{dt}C(t)\right)\Omega\eta(t)\,A(t)\,W\pi\right)\varepsilon + O\left(\varepsilon^2\right)$$

$$We := \int_0^{2\cdot Pi} dwt^2 \, d\varphi$$

$$W^2\,\rho 0\left(\frac{d}{dt}A(t)\right)^2\pi + W^2\,\rho 0\left(\frac{d}{dt}B(t)\right)^2\pi + \left(\frac{1}{2}W^2\,\rho 0\left(\frac{d}{dt}A(t)\right)^2\rho C_6\,\pi\right. \tag{22}$$
$$-\frac{1}{2}W^2\,\rho 0\left(\frac{d}{dt}B(t)\right)^2\rho C_6\,\pi + W^2\,\rho 0\left(\frac{d}{dt}A(t)\right)\left(\frac{d}{dt}B(t)\right)\rho S_6\,\pi$$
$$+W\,\rho 0\,\Omega\xi(t)\,C(t)\left(\frac{d}{dt}B(t)\right)V\pi - W\,\rho 0\,\Omega\xi(t)\,S(t)\left(\frac{d}{dt}A(t)\right)V\pi$$
$$-W\,\rho 0\,\Omega\eta(t)\,C(t)\left(\frac{d}{dt}A(t)\right)V\pi - W\,\rho 0\,\Omega\eta(t)\,S(t)\left(\frac{d}{dt}B(t)\right)V\pi$$
$$-W\,\rho 0\,\Omega\eta(t)\,C(t)\left(\frac{d}{dt}A(t)\right)U\pi - W\,\rho 0\,\Omega\eta(t)\,S(t)\left(\frac{d}{dt}B(t)\right)U\pi$$
$$\left.+W\,\rho 0\,\Omega\xi(t)\,C(t)\left(\frac{d}{dt}B(t)\right)U\pi - W\,\rho 0\,\Omega\xi(t)\,S(t)\left(\frac{d}{dt}A(t)\right)U\pi\right)\varepsilon + O\left(\varepsilon^2\right)$$

$$u1 := convert\left(int\left(dut^2, \varphi = 0..2\cdot \mathrm{Pi}\right), polynom, simplify\right)$$

$$U^2\,\rho 0\left(\frac{d}{dt}C(t)\right)^2\pi + U^2\,\rho 0\left(\frac{d}{dt}S(t)\right)^2\pi + \left(\frac{1}{2}U^2\,\rho 0\left(\frac{d}{dt}C(t)\right)^2\rho C_4\,\pi\right. \tag{23}$$
$$-\frac{1}{2}U^2\,\rho 0\left(\frac{d}{dt}S(t)\right)^2\rho C_4\,\pi - 2\,U\,\rho 0\left(\frac{d}{dt}S(t)\right)\Omega\zeta(t)\,C(t)\,V\pi$$
$$+2\,U\,\rho 0\left(\frac{d}{dt}C(t)\right)\Omega\zeta(t)\,S(t)\,V\pi - U\,\rho 0\left(\frac{d}{dt}C(t)\right)\Omega\xi(t)\,B(t)\,W\pi$$
$$+U\,\rho 0\left(\frac{d}{dt}S(t)\right)\Omega\xi(t)\,A(t)\,W\pi + U\,\rho 0\left(\frac{d}{dt}S(t)\right)\Omega\eta(t)\,B(t)\,W\pi$$
$$\left.+U\,\rho 0\left(\frac{d}{dt}C(t)\right)\Omega\eta(t)\,A(t)\,W\pi + U^2\,\rho 0\left(\frac{d}{dt}C(t)\right)\left(\frac{d}{dt}S(t)\right)\rho S_4\,\pi\right)\varepsilon$$

$$v1 := convert\left(int\left(dvt^2, \varphi = 0..2\cdot \mathrm{Pi}\right), polynom, simplify\right)$$

$$V^2\,\rho 0\left(\frac{d}{dt}C(t)\right)^2\pi + V^2\,\rho 0\left(\frac{d}{dt}S(t)\right)^2\pi + \left(-2\,U\,\rho 0\left(\frac{d}{dt}S(t)\right)\Omega\zeta(t)\,C(t)\,V\pi\right. \tag{24}$$
$$+2\,U\,\rho 0\left(\frac{d}{dt}C(t)\right)\Omega\zeta(t)\,S(t)\,V\pi + \frac{1}{2}V^2\,\rho 0\left(\frac{d}{dt}S(t)\right)^2\rho C_4\,\pi$$
$$-\frac{1}{2}V^2\,\rho 0\left(\frac{d}{dt}C(t)\right)^2\rho C_4\,\pi - V^2\,\rho 0\left(\frac{d}{dt}C(t)\right)\left(\frac{d}{dt}S(t)\right)\rho S_4\,\pi$$
$$-V\,\rho 0\left(\frac{d}{dt}C(t)\right)\Omega\xi(t)\,B(t)\,W\pi + V\,\rho 0\left(\frac{d}{dt}S(t)\right)\Omega\xi(t)\,A(t)\,W\pi$$
$$\left.+V\,\rho 0\left(\frac{d}{dt}S(t)\right)\Omega\eta(t)\,B(t)\,W\pi + V\,\rho 0\left(\frac{d}{dt}C(t)\right)\Omega\eta(t)\,A(t)\,W\pi\right)\varepsilon$$

$$w1 := convert\left(int\left(dwt^2, \varphi = 0..2\cdot \mathrm{Pi}\right), polynom, simplify\right)$$

$$W^2\,\rho 0\left(\frac{d}{dt}A(t)\right)^2\pi + W^2\,\rho 0\left(\frac{d}{dt}B(t)\right)^2\pi + \left(\frac{1}{2}W^2\,\rho 0\left(\frac{d}{dt}A(t)\right)^2\rho C_6\,\pi\right. \tag{25}$$
$$-\frac{1}{2}W^2\,\rho 0\left(\frac{d}{dt}B(t)\right)^2\rho C_6\,\pi + W^2\,\rho 0\left(\frac{d}{dt}A(t)\right)\left(\frac{d}{dt}B(t)\right)\rho S_6\,\pi$$
$$+W\,\rho 0\,\Omega\xi(t)\,C(t)\left(\frac{d}{dt}B(t)\right)V\pi - W\,\rho 0\,\Omega\xi(t)\,S(t)\left(\frac{d}{dt}A(t)\right)V\pi$$
$$-W\,\rho 0\,\Omega\eta(t)\,C(t)\left(\frac{d}{dt}A(t)\right)V\pi - W\,\rho 0\,\Omega\eta(t)\,S(t)\left(\frac{d}{dt}B(t)\right)V\pi$$
$$-W\,\rho 0\,\Omega\eta(t)\,C(t)\left(\frac{d}{dt}A(t)\right)U\pi - W\,\rho 0\,\Omega\eta(t)\,S(t)\left(\frac{d}{dt}B(t)\right)U\pi$$
$$\left.+W\,\rho 0\,\Omega\xi(t)\,C(t)\left(\frac{d}{dt}B(t)\right)U\pi - W\,\rho 0\,\Omega\xi(t)\,S(t)\left(\frac{d}{dt}A(t)\right)U\pi\right)\varepsilon$$

$$collect\left(combine(u1 + v1 + w1), [\varepsilon, \rho 0, \rho C[4], \rho S[4], diff, \Omega\xi, \Omega\eta, \Omega\zeta, \rho C[6], \rho S[6]], factor\right)$$

$$\left(\left(\frac{1}{2}\pi\,(U-V)\,(V+U)\left(\frac{d}{dt}C(t)\right)^2 - \frac{1}{2}\pi\,(U-V)\,(V+U)\left(\frac{d}{dt}S(t)\right)^2\right)\rho C_4 + \pi\,(U\right. \tag{26}$$
$$\left.-V)\,(V+U)\left(\frac{d}{dt}S(t)\right)\left(\frac{d}{dt}C(t)\right)\rho S_4 + \frac{1}{2}W^2\left(\frac{d}{dt}A(t)\right)^2\rho C_6\,\pi\right.$$

$$+\left(W^2\left(\frac{\mathrm{d}}{\mathrm{d}t}B(t)\right)\rho S_6\,\pi-\pi\,S(t)\,W(V+U)\,\Omega\xi(t)-\pi\,C(t)\,W(V\right.$$
$$\left.+U)\,\Omega\eta(t)\right)\left(\frac{\mathrm{d}}{\mathrm{d}t}A(t)\right)-\frac{1}{2}\,W^2\left(\frac{\mathrm{d}}{\mathrm{d}t}B(t)\right)^2\rho C_6\,\pi+\left(\pi\,C(t)\,W(V+U)\,\Omega\xi(t)\right.$$
$$\left.-\pi\,S(t)\,W(V+U)\,\Omega\eta(t)\right)\left(\frac{\mathrm{d}}{\mathrm{d}t}B(t)\right)+\left(-\pi\,B(t)\,W(V+U)\,\Omega\xi(t)+\pi\,A(t)\,W(V\right.$$
$$\left.+U)\,\Omega\eta(t)+4\,\pi\,\Omega\zeta(t)\,S(t)\,UV\right)\left(\frac{\mathrm{d}}{\mathrm{d}t}C(t)\right)+\left(\pi\,A(t)\,W(V+U)\,\Omega\xi(t)\right.$$
$$\left.+\pi\,B(t)\,W(V+U)\,\Omega\eta(t)-4\,\pi\,\Omega\zeta(t)\,C(t)\,UV\right)\left(\frac{\mathrm{d}}{\mathrm{d}t}S(t)\right)\rho0\,\varepsilon$$
$$+\left(\left(\frac{\mathrm{d}}{\mathrm{d}t}A(t)\right)^2W^2\,\pi+\left(\frac{\mathrm{d}}{\mathrm{d}t}B(t)\right)^2W^2\,\pi+\pi\left(U^2+V^2\right)\left(\frac{\mathrm{d}}{\mathrm{d}t}C(t)\right)^2+\pi\left(U^2\right.\right.$$
$$\left.\left.+V^2\right)\left(\frac{\mathrm{d}}{\mathrm{d}t}S(t)\right)^2\right)\rho0$$